University of Groningen

Steady state and time resolved spectroscopy of photoswitchable systems

Hou, Lili

IMPORTANT NOTE: You are advised to consult the publisher's version (publisher's PDF) if you wish to cite from it. Please check the document version below.

Document Version
Publisher's PDF, also known as Version of record

Publication date:
2013

Link to publication in University of Groningen/UMCG research database

Citation for published version (APA):
Hou, L. (2013). *Steady state and time resolved spectroscopy of photoswitchable systems*. s.n.

Steady State and Time Resolved Spectroscopy of Photoswitchable Systems

Lili Hou

RIJKSUNIVERSITEIT GRONINGEN

Steady State and Time Resolved Spectroscopy of Photoswitchable Systems

Proefschrift

ter verkrijging van het doctoraat in de
Wiskunde en Natuurwetenschappen
aan de Rijksuniversiteit Groningen
op gezag van de
Rector Magnificus, dr. E. Sterken,
in het openbaar te verdedigen op
dinsdag 10 december 2013
om 11:00 uur

door

Lili Hou

geboren op 5 juni 1984

te Jilin, China

Promotores : Prof. dr. B.L. Feringa
Prof. dr. W.R. Browne

Beoordelingscommissie : Prof. dr. S. Harutyunyan
Prof. dr. W.J. Buma
Prof. dr. J.M. Kelly

CONTENT

CHAPTER 1

Molecular Organic Photochemistry

Organic molecules often interact with light and undergo structural changes and initiate dynamic processes, which occur from a wide variety of electronically excited states. Understanding these processes is crucial to investigate photosynthesis in nature, develop 'green' solutions to energy production, and develop new optoelectronic devices for application in information technology. In this chapter the most commonly encountered molecular organic photochemical processes are described, with selected examples of photochemical reactions and bimolecular photochemical processes.

1.1 Introduction

Molecular organic photochemistry is concerned with the chemical reactions and physical changes of organic molecules initiated by absorption of light. Photochemistry has always played an important role in the fields of chemical physics, molecular spectroscopy, physical organic chemistry, supramolecular organic chemistry, etc.[1] Organic molecules (R) absorb photons (*hv*), whose frequency matches the energy gap between two electronic states, and are promoted to an electronically excited state (R*). Upon excitation, molecules undergo either relaxation back to their ground state, or a chemical reaction to form new products (P). If, overall, the molecules do not undergo a net chemical change, then the processes are described as photophysical processes (1.1). On the other hand, if the processes involve the formation of products, they are described as photochemical processes (1.2).

$$R + hv \rightarrow R^* \rightarrow R \qquad\qquad (1.1)$$

$$R + hv \rightarrow R^* \rightarrow P \qquad\qquad (1.2)$$

Photochemistry is at the foundation of many important processes involved in living systems and the environment. The premier example is natural photosynthesis, including absorption of sunlight by plants to produce food and energy, and the production of vitamin D in the body.[2,3] Vision is achieved by light induced *cis-trans* isomerization of retinal in rhodopsin, which triggers a signal transducing ion cascade.[4,5] Photochemistry also plays an important role in health sciences, e.g. photodynamic therapy, which is used to treat some forms of tumors and diseases with light irradiation.[6,7] Many polymerizations are induced by photochemical processes, in which molecules are decomposed upon absorbing light to produce free radicals for radical polymerization.[8,9] Photoinduced polymerization has been applied to produce protective coatings for a variety of high-value materials, e.g. optical fibers.[10] Photochemistry also plays an important role in artificial lighting,[11] solar cells[12,13] and computer chips manufactured with photolithography.[14]

1.2 Photophysical processes

The photophysical processes of organic molecules interacting with light are usually illustrated with a Jablonski diagram, which is often used to describe the light absorption and emission processes.[15] Figure 1 shows a Morse potential surface of the ground state (S_0), the lowest-energy excited singlet state (S_1), and the lowest-energy excited triplet state (T_1). Each energy level is comprised of a number of coupled vibrational states. The electronic configuration of the highest occupied molecular orbital (HOMO) and the lowest unoccupied molecular orbital (LUMO) of each energy level is also shown. Higher energy excited singlet (S_2, S_3, etc.) and triplet states (T_2, T_3, etc.) are excluded in Figure 1, because experience has shown that excitation of these higher energy excited states generally results in deactivation to S_1 and T_1, which are much faster than any other measurable processes. It is termed as Kasha's rule.[16] In Figure 1, the dynamics of transitions corresponding to all possible photophysical processes that interconnect S_0, S_1, and T_1 are also presented.
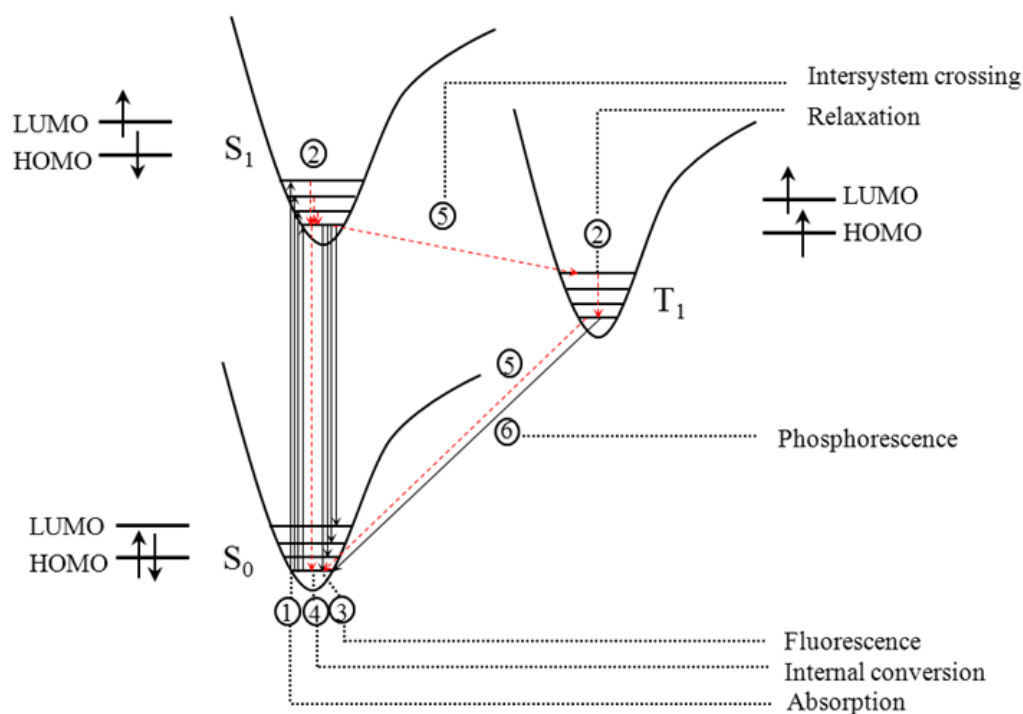
Figure 1. Morse potential for the ground state and the lowest-energy singlet and triplet states.

1.2.1 Absorption

When irradiated with light, molecules absorb photons with an energy that matches the energy gap between the ground state (S_0) and an electronically excited state. The electronic configuration of the ground state of most organic compounds is generally $HOMO^2$ $LUMO^0$ with the spin of the two electrons in HOMO paired, due to the Pauli Exclusion Principle. In Figure 1, the antiparallel spins of the electrons is symbolized as ↑↓, which corresponds to a singlet spin configuration. When molecules absorb photons and excited electronic states are generated, electrons are promoted to unoccupied molecular orbitals, and the electrons in two different half-filled orbitals (e.g. HOMO and LUMO) are not required to follow the Pauli Exclusion Principle, so the spin of the electrons can be either paired or unpaired. The unpaired electrons have parallel spins, which corresponds to a triplet spin configuration or triplet state.

The transition time from S_0 to S_1 occurs over 10^{-16} to 10^{-14} s, which no chemical process can compete with. The process of absorption only involves the movement of electrons. According to the Franck-Condon principle,[17,18] electronic transitions occur faster than nuclear motion, which means that electronic transitions are most favorable when the geometries of the initial and final states are the same.

Light absorption by compounds follows the Lambert-Beer Law (equation 1.3).[19] The absorbance or optical density (OD), *A*, is linearly dependent on the concentration and the distance the light travels through the material. The molar absorptivity expresses the efficiency of light absorption, which depends primarily on the intrinsic properties of the molecules.

$$A = log \ (I_0/I) = \varepsilon bc \tag{1.3}$$

Where I_0 is the intensity of the incident light, I is the intensity of the transmitted light, ε is molar absorptivity, *b* is the path length, and *c* is the concentration of the compound of interest.

The UV/vis absorption spectrum is plotted with absorption as a function of wavelength. Typically, broad transitions are observed in the UV/vis absorption spectrum, instead of detailed vibrational structures (Figure 2). The reason is that

most molecules under normal conditions are present in a range of micro environments and many vibrational and rotational levels overlap. For very rigid molecules, e.g. anthracene (Figure 2c), or at very low temperature, the vibrational structure is often resolved with narrow absorption bands.
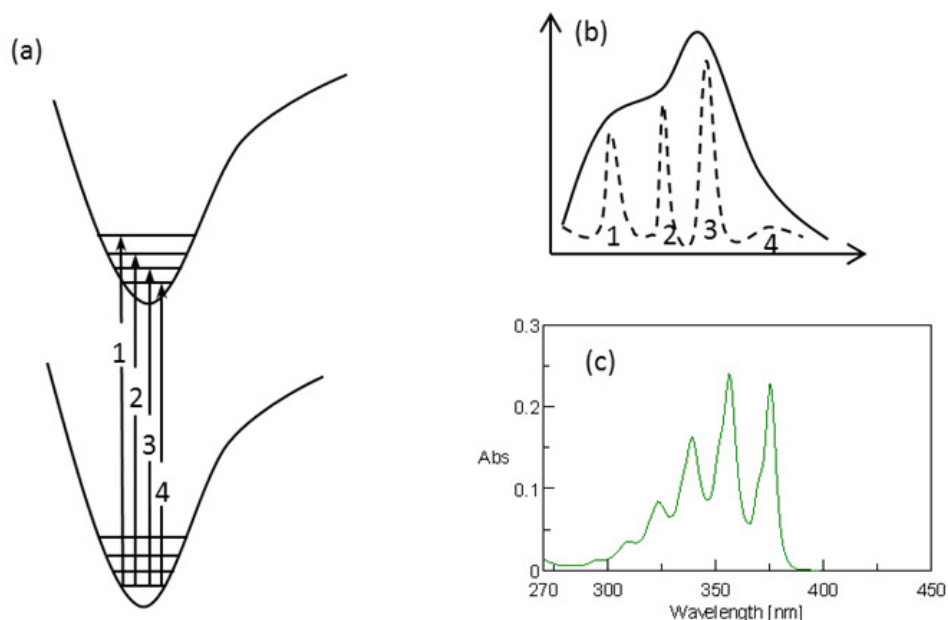
Figure 2. (a) Excitation upon absorption of light to different vibrational excited electronic states. (b) A typically absorption spectrum with a broad absorption band. (c) Absorption spectrum of anthracene in ethanol.

1.2.2 Emission

In condensed phases, after absorbing light, molecules (e.g. at a higher vibrational level of S_1 or T_1) rapidly relax to the lowest vibrational level of the excited state, which is termed vibrational relaxation (Figure 1, process 2). This process generally occurs within 10^{-12} s or less, and it is generally complete prior to emission.

There are four possible photophysical processes that result in molecules returning to the ground state from the lowest vibrational level of the excited states: fluorescence, phosphorescence, internal conversion and intersystem crossing (Figure 1, process 3, 6, 4, 5, respectively). Internal conversion is a non-radiative process, which generates heat instead of photons and transfers energy to the environment. Intersystem crossing that occurs from S_1 to T_1, or from T_1 to S_0 is

also a non-radiative process. The difference compared to internal conversion is that intersystem crossing involves a change of electron spin.

Molecules relax to the ground state also by releasing energy though emission of photons. The emission of light from the molecules is called luminescence, which is formally divided into two categories, fluorescence and phosphorescence, depending on the nature of the excited state. Fluorescence is emission from the singlet excited state to the ground state, which is a spin allowed process with fluorescence lifetime typically in the nanosecond time scale. While, emission from a triplet excited state to the ground state is termed phosphorescence, in which the transition is forbidden, and thus phosphorescence lifetimes are several orders of magnitude longer than those of fluorescence, and typically lasts from microseconds to seconds. The triplet excited state is generally lower in energy than the singlet excited state, and therefore phosphorescence is shifted to longer wavelength relative to fluorescence from the same compound. These two processes are one of the central points of interest in this thesis.

Fluorescence or emission spectra are plotted as fluorescence intensity as a function of wavelength. Fluorescence spectra are generally independent of the excitation wavelength, following Kasha's rule.[16] As with absorption spectra, fluorescence spectra usually show broad bands without vibrational structures, due to the strong overlap of numerous states of nearly equal energy. The fluorescence spectra of most compounds typically follow the mirror-image rule, in which the absorption and fluorescence spectra are mirror images, e.g. anthracene (Figure 3). The symmetric relation between absorption and emission spectra is due to the similarity of the vibrational energy levels of the S_1 and S_0 states. The difference between the longest wavelength absorption band and the shortest wavelength emission band is termed the Stokes shift.[20] The Stokes shift is energy loss between excitation and emission. Solvent effects, complex formation, etc. can result in an increased Stokes shift and deviation from the mirror-image rule.
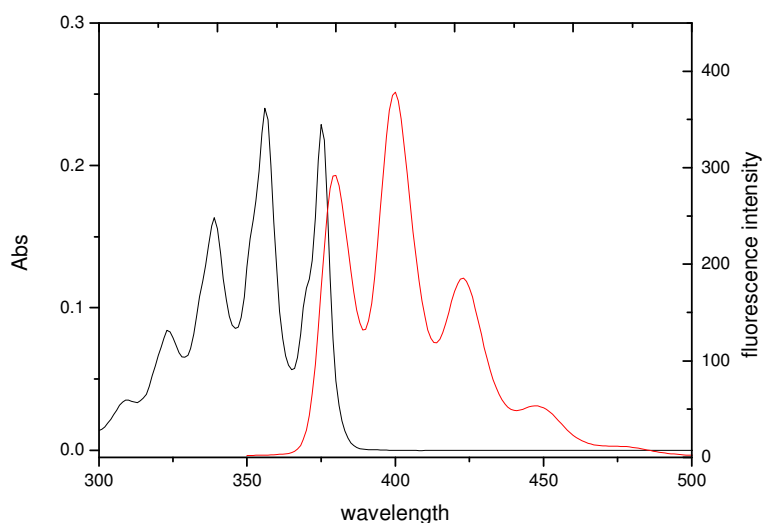
Figure 3. The absorption and emission spectra of anthracene in ethanol.

Phosphorescence spectra are usually not observed in fluid solutions at room temperature, due to several deactivation processes that compete with phosphorescence, such as non-radiative decay and oxygen sensitization. Intersystem crossing from singlet excited state to triplet state can be enhanced by the heavy atom effect,[21] e.g., Br, I or metal. Introducing heavy atoms increase mixing of spin and orbital angular momentum, or coupling of spin orbitals (e.g., in porphyrins), and thus enhance the phosphorescence quantum yield. This leads to the possibility to observe phosphorescence at room temperature, e.g., metal-porphyrins,[22] and coordination complexes.[23]

1.3   Photochemical reactions

Photochemical reactions are chemical reactions initiated by the absorption of light. After absorbing light, the molecules go to transient excited states to yield new chemical species, or transfer electrons, protons, H atoms or energy to other molecules. Photochemical reactions can occur when internal conversion and relaxation of an excited state leads to a ground state different to that of the initial molecules, or when an excited state performs an intermolecular addition to another molecule in the ground state. Photochemical reactions have proven to be a useful tool to synthesize organic compounds.
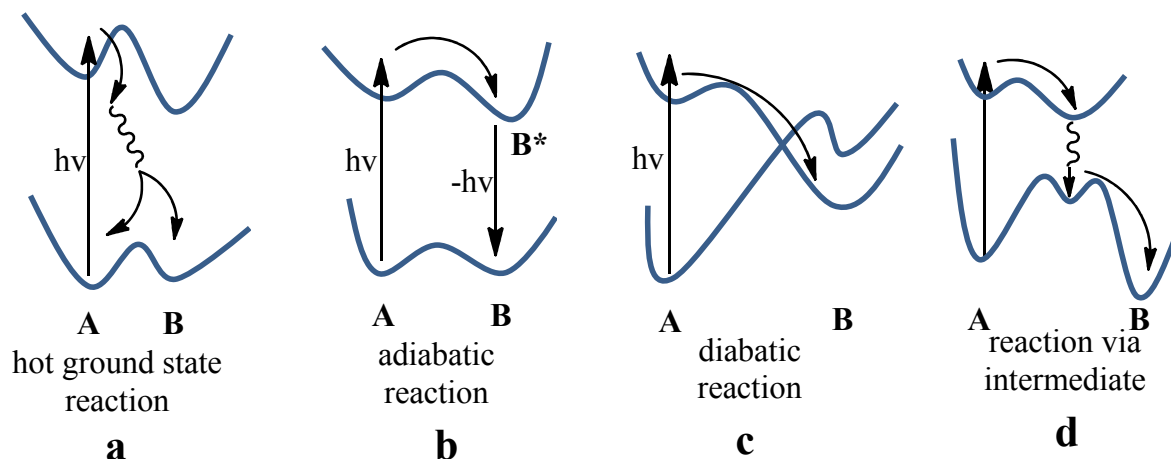
Figure 4. Classification of photochemical reactions.

Four types of photochemical reactions are distinguished: (a) Hot ground state reactions, in which the molecule relaxes from the local minimum excited state to the ground state through internal conversion (Figure 4a); (b) Photochemical reactions proceed on an excited state surface B* (adiabatic reaction, Figure 4b); (c) Diabatic reactions, which take place directly by crossing of the ground and excited state energy surfaces (Figure 4c); (d) Photochemical reactions that proceed via the formation of intermediates, such as carbenes, biradicals or zwitterions (Figure 4d). The following section summarizes some typical photochemical reactions, including photocycloaddition, photoreduction and photoisomerization.

1.3.1 Photocycloaddition reactions

An example of a photocycloaddition reaction is the addition of a carbonyl to an olefin to form a four-membered oxetane ring (Scheme 1).[24] The reaction takes place from the singlet or triplet n→π* states of the carbonyl, via a biradical intermediate.
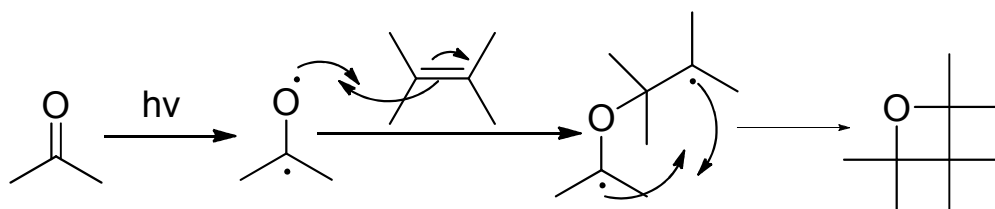
Scheme 1. Formation of four-membered ring oxetane.

1.3.2 Photoreduction reactions

Ketones can be reduced to alcohols upon irradiation in the presence of hydroxylic solvents.[16] Scheme 2 shows an example of the reduction of benzophenone by 2-propanol. The ketone can abstract H from the C-H bond of 2-propanol to form two radicals. Then the reaction proceeds via either of two routes: formation of benzhydrol by abstraction of H, or formation of benzpinacol via dimerization.
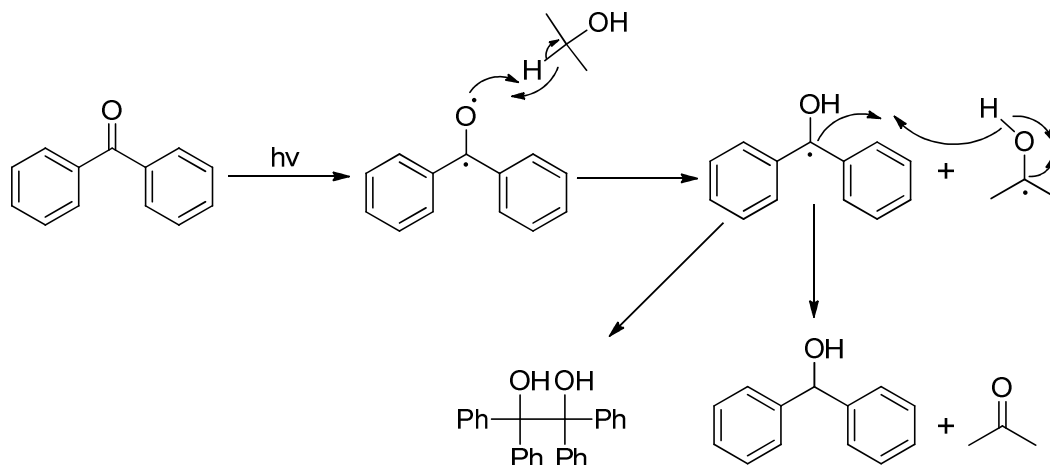
Scheme 2. Reduction of benzophenone by isopropanol to benzhydrol or benzpinacol upon irradiation.

1.3.3 Photoisomerizations

Photoisomerization converts molecules from one isomer to another isomer using light. Here, the photoisomerization of the commonly used molecular switches/motors will be discussed briefly. [25]

Stilbene

Stilbene, a diarylethene compound, has been studied extensively over the past decades.[26,27] It has two isomeric forms, E and Z. The E-form of stilbene can be converted to the Z-form upon irradiation with light. The Z-form can revert to the E-form using light or heat (Scheme 3). Besides the *cis/trans* isomerization, the Z-form of stilbene can also undergo a 6-π electrocyclization to form dihydrophenanthrene (which has never been isolated but can be detected spectroscopically), which is prone to be oxidized irreversibly to phenanthrene by

molecular oxygen. A bimolecular reaction between two stilbene molecules can also occur to form 1,2,3,4-tetraphenylcyclobutane (not shown). These side reactions of stilbene limits its use as an optical switch.
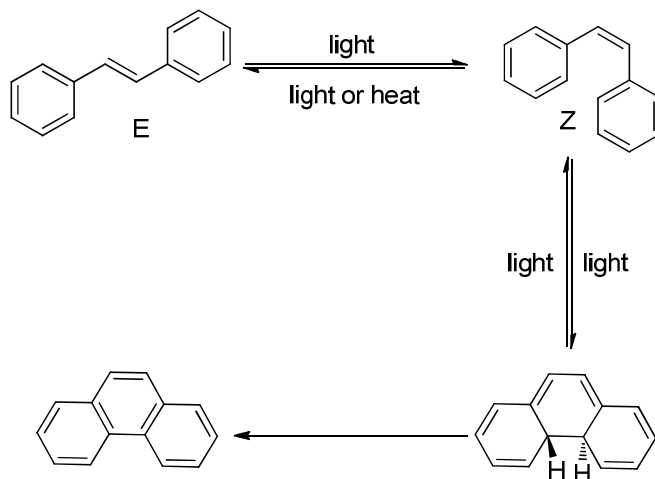
Scheme 3. Isomerization and cyclization processes of stilbene.

Azobenzenes

Azobenzenes are another kind of well-known optical switch and are composed of two phenyl rings linked by a central N=N bond.[28] The *cis/trans* isomers can be switched using ultraviolet and blue light (Scheme 4). The *cis* isomer is less stable than the *trans* isomer. Therefore, the *cis* isomer can thermally relax back to the stable *trans* isomer. The two isomers show well-separated absorption bands and different physical properties (e.g. dielectric constant, refractive index).
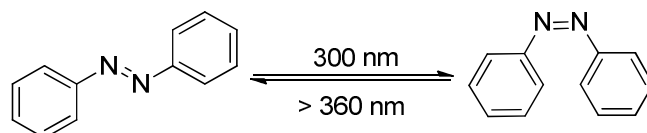
Scheme 4. Photochemical isomerization of azobenzene.

Dithienylethenes

One of the most successful of diarylethene switches are the dithienylethenes (alkenes with a thiophene ring on each side, Scheme 5).[29] The open form of the

dithienylethene switch is normally colourless and can convert to the closed form upon irradiation with UV light. The closed form is coloured and can go back to the open form by irradiation with visible light.
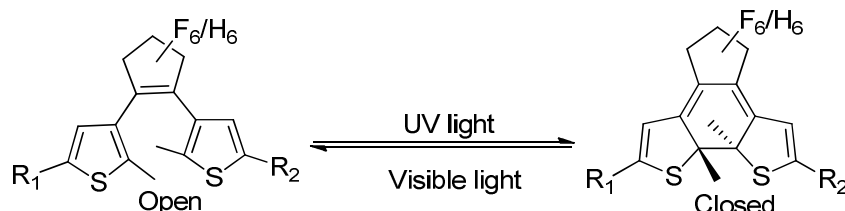
Scheme 5. Photoswitching of dithienylethene switches.

Overcrowded alkenes

In 1999, Feringa et al. reported a unidirectional molecular motor based on overcrowded alkenes.[30] The molecular motors consist of a central double bond, naphthalene groups and a stereogenic center. The unidirectional rotation of the motor involved four steps: two reversible photoisomerization steps and two irreversible thermal isomerization steps (Scheme 6). The helicity of the motor changes during each step, and the direction of the rotation is determined by the configuration of the stereo-centers.
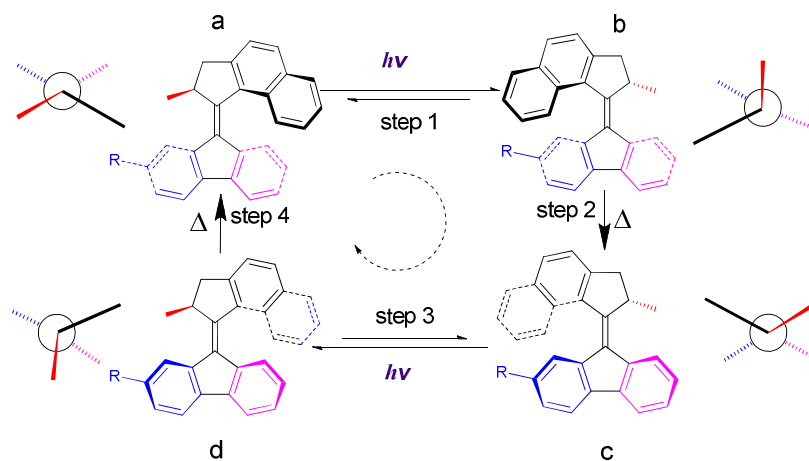
Scheme 6. 360° rotary cycle of an overcrowded alkene based molecular motor.

1.4   Bimolecular photochemistry

When molecules in an excited electronic state encounter a second molecular species in its ground state, more complex photochemical processes can occur, for

example, photoinduced electron transfer, energy transfer and formation of excimers or exciplexes. These processes compete with direct emission of light and facilitate non-radiative relaxation. Bimolecular photochemical processes are useful to further study the nature of the excited states and provide guidance to build artificial systems.

1.4.1 Quenching

Bimolecular photochemical processes can decrease the intensity of fluorescence or phosphorescence and diminish excited state lifetime, both of which are termed quenching, and the molecules that deactivate the luminophores are termed quenchers. The most common quenching process is collisional quenching. The molecules in an excited state encounter the quenchers before returning to their ground state resulting in non-radiative relaxation. The molecules are not chemically altered by this process.

The Stern-Volmer equation is used to determine the rate of collisional quenching:[31]

$$F_0/F = \tau_0/\tau = 1 + k_q\tau_0[Q] \tag{1.4}$$

Where F_0 and F are the fluorescence or phosphorescence intensity in the absence and presence of the quencher, and τ_0 and τ are the lifetime of molecules in absence and presence of the quencher, respectively; $[Q]$ is the concentration of the quencher, and k_q is the bimolecular quenching constant, which reflects the efficiency of quenching or the accessibility of the luminophores to the quencher.

Collisional quenching is a time-dependent process. Quenching can also occur when the quencher is bound to the luminophores in their ground state and forms non-luminescent complexes, it is referred as static quenching. A Stern-Volmer plot, where static quenching is involved will show a linear dependence of F_0/F on the concentration of the quencher, with the quenching constant of static quenching being essentially the association constant. The emission lifetime, in the case of static quenching does not decrease because only the unbound luminophores are observed, which have the unquenched lifetime τ_0, and bound luminophores are non-emissive. A plot of τ_0/τ versus $[Q]$ can be used to distinguish collisional quenching from static quenching, for static quenching

$\tau_0/\tau=1$, while for dynamic quenching $\tau_0/\tau= F_0/F$. The absorption spectra of luminophores can be also used to distinguish static and dynamic quenching. If there are no changes in the absorption spectrum of a luminophore, then they are likely to be involved in dynamic quenching, while the formation of a ground-state complex in the static quenching event can result in a change in the absorption spectrum.

1.4.2 Electron Transfer

Electron transfer from molecules in the excited state to a second molecular species is a further process that can also lead to quenching of emission. Electron transfer requires a compatible acceptor (A) to be in proximity to a donor (D). The donor is a molecule with a low ionization potential, and the acceptor has a high electron affinity.
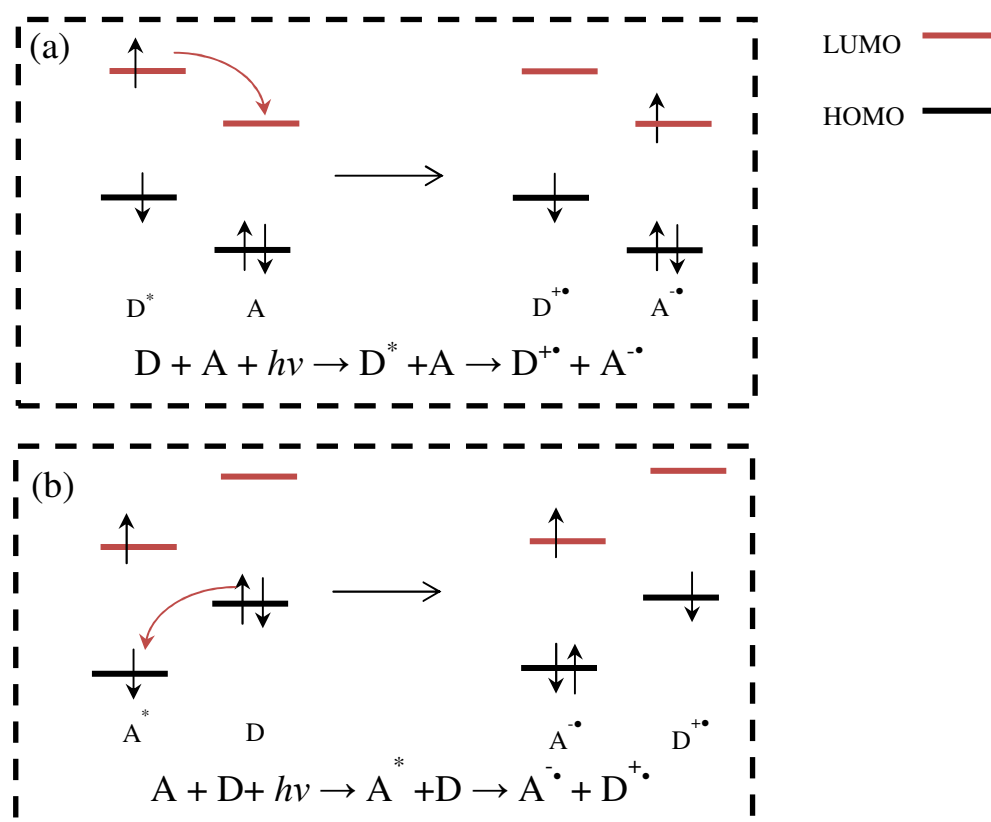
Figure 5. The mechanism of oxidative electron transfer where the LUMO of the excited molecules is above the LUMO of the ground state of the acceptor (a), and reductive electron transfer where the HOMO of the excited molecules is below the HOMO of the ground state of the donor (b).

There are two mechanisms for electron transfer: oxidative and reductive (Figure 5). The molecules in an excited state have a significantly different oxidation and reduction potential than the ground state, due to occupation of the LUMO level. If the donor molecular species has a higher LUMO energy than that of the acceptor, the excited donor will transfer electrons to the lower energy orbital of the acceptor. The excited state of molecules, which absorbed light, is considered to be a good donor (Figure 5, a). Since the electron is moved to a higher orbital, there is a vacancy in the lower energy orbital (HOMO), which facilitates reduction. In the presence of a donor with a higher lying HOMO, an electron is accepted from the donor and transferred to the HOMO of the excited molecules (Figure 5, b).

Photoinduced electron transfer promotes charge separation, which has several manifestations in photochemical reactions, and is also a key step in the function of photosynthesis, and of materials developed for photovoltaic and molecular electronics applications.

One example based on photoinduced electron transfer processes in nature is that photosystem II absorbs light to provide electrons for photosynthesis in thylakoid membranes of plants, algae, and cyanobacteria.[32] The crystal structure of photosystem II was determined by Ferreira et al.,[34] which is shown in Figure 6. Excitation of the reaction center via four chlorophylls (Chl_{D1}, Chl_{D2}, P_{D1} and P_{D2}) initiates electron transfer to the primary electron acceptor pheophytin (Pheo). The formation of the primary radical pair of $P_{D1}^{\cdot}$ and $Pheo^{\cdot-}$ takes place in a few picoseconds. Stabilisation of the $P_{D1}^{\cdot}$ and $Pheo^{\cdot-}$ state is accomplished by electron transfer from $Pheo^{\cdot-}$ to a plastoquinone acceptor Q_A then to a second plastoquinone Q_B. This electron transfer is aided by the presence of a non-haem iron (Fe) located mid-way between them and it occurs over the microsecond to millisecond time domain according to its redox state. The charge recombination in photosystem II is in the 10^{-8} to 10^{-4} s time range,[33] which is long enough to oxidize water to oxygen and reduces plastoquinone to plastoquinol, simultaneously serving as the ultimate electron source for biosynthesis of organic matter and contributing to the pH gradient across the photosynthetic membrane for ATP synthesis.
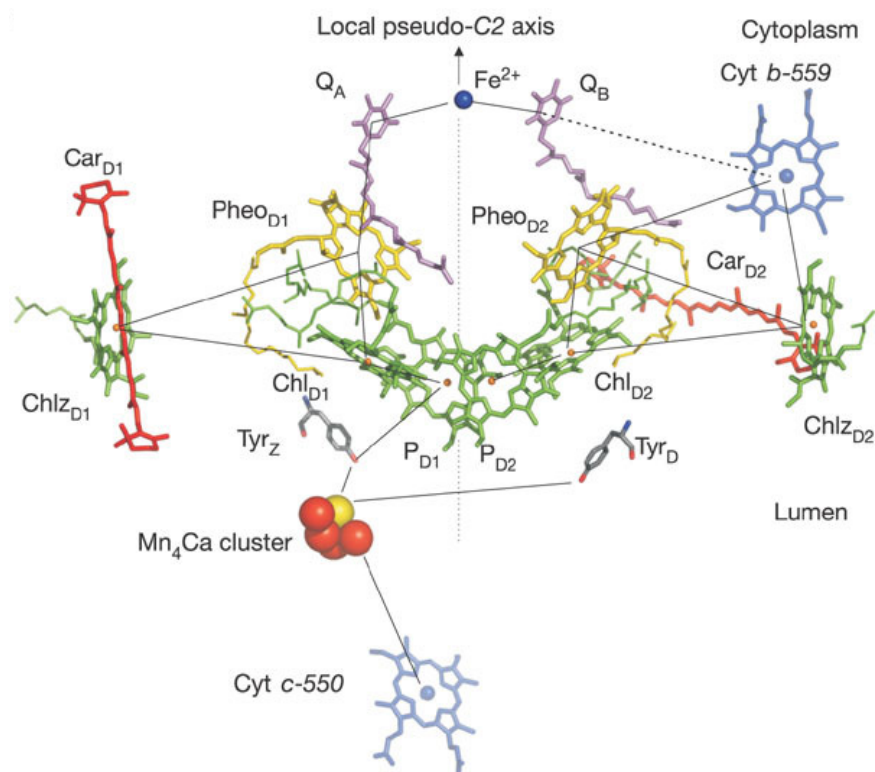
Figure 6. Organisation of the electron transfer cofactors that make up the reaction center of Photosystem II as revealed by X-ray crystallography.[34] Reproduced from ref. 34 with permission. Copyright the American Association for the Advancement of Science (2005).

Another example related to photoinduced electron transfer is found in semiconducting solar cells based on n- and p- type dye. The charge separation between the donor/acceptor interfaces of semiconducting solar cells converts energy to an electrical signal.[35,36] Figure 7 shows the principle of operation of photoelectrochemical cells based on n-type semiconductors. Light excitation induces an ultrafast initial charge separation, which occurs in femtoseconds. The electric field present in the space-charge layer leads to a relatively slower charge recombination, which allows the charge carriers to be collected as an electric signal. The negative charge carriers move through the bulk of the semiconductor to the current collector and the external circuit. The positive holes are driven to the surface where they are scavenged by the reduced form of the redox relay molecule.
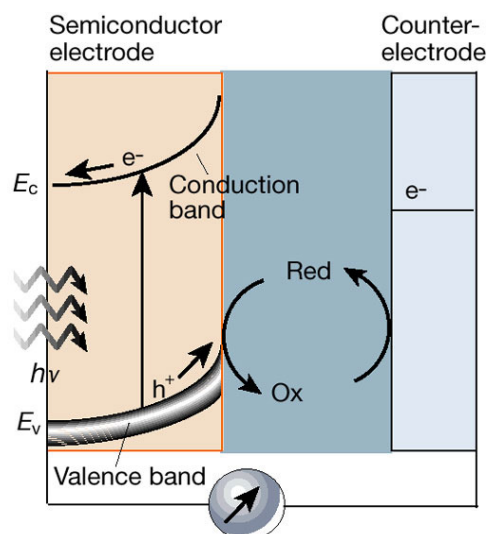
Figure 7. Principle of operation of photoelectrochemical cells based on n-type semiconductors.[37] Reproduced from ref. 37 with permission. Copyright the American Association for the Advancement of Science (2001).

1.4.3   Energy transfer

As with electron transfer, when an energy acceptor with suitable excited state energy and distance is present, energy transfer can occur from the excited molecule (donor) to an acceptor. Instead of formation of a charge separated state due to electron transfer, energy transfer produces an excited electronic state in the acceptor.

Energy transfer processes are rationalized through many possible mechanisms. The most trivial form of energy transfer is radiative transfer, which occurs when a donor molecule emits a photon upon excitation and an accepter molecule reabsorbs that photon (Figure 8 and equation 1.5).[38]

$$D + h\nu \rightarrow D^* \xrightarrow{A} D + A^*$$ (1.5)

Radiative transfer occurs when the emission spectrum of the donor substantially overlaps with the absorption spectrum of the acceptor. The rate or efficiency of radiative transfer is dependent on a number of factors, including the quantum yield of the donor, the concentration of acceptor molecules, and the molar absorption of the acceptor at the wavelength of emission of the donor. In dilute solution, the probability of radiative transfer is very low.
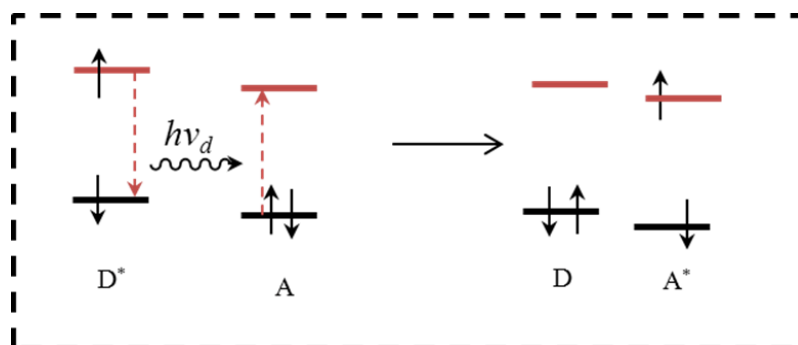
Figure 8. Trivial energy transfer processes.

There are two main mechanisms of energy transfer in molecular organic photochemistry (Figure 9). One is the electron exchange interaction, which is also referred as orbital overlap electron exchange (Figure 9, a). The other is the dipole-dipole interaction, which is also referred as Coulombic or resonant energy transfer (Figure 9, b). These two mechanisms are named as Dexter energy transfer[39] and Förster resonance energy transfer,[40] respectively.
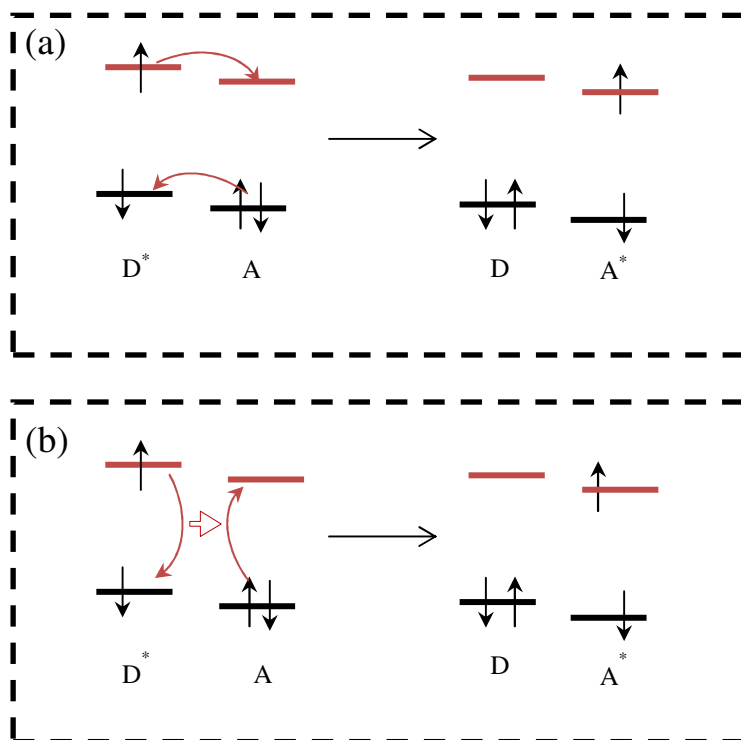
Figure 9. (a) Dexter energy transfer and (b) Förster resonance energy transfer mechanisms.

Dexter energy transfer

Dexter energy transfer involves electron exchange mediated by the overlap of orbitals of the excited state donor and the ground state acceptor (Figure 8, a). When light is absorbed by the donor, an electron in the LUMO transfers to the LUMO of the acceptor, which is equal or lower than that of the donor. Meanwhile, one electron in the HOMO of the acceptor transfers to the HOMO of the donor.

The rate of electron exchange (k_{ee}) in Dexter energy transfer is determined by the magnitude of the specific orbital interaction (K) that promotes the electron exchange, the magnitude of the spectral overlap integral (J), and the distance between the donor and acceptor (r_{DA}). Equation 1.6 describes the electron exchange energy transfer rate, in which L is the sum of the van de Waals radii.

$$k_{ee} = KJe^{-(2r_{DA}/L)} \tag{1.6}$$

Equation 1.6 indicates that the efficiency of Dexter energy transfer decreases steeply as the separation between the donor and acceptor increases because of it is an exponential relationship. Dexter energy transfer typically occurs within 10 Å, and it is a short-range energy transfer mechanism. To achieve efficient Dexter energy transfer, the donor and acceptor are usually held in a fixed position, for example, covalently connecting the donor and acceptor at a fixed distance.

Dexter energy transfer can also occur through the excited triplet state, which is termed as triplet state sensitization (Figure 10). Energy transfer from the triplet excited state of the donor to the acceptor is accompanied by intersystem crossing. To conserve spin, electron exchange processes allows the formation of the triplet excited state of the acceptor. The quantum yield of the triplet state of many organic molecules is low, since other processes with faster rates are observed mainly, e.g. fluorescence. Triplet state sensitization through a donor that has efficient intersystem crossing can yield sufficient triplet state in the acceptor. This allows the photochemistry of the triplet state of the organic molecules to be studied and used.
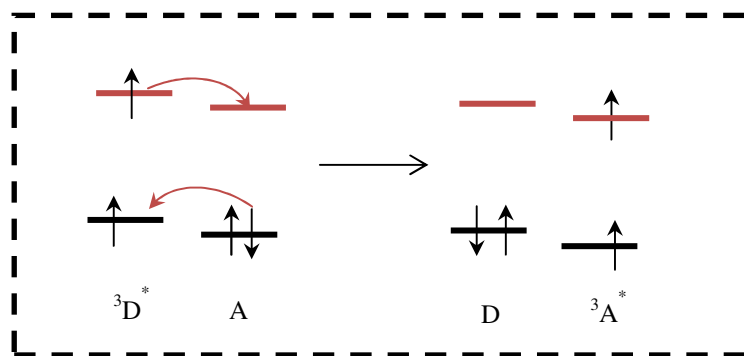
Figure 10. Dexter energy transfer through triplet states of the donor and acceptor.

Whitten et al. investigated complexes in which metalloporphyrins were bound to stilbene and its derivatives (Figure 11).[41,42] Isomerization was achieved through triplet state sensitization by irradiation with visible light of 400-600 nm, while UV or near UV light is needed to directly induce the photoisomerization of stilbene and related compounds. The long triplet lifetimes and high triplet quantum yield of metalloporphyrins enable energy transfer to produce the triplet state of stilbenes. The triplet sensitization results in a *cis* or *trans* excited state converting to the perpendicular triplet excited state ($^pT_1$) and relaxing to the ground state, by which the isomerization takes place.
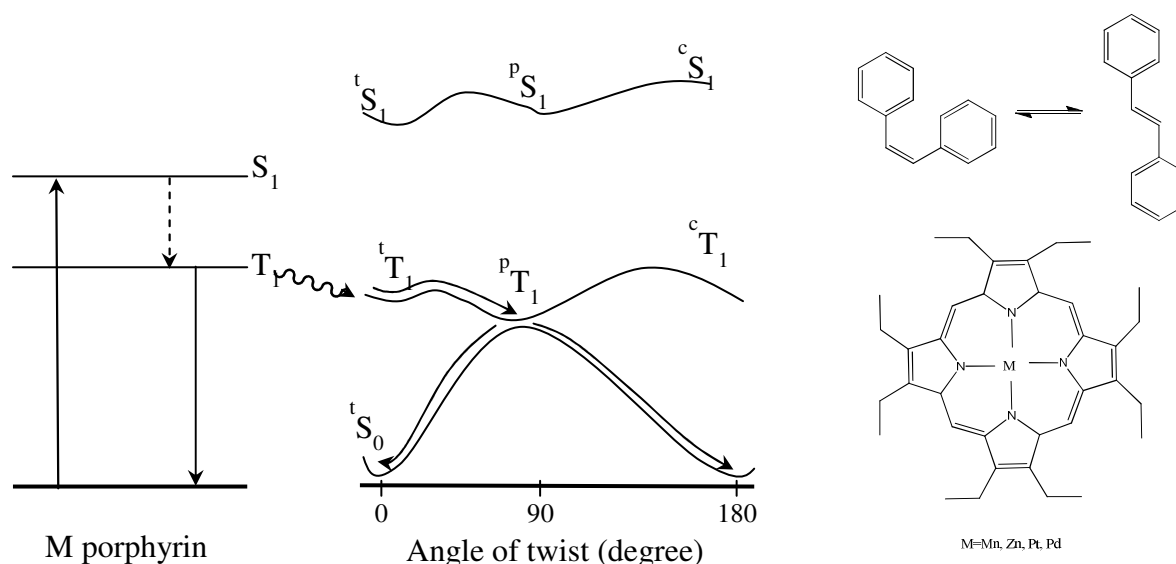
Figure 11. The structures of stilbene and metalloporphyrins. The photochemical process is described on the left.

Triplet state sensitization is also widely applied in energy up-conversion systems, which provides a promising way to produce high-energy light using medium-

energy light. Two steps are involved in up-conversion: the first is triplet-triplet Dexter energy transfer between the donor and acceptor, and the second step is triplet-triplet annihilation of the acceptor. Triplet-triplet annihilation occurs when two acceptor molecules in their triplet excited state encounter and produce one molecule in a singlet excited state and the other relaxes to its ground state. One example of up-conversion is shown in Figure 12, in which Pt(II)-octaethylporphryin (PtOEP) acts as the donor and 9, 10-diphenylanthracene (DPA) as the acceptor.[43] PtOEP is promoted to its first singlet excited state (2.33 eV) upon excitation at 532 nm, and relaxes to the triplet excited state (1.91 eV) through efficient intersystem crossing. Energy transfer occurs from the triplet excited state of PtOEP to the triplet excited state of DPA (1.78 eV). Triplet-triplet annihilation promotes triplet DPA to its higher singlet excited state (e.g. S_2 or S_3) and relaxes rapidly to the first excited state (2.83 eV). The emission band of this up-conversion system has a maximum located at 430 nm upon excitation at greater than 500 nm.
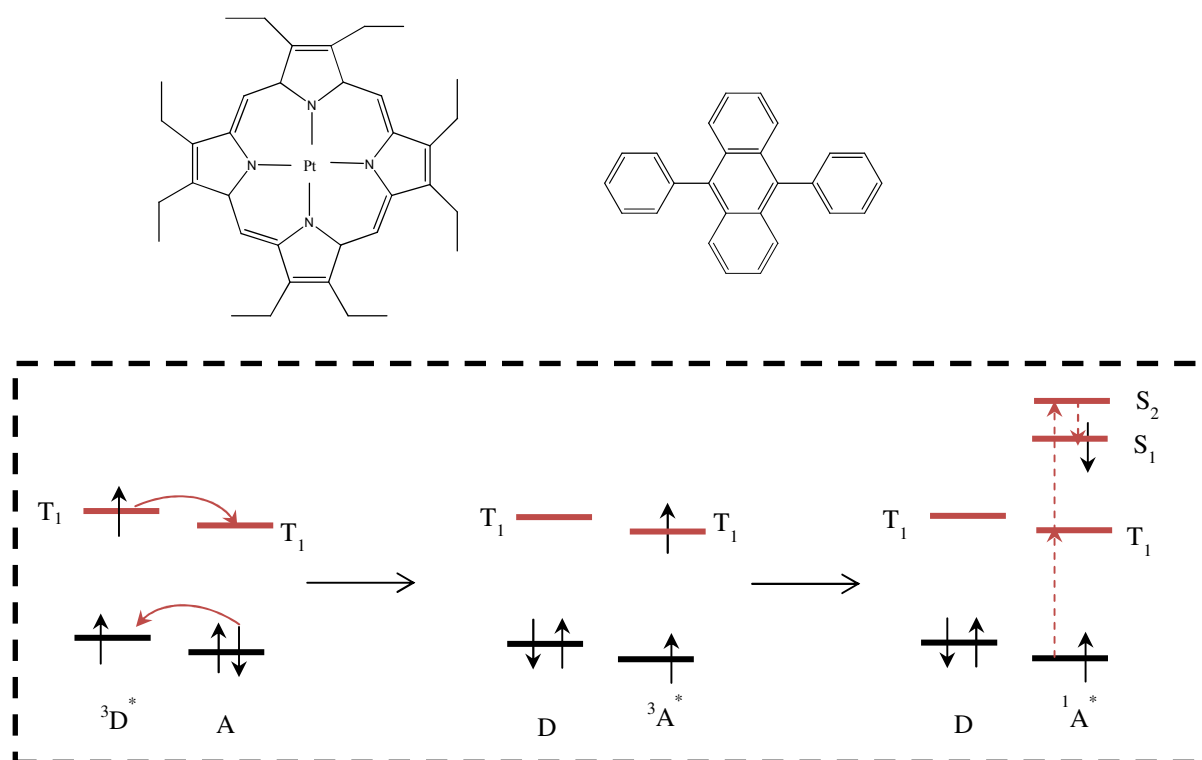
Figure 12. The generation of the up-converted fluorescence through Dexter energy transfer of Pt(II)-octaethylporphyrin and 9, 10-diphenylanthracene.

Triplet energy transfer is also used extensively to sensitize triplet oxygen to form singlet oxygen, and it is applied in a wide range of areas in photooxidation, DNA

damage, and photodynamic therapy.[44, 45] The ground state of oxygen molecules is a spin triplet termed ($^3\Sigma_g^-$, or generally $^3O_2$). There are two accessible excited states of triplet oxygen termed singlet oxygen, $^1\Sigma_g^+$ and $^1\Delta_g$ (generally $^1O_2$), which are spin singlets with 158 and 95 kJ/mol above the triplet state, respectively. Relaxation from $^1\Sigma_g^+$ to $^1\Delta_g$ is very fast, while the transition from $^1\Delta_g$ to $^3\Sigma_g^-$ is spin forbidden, thus singlet oxygen is a relatively long-lived species and highly reactive. Photosensitization is a simple and controllable method for generation of singlet oxygen, in which the photosensitizer transfers its energy of excitation to $^3\Sigma_g^-$ to generate singlet oxygen. Achieving a high singlet oxygen quantum yield requires that the photosensitizer has a high triplet state quantum yield (>0.4), an electronic energy of the triplet state at least 20 kJ/mol above that of singlet oxygen, a long triplet lifetime and high photostability. Common photosensitizers used to generate singlet oxygen are some organic dyes[46] e.g. rose Bengal, methylene blue, porphyins,[47] phthalocyanines,[48] and transition metal complexes.[49]

Förster resonance energy transfer

Förster resonance energy transfer (FRET) involves a through space dipole-dipole interaction with overlap of dipolar electric fields of the excited state of the donor and the ground state of the acceptor (Figure 10, b). This interaction does not require overlap of the orbitals or a van der Waals contact between the donor and acceptor as in Dexter energy transfer, because it operates through electric fields created as the excited state donor relaxes and the ground state acceptor is excited.

The rate of FRET (k_{ET}) is inversely proportional to the distance and extent of spectral overlap (r) of the donor emission and acceptor absorption. Equation 1.7 describes the energy transfer rate in terms of the Förster distance (R_0) and the lifetime of the donor (τ_D) in the absence of the acceptor.

$$k_{ET} = (1/\tau_D)\ (R_0/r)^6 \tag{1.7}$$

The Förster distance (R_0) is the distance at which the energy transfer efficiency is 50%. R_0 is determined by the overlap integral (J) between the emission spectrum of the donor and the absorption spectrum of the acceptor. R_0 is expressed in Equation 1.8:[50]

$$R_0^6 = 9\, Q_0\, (ln\ 10)\, k^2 J\, /(128\, \pi^5 n^4 N_A) \tag{1.8}$$

where Q_0 is the fluorescence quantum yield of the donor, k is the orientation between the dipoles of the donor and acceptor, n is the refractive index of the solvent or environment, and N_A is Avogadro's number.

FRET does not require overlap of the orbitals of the donor and acceptor, so energy transfer occurs over much longer distances than with Dexter energy transfer. The Förster radius in FRET can reach to ca. 80 Å, which allows FRET to be applied in probing biological structures,[51] and studying interactions at interfaces.[52] Biological structures can be labeled with two different fluorescent groups, which are referred as the donor and acceptor, respectively, and the emission spectrum of the donor overlaps with the absorption spectrum of the acceptor (Figure 13). The closer the donor and acceptor are, the more efficient the FRET is, thus the fluorescence intensity of the acceptor increases, meanwhile, the donor's fluorescence intensity decreases. The ratio of the two emission bands can be used to determine the distance between the donor and acceptor.
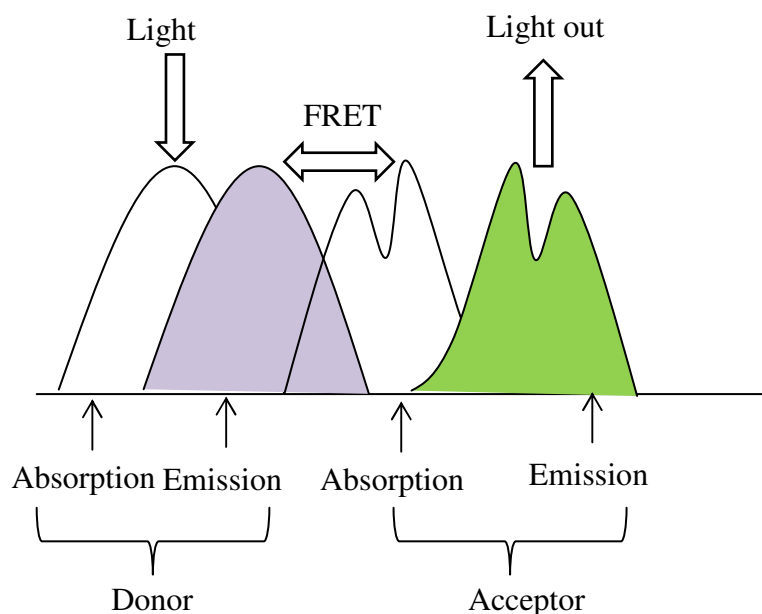
Figure 13. Overlap of the absorption and the emission spectra of the donor and acceptor used for probing, e.g. biology structures.

For example Chu et al. used dye labeled individual tethrahymena thermophila ribozyme molecules to study the processes of catalysis by RNA and folding with

fluorescence microscopy.[53] A donor Cy3 dye was attached to the region that moves during the docking, and an acceptor Cy5 dye was bound near the immobilization site, which is shown in Figure 14. The emission from the acceptor was monitored when the donor was excited. The real-time observation of a single molecule was observed by emission intensity versus time. FRET studies indicated that the distance between the donor and acceptor changed from 10-20 Å to 70 Å upon docking.
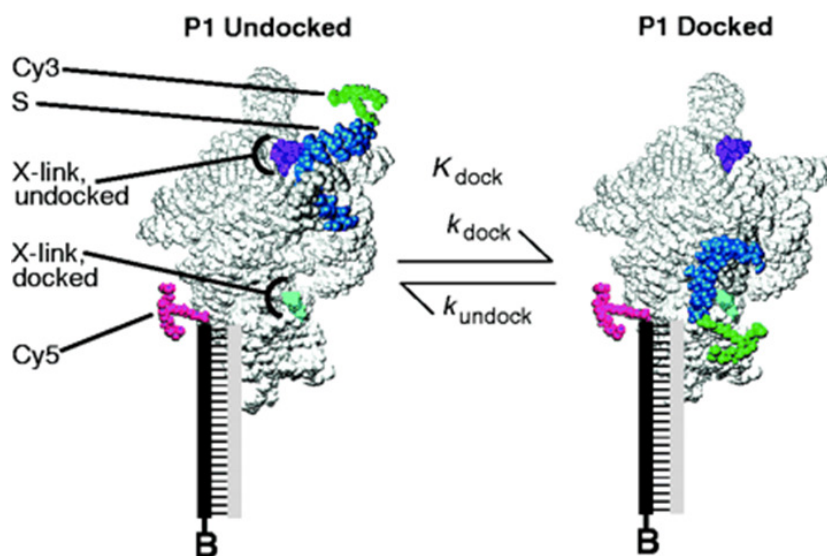
Figure 14. FRET between Cy3 (green) and Cy5 (red) in tethrahymena thermophila ribozyme molecule gives a signal for docking.[53] Reproduced from ref. 53 with permission. Copyright American Association for the Advancement of Science (2000).
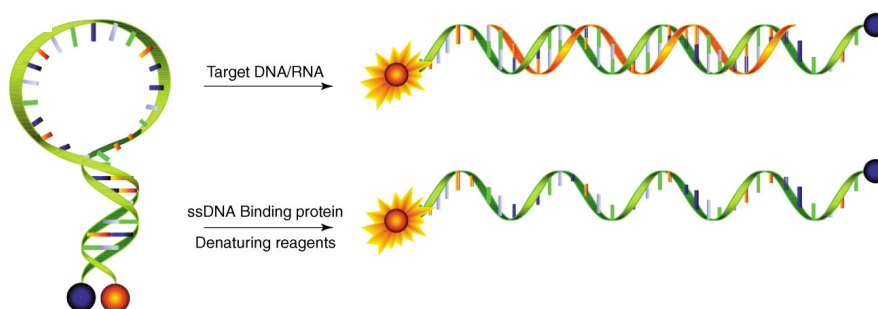
Figure 15. The principle of molecular beacon.[54] Reproduced from ref. 57 with permission. Copyright American Association for the Advancement of Science (2004).

Another application of FRET is molecular beacons, which act like switches that are normally closed and do not emit. Binding induces conformational changes that open the hairpin and, as a result, the fluorescence is turned on (Figure 15). Molecular beacons have been used widely as probes in chemistry, biology, biotechnology and medical sciences for biomolecular recognition.[55, 56, 57]

1.5 Thesis overview

This thesis describes the techniques and methods used to characterize molecular organic photochemical processes and explored several photochemical systems including smart molecules (molecular switches and molecular motors) and materials, in which the functions and properties are controlled or modified through energy transfer, electron transfer, or photochemical reactions.

Chapter 2 describes several home-built instruments capable of transient luminescence, transient absorption and near-infrared emission spectroscopies. These home-built systems were used to study the photochemical processes in the following chapters.

In chapter 3 a photoswitchable magnetic system is described. Two organic radical centers are attached to an overcrowded alkene photochromic unit, and the through space magnetic interaction was switched on and off by photoisomerization. The function of this system was characterized by UV/vis absorption, ^{1}H-NMR, and EPR spectroscopies.

In chapter 4 porphyrins were used to modify the properties of graphene, and sensitize the rotation of molecular motors. Energy and/or electron transfer from porphyrins was studied by transient absorption spectroscopies. UV/vis absorption and CD spectroscopies were used to determine the properties of the graphene-based hybrid materials and the functionality of visible light driven molecular motors.

In chapter 5 singlet oxygen generation was switched on and off using diarylethene switches. The on and off states of ^{1}O$_2$ generation were accessed by alternate irradiation with UV and visible light, and the systems were characterized by UV/vis absorption and emission spectroscopies. The energy

transfer from the photosensitizer to diarylethene switches was studies by transient absorption spectroscopy.

In chapter 6 a series of variously substituted molecular motors were characterized by transient absorption and UV/vis absorption spectroscopy. The rotation speeds and energy barriers to helix inversion of these molecular motors were determined.

1.6 References

[1] N. J. Turro, V. Ramamurthy, J. C. Scaiano, *Principles of Molecular Photochemistry*, University Science Book, Sausalito, California, **2008**.

[2] J. F. Talling, *Annu. Rev. Plant. Physiol.,* **1961**, *12*, 133-154.

[3] Y. C. Cheng, G. R. Fleming, *Annu. Rev. Phys. Chem.,* **2009**, *60*. 241-262.

[4] R. R. Birge, L. M. Hubbard, *J. Am. Chem. Soc.*, **1980**, *102,* 2195–2205.

[5] H. Kandori, Y. Schichida, T. Yoshizawa, *Biochemistry (Moscow),* **2001**, *66,* 1197-1209.

[6] T. J. Dougherty, C. J. Gomer, B. W. Henderson, G. Jori, D. Kessel, M. Korbelik, J. Moan, Q. Peng, *J. Natl. Cancer Inst*. **1998**, *90*, 889-905.

[7] D. E. Dolmans, D. Fukumura, R. K. Jain, *Nat. Rev. Cancer,* **2003**, *3,* 380-387.

[8] H. Ma, R. H. Davis, C. N. Bowman, *Macromolecules*, **2000**, *33*, 331–335.

[9] T. F. Scott, A. D. Schneider, W. D. Cook, C. N. Bowman, *Science*, **2005**, *308,* 1615-1617.

[10] L. Eldada, *IEEE J. Sel. Top. Quantum Electron*, **2000**, *6*, 54-68.

[11] M. Saquib, M. Muneer, *Dyes and Pigments*, **2002**, *53*, 237-249.

[12] M. Grätzel, *J. Photochem. Photobiol.,C,* **2003**, *4*, 145-153.

[13] F. C. Krebs, *Sol. Energy Mater. Sol. Cells*, **2009**, *93*, 394-412.

[14] M. D. Levenson, *Phys. Today,* **1993**, *46*, 28.

[15] A. Jablonski, Z. Phys. **1935**, *94*, 38-4.

[16] M. Kasha, *Discuss. Faraday Soc.,* **1950**, *9,* 14-19.

[17] J. Franck, E. G. Dymond, *Trans. Faraday Soc.*, **1926**, *21*, 536-542.

[18] E. U. Condon, *Phys. Rev.,* **1926**, *28*, 1182-1201.

[19] A. Beer, *Annalen der Physik und Chemie*, **1852**, *86*, 78-88.

[20] G. G. Stocks, *Phil. Trans. R. Soc. (London),* **1852**, *142*, 463-562.

[21] E. U. Condon and G. H. Shortley, *The Theory of Atomic Spectra*, Cambridge University Press, **1935.**

[22] A. Harriman, *J. Chem. Soc., Faraday Trans. 2.* **1981**, *77*, 1281-1291.

[23] R. C. Evans, P. Douglas, C. J. Winscom, *Coord. Chem. Rev.*, **2006**, *250*, 2093-2126.

[24] E. V. Anslyn, D. A. Dougherty. *Modern Physical Organic Chemistry.* University Science Books, Sausalito, California, **2006**.

[25] B. L. Feringa, W. R. Browne, *Molecular Switches,* Vol 1-2, Wiley-VCH, Weinheim, Germany, **2011**.

[26] H. Meier, *Angew. Chem., Int. Ed.* **1992**, *31*, 1399-1420.

[27] A. Momotake, T. Arai, *J. Photochem. Photobiol.,C,* **2004**, *5*, 1-25.

[28] J. F. Rabek, *Photochemistry and Photophysics*, CRC Press. Boca Raton, USA, **1991**.

[29] H. Tian, S. Yang, *Chem. Soc. Rev.* **2004**, *33*, 85-97.

[30] N. Koumura, R. W. J. Zijlstra, R. A. van Delden, N. Harada, B. L. Feringa, *Nature,* **1999**, *401*, 152-155.

[31] J. R. Lakowicz, *Principles of Fluorescence Spectroscopy,* Springer, Singapore, **2006**.

[32] E. M. Aro, I. Virgin, B. Andersson, *Biochim. Biophys. Acta, Bioenerg.* **1993**, *1143*, 113-134.

[33] M. J. Schilstra, F. Rappaport, J. H. A. Nugent, C. J. Barnett, D. R. Klug, *Biochemistry*, **1998**, *37*, 3974–3981.

[34] B. Loll, J. Kern, W. Seanger, A. Zouni, J. Biesiadka, *Nature*, **2005**, *438*, 1040-1044.

[35] G. Yu, J. Gao, J. C. Hummelen, F. Wudl, A. J. Heeger. *Science,* **1995**, *270*, 1789-1791.

[36] S. Günes, H. Neugebauer, N. S. Sariciftci, *Chem. Rev.* **2007**, *107*, 1324-1338.

[37] M. Grätzel, *Nature*, **2001**, *414*, 338-344.

[38] J. B. Birks, *Photophysics of Aromatic Molecules,* Wiley-Interscience, London, **1970**.

[39] D. L. Dexter, *J. Chem. Phys.* **1953**, *21*, 836-850.

[40] T. Förster, *Fluorenzenz Organische Verbindungen*. Vandenhoech and Ruprcht, Gottingen, Germany, **1951.**

[41] D. G. Whitten, P. D. Wildes, C. A. DeRosier, *J. Am. Chem. Soc.* **1972**, *94*, 7811-7823.

[42] J. A. Mercer-Smith, D. G. Whitten, *J. Am. Chem. Soc.* **1978**, *100*, 2620-2625.

[43] A. Monguzzi, R. Tubino, F. Meinardi, *Phys. Rev. B,* **2008**, *77*, 155122.

[44] D. R. Kearns, *Chem. Rev.,* **1971**, *71*, 395-427.

[45] M. C. DeRosa, R. J. Crutchley, *Coord. Chem. Rev.*, **2002**, *233-234*, 351-371.

[46] R. W. Redmond, J. N. Gamlin, *Photochem. Photobiol.,* **1999**, *70*, 391-475.

[47] A. E. O'Connor, W. M. Gallagher A. T. Byrne, *Photochem. Photobiol.,* **2009**, *85*, 1053–1074.

[48] D. Wöhrle, A. Hirth, T. Bogdahn-Rai, G. Schnurpfeil, M. Shopova, *Russ. Chem. Bull.,* **1998**, *47*, 807-816.

[49] D. Garcìa-Fresnadillo, Y. Georgiadou, G. Orellana, A. M. Braun, E. Oliveros, *Helv. Chim. Acta.,* **1996**, *79*, 1222-1238.

[50] T. Förster, *Delocalized Excitation and Excitation Transfer*, Florida State University, **1965**.

[51] R. B. Sekar, A. Periasamy, *J. Cell. Biol.,* **2003**, *160*, 629-633.

[52] J. R. Silvius, I. R. Nabi, *Mol. Membr. Biol.,* **2006**, *23*, 5-16.

[53] X. Zhuang, L. E. Bartley, H. P. Babcock, R. Russell, T. Ha, D. Herschlag, S. Chu, *Science*, **2000**, *288*, 2048-2051.

[54] W. Tan, K. Wang, T. J. Drake, *Curr. Opin. Chem. Biol.*, **2004**, *8*, 547-553.

[55] S. Tyagi, F. R. Kramer, *Nat. Biotechnol.,* **1996**, *14*, 303-308.

[56] O. Noya, M. E. Patarroyo, F. Guzman, B. A. de Noya, *Curr. Protein. Pept. Sci.*, **2003**, *4*, 299-308.

[57] X. Fang, J. J. Li, J. Perlette, W. Tan, K. Wang, *Anal. Chem.,* **2000**, *72*, 747 A–753 A.

CHAPTER 2

Instrumentation

In this chapter, the design and construction of three home-built instrument systems are described. The first system was built in order to detect medium to long lived luminescence, with better efficiency than that can be achieved with the single photon counting technique and can extend to time scales of seconds. Based on this time-resolved luminescence system, a laser flash photolysis system was constructed to achieve time-resolved absorption from the micro to millisecond time scale, which can be used to study slow relaxation and chemical reactions. The system was extended to allow for infrared luminescence measurement. With phase locked signal amplification, the sensitivity of infrared system substantially improved.

2.1 Introduction

Since the first ruby laser was built in 1960, [1] laser technology has developed rapidly and widely applied in spectroscopy, because of its excellent properties, e.g., high intensity, monochromaticity, polarization, etc. Thanks to the development of ultra-fast lasers, dynamic physical and chemical processes can be probed on picosecond (ps) and even femtosecond (fs) time scales. In 2001, an attosecond (as) pulsed laser was developed, [2,3] which opened up an unexplored timescale for the study of dynamics of molecules. [4,5] However, these advances have overshadowed longer time scale time-resolved spectroscopy. The time scale of photoreactions covers a wide range, from attosecond to second and the range is almost 20 orders of magnitude. In Table 1, some typical time scales of interesting photochemical events are listed. [6] If the measurement focuses on rotational and translational motion, fast chemical reactions, or longer luminescence lifetimes, which occur over tens of nanosecond (ns) to millisecond (ms) or even to the seconds scale, applying ultra-fast technology to measure these events is cumbersome or even totally unsuitable.

For dynamic processes from nanosecond to millisecond time scales, the most common technology is flash photolysis, which was invented in 1949 by Manfred Eigen, Ronald G. W. Norrish and George Porter, [7, 8,9] who won the 1967 Nobel Prize in Chemistry for their contributions in this field. In flash photolysis, the sample is firstly excited by an intense light pulse, which populates electronic states other than the ground state and lead to ultrafast chemical reactions. A synchronized probe light source monitors the changes in absorption, since molecules in an excited state have different absorption spectra compared with the ground state, to follow relaxation or chemical processes in real time. Nowadays, the gas-filled flash discharge tubes used as pump sources have been replaced by a nanosecond pulse laser, such as Q-switch Nd:YAG laser, Nd:YLF laser, or argon lasers. These lasers can generate much more intense light with nanosecond pulse width. An intense xenon lamp or a laser can be used as probe source.

Table 1. Time scales of typical photochemical events.

Time scale(s)	Rate (s^{-1})	Dynamic events	
10^{-18}=1 as ↓	10^{18} ↓	Motion in nucleus	
10^{-15}=1 fs ↓	10^{15} ↓	Electronic motion Electron orbital jumps Electron transfer Proton transfer	
10^{-12}=1 ps ↓	10^{12} ↓	Vibrational motion Bond cleavage Rotational and translational motion (small molecules) Spin-orbit coupling	Fluorescence
10^{-9}=1 ns ↓	10^{9} ↓	Rotational and translational motion (large molecules) Hyperfine coupling	Fluorescence
10^{-6}=1 μs ↓	10^{6} ↓	Ultrafast chemical reactions Rotational and translational motion (large molecules)	Phosphorescence
10^{-3}=1 ms ↓	10^{3} ↓	Ultrafast chemical reactions Rotational and translational motion (large molecules)	Phosphorescence
10^{0}=1 s ↓	10^{0} ↓	Fast chemical reactions	

Some molecules in nature or synthetized by chemists show relatively strong luminescence. Measuring emission light has been widely applied in chemistry, biology and nanotechnology, [10] including visualizing the interactions between molecules in different environments, locating target biomolecules or cells, determining the distance between sites in large molecules, etc. Steady-state luminescence measurements are straightforward, while time-resolved studies require much more complex instrumentation, but can provide more information. For instance, luminescence lifetime reports whether the quenching of the emission is due to a static or a dynamic process. Time-correlated single-photon counting (TCSPC) is the most popular method for time-domain fluorescence measurements. [11, 12] However, if the luminescence lifetime is longer than 1 μs,

which is mostly the case with phosphorescence, TCSPC systems have difficulty to reach this range or take an extremely long time to obtain a good quality signal. This is because a delay of 10 lifetimes is needed between each event (1 μs lifetime, hence a maximum of 10,000 counts per seconds). A more economic approach is to use a laser flash photolysis setup without the probe beam. The sample is initially excited by a pulsed light source, a nanosecond pulse laser for instance, and detected by a synchronized photodetector together with a date acquisition card, which has sufficient time resolution. This method can measure lifetimes from the nanosecond to the second time scales.
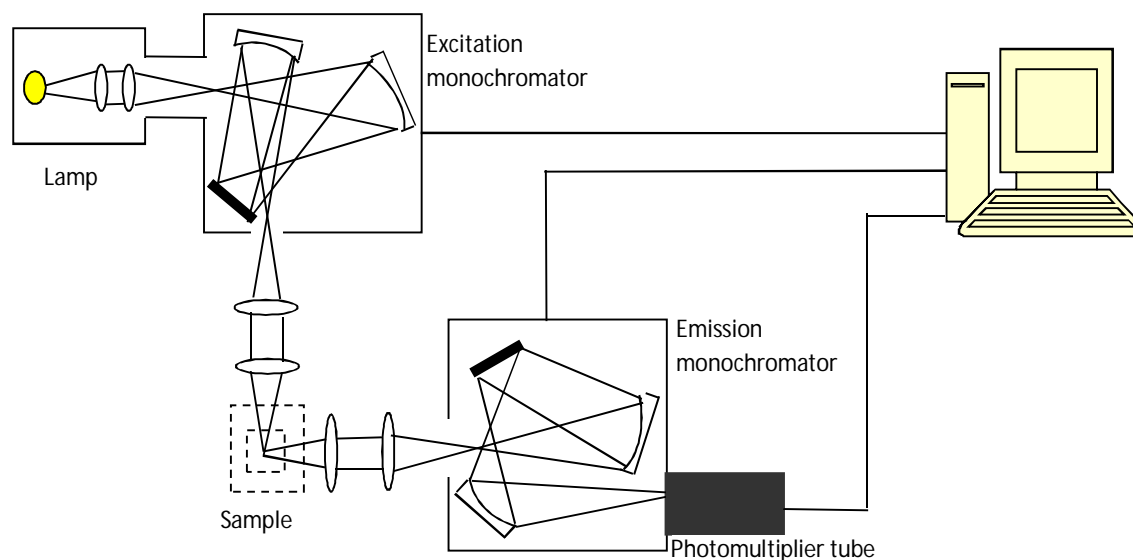
2.2 Time-resolved luminescence spectrometer

The typical design of standard spectrofluorometers used to record steady-state excitation and emission spectra is shown in Scheme 1. The excitation light passes through a monochromator or filter to select a fixed wavelength to irradiate the sample, and the liquid sample is commonly prepared in a glass or silica cuvette and placed into a cuvette holder in the spectrofluorometer. The emission is collected at 90° to the excitation beam by a photo sensitive detector, coupled to a second monochromator or filter. The angle is used to minimize incident or reflected light reaching the detector.

The light source in a spectrofluorometer should be strong enough to excite the maximum number of the molecules any one point in time. The most common light sources are mercury vapor lamps and/or xenon arc lamps. The mercury lamp provides excitation at essentially all wavelengths primarily from 200-600 nm. Xenon arc lamps have a nearly continuous emission spectrum in the range from 300-800 nm, and this source allows for recording of both emission and excitation spectra. In addition, laser, LED and other light sources can be used as well. A laser has a narrow wavelength range, which means that it is not necessary to equip the source with excitation monochromator or filter.

Monochromators or filters are used to transmit a mechanically selectable narrow band of wavelengths of excitation source and emission of the samples. The collimated light from the entrance slit of the monochromator is reflected on to the first mirror and to a grating, in which different wavelengths exit at a different angle, and the second mirror refocuses the light on to the exit slit. However, no monochromator is perfect and stray light, i.e. light that follows a random path, must be suppressed. The 90° arrangement can reduce stray light, but the light

scattered from the sample can still be detected. To avoid this, spectroscopists usually set the start emission wavelength 20 nm longer than the excitation wavelength and/or put a filter in front of the emission monochromator, which can cut of the excitation light.

There are several possible photosensitive detectors that can be utilized in spectrofluorometers. Photomultiplier tubes (PMTs), photodiodes and charge-coupled devices (CCD). PMTs are the most common detector used in spectrofluorometers. [13] They can convert the incident light to current, and the current can be amplified as much as 100 million times in the photocathode and multiple dynode stages. A stable high voltage supply is needed to operate PMTs. A photodiode has the capability to convert light either to current or voltage, and it is much less costly but is also less sensitive than a PMT. CCDs show growing application in fluorescence spectroscopy. [14] The pixels in a CCD enable conversion of the photons into charge and the charge at each pixel can be read out when desired. This enables a luminescence spectrum to be obtained in two- or three-dimensions. [15] Most CCDs are more expensive than PMTs and an additional cooling unit is required to achieve a sufficient signal to noise ratio (SNR).

Scheme 1. Arrangement of a typical spectrofluorometer.

Based on the basic scheme for a spectrofluorometer, a time-resolved luminescence system was built (Scheme 2). This system is focused on detecting emissions with longer lifetimes, including fluorescence lifetimes longer than 100

ns and phosphorescence lifetimes. A Nd:YAG pulsed laser [16] is used as an excitation light source, which can generate 6 ns pulses at up to 10 Hz and the excitation wavelengths at 266 nm, 355 nm, 532 nm, 1064 nm, and more wavelengths available through the use of a Raman shifter. [17] A xenon arc lamp with a pulse generator is also available to work as the excitation light source, which can be used to detect microsecond and/or steady state luminescence spectra. The emission is detected as in a standard spectrofluorometer. The difference is that the light falling on the PMT is recorded at a fixed wavelength as a series of decays trigged when the laser pulse irradiated the sample. In order to achieve this goal, a second photodiode detector is used and the signals of two detectors are sent into separate channels of an oscilloscope. The first channel records the time-resolved luminescence signal, and the second channel acts as a trigger source. When the pulsed light irradiates the sample, a small fraction (less than 1%) is reflected onto the photodiode and this triggers the oscilloscope to start capturing the data and record the emission signal. The oscilloscope not only records the signal, but also can do some preliminary data processing, e. g. averaging to improve the signal to noise ratio. The devices control and data transfer and analysis are accomplished by the home-built software with a computer, which is described in detail in the software section below. The main specifications of each component are summarized in Table 2.
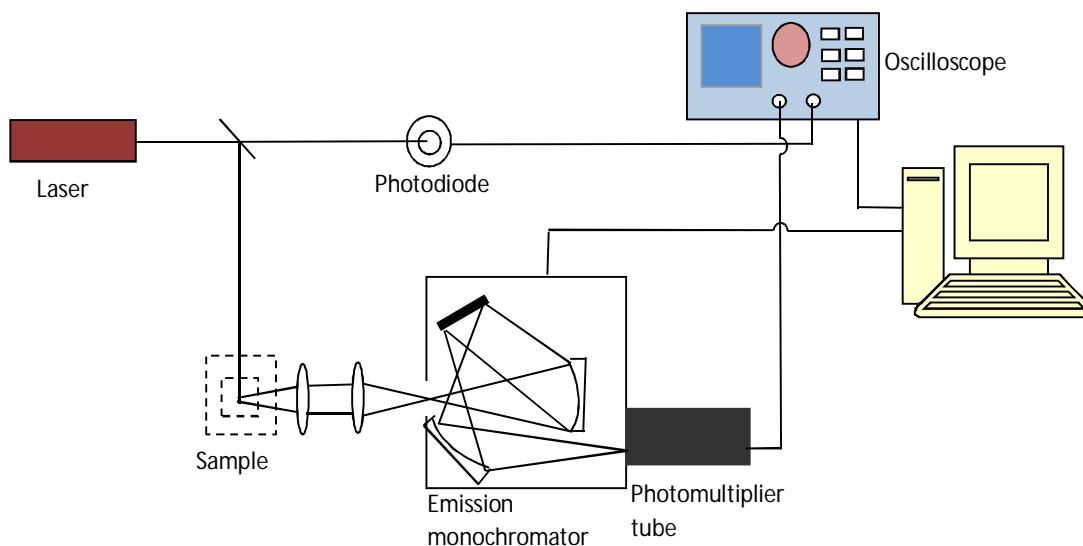
Scheme 2. Layout of transient luminescence system.

Table 2. Specifications of home-built transient luminescence system.

Light sources	Xenon Arc lamp with the pulser (Applied Photophysics Co., Ltd. SX20) [18]	Power:150 W Wavelength range: 250 nm-800 nm Pulsed beam: 400 μs plateau region
Light sources	Flash lamp pumped Nd:YAG laser (INNOLAS. SpitLight 400)[19]	Repetition Rate: from 1 to 10 Hz Pulse Energy at 1064 nm: > 400 mJ Pulse Energy at 532 nm: > 240 mJ Pulse Energy at 355 nm: > 100 mJ Beam Diameter: 6 mm Pulse width: < 8 ns Temporal Jitter: < ± 1 ns
Monochromators	Excitation monochromator (Zolix Instruments. Omni-λ150)[20]	Scanning range: 0-900 nm Resolution: 0.4 nm Wavelength accuracy: ±0.25nm Focal length: 150 mm Relative aperture: f/4.2 Slit width: 0.01-3 mm Blazing: 500 nm
Monochromators	Emission monochromator (Zolix Instruments. Omni-λ300)[22]	Scanning range: 0-1200 nm Resolution: 0.1 nm Wavelength accuracy: ±0.2nm Focal length: 300 mm Relative aperture: f/3.9 Slit width: 0.01-3 mm Blazing: 500 nm
Detector	PMT (Zolix Instruments, PMTH-S1-CR131)[21]	Wavelength range: 185-900 nm Dynode gain: 1×10^7 Anode dark current:3×10^{-9} A Single electron jitter: 22 ns
Detector	Photodiode (Thorlabs SM05PD/A)[22]	Cathode grounded photodiode Wavelength range: 200-1100 nm Material: Si
Oscilloscope	Tektronix DPO 4032 Digital Phosphor Oscilloscope[23]	Channel Model: 2 Maximum Sample Rate : 2.5 GS/s Maximum Record Length: 10 M points Timebase Range (s/div): 1 ns to 400 s Calculated Rise Time: 1 ns

Compared to the TCSPC, this method can extend the time scale to seconds and less time is required to record decay traces. The typical transit time range of PMTs is from 20-50 ns, and this means the system has the ability to detect luminescence lifetime longer than 100 ns. The use of a PMT instead of an iCCD detector for the time-resolved measurements not only reduces costs but also ensures that the sample is irradiated with fewer pulses, which can protect the sample from photodecomposition.

This system can work as a normal spectrofluorometer by replacing the Nd:YAG pulsed laser with a xenon arc lamp together with an excitation monochromator. By controlling the scan of the emission monochromator, the oscilloscope can record the emission spectrum of the sample. Figure 1 shows a comparison of the emission spectrum obtained with the home-built system and a commercial spectrofluorometer (JASCO FP6200). The sample tested was palladium tetraphenylporphyrin (PdTPP) dissolved in aerated 1,2-dichloroethane with excitation at 532 nm, which should give a fluorescence maximum at 610 nm and phosphorescence maximum at 710 nm, however because of oxygen, the phosphorescence is totally quenched and the latter signal does not appear in the spectrum. [24] The correspondence of the two spectra demonstrates the performances of the home-built system as a spectrofluorometer.

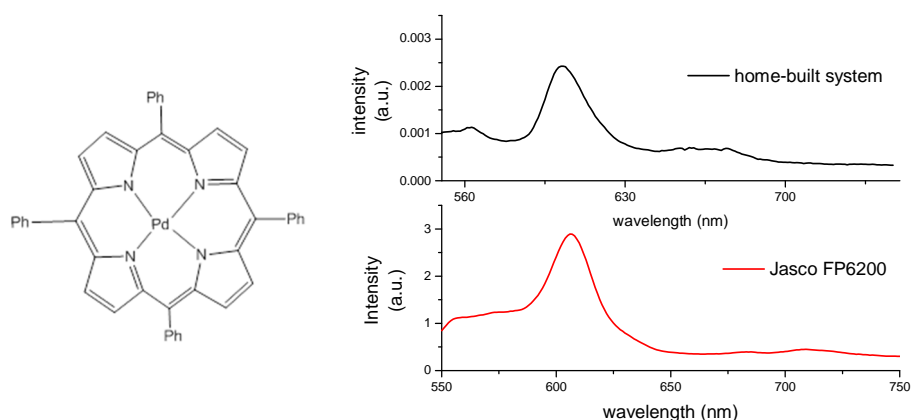**Figure 1**. Comparison between spectra recorded on a home-built system and commercial spectrofluorometers.

Time-resolved luminescence was studied by measuring the lifetime of $[Ru(bpy)_3]^{2+}$ in deaerated acetonitrile solution. Degassing was achieved by at least three cycles of freeze-pump-thaw. The sample was excited at 532 nm, and the lifetime is record at 607 nm, where the maximum emission occurs. Fitting

with a first order exponential decay gave a lifetime of 1.1 ±0.2 µs which corresponds to the literature value. [25] This system is further used to detect phosphorescence lifetimes as described in Chapter 4.
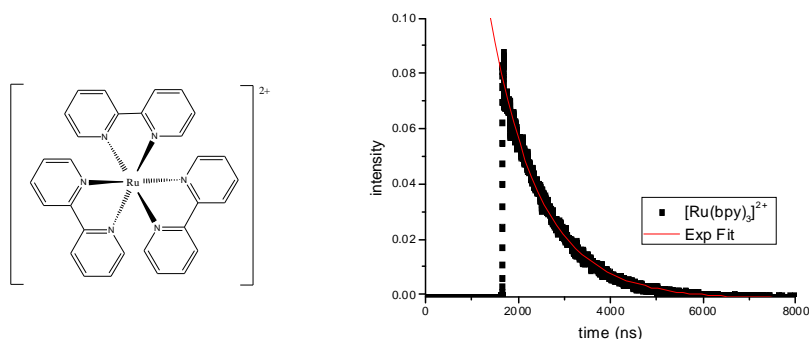

Figure 2. Luminescence decay of $[Ru(bpy)_3]^{2+}$ at 607 nm measured on a home-built transient luminescence system.

2.3 Laser flash photolysis

Laser flash photolysis technique has seen wide application in the study of transient species, such as radicals or ions[26], fast photochemical reaction, [27, 28] changes in conformation, [29] and slow electron or energy transfer in chemical and biological systems. [30, 31] The concept of laser flash photolysis is using a pulsed light source, a flash lamp or laser with a flash duration at least 10 times shorter than the process of interest, to drive the molecules into excited states and/or start a reaction. The excitation causes a change in absorbance, by following which the kinetics of processes can be determined.

The time-resolved luminescence setup can be modified to accomplish the above purpose by placing a xenon arc lamp in front of the sample (Scheme 3). The pulse generator of the xenon arc lamp is used here to provide a more intense monitoring beam for samples that do not show strong enough transient signals due to the weak probe light source. The pulse generator is synchronized to the flash lamp inside the Nd:YAG laser, so once the pulsed laser emits, the lamp would produce a flash of white light at the same time. The delay between the laser pulse and flash light can be manually adjusted on the front panel of pulse generator. The intensity of UV light from the flash lamp can be increased 150 times than without the flash function and the visible region can be increased around 35 times. The overall pulse duration is 2 ms with a 400 µs plateau region.

Other components have the same function as in the time-resolved luminescence system.
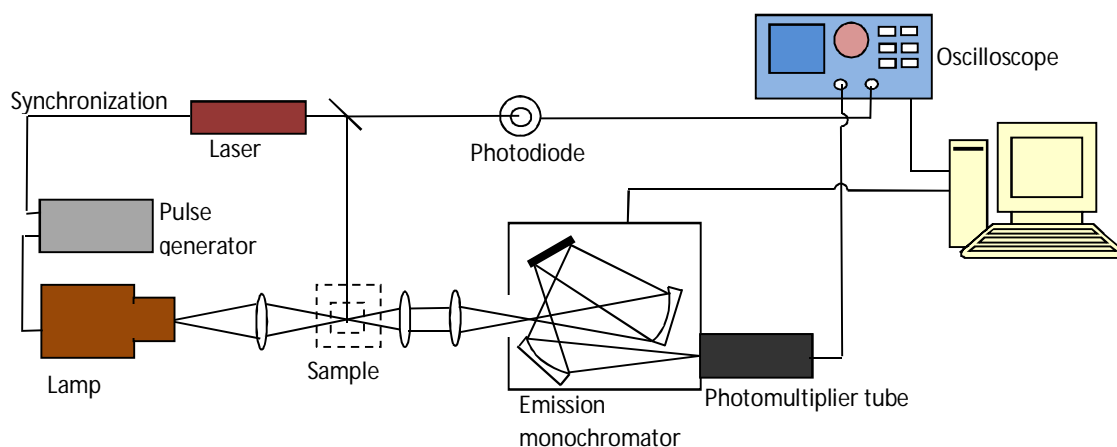
Scheme 3. Layout of the laser flash photolysis system.

The signal of transient absorption is much more difficult to monitor than transient luminescence. Since it focuses on the change in the optical density (ΔOD), the background is required, which is the light absorbed by the ground state of the samples. The ground-state absorption can be as much as four orders of magnitude more intense than ΔOD. To obtain a reliable signal, the pump source should be strong enough to generate as much change (ΔOD) as possible and the detector itself should be sensitive enough to distinguish the change in absorbance. [32,33] Some other parameters should be considered in advance as well, such as the concentration of the sample and the overlap area of the pump source and monitoring beam in the sample.

The change in the optical density (ΔOD) is defined by the Beer-Lambert law (2-1),

$$\Delta OD = \Delta \varepsilon c l = \varepsilon_{GS} c_{GS} l - \varepsilon_{ES} c_{ES} l \qquad (2\text{-}1)$$

Where $\Delta \varepsilon$ is the molar absorptivity change between the transient and ground state spectrum at the monitoring wavelength, l is the optical path along the monitoring beam, and c is concentration.

Most samples measured in laser flash photolysis are prepared in a standard 1×1 cm cuvette with a volume of ca. 3 ml. Using longer optical path cuvettes could not increase the signal, since the pump pulse only focuses on a certain portion of

the entire probe length, and large l means a decrease in the ratio between transient and ground state and it can overwhelm the signal. $\Delta\varepsilon$ is determined by the intrinsic characteristics of the sample and can be controlled only to a limited extent. Normally a monitoring wavelength near the absorption maximum is chosen.

The concentration of the transient species c is determined by several parameters, e.g., pump pulse power density, quantum yield, the absorbance of the sample at the pump wavelength, beam alignment, etc. An intense pump pulse and high quantum yield can result in a large value of c, however a high pump power might bleach the sample permanently, so it should be always checked whether the sample is bleached after the laser flash photolysis study.

If a 3 ml sample in 1×1 cm cuvette is considered, only a small volume is irradiated by the probe beam (2-2).

$$V_{probe} = \frac{\pi l d^2}{4} \qquad\qquad (2\text{-}2)$$

Where d is the diameter of the probe beam. Figure 3 shows the overlap of the probe beam with the pump beam, and the front view and side view is drawn as well. Here it is assumed that the diameter of the probe beam is larger than the pump beam. In the case of the diameter of the probe beam $d = 3\ mm$, only 2.4% of the total volume is probed. In this volume, the absorbance of the sample influences the absorption efficiency of the pump beam. The pump beam has to first transit the distance s (in the side view of Figure 3), in which the probe beam is absent, and afterwards overlap with the monitor light. The transmittance of the pump beam in the overlap area can be calculated by equation 2-3:

$$T_d = T_s - T_{s+d} = 10^{-sA} - 10^{-(s+d)A} \qquad\qquad (\,2\text{-}3)$$

Where T_s is the transmittance in the distance of s, T_{s+d} is the transmittance in the distance of $s + d$, and A is absorbance at the excitation wavelength. Figure 4 shows a plot of T_d *vs.* A for several values of d. Here it is assumed that the probe beam is at the center of the cuvette.
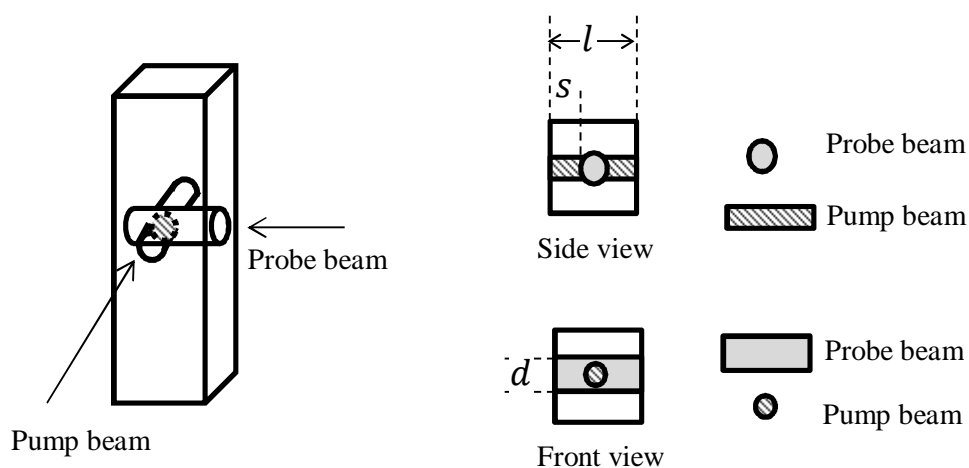
Figure 3. Overlap of pump and probe beam in a 1×1cm cuvette.
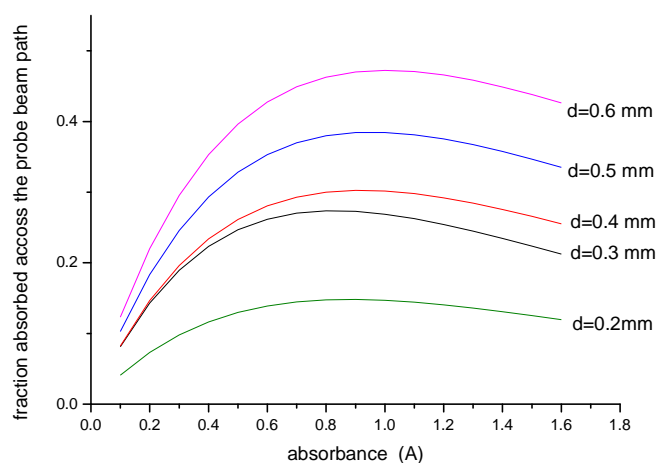
Figure 4. The efficiency of the pump pulse in the overlap region as a function of sample absorbance with different sizes of probe beam.

It can be seen in Figure 4 that the optimal absorbance is ca. 0.8 in a typical experimental system. However, signal quality also depends on the individual setup and the samples. In general, the absorbance is chosen between 0.5 and 1.0. Figure 4 indicates that the larger value of d provides better efficiency in regard to the pump beam. However, if the size of the beam is too large, a decrease in the ratio between transient and ground state molecules occurs because the irradiated area of the laser is much smaller, and the signal would be too weak to be detected. If a larger value of d together with an broaden pump beam is used, it seems that both the effective fraction and the ratio between transient and ground state molecules is improved, however, the transient concentration is lower because the same number of photons are distribute over a larger volume.

In addition to the factors disscussed above, the voltage across the PMT, the width of slits both at the entrance and exit of the monochromator are amongst factors that should be taken into consideration to obtain optimized transient signals.

To test the performance of the home-built laser flash photolysis system, the first measurement is to acquire a steady-state absorption spectrum as a basic function. The pulsed laser and pulse generator of the lamp are not required for this measurement. Light from the xenon arc lamp passes through the sample and transmitted light is detected after the sample through a monochromator by a PMT. The sample examined was an aerated solution of $[Ru(bpy)_3]^{2+}$ in acetonitrile. The spectrum recorded was compared with the spectrum on a commercial UV/vis absorption spectrophotometer (Figure 5). The obtained overlap of the two spectra demonstrates that the system can be used as a UV/vis absorption spectrophotometer.
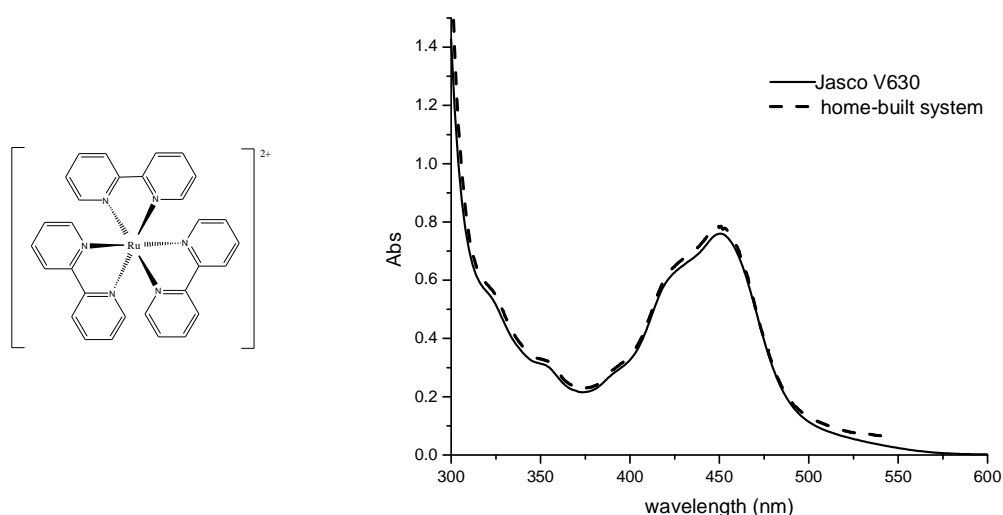
Figure 5. UV/vis absorption spectra recorded on a home-built system and a commercial spectrophotometer.

The second and key measurement is to test the capability of this system to do time-resolved absorption of the compounds of which the transient absorption lifetimes are known. One of overcrowded alkene-based molecular motors that undergo fast thermal relaxation (the structure is shown in Figure 6, left) was examined. The upper part of molecular motor undergoes unidirectional rotation relative to the lower part upon excitation with UV light and thermal relaxation, [34,35] and the absorption spectrum undergoes a red shift with the absorbance at 375 nm decreases and a concomitant increase in absorption at 450 nm. The thermal step has a lifetime of ca. 3 μs at 20 °C. [36] Due to the short lifetime, it cannot be

determined by using a steady state spectrophotometer. For laser flash photolysis, the sample was prepared in hexane purged with argon, and the absorbance was adjusted to 0.46 at 355 nm (the pump wavelength). The change in the absorbance was monitor at 475 nm, and the result is shown in Figure 6 (a). The fitting gives a thermal lifetime of 3.1 ± 0.3 μs at room temperature in agreement with the literature value.[36] The quality of transient absorption signals was further studied by measuring the samples with different concentration. Five samples with various absorbances at 355 nm from 0.33 to 1.16 were used, and the time-resolved absorption spectra are shown in Figure 6 (b). The sample with an absorbance of 0.80 shows largest change between ground state and excited state, and this is in accordance with expectations (Figure 4).
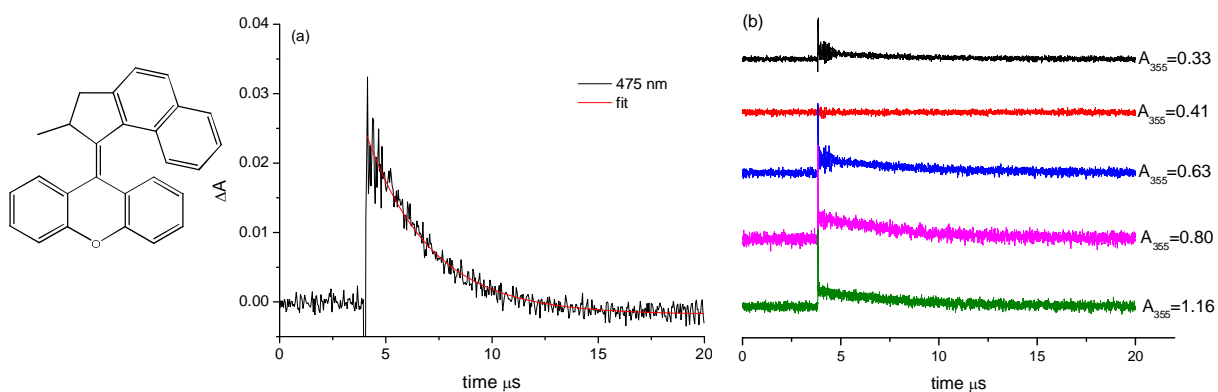

Figure 6. Transient absorption trace for molecular rotary motor (a) at 475 nm with 355 nm pump, recorded with the home-built laser flash photolysis system. (b) The transient absorption traces are measured with various absorbances at 355 nm.

The performance towards the measurement of transient absorption spectra was examined further using PdTPP in 1,2-dichloroethane in which oxygen was removed by purging with argon. The sample was excited at 532 nm by the Nd:YAG laser (10 Hz, 35 mW), and the absorbance at 532 nm was ca. 0.5. The change in absorbance was monitored at 475 nm, where the ground state has almost no absorbance (Figure 7 (a), black line). When the compound is excited, the absorbance at 475 nm increased immediately and decayed as it relaxes to the ground state (Figure 7 (b)). The relaxation time was fitted to a first order exponential decay, which gives a lifetime of 19 ± 0.5 μs, which is similar to the literature value. [23] The phosphorescence lifetime at 710 nm of the same sample was also measured (Figure 7 (c)). Fitting gave an emission decay of 20 ±0.5 μs.

The same value obtained from the transient absorption and phosphorescence is expected since both signals are due to molecules in the triplet excited state.
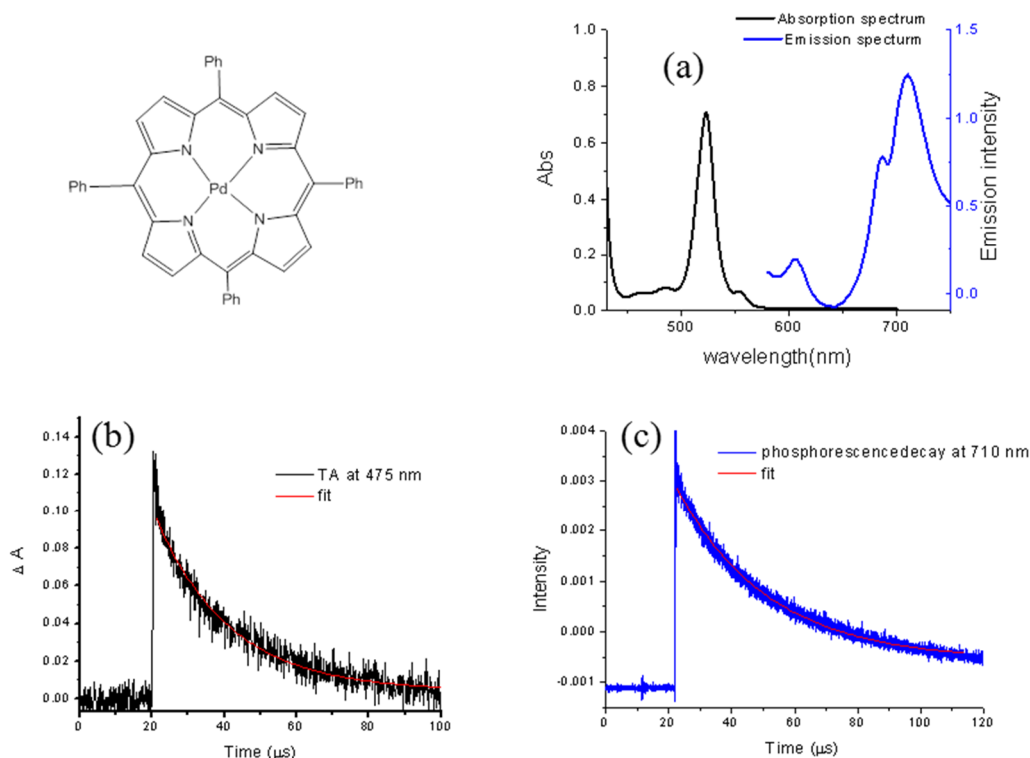

Figure 7. (a) UV/vis absorption and emission spectrum of PdTPP. (b) The transient absorbance at 475 nm and (c) the phosphorescence decay at 710 nm with 532 nm excitation.

2.4 Infrared luminescence spectrofluorometer

Studying the molecules in a living body or cell in *vivo* is challenging due to the absorbed visible light, and one approach is to label the target with an infrared luminophore, which can emit infrared light and hence allow for deeply tissue penetration. [37] The detectors in a standard spectrofluorometer only cover the visible and/or UV range,[38] and to extend to the infrared range, an extra detector is required. Various types of IR photo detectors are available for particular applications, e.g. Indium gallium arsenide (InGaAs), Lead sulfide (PbS), Indium antimonide (InSb).[39]

The system built to measure the steady-state and time-resolved luminescence, which is described in section 2.2, uses a PMT detector with the sensitivity typically from 185 nm to 850 nm that is unable to detect most of the infrared radiation (IR). To broaden the wavelength range to IR, an InGaAs pin detector

was added. The principle of an InGaAs detector is similar to that of the Si photodiode, which has p-n junctions. When light shines on the detector, electrons are excited to populate the conduction band between the p-n junctions and be converted to a voltage or current signal. The energy gap of InGaAs is smaller than that of Si photodiodes, which provides high sensitivity at longer wavelengths. The main specifications of the InGaAs detector used in the home-built system are listed in Table 3. Due the slow response time of this particular detector, this setup is mainly focus on testing steady-state or dynamic process slower than 10 ms.

Table 3. Performance of InGaAs detector. [40]

Parameters	*Specifications*
Detector name	Zolix DInGaAs 1600
Active diameter (mm)	1.5
Available range (nm)	900-1600
Responsivity (A/W)	0.8-0.85 (1300 nm)
	0.85-0.90 (1550 nm)
Dark Current (nA)	0.1-1
Shunt resistance (Ω)	1M
Junction capacitance (pF)	300
Response time (μs)	660

The InGaAs detector does not show an SNR as good as other photo detectors used in the UV and visible range. The output electronic signal is weaker, and in most cases, needs to be combined with a preamplifier and a lock-in amplifier. The weak electrical signal is first amplified by a preamplifier without significantly increasing the SNR, and the amplification amplitude can be tuned. To detect weak IR luminescence, a chopper (Model SR540 Optical Chopper, Stanford Research Systems INC.) and a lock-in amplifier (Model SR850 DSP Lock-in Amplifier, Stanford Research Systems INC.) are needed also. The excitation beam is chopped by the slots of the chopper, and the reference output from the chopper controller is used to lock the lock-in amplifier to a chopped frequency. The layout of home-built infrared luminescence spectrofluorometer is shown in Scheme 4.
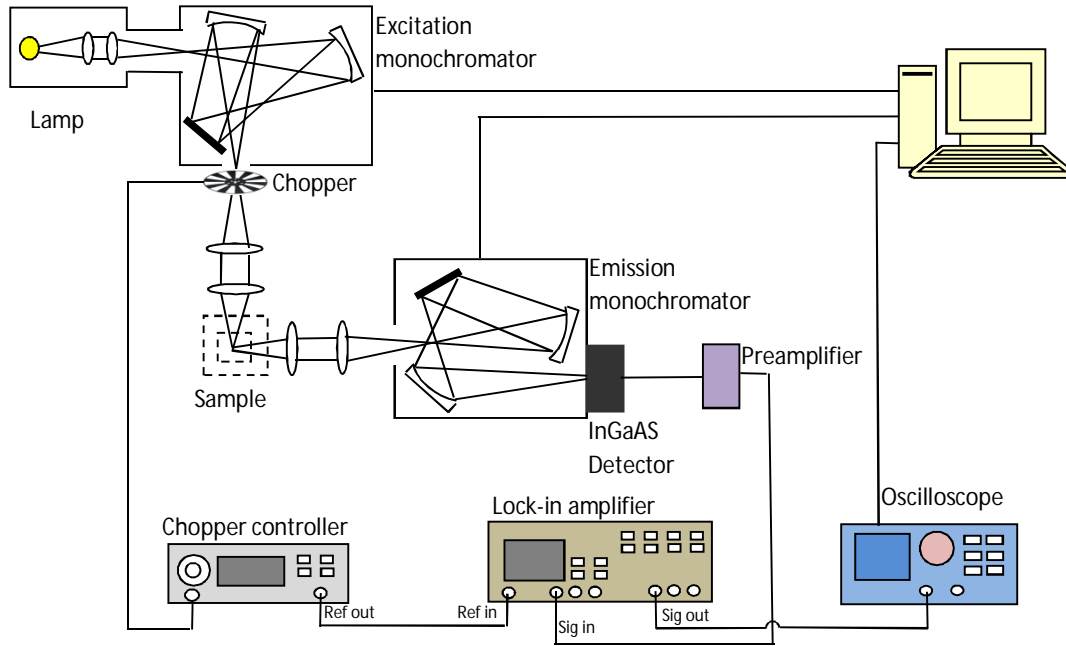
Scheme 4. Schematic diagram of home-built IR spectrofluorometer system.

A lock-in amplifier is widely used to extract an extremely weak signal as low as a few nanovolts in a noisy environment with a known carrier wave.[41] The basic functions of a lock-in amplifier are shown in Scheme 5. To get a stable amplified signal, there are two multipliers stabilizing the phase between signal and reference.

Assuming the tested signal is:

$$V_{sig} Sin(\omega_{sig}t + \theta_{sig}) \tag{2-4}$$

And the reference signal is:

$$V_{ref} Sin(\omega_{ref}t + \theta_{ref}) \tag{2-5}$$

The output after the first multiplier unit is:

$$
\begin{aligned}
V_1 &= V_{sig} sin(\omega_{sig}t + \theta_{sig}) \times V_{ref} sin(\omega_{ref}t + \theta_{ref}) \\
&= \frac{1}{2} V_{sig} V_{ref} \cos[(\omega_{sig-}\omega_{ref})t + \theta_{sig} - \theta_{ref}] \\
&\quad - \frac{1}{2} V_{sig} V_{ref} \cos[(\omega_{sig+}\omega_{ref})t + \theta_{sig} + \theta_{ref}]
\end{aligned} \tag{2-6}
$$

If the signal and the reference have the same frequency, the difference frequency component will be a DC signal, after passing through a low pass filter the sum frequency component is removed. The output after the filter is:

$$\frac{1}{2} V_{sig} V_{ref} \cos(\theta_{sig} - \theta_{ref}) \qquad (2\text{-}7)$$

The same operation can be applied at the second multipliers, and the only difference is that the phase of both the signal and the reference are offset by 90º. So the output after the second unit is

$$
\begin{aligned}
V_2 &= V_{sig} Sin(\omega_{sig} t + \theta_{sig}) \times V_{ref} Sin(\omega_{ref} t + \theta_{ref}) \qquad (2\text{-}8)\\
&= \frac{1}{2} V_{sig} V_{ref} \cos\left[(\omega_{sig} - \omega_{ref})t + \theta_{sig} - \theta_{ref} + \frac{\pi}{2}\right]\\
&\quad - \frac{1}{2} V_{sig} V_{ref} \cos\left[(\omega_{sig} + \omega_{ref})t + \theta_{sig} + \theta_{ref} + \frac{\pi}{2}\right]
\end{aligned}
$$

With the same frequency, the output after the low pass filter would be

$$\frac{1}{2} V_{sig} V_{ref} \cos(\theta_{sig} - \theta_{ref} + \frac{\pi}{2}) = \frac{1}{2} V_{sig} V_{ref} \sin(\theta_{sig} - \theta_{ref}) \qquad (2\text{-}9)$$

So both the outputs are DC signals carried by a sine and cosine function, respectively, and these signals are proportional to actual signal amplitude.
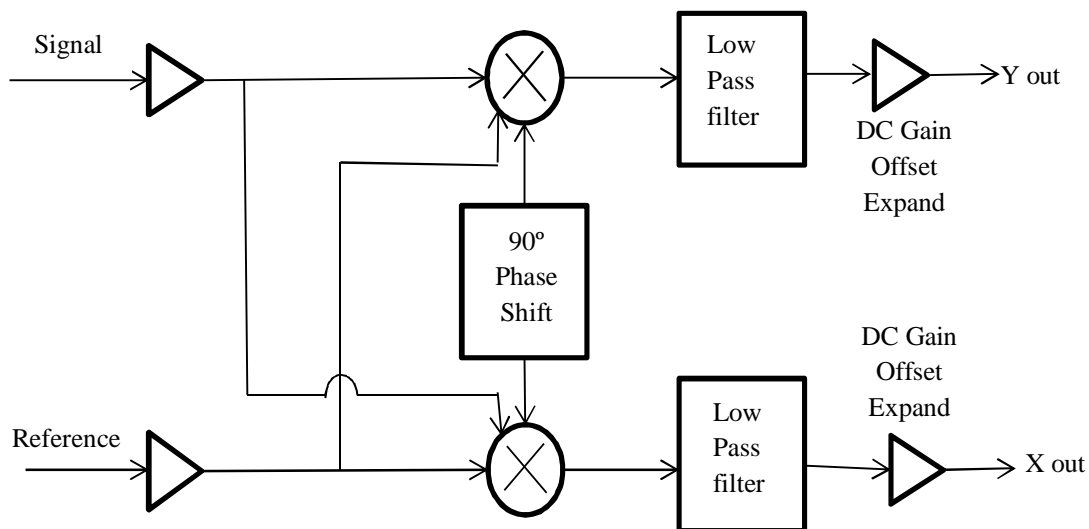
Scheme 5. The principle of lock-in amplifier.

The contrast between spectra recorded with and without a lock-in amplifier in the home-built system is shown by the luminescence spectrum of a 7 W energy saver bulb. This light source has several strong emission lines in the infrared region. [42] The test bulb was placed at the position of the sample holder. The monochromator was set to scan from 800 nm to 1600 nm and the spectrum was directly recorded on the screen of an oscilloscope (shown in Figure 8). The spectrum in Figure 8 (a) is the result of directly measuring the signal from the preamplifier, and some of the IR emission lines can be observed but with a poor SNR. By using a lock-in amplifier and a chopper to modulate the excitation beam, the quality of the spectrum of the bulb was improved significantly and the noise was suppressed (Figure 8, b).
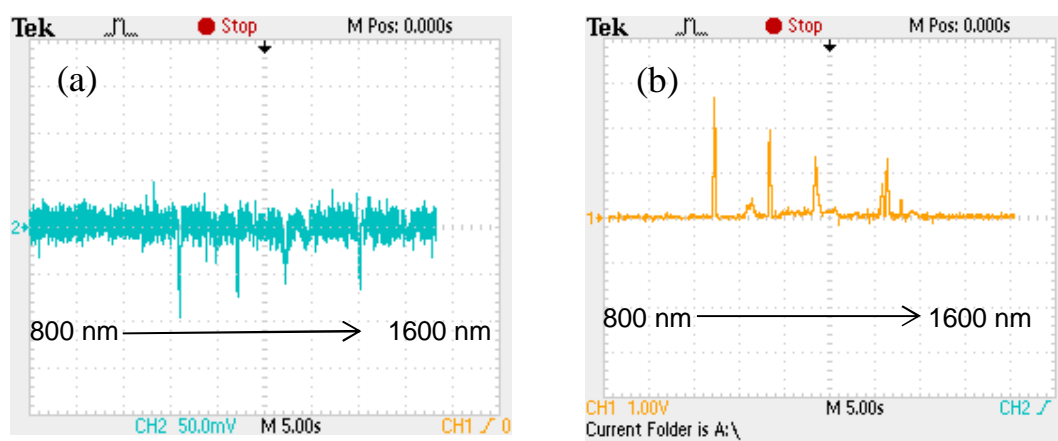
Figure 8. Near IR spectra of an energy save bulb measured without (a) and with (b) a lock-in amplifier.

The system was also used to test the emission of a NIR dye, 1,1',3,3,3',3'-hexamethylindotricarbocyanine iodide (HITCI), which shows a fluorescence peak centered at 780 nm, with ~60 nm FWHM, and a shoulder at long wavelength side with peak center at 855 nm. [43] Figure 9 (b) shows the spectrum measured by the home-built system, and this spectrum was calibrated by using NIR emission lines of energy saver bulb[42] and the spectrum response of the NIR detector. [44] The correspondence of the two spectra demonstrates the performances of the home-built system in detecting IR emission.

Figure 9. The NIR emission spectrum of the HITCI NIR dye from the literature[42] (a) and measured on a home-built NIR system (b).

2.5 Conclusion

In conclusion, three systems have been built to measure transient luminescence, transient absorption, and IR emission spectra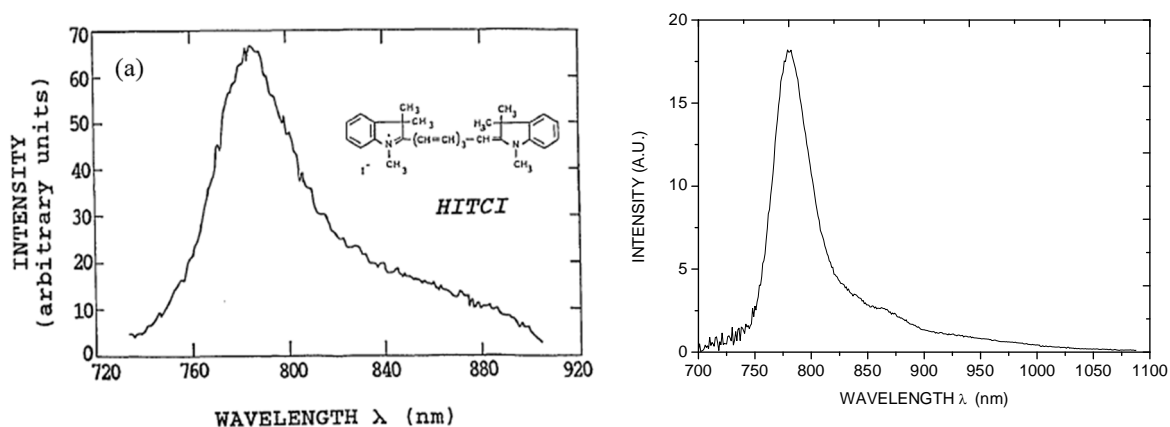. The basic functions of these systems working as normal steady state spectrophotometers are maintained, which is demonstrated by comparing the spectra obtained on home-built systems with those measured on the commercial spectrophotometers. The transient performances were characterized by measuring the solutions of PdTPP, $[Ru(bpy)_3]^{2+}$ and overcrowded molecular motors, and the lifetimes of the transient processes obtained on home-built systems are the same as the reported values, which demonstrates the accuracy of transient detections. Using a preamplifier and lock-in amplifier, the SNR of home-built infrared luminescence spectrofluorometer has been substantially improved. A series of programs to control these home-built spectroscopic systems were developed in the LabVIEW programming environment, which is described in appendix. The software also enables recording and preliminary analysis of spectra and transients.

2.6 References

[1] T. H. Maiman, *Nature*, **1960**, *187*, 493-494.

[2] M. Hentschel, R. Kienberger, Ch. Spielmann, G. A. Reider, N. Milosevic, T. Brabec, P. Corkum, U. Heinzmann, M. Drescher, F. Krausz, *Nature*, **2001**, *414*, 509-513.

[3] P. B. Corkum, F. Krausz, *Nature Physics*, **2007**, *3*, 381–387.

[4] S. Baker, J. S. Robinson, C. A. Haworth, H. Teng, R. A. Smith, C. C. Chirilă, M. Lein, J. W. G. Tisch, J. P. Marangos, *Science*, **2006**, *21*, 424-427.

[5] O. Smirnova, Y. Mairesse, S. Patchkovskii, N. Dudovich, D. Villeneuve, P. Corkum, M. Y. Ivanov, *Nature*, **2009**, *460*, 972-977.

[6] N. J. Turro, V. Ramamurthy, J. C. Scaiano, *Principles of Molecular Photochemistry*, University Science Books, Sausalito, California, **2009**.

[7] R. G. W. Norrish, G. Porter, *Nature,* **1949**, *164*, 658.

[8] G. Porter, *Proc. R. Soc. Lond. A,* **1950**, *200*, 284-300.

[9] G. Porter, *Science*, **1968**, *160*, 1299-1307.

[10] J. Lakowicz, *Principles of Fluorescence Spectroscopy*, Springer, Singapore, **2006**.

[11] D. V. O'Çonnor, D. Phillips. *Time-correlated single-photon counting*. Academic Press, New York. **1984.**

[12] W. Becker, H. Hickl, C. Zander, K. H. Drexhage, M. Sauer, S. Siebert, J. Wolfrum, *Rev. Sci Instrum*, **1999**, *70*, 1835-1841.

[13] Hamamatsu, *Photomultiplier tubes: basics and application*, Third edition, **2007**. http://www.hamamatsu.com/resources/pdf/etd/PMT_handbook_v3aE.pdf.

[14] Ocean Optics In., http://www.oceanoptics.com/Products/usbnow.asp.

[15] Y. Hiraoka, J. W. Sedat, D. A. Agard, *Science,* **1987**, *238*, 36-41.

[16] T. M. Baer, M. S. Keirstead, US Patent 4,653,056, **1987**.

[17] G. B. Jarvis, S. Mathew, J. E. Kenny, *Appl. Opt.,* **1994**, *33*, 4938-4946.

[18] Xenon arc lamp, Applied Photophysics Co., Ltd. http://www.photophysics.com/tutorials/stopped-flow-spectrometry/sx20-performance-0.

[19] Flash lamp pumped Nd: YAG laser, InnoLas Laser GmbH. http://www.innolas-laser.com/index.php/en/scientific-laser/flash-lamps/spitlight-compact-400.html.

[20] Monochromators, Zolix Instruments CO.,LTD. http://www.zolix.com.cn/en/prodcon_370_376_346.html.

[21] PMT, Zolix Instruments CO.,LTD. http://www.zolix.com.cn/en/prodcon_370_379_386.html.

[22] Photodiode, Thorlabs Inc. http://www.thorlabs.de/newgrouppage9.cfm?objectgroup_id=1285.

[23] Oscilloscope, Tektronix, Inc. http://www.tek.com/datasheet/dpo4032-oscilloscope.

[24] J. E. Rogers, K. A. Nguyen, D. C. Hufnagle, D. G. McLean, W. Su, K. M. Gossett, A. R. Burke, S. A. Vinogradov, R. Pachter, P. A. Fleitz, *J. Phys. Chem. A,* **2003**, *107*, 11331-11339.

[25] K. Nakamaru, *Bull. Chem. Soc. Jpn.*, **1982**, *55*, 1639-1640.

[26] A. Beckett, G. Porter, *Trans. Faraday Soc.*, **1963**, *59*, 2038-2050.

[27] P. K. Das , M. V. Encinas , J. C. Scaiano*, J. Am. Chem. Soc.*, **1981**, *103*, 4154–4162.

[28] J. C. Scaiano, *Acc. Chem. Res.,* **1982**, *15*, 252–258.

[29] C. A. Sawicki, Q. H. Gibson, *J. Biol. Chem.,* **1976**, *251*, 1533-1542.

[30] A. Watanabe , O. Ito, *J. Phys. Chem.*, **1994**, *98*, 7736–7740.

[31] M. E. Sigman , G. L. Closs , *J. Phys. Chem.*, **1991**, *95*, 5012–5017.

[32] J. Jasny, J. Sepit, J. Karpiuk, J. Gilewski, *Rev. Sci. Instrum.,* **1994**, *65*, 3646-3652,

[33] V. I. Vullev, G. Jones, *Journal of Applied Science*, **2005**, *5*, 517-526.

[34] B. L. Feringa, *J. Org. Chem.,* **2007**, *72*, 6635-6652.

[35] M. M. Pollard, M. Klok, D. Pijper, B. L. Feringa, *Adv. Funct. Mater.,* **2007**, *17*, 718-729.

[36] M. Klok, N. Boyle, M. T. Pryce, A. Meetsma, W. R. Browne, B. L. Feringa, *J. Am. Chem. Soc.* **2008**, *130*, 10484–10485.

[37] S. A. Hilderbrand, R. Weissleder, *Curr. Opin. Chem. Biol.*, **2010**, *14*, 71-79.

[38] The wavelength range of the PMTs manufactured in Hammamatsu Inc. http://www.hamamatsu.com/resources/pdf/etd/PMTmodules_TPMO0010E02.pdf.

[39] Revised from commercial literature provided by Hammamatsu Inc. http://www.slac.stanford.edu/grp/arb/tn/arbvol5/AARD460.pdf.

[40] InGaAs detector DinGaAs1600, Zolix Instruments Co., Ltd. http://www.zolix.com.cn/en/prodcon_370_379_388.html.

[41] R. R. Alfano, N. Ockman*, J. Opt. Soc. Am*, **1968**, *58*, 90-93.

[42] The IR spectrum of energy saver bulb can be revised from commercial document of Olis Inc. http://olisweb.com/literature/pdf/nir_fluorescence_brochure.pdf.

[43] J. Ivri, Z. Burshtein, E, Miron, *Appl. Opt.*, **1991**, *30*, 2484-2488.

[44] Corrected using the response spectra in operation manual of InGaAs series detectors, version 1.0, **2008**, Zolix Instruments CO., LTD.

CHAPTER 3

Photoswitchable Intramolecular Through-Space Magnetic Interaction[1]

A light driven molecular motor, which bears two TEMPO spin centers, has been developed. In this system, the distance between spin centers can be changed with light. The interaction between two TEMPO spin centers connected to a photoswitchable overcrowded alkene changes upon photoswitching from non-coupled (3-line EPR spectrum) in the trans state, where the two spin centers are separated by ca. 22 Å, to strongly coupled (5-line EPR spectrum) in the cis state, with the separation is ca. 7 Å. Importantly, the alkene switching unit's performance is essentially unaffected by the spin centers.

3.1 Introduction

Dynamic photocontrol over magnetic interactions between stable organic radical centers (RCs) is a promising strategy towards molecular-scale information processing and memory devices.[1, 2] Several photochromic units (PU),[3] such as azobenzenes,[4] diarylethenes,[5, 6, 7, 8] and Schiff bases[9] have been functionalized with RCs to construct systems, in which photoswitching of the PU modulates the through-bond interaction between RCs, producing a readable magnetic signal. An impressive series of RC-PU-RC compounds have been reported by Irie and coworkers.[6, 7, 8] In these systems, reversible photocyclization of the diarylethene PU can switch a through-bond spin-spin coupling of pairs of nitronyl nitroxide RCs on and off, manifested in substantial changes in the electron paramagnetic resonance (EPR) spectra.[4] However, in these π-conjugated RC-PU-RC systems, modulating the extent of π-delocalization by photo-isomerization of the PU unit was used to control the spin-spin interaction. Nevertheless, it is a challenging task to achieve a system that operates by switching on and off the electronic interaction between RC units through the π-system of the PU unit, without compromising the efficiency of photoswitching processes. This requires careful optimization of the photochromic π-conjugated structures.[5]

In this chapter a highly efficient photoswitchable magnetic system by which intramolecular through-space magnetic interactions between two RCs can be switched on and off reversibly, is described. The molecular design, which does not rely on through-bond interactions between the RCs, avoids loss in photochemical performance. In this system (Figure 1), the RC-PU-RC functional subunits are connected in a non-π-conjugate manner via alkylamide spacers to minimize the electronic interference between PU and RC units. The switching unit (see *trans*-1) is based on the well-known overcrowded alkenes (OA),[10, 11, 12, 13, 14] to which a pair of stable 2,2,6,6-tetramethyl-piperidine-1-oxyl (TEMPO) radicals are attached via amide bonds. Light-driven *cis-trans* isomerization of the OA unit can switch the through-space magnetic interactions between the TEMPO radical pair. In the *trans*-state, the TEMPO units are kept apart, and the three-line EPR spectrum is assigned to that of monomer-like TEMPO unit. In stark contrast, in the *cis*-state, the two TEMPO units are in sufficient proximity to allow for strong spin-spin coupling, manifested in a five-line EPR spectrum.[15, 16] These two states can be interconverted by alternate irradiation at λ_{irr} 312 and 365 nm at room temperature in several solvents.
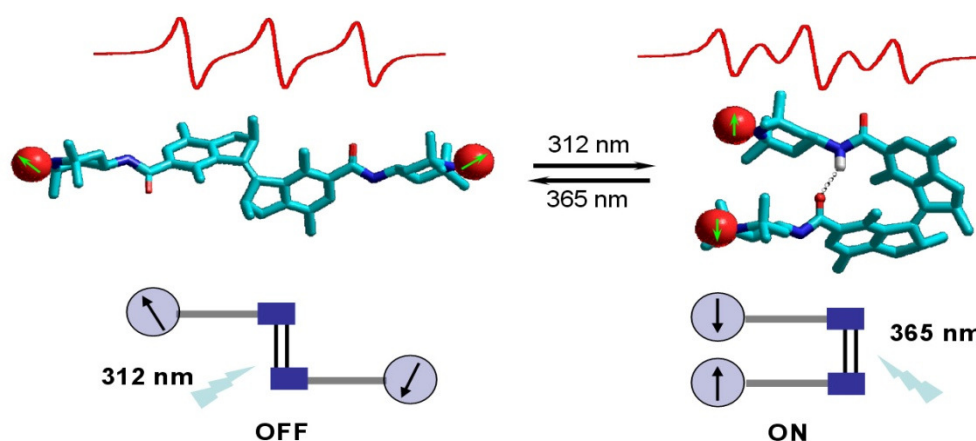
Figure 1. Photoswitching of intramolecular through-space magnetic interaction.

3.2 Molecular design

A TEMPO unit was attached to each end of the PU via amide bonds as *trans*-**1** (Figure 1). The mono-TEMPO substituted *trans*-**2** was prepared to confirm the intramolecular nature of the photoswitchable spin-spin coupling observed for *trans/cis*-**1**. *Bis*-cyclohexylamine substituted *trans*-**3**, which does not bear RCs, was used for comparison.

trans-**1**   *trans*-**2**   *trans*-**3**
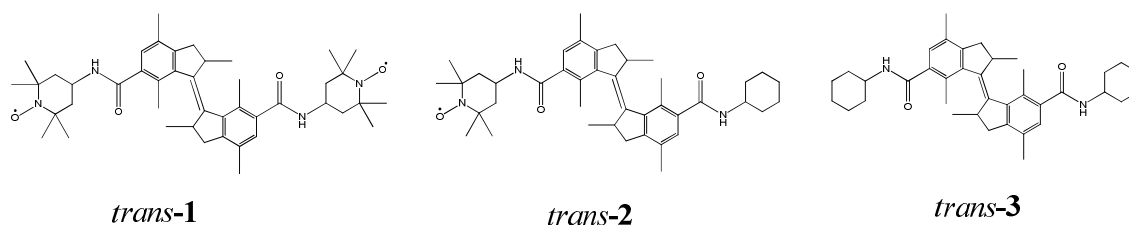
Scheme 1. Molecular structure of *trans* **1-3**.

3.3 Results and Discussion

The compounds *trans*-**1-3** display similar UV/vis absorption spectra (Figure 2, Figure 3) with the maximum centered at 297 nm, which is ascribed to absorption by the *trans*-OA unit. Irradiation at 312 nm results in a decrease in the absorption of *trans*-**1** (Figure 2a) at 297 nm with a concomitant increase of a new absorption band at 350 nm. An isosbestic point was maintained at 319 nm over the course of the irradiation. At the photo stationary state (PSS), 89% of *cis*-**1** is formed as determined by ^{1}H NMR. *Trans*-**1-3** all exhibit essentially identical changes in their absorption spectra upon irradiation at 312 nm. The spectral changes are

assigned to the *trans→cis* photo-switching of the OA unit.[10, 11] For the reference compound **3**, ^{1}H-NMR spectroscopy was employed to monitor the photoswitching. The aromatic proton H_a shifts from 7.02 to 6.95 ppm (Figure 3c), characteristic[6a,6b] of the formation of *cis*-**3**.
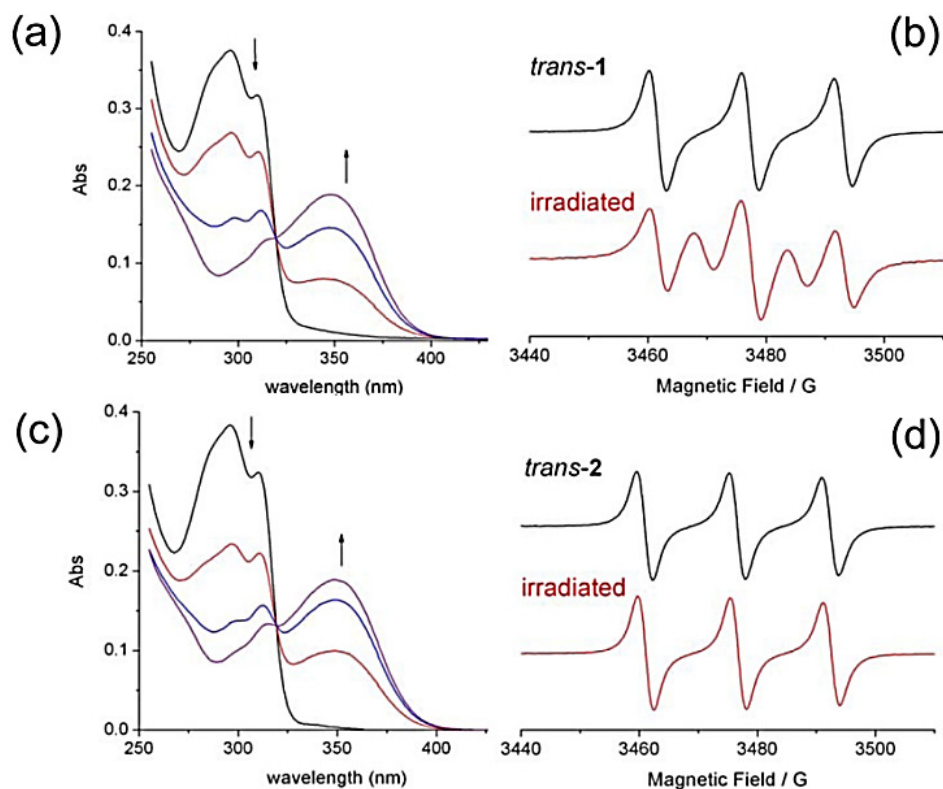

Figure 2. UV/vis absorption (1.5×10^{-5} M) and EPR spectroscopy (1.0×10^{-3} M) of *trans*-**1** (a, b) and *trans*-**2** (c, d) upon irradiation at 312 nm for 70 s in ethyl acetate at 20 ˚C.
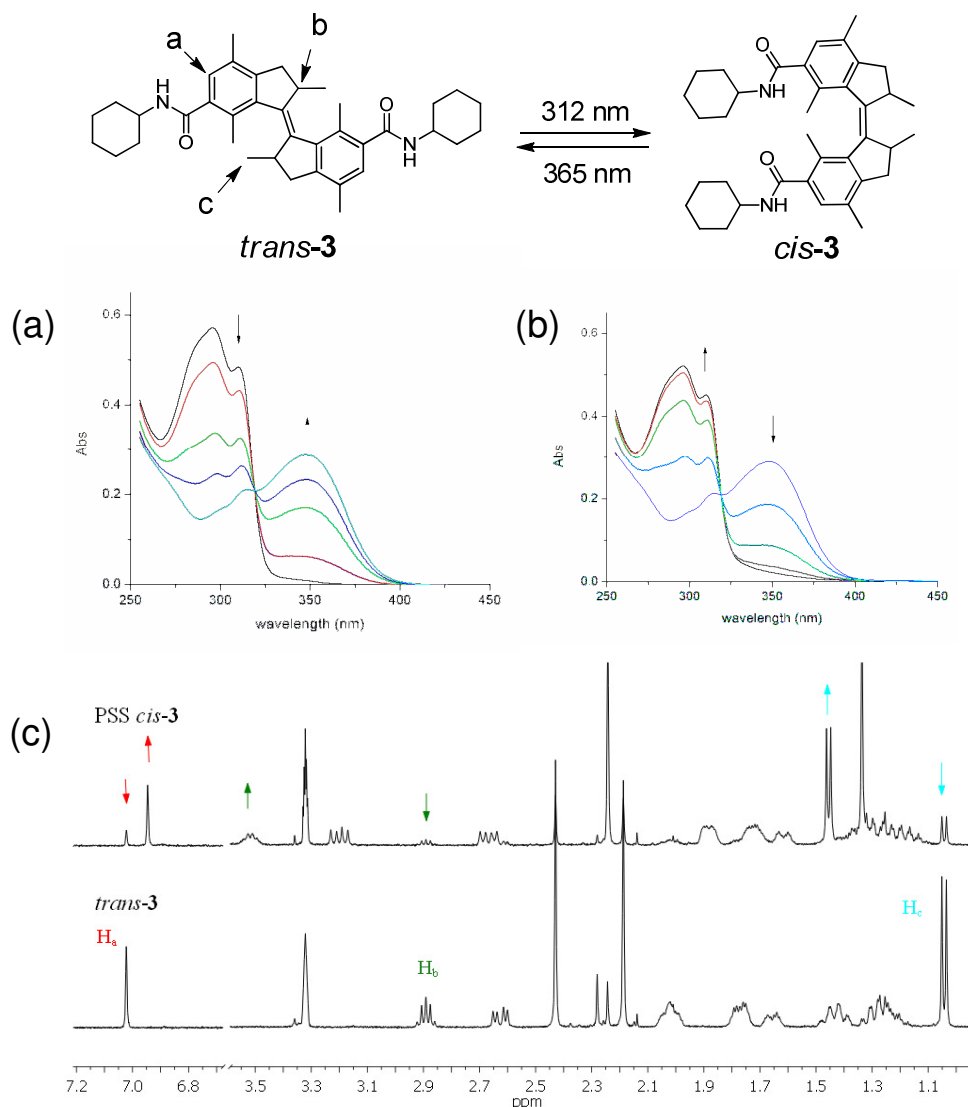
Figure 3. Changes to the UV-vis absorption spectrum of *trans*-**3** (2.3×10^{-5} M) upon irradiation at 312 nm (a). Irradiation of *cis*-**3** at the PSS by 365 nm drives a reverse *cis*→*trans* isomerization (b). The formation of *cis*-**3** was confirmed by ^{1}H-NMR spectroscopy (c). The arrows indicate the signal changes upon irradiation at 312 nm for 6 min in CD_2Cl_2/CD_3OD (3/1) at 20 ˚C.

The changes in the magnetic interaction between the two TEMPO radical units of compound **1** upon photoswitching were monitored by EPR spectroscopy (Figure 2b). A three-line spectrum (g = 2.006, A_N = 15.5 G) typical of TEMPO was observed for *trans*-1, indicating the absence of significant spin coupling between the two radicals.[17, 18] The EPR spectra showed substantial changes from a three- to a five-line spectrum upon irradiation at 312 nm. The mixture of three- and five-line EPR signals observed at the PSS (>71% *cis*-**1**) was in agreement with the PSS determined by UV/vis absorption and ^{1}H NMR spectroscopy. The

changes in the EPR spectrum upon switching to the *cis* state are indicative of coupling between the two TEMPO RCs, which is larger than the ^{14}N hyperfine coupling constant.[15] Density functional theory (DFT) molecular modeling studies at the DFT B3LYP/6-31G* level (Figure 4) indicated that the two TEMPO units are in proximity in the *cis*-state with a separation ca. 7.1 Å (between the N-O centers), coinciding with the reported distance through which substantial spin-spin interaction occurs.[17] In contrast, in the *trans*-state, the two TEMPO units are sufficiently isolated from each other (ca. 22.4 Å) to preclude significant spin coupling. The EPR spectrum of the mono-substituted reference *trans*-**2** is unaltered (Figure 2d) upon photoisomerization of the OA unit (Figure 2c), supporting the assignment of intramolecular coupling in *cis*-**1**.
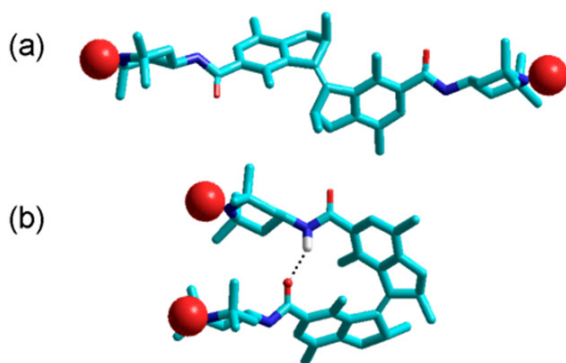

Figure 4. Energy minimized structures of *trans*-**1** (a) and *cis*-**1** (b) optimized using density functional theory (DFT) methods with the B3LYP/6-31G (d,p) basis set.

Molecular modeling studies also suggest the presence of an intra-molecular hydrogen bond (Figure 4) between the amide groups in the *cis* state, which cooperates with the OA platform to direct the two TEMPO arms in a proper orientation for spin-spin interaction. This conclusion is further supported by the experimental observation that in a protic solvent such as ethanol, the coupled EPR signal is less evident (Figure 5) compared with that observed in an aprotic solvent (e.g. THF). In the PSS state, the UV/vis absorption spectra are quite similar (see Figure 5, a,b), but the change in the EPR signal to the five line spectrum is less evident in ethanol compared with that in THF (see the region marked with a double arrow).
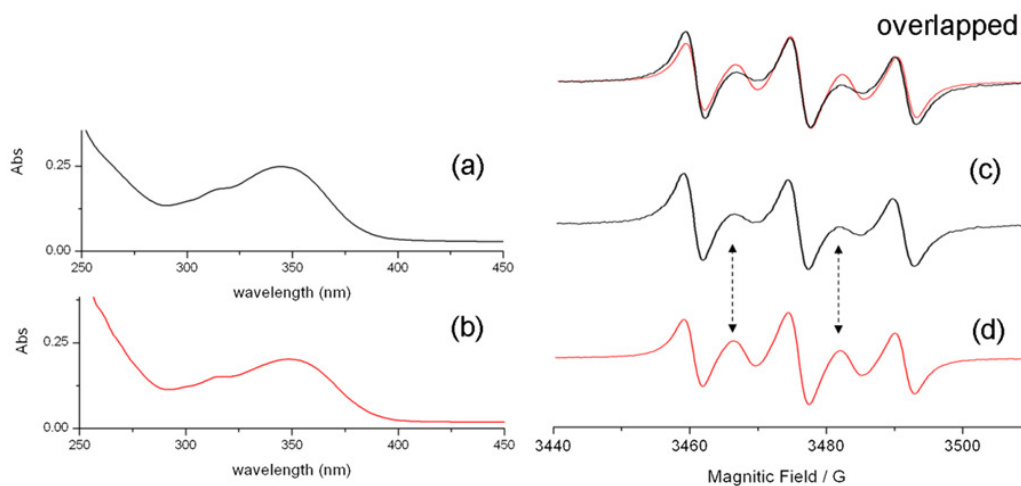
Figure 5. UV/vis absorption spectra and EPR spectra of PSS *cis*-**1** in ethanol (a, c) and THF (b,d) at 20 ˚C.

The photoswitching is reversible (Figure 6, Figure 7). Irradiation at 365 nm drives the reverse *cis→trans* isomerization, with the absorption band at 350 nm decreasing in intensity (Figure 7a), and a recovery in the initial absorption of *trans*-**1** at 297 nm (PSS, 86% *trans*-**1**). Concomitant recovery of the three-line EPR spectrum is observed also (Figure 7b).
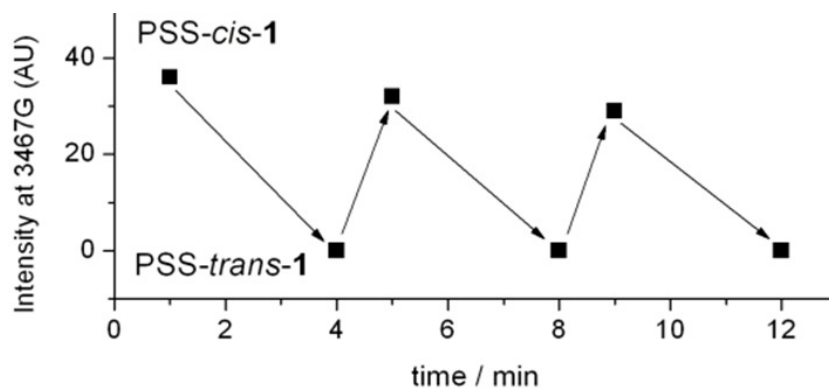

Figure 6. Reversibility of the switching monitored by EPR spectroscopy upon alternate irradiation of PSS mixture of *cis/trans*-**1** at 365 and 312 nm, respectively.
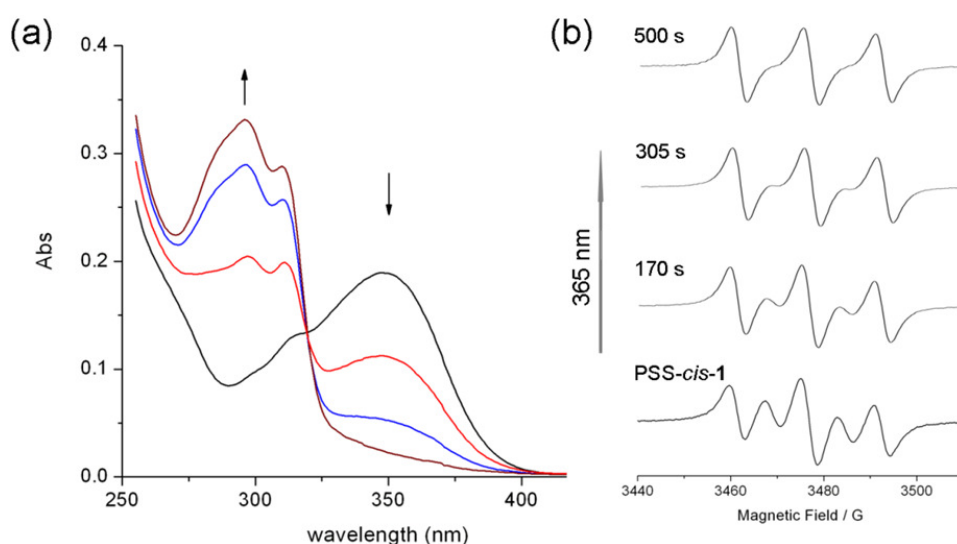
Figure 7. UV-vis absorption spectra (a, 1.5× 10^{-5} M) and EPR spectra (b, 1.0× 10^{-3} M) of PSS *cis*-**1** upon irradiation at 365 nm in ethyl acetate at 20 ˚C.

An important feature of the present system is that the radical centers do not interfere with the photochemical properties of the switching unit. Comparison of the quantum yields (Table 1) of photoswitching for compounds **1**-**3** indicates that TEMPO functionalization does not affect the isomerization significantly in either direction. This is a remarkable feature when it is considered that orders of magnitude decrease in the quantum efficiency has been observed in π-conjugated RC-PU-RC systems.[7] In addition, the intramolecular nature of the magnetic interaction in the current study, in contrast to those showing intermolecular interactions,[9] allows for this dynamic system to operate under a wide range of concentrations. Photoisomerization results in substantial changes to the EPR spectrum in solvents (Figure 8), such as ethyl acetate, dichloromethane, toluene, and acetonitrile (Figure 9).

Table 1. Quantum yields of photoisomerization of compounds **1**-**3**[*].

compound	Φ_{312}	Φ_{365}
1	0.131 ±0.03	0.023±0.03
2	0.136 ±0.03	0.029±0.03
3	0.148 ±0.03	0.038±0.03

* the quantum yields were independently determined at least 3 times.
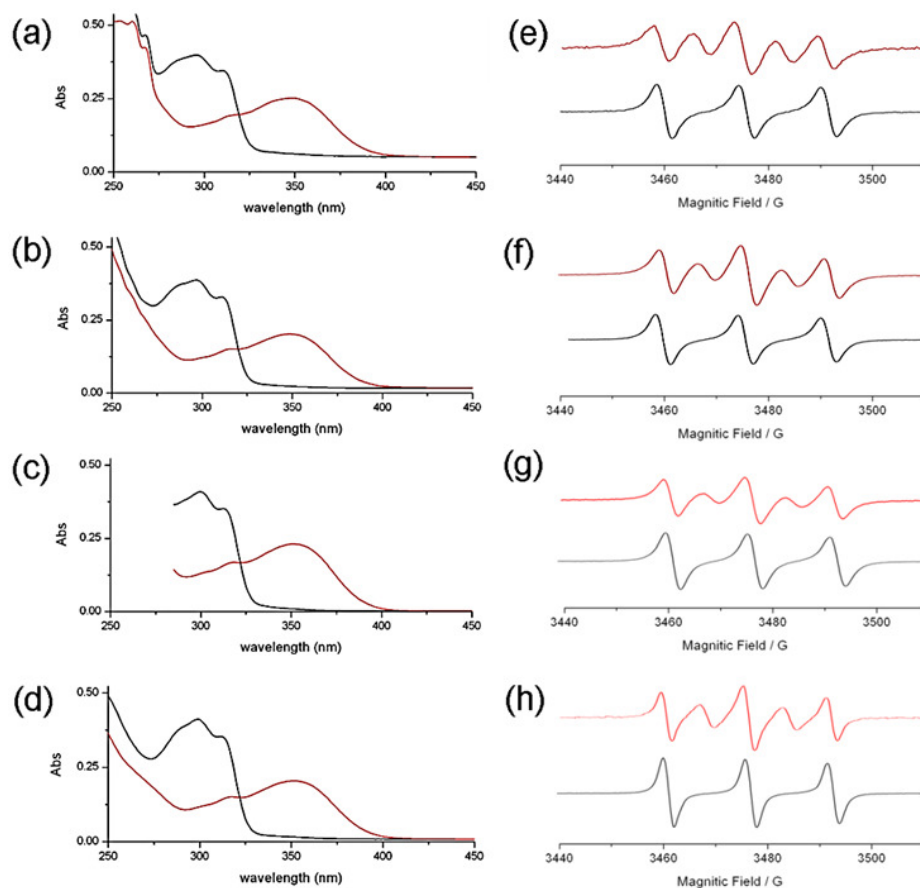
Figure 8. UV/vis absorption spectra (a-d, 1.5× 10^{-5} M) and EPR spectra (e-h, 1.0× 10^{-4} M) of *trans*-**1** upon UV irradiation at 312 nm in acetonitrile, a,e; tetrahydrofuran, b,f; toluene, c,g and dichloromethane, d,h at 20 ˚C.
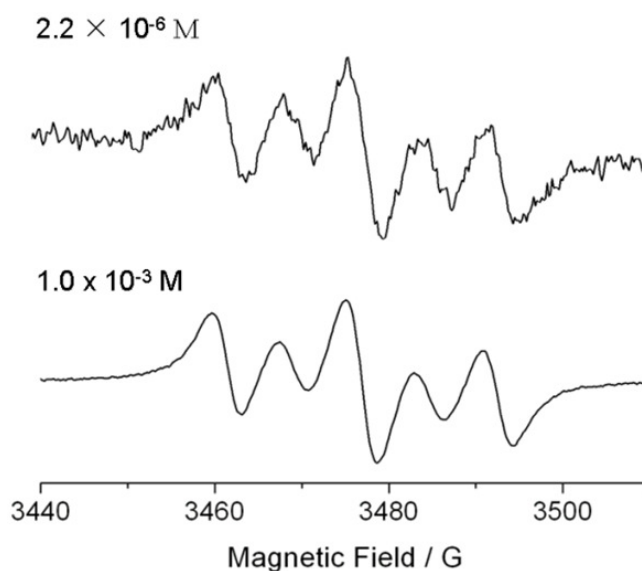

Figure 9. EPR spectroscopy of PSS *cis*-**1** (1.0× 10^{-3} M, or 2.2× 10^{-6} M) in ethyl acetate at 20 ˚C.

3.4 Conclusion

A photoswichable magnetic system is described, in which the photochromic units (PU) based on the well-known overcrowded alkenes and the organic radical centers (RC) 2,2,6,6-tetramethyl-piperidine-1-oxyl (TEMPO) are attached to both ends of the PU via amide bonds. The RC-PU-RC functional subunits are connected in a non-π-conjugate manner via alkylamide spacers to minimize the electronic interference between PU and RC units. The light-driven isomerization of the overcrowded alkenes changes the interaction between two spin centers from a non-coupled *trans* state separated by ca. 22 Å, to strongly coupled *cis* state, with a separation of ca. 7 Å by alternate irradiation aṭ λ_{irr} 312 and 365 nm at room temperature in several solvents. The isomerization of the overcrowded alkenes was monitored by UV/visible absorption and ^{1}H-NMR spectroscopy. The magnetic interaction of the two spin centers was characterized by EPR spectroscopy, from a three-line EPR spectrum to a strong spin-spin coupling, manifested in a five-line EPR spectrum upon light irradiation. The photoswitching of magnetic interaction is reversible. RC interaction in this system is intramolecular through-space rather than through-bond interactions between the RCs, without compromising the efficiency of the photoswitching processes. This approach shows potential application in molecular-scale information processing and memory devices.

3.5 Experimental section

General remarks

Chemicals were purchased from Aldrich. Freshly distilled tetrahydrofuran (THF), dichloromethane (DCM), and toluene were used for synthesis. UVASOL grade solvent were used for spectroscopic measurements. Technical grade solvents were used for extraction and chromatography. Merck silica gel 60 (230-400 mesh ASTM) was used in flash chromatography. NMR spectra were obtained using a Varian Mercury Plus (400 MHz). EPR spectra were obtained using a Bruker ECS 080 spectrometer. FT-IR spectra were obtained using a Perkin Elmer Spectrum 400 spectrometer. UV/Vis measurements were performed on a JASCO V-630 spectrophotometer. UV irradiation experiments were carried out using a Spectroline model ENB-280C/FE lamp. In general, the PSS can be reached

within 40 s of irradiation at 312 nm and the recovery of *trans*-form occurs within 2 min by 365 nm irradiation.

Synthesis[2*]:
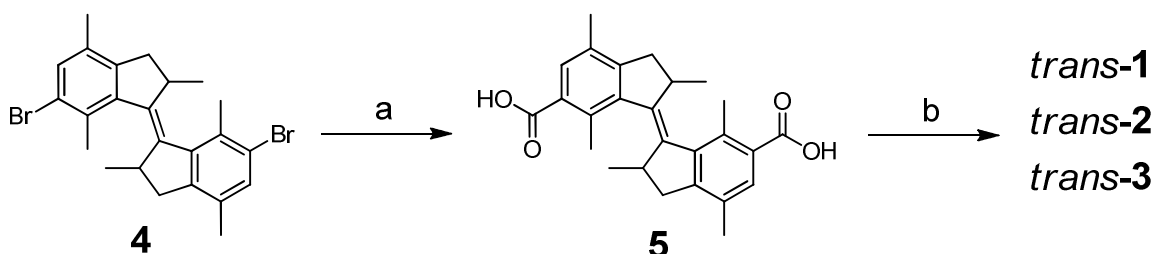
(a) ^{n}BuLi, CO_2, THF, -85 °C, 93%

(b) i), DCC, HOBt, 4-Amino-TEMPO, DMF, rt, 6h; ii), Cyclohexylamine, 1h, **1** (23%), **2** (35%), **3** (26%)

To a solution of compound **4**[11] (0.5 g, 1.05 mmol) in 30 mL dry THF was added 2.3 mL of ^{n}BuLi (1.6 M solution in THF) at -90 °C. The solution was stirred at this temperature for 0.5 h before addition of dry ice (3.0 g, 68.0 mmol). After warming to room temperature, the mixture was slowly poured into 50 mL of water. The precipitate was collected and washed with pentane (50 mL) affording 384 mg (0.95 mmol, 90%) of the diacid **5** as a white solid. mp: >300 °C (dec.). ^{1}H NMR (CD_3OD/CD_2Cl_2): δ = 7.65 (s, 2H), 2.94-2.82 (m, 2H), 2.70-2.55 (m, 8H), 2.30-2.21 (m, 8H), 1.08 (d, $J = 6.3$Hz, 6H). ^{13}C NMR (CD_3OD/CD_2Cl_2): 169.5, 146.3, 142.3, 141.7, 132.4, 131.5, 131.0, 130.0, 42.1, 31.1, 21.6, 18.9, 18.1. HRMS: m/z calcd for $C_{26}H_{27}O_4$ [M-H]$^{-}$: 403.1904; found: 403.1907.

Compounds *trans*-**1-3**. To a solution of diacid **5** (150 mg, 0.37 mmol) in 20 mL of dry DMF was added 4-amino-TEMPO (76 mg, 0.44 mmol), HOBt (N-Hydroxybenzotriazole, 150 mg, 1.11 mmol), and DCC (Dicyclohexylcarbodiimide, 229 mg, 1.11 mmol) under N_2. The mixture was stirred at room temperature for 6h. Next cyclohexylamine (550 mg, 5.55 mmol) was added. After stirring at room temperature for another 0.5 h, the mixture was poured into 100 mL water and extracted with ethyl acetate (2 × 60 mL). The combined organic phase was dried and the solvent was removed under vacuum. The residue was purified by silica gel column chromatography using n-

---

[*] Dr. Jiaobing Wang is acknowledged for the synthesis compounds *trans* **1-3**.

heptane/ethyl acetate (1/1) as the eluant affording compounds *trans*-**1** and **2** as a slightly pink solid and *trans*-**3** as a white solid.

trans-**1**. mp: 159.3-161.8 °C. FTIR: 2972 ($^{TEMPO}CH_3$), 2929, 2851, 1625 (C=O, amide), 1525, 1457, 1364 (N–O), 1245 cm^{-1}. EPR (ethyl acetate): 3 lines, g = 2.006, A_N = 15.5 G. UV-vis (ethyl acetate): λ_{max}(nm) = 297 (ε = 2.57 × 10^4 M^{-1}cm^{-1}). HRMS: m/z calcd for $C_{44}H_{63}N_4O_4$ [M+H]$^+$: 711.4844; found: 711.4879.

trans-**2**. mp: 169.1-170.7 °C. FTIR: 2972 ($^{TEMPO}CH_3$), 2927, 2852, 1627 (C=O, amide), 1531, 1459, 1363 (N–O), 1244 cm^{-1}. EPR (ethyl acetate): 3 lines, g = 2.006, A_N = 15.5 G. UV-vis (ethyl acetate): λ_{max}(nm) = 297 (ε = 2.57 × 10^4 M^{-1}cm^{-1}). HRMS: m/z calcd for $C_{41}H_{57}N_3O_3$ [M+H]$^+$: 639.4394; found: 639.4419.

trans-**3**. mp: 175.3-177.5 °C. IR: 2930, 2855, 1622 (C=O, amide), 1435, 1153 cm^{-1}. UV-vis (AcOEt): λ_{max}(nm) = 297 (ε = 2.57 × 10^4 M^{-1}cm^{-1}). ^{1}H NMR (CD$_2$Cl$_2$/MeOD = 1/0.6): δ = 7.01 (s, 2H), 3.91-3.81 (m, 2H), 2.93-2.84 (m, 2H), 2.61 (dd, J = 14.8, 5.6 Hz, 2H), 2.42 (s, 6H), 2.27 (d, J = 14.8 Hz, 2H), 2.16 (s, 6H), 2.06-1.95 (m, 4H), 1.81-1.71 (m, 4H), 1.69-1.58 (m, 2H), 1.48-1.35 (m, 4H), 1.33-1.18 (m, 6H), 1.03 (d, J = 6.4 Hz, 6H). ^{13}C NMR (CD$_2$Cl$_2$/MeOD = 1/0.6): 170.9, 143.9, 141.9, 141.7, 136.2, 131.4, 128.3, 126.6, 48.8, 42.0, 38.7, 32.7, 25.4, 24.9, 19.1, 18.3, 17.5. HRMS: m/z calcd for $C_{38}H_{51}N_2O_2$ [M+H]$^+$: 567.3945; found: 567.3964.

3.6 References

[1] O. Sato, J. Tao, Y.-Z. Zhang, *Angew. Chem. Int. Ed.,* **2007**, *46*, 2152.

[2] S. Nakatsuji, *Chem. Soc. Rev.,* **2004**, *33*, 348.

[3] B. L. Feringa, W. R. Browne, *Molecular Switches*, Wiley-VCH, Weinheim, **2001.**

[4] An azobenzene based dynamic magnetic system has been reported. However, a change in EPR signal is only observable for a pre-irradiated sample at cryogenic temperatures (10 K). see, Hamachi, K.; Matsuda, K.; Itoh, T.; Iwamura, H. *Bull. Chem. Soc. Jpn.* **1998**, *71*, 2937.

[5] N. Tanifuji, M. Irie, K. Matsuda, *J. Am. Chem. Soc.,* **2005**, *127*, 13344.

[6] K. Matsuda, M. *J.* Irie, *Am. Chem. Soc.,* **2001**, *123*, 9896.

[7] K. Matsuda, M. *J.* Irie, *Am. Chem. Soc.,* **2000**, *122*, 7195.

[8] K. Matsuda, M. *J.* Irie, *Am. Chem. Soc.,* **2000**, *122*, 8309.

[9] Ratera, I.; Ruiz-Molina, D.; Vidal-Gancedo, J.; Wurst, K.; Daro, N.; Létard, J.-F.; Rovira, C.; Veciana, J. *Angew. Chem. Int. Ed.* **2001**, *40*, 919.

[10] M. M. Pollard, A. Meetsma, B. L. Feringa, *Org. Biomol. Chem.,* **2008**, *6*, 507.

[11] J. Wang, A. Kulago, W. R. Browne, B. L. Feringa, *J. Am. Chem. Soc.,* **2010**, *132*, 4191.

[12] J. Wang, B. L. Feringa, *Science,* **2011**, *331*, 1429.

[13] W. R. Browne, B. L. Feringa, *Nature Nanotech.,* **2006**, *1*, 25.

[14] B. L. Feringa, *J. Org. Chem.,* **2007**, *72*, 6635.

[15] M. Porel, M. F. Ottaviani, S. Jockusch, N. Jayaraj, N. J. Turro, V. Ramamurthy, *Chem. Commun.,* **2010**, *46*, 7736.

[16] E. Sartori, I. V. Khudyakov, X. Lei, N. J. Turro, *J. Am. Chem. Soc.,* **2007**, *129*, 7785.

[17] D. Bardelang, K. Banaszak, H. Karoui, A. Rockenbauer, M. Waite, K. Udachin, J. A. Ripmeester, C. I. Ratcliffe, O. Ouari, P. Tordo, *J. Am. Chem. Soc.,* **2009**, *131*, 5402.

[18] K. Matsuda, M. T. Stone, J. S. Moore, *J. Am. Chem. Soc.,* **2002**, *124*, 11836.

CHAPTER 4

Energy and Electron transfer between Porphyrins, Graphene and Molecular Motors[1]

Two bicomponent systems based on porphyrins are presented; the first is used to modify graphene, and the second to study triplet sensitization of covalently and non-covalently attached molecular motors. The characteristics of two systems are studied by steady state spectroscopy, i.e. UV/vis absorption, emission and CD spectroscopies. The energy and/or electron transfer processes were studied by laser flash photolysis. The properties of the new graphene materials and the visible light driven operation of molecular motors have been demonstrated.

4.1 Introduction

Porphyrins are heterocyclic macrocycles that are based on four pyrrole subunits connected at their α carbons by methine bridges. They are relatively large, highly symmetric and conjugated systems, and typically exhibit strong absorption and emission in the visible region. Due to their spectroscopic properties, porphyrins have attracted significant attention in chemistry, nanotechnology and biology.[1] For example, supramolecular chemists have taken advantage of the delocalized π-electron system or Lewis acidity of the central metal ion of metalloporphyrins to form supramolecular system; the strong absorption and efficient energy and/or electron transfer drives the conversion of light to chemical energy, with porphyrins acting as photosensitizers in photodynamic therapy[2] and dye-sensitized solar cells.[3]

Recently several groups have combined porphyrins with fullerenes (C_{60}) and carbon nanotubes to form hybrid materials as artificial electron-donor-acceptor ensembles. Researches on novel functional materials have focused on applications in solar cells, photodiodes and light-harvesting systems.[4]

Graphene, a single-atom-thick layer of graphite, has drawn tremendous attention and intense research activities by scientists because of its extraordinary properties.[5] Its characteristics such as thermal conductivity and a near-room temperature Quantum Hall effect, 0 to 0.25 eV tunable bandgap and electron-hole symmetry, remarkably high electron mobility, nonlinear phase shift under intense laser illumination, etc, makes graphene to be one of the most promising candidates for applications in supercapacitors,[6] nanoelectronics devices,[7] chemical sensors[8] and reinforced composite materials.[9]

Inspired by porphyrin-C_{60} and porphyrin-carbon nanotube hybrid systems, a hybrid material combining graphene with porphyrins was envisaged. Graphene-TPP (TPP: tetraphenylporphyrin) and graphene-PdTPP (PdTPP: palladium tetraphenylporphyrin) hybrid materials were prepared by a one pot cycloaddition reaction (Scheme 1).[10] This covalent functionalization provides a stable connection between porphyrins and graphene. Because of the accessibility of the edge and both faces of the carbon sheet as well as the other extraordinary properties of graphene, which are distinct from those of C_{60} and carbon nanotubes, understanding the interaction between graphene and porphyrins is of interest.

Several spectroscopic techniques, including UV/vis absorption, emission and laser flash photolysis, were used to characterize the graphene-TPP and graphene-PdTPP hybrid materials. The new hybrid materials hold the potential for application in solar cells, electronic sensors and devices and in catalysis.
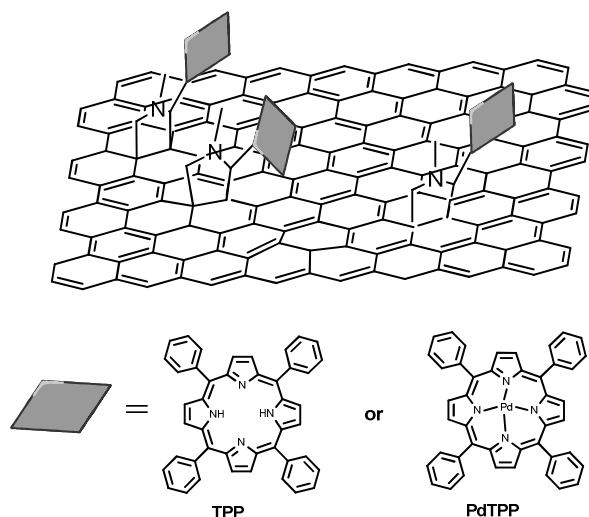
Scheme 1. Hybrid materials based on graphene modified by TPP or PdTPP.

The second part of this chapter described a unidirectional molecular rotary motor driven by visible light through intra- and intermolecular energy transfer from palladium porphyrins. Light driven molecular motors based on overcrowded alkenes undergo photochemical and thermal isomerization, showing a full 360° unidirectional rotary behavior.[11] A number of systems based on these molecular motors have been developed and applied to catalysis,[12] modified surfaces,[13] nanoscale machines,[14] etc. Near and mid UV light is typically required to operate most molecular motors and photoresponsive switches, however, red and near IR light-driven molecular components are highly desirable in expanding their applicability to biological systems. One solution is to sensitize molecular motors through energy transfer from appended chromophores to induce isomerization. We were inspired by the processes used by deep-sea fish for vision, which is used an exogenous chromophore to trigger rhodopsin with long wavelength light.[15] Furthermore, we were motivated by a number of examples of metalloporphyrins that can sensitize the isomerization of stilbene and its derivatives when irradiated at wavelengths longer than the longest wavelength absorption of stilbene.[16] The triplet excited state of a palladium(II) tetraphenylporphyrin (PdTPP) is used to drive the photochemical E-Z isomerization of a unidirectional molecular rotary motor using visible light both by intra- and intermolecular energy transfer

(scheme 2).[17] Visible light driven rotation was confirmed by UV/vis absorption and circular dichroism (CD) spectroscopies. Energy transfer from a triplet excited state was demonstrated by emission spectroscopy and phosphorescence lifetime measurements.
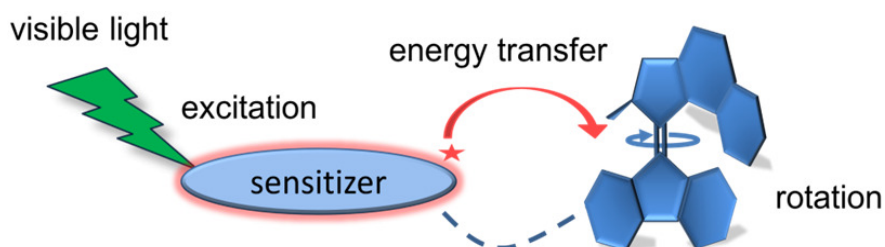

Scheme 2. The rotation of molecular motors can be driven by energy transfer from a triplet photo-sensitizer.

4.2 Porphyrins and Graphene

4.2.1 System design

The hybrid materials, graphene-TPP (TPP: tetraphenylporphyrin) and graphene-PdTPP (PdTPP: palladium tetraphenylporphyrin), studied here were prepared by using a one pot cycloaddition reaction (Scheme 3).[18] The covalent bonding between graphene and porphyrin provides stable and well defined systems compared to the non-covalent system.
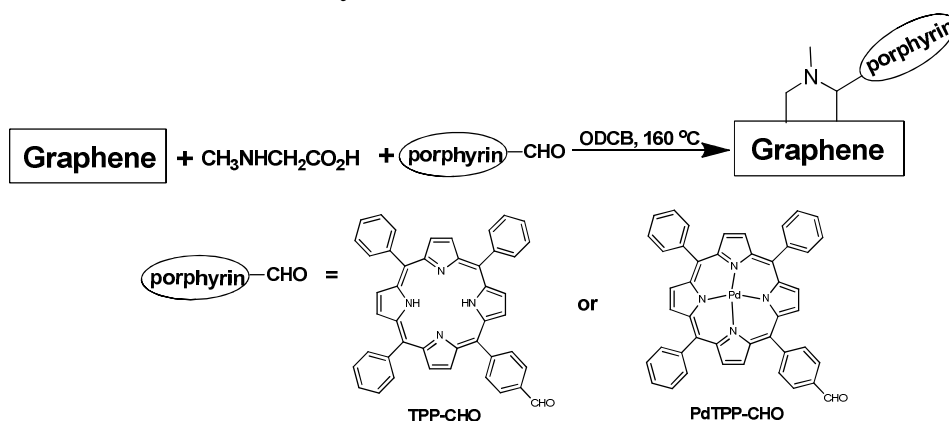
Scheme 3. Synthesis of graphene-TPP and graphene-PdTPP hybrid materials. (Synthesis by Xiaoyan Zhang)

4.2.2 Results and discussion

UV/vis absorption spectroscopy was used to confirm the presence of porphyrin after modification of the graphene. TPP-CHO shows a strong Soret band at 419 nm and four weaker Q bands between 500 nm to 650 nm (Figure 1(a) thick solid line). As for TPP-CHO, PdTPP-CHO shows a strong Soret band at 416 nm and one weaker Q band at 523 nm (Figure 1 (b) thick solid line). In the case of hybrid materials, the typical Soret and Q bands of porphyrin are obtained when suspended in DMF, a broad absorption at 421 nm and a weaker Q band in the graphene-TPP (Figure 1(a) thin solid line), and two broad bands at 419 nm and 525 nm for the graphene-PdTPP (Figure 1(b) thin solid line). These spectra confirmed the presence of the porphyrin unit in the graphene-porphyrin hybrid materials. In control reactions with TPP and PdTPP, where the reaction was performed without sarcosine (see the synthesis in scheme 3), the UV/vis absorption spectra of the graphene materials recovered did not exhibit the typical porphyrin absorption bands (Figure 1, dashed line). This supports the conclusion that the porphyrins in the graphene-TPP and graphene-PdTPP hybrid materials are attached covalently and are not physisorbed.
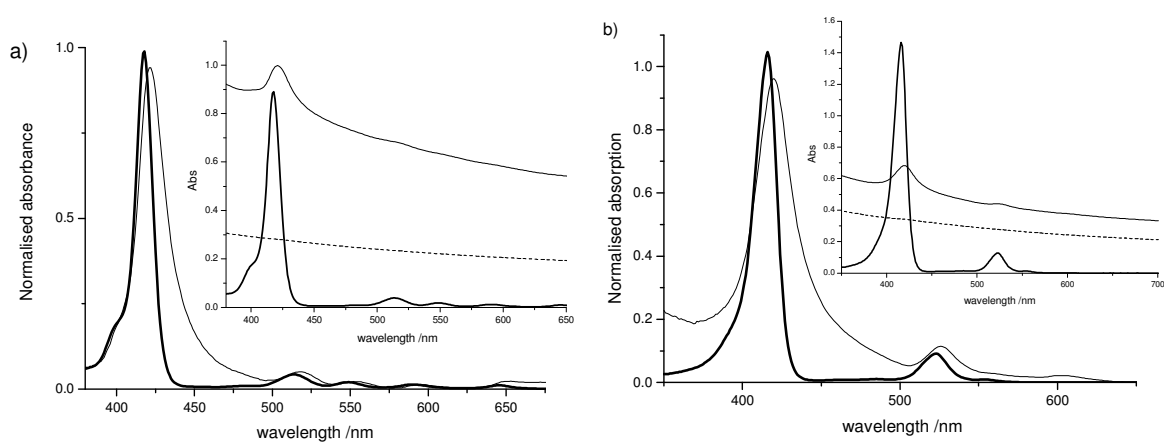

Figure 1. UV/vis absorption spectra of (a) TPP-CHO (thick solid line), graphene-TPP (thin solid line, baseline corrected) {Inset: TPP-CHO (thick solid line), graphene-TPP (thin solid line) and the control sample (dashed line)} in DMF. (b) PdTPP-CHO (thick solid line), graphene-PdTPP (thin solid line, baseline corrected) {Inset: PdTPP-CHO (thick solid line), graphene-PdTPP (thin solid line) and the control sample (dashed line)} in DMF.

The Soret band of both graphene-PdTPP and graphene-TPP shows a small red-shift when covalently attached to graphene, which suggests that there are

interactions between graphene and the porphyrins in the hybrid materials. To further study the interactions, fluorescence (and phosphorescence, in the case of PdTPP) spectroscopy was carried out. The emission spectra of both free porphyrin and the hybrid materials were measured with excitation at 410 nm, where the absorbance is relatively strong. The samples were prepared with the same optical density at the Soret band, and for the hybrids materials the scattering by graphene was taken into consideration. Figure 2, left, shows the fluorescence of free TPP-CHO with the maxima at 650 nm and 710 nm. In contrast, for the graphene-TPP hybrid, the fluorescence is quenched significantly (Figure 2a, dotted line). The fluorescence quantum yield is reduced from 4% to 0.3% for TPP-CHO and graphene-TPP, respectively. A similar quenching behavior is observed for the graphene-PdTPP hybrid material (Figure 2, right). The strong phosphorescence with the maxima at 710 nm for PdTPP is also quenched in the hybrid material. The phosphorescence quantum yield is reduced from 0.62% for PdTPP to below 0.01% for graphene-PdTPP.

A mixture of porphyrin and graphene was compared also, i.e., comparison of the porphyrin, the porphyrin hybrid material and a non-covalent mixture. The phosphorescence measurement of PdTPP related materials at room temperature was carried out by preparing the tested samples either by degassing with argon or by at least three freeze-pump-thaw cycles. The absorption at 410 nm attributed to the porphyrin component in each case was matched for comparison (Figure 3, left). Figure 3, right, shows that the emission intensity of the graphene-porphyrin is almost half of the intensity of TPP-CHO, when the scattering by the graphene is taken into consideration, i.e. attenuation of the emission intensity by ca. 50%. Hence, the decrease in emission intensity of the TPP-CHO in the presence of graphene is attributed primarily to attenuation and not dynamic quenching. The same comparison was carried out for the Pd-TPP/graphene. The absorbance was again matched (Figure 4, left) to compare the intensity of emission. The emission spectra of the non-covalent mixture and the hybrid material are shown in Figure 4, right. The attenuation due to the scattering by the graphene in the wavelength range of the phosphorescence and at 410 nm is estimated to result in a ca. 40% loss in emission intensity. Hence the decrease in emission intensity of the PdTPP-CHO in the presence of graphene is attributable primarily to attenuation also and not only dynamic quenching. The distinct emission behaviors of the non-covalent graphene and porphyrins and covalent hybrid materials indicates that there is no strong interaction between the porphyrins and graphene by directly mixing, while

the covalent system shows a much stronger interaction, in which the emission of the porphyrins is heavily quenched.
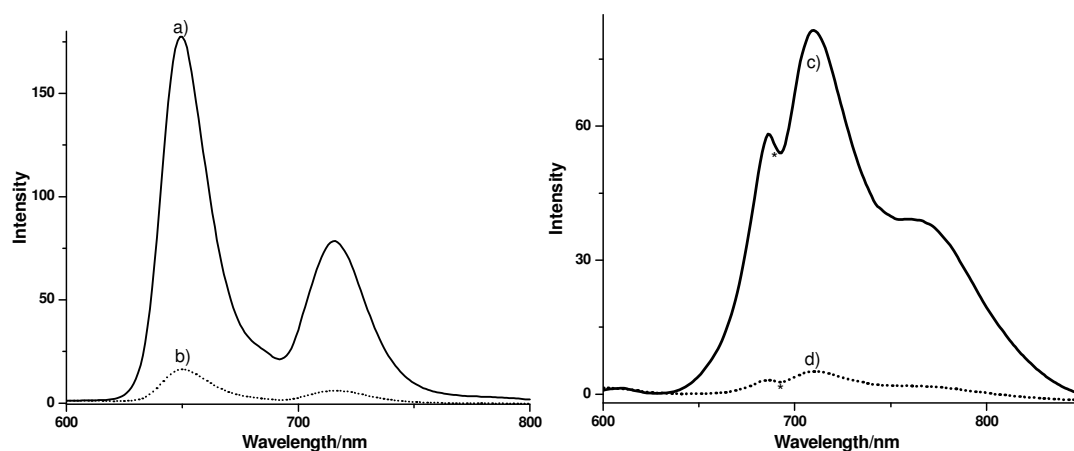

Figure 2. (left) Fluorescence emission spectra of a) TPP-CHO (solid line) and b) graphene-TPP (dotted line) at λ_{exc} 410 nm in DMF. The concentration of porphyrin in both samples (i.e., TPP-CHO and graphene-TPP) was equivalent (0.7 µM) as determined by the intensity of the Soret band taking into account the background due to the porphyrin (right). Phosphorescence emission spectra of (c) PdTPP-CHO (solid line) and (d) graphene-PdTPP (dotted line) λ_{exc} 410 nm. The concentration of porphyrin in both TPP-CHO and graphene-TPP were kept the same (0.6 µM) according to the Soret band absorption intensity. For both of graphene-TPP and graphene-PdTPP, the absorption spectra were corrected by subtracting the scattering of the graphene. *The dip in the spectrum is an instrumental artifact.
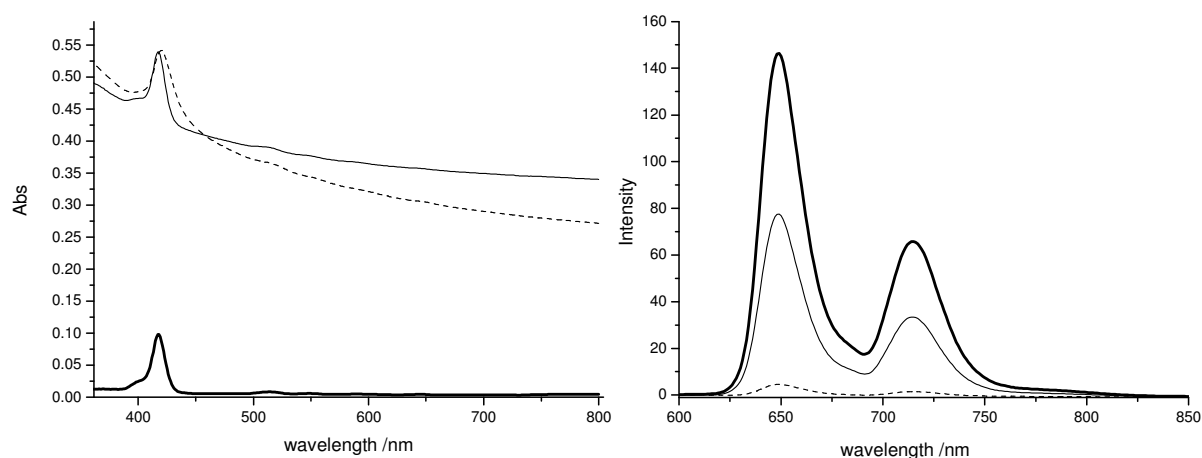

Figure 3. (left) UV/Vis absorption and (right) fluorescence (λ_{exc} 410 nm) spectra of solutions of TPP-CHO (thick solid line), graphene-TPP (thin dotted line) and a mixture of TPP-CHO and graphene (thin solid line).
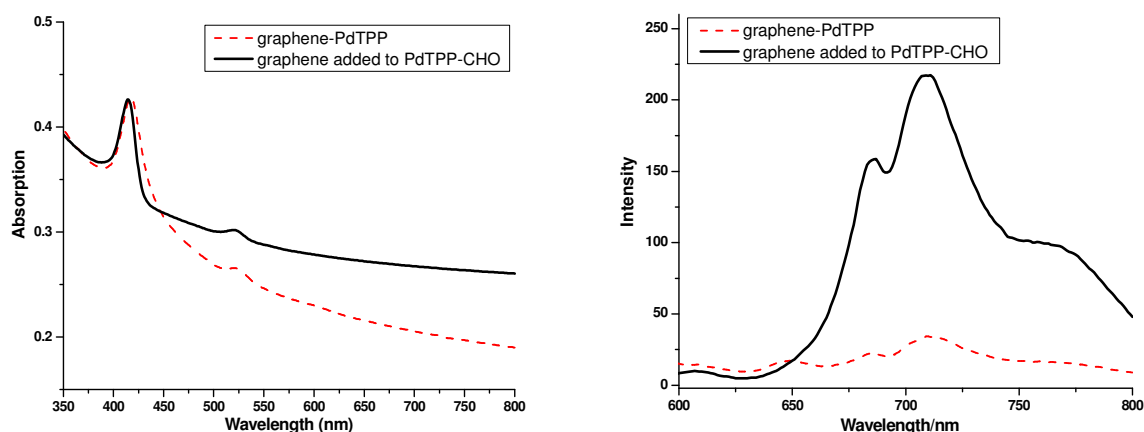
Figure 4. (left) UV/Vis absorption and (right) phosphorescence (λ_{exc} 410 nm) spectra of solutions of graphene-PdTPP (dash line) and a mixture of PdTPP-CHO with graphene (line).

The interaction between graphene and porphyrins in the novel hybrid materials was further examined by determining luminescence lifetimes. The fluorescence lifetime of TPP is around 10 ns, while the phosphorescence lifetime of Pd-TPP is tens of microseconds,[19] so two different techniques for luminescence lifetime measurement were used. For the nanosecond scale lifetimes, a time-correlated single photon counting system was used, and for the longer luminescence lifetimes, the laser flash photolysis system described in chapter 2 was applied. Figure 5 shows that TPP-CHO has a fluorescence lifetime of ca.10.5 ns, and could be fit to a single exponential decay, while the fluorescence decay of the hybrid graphene-TPP was biexponential, with a short component of <500 ps and a longer component of 6.2 ns. The short component accounts for the major part of the decay and confirms that rapid quenching of the porphyrin singlet excited state occurs. The biexponential nature of the decay may reflect the location of the porphyrins on the graphene, i.e. on the basal plane or near the edge. The relatively minor contribution of the longer lifetime component is consistent with such an assignment.

The phosphorescence decay lifetime of PdTPP-CHO is 44 μs whereas for the graphene-PdTPP hybrid material the phosphorescence quantum yield and lifetime are diminished considerably and the latter was non-single exponential (Figure 6). Fitting of the decay of graphene-PdTPP with a biexponential function gives the values 80 and 660 ns, and the main decay component is the shorter one (80 ns).

The phosphorescence decay lifetime of the palladium porphyrin was in the microsecond time range and hence in contrast to fluorescence, phosphorescence can be quenched dynamically as well as statically.
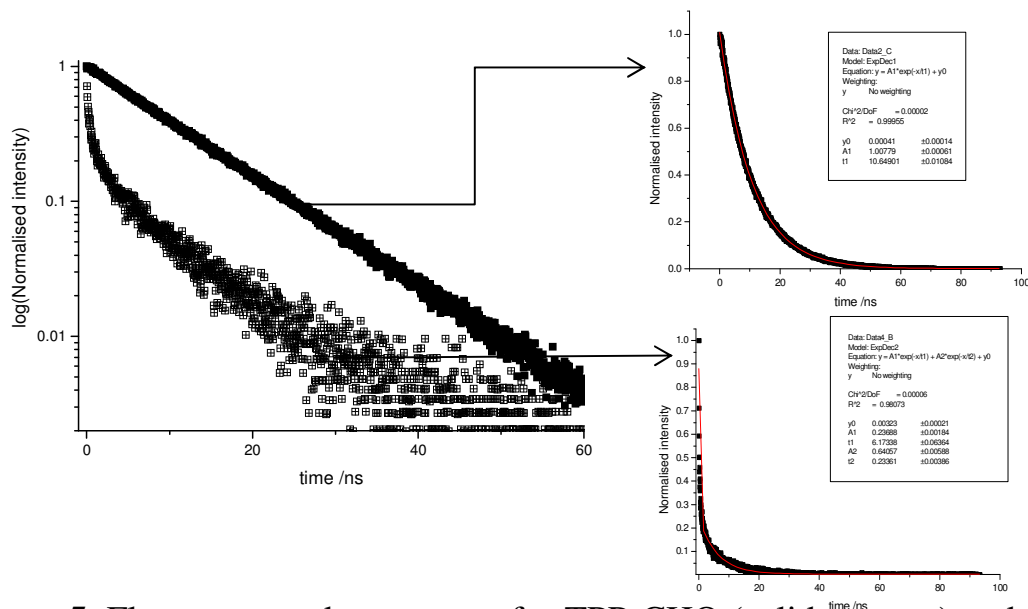

Figure 5. Fluorescence decay traces for TPP-CHO (solid squares) and graphene-TPP hybrid material (open squares) in DMF. Fits are shown on the right.
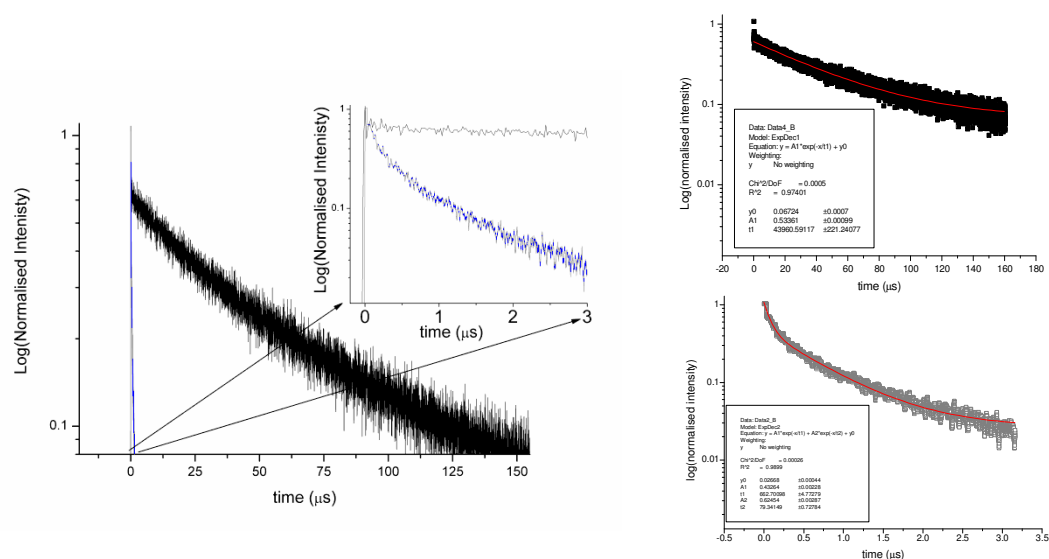

Figure 6. (left) Phosphorescence decay for PdTPP-CHO (black line) and the graphene-PdTPP hybrid material (blue line). The inset shows an expansion of the figure between 1-3 µs. (right) Phorescence lifetime decays for (top) PdTPP-CHO and (bottom) graphene-PdTPP in DMF together with a mono and bi-exponential decay fitting, respectively.

The luminescence lifetimes of both TPP-CHO (or PdTPP-CHO) and graphene-TPP (or PdTPP) show that there are strong interactions between the graphene and TPP (or PdTPP). Comparison of the emission spectra of the covalently modified graphene-TPP (or PdTPP) with both free TPP-CHO (or PdTPP) and a absorbance matched mixture of TPP-CHO with graphene show that collisional (dynamic) quenching is not significant (Figure 3 and Figure 4). The reduced emission lifetimes for both of the hybrid materials is in agreement with the fluorescence (or phosphorescence) quenching and the reduction in emission quantum yield, indicates that either energy or electron transfer process between graphene and the attached porphyrin occurs.[20]

The absence of absorption bands of the porphyrin in UV/Vis absorption spectra for the control samples, prepared by the same procedures as for graphene-TPP and graphene-PdTPP, the disappearance of aldehyde bands in the FTIR spectra of graphene-TPP and graphene-PdTPP, the presence of Pd revealed by XPS and the increased D/G ratio in the Raman spectra for both of the hybrid materials,[10] all indicate the successful functionalization of graphene. Based on TGA data, the degree of functionalization of these two hybrid materials is relatively low, which allows for extended patches of undisturbed graphene. The reduced emission lifetimes for both of the hybrid materials is in agreement with the fluorescence (or phosphorescence) quenching and the reduction in emission quantum yield data, indicates that either energy or electron transfer processes between graphene and the attached porphyrin molecules occurs.[27]

4.3 Porphyrins and molecular motors

4.3.1 System design

The unidirectional rotary motion of overcrowded alkene molecular rotary motors can be driven by a combination of UV light and heat.[21] Photochemical *trans-cis* isomerization of the central double bond and thermal helix inversion, allows for the fully unidirectional rotation to be achieved (scheme 4). A molecular rotary motor, for example **1**, includes an upper part referred to as a rotor, with respect to the symmetrical lower part referred to as a stator. The upper part rotates in four steps driven by UV light and heat, and can be unidirectional with respect to the lower part. When irradiated by UV light, the upper part undergoes a *trans-cis* isomerization of the central double bond which acts as the axis of rotation to form

the unstable form (Scheme 4, step 1). Upon a subsequent thermal step that releases the strain of the helix, with a concomitant slippage of the methyl over the lower part, 180° rotation is achieved (Scheme 4, step 2). The full 360° rotation is completed by another photoisomerization and thermal isomerization step (Scheme 4, step 3 and step 4).
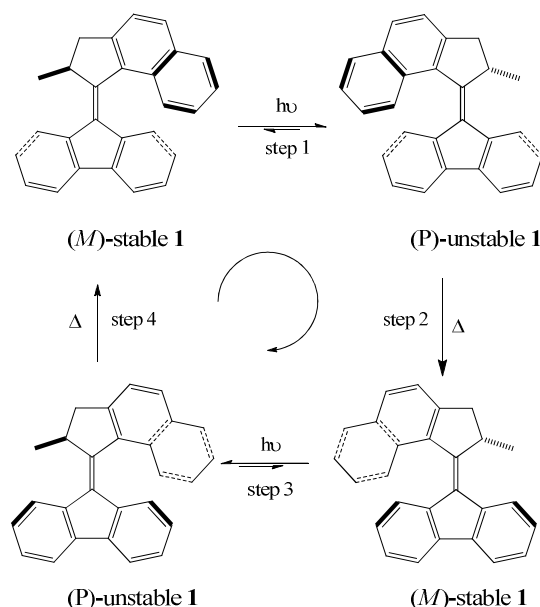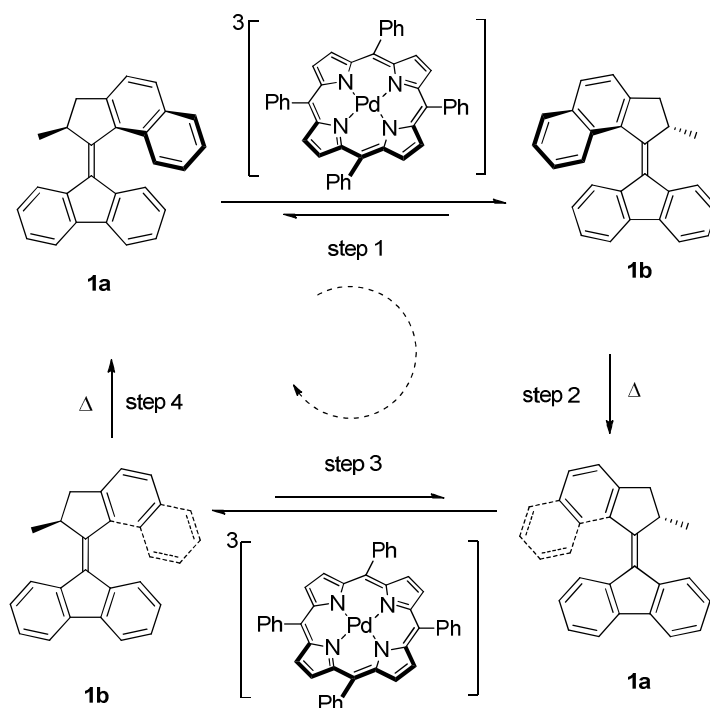

Scheme 4. Isomerization of a molecular motor driven by light and heat to achieve unidirectional rotation.

The triplet excited state of molecular rotary motors has not been directly measured to date, but it can be estimated using time-dependent density functional theory (TD-DFT) calculations. TD-DFT calculations at the B3LYP/6-31G(d,p)[22,23,24] level of theory gives a value of 182 kJ/mol. [25] Accessing the triplet state of the motor requires a photosensitizer, which has a similar triplet energy state and high triplet quantum yield. Palladium tetraphenylporphyrin (PdTPP) is chosen as a candidate, as it has a relatively long-lived triplet state lifetime (up to 2 ms) and relatively high triplet quantum yield (ca. 0.5). [19] In addition, it has a strong absorption in the visible region, which allows for selective excitation of PdTPP in the presence of **1**. The triplet energy of PdTPP is 178 kJ/ mol,[26] which is similar to that predicted for the molecular motor.

Both inter- and intramolecular energy transfers from PdTPP to **1** to drive unidirectional rotation were studied. Intermolecular energy transfer involves directly mixing **1** with PdTPP in solution. Step 1 and step 3 in scheme 3 would be driven by collisional energy transfer from PdTPP, which was excited by visible

light (scheme 5). A covalent system was designed to allow for intramolecular energy transfer (scheme 6) to increase the effective molarity and thus the efficiency of energy transfer. In energy transfer processes, the distance and orientation between the donor and acceptor is important. In the covalent system employed a flexible, non-conjugated linker was used, which precludes through-bond interactions, with an ester formation as the final coupling step.

Scheme 5. Excitation of PdTPP with visible light followed by efficient intersystem crossing generates the triplet excited state in porphyrin. Intermolecular energy transfer to the molecular motor drives isomerization of the central olefinic bond. Thermal helix inversion of the unstable form completes one half rotation. (Synthesis by Arjen Cnossen).
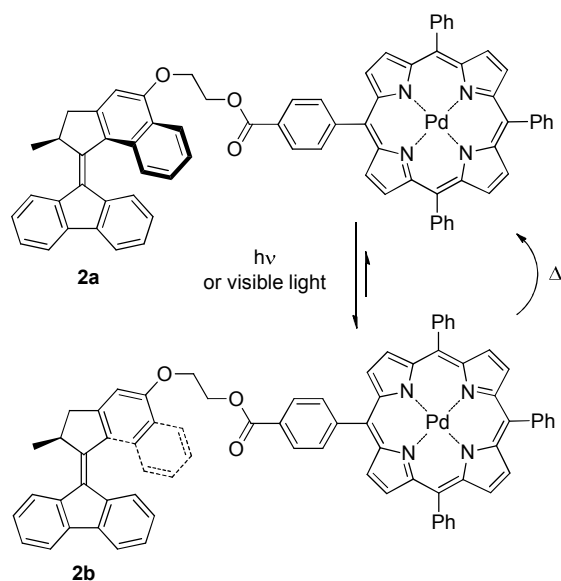
Scheme 6. Expected isomerization behaviour of **2**. (Synthesis by Arjen Cnossen)

4.3.2 Results and discussion

4.3.2.1 Intermolecular energy transfer to drive the molecular motors using PdTPP

The photoisomerization of molecular motor **1** can be monitored by UV/vis absorption spectroscopy. The band at ca. 375 nm broadens and undergoes a red shift upon irradiation at e.g. 365 nm (the solid line and dashed line in the Figure 7, respectively). For **1** in 1,2-dichloroethane at 293 K, the photo stationary state (PSS) was reached within 3 min by irradiated at 365 nm. The absorption spectrum of PdTPP (Figure 7) overlaps partially with that of **1** with the Soret band dominating the absorption spectrum.
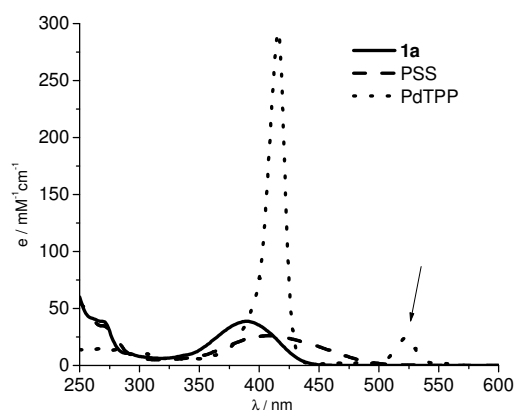

Figure 7. UV/vis absorption spectra of **1a** (solid line), the PSS mixture of **1a** and **1b** obtained by irradiation at 365 nm (dashed line) and PdTPP (dotted line).

Irradiation of the porphyrin at 420 nm would also lead to direct excitation and isomerization of **1**. Hence irradiation was carried out at a wavelength resonant with one of the Q-bands (indicated by the arrow in Figure 7) of the porphyrin, at longer wavelengths than the absorption of both the stable and the unstable forms of **1**. Excitation at 530-550 nm was achieved by the use of a visible light source with an appropriate band pass filter or a 532 nm pulsed laser.

An argon purged solution of **1** alone and a 1:1 mixture of PdTPP and **1** (5 µM) were irradiated at 532 nm (pulsed laser, 6 ns, 10 Hz). A red shift in the absorption was observed, corresponding to the photoisomerization of motor **1** (Figure 8), as observed before upon direct irradiation of **1** with UV light. The change in absorption is minor and partially obscured by the overlap with the porphyrin absorption, but is nevertheless reproducible, and the spectrum recovers in the dark within 20 min due to the thermal helix inversion. In contrast, when a solution of **1** only was irradiated under the same conditions, changes were not observed in the UV/vis absorption spectrum, confirming that the photochemistry of **1** cannot be driven directly at 532 nm.

Figure 8. UV/vis absorption spectra of a mixture of **1** and PdTPP (full line) and the same mixture after irradiation at 532 nm (dashed line). Inset: expansion of the 350-400 nm region.

CD spectroscopy was employed to further characterize the photoisomerization of **1**. Enantiomerically pure *(S)*-**1** was obtained by preparative chiral stationary phase HPLC. Upon irradiation at 546(±5) nm of a solution of *(S)*-**1**, the major bands in the CD spectrum decrease in intensity, which implies the formation of

the unstable form with opposite helicity (Figure 9). The bands do not invert fully, even upon prolonged irradiation, which can be rationalized by a relatively low PSS; from the decrease in signal intensity a ratio **1a**:**1b** of about 75:25 can be estimated. Upon heating to 40 °C for 20 min, the spectral changes in both the UV/vis absorption and the CD spectra are reversed.

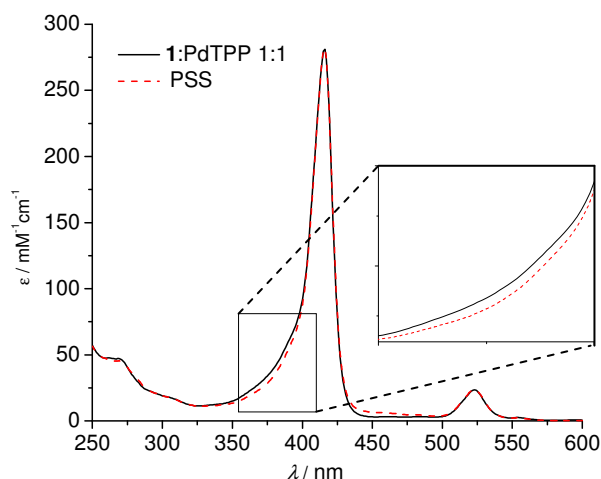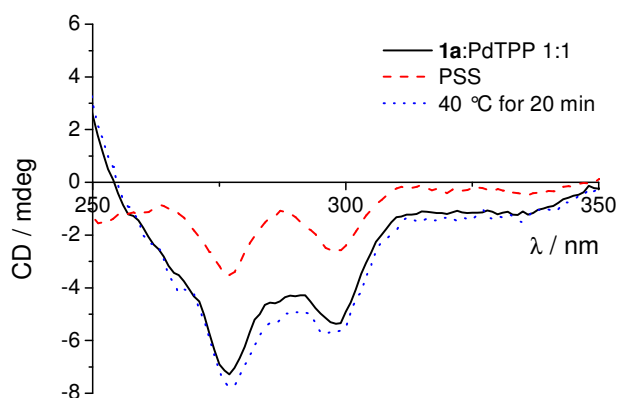**Figure 9.** CD spectra of a mixture of **1** and PdTPP (full line) and the same mixture after irradiation at 532 nm (dashed line) and subsequent heating to 40 °C for 20 min (dotted line).

The unidirectional rotation of the motor by triplet sensitization was characterized by ^{1}H NMR. A methoxy substituent was introduced in the lower half, which enable to distinguish the four distinct steps in the rotary cycle of the motor. The detailed ^{1}H NMR spectra and discussion can be found in the published paper.

4.3.2.2 Intramolecular energy transfer to drive the molecular motors using PdTPP

As for the intermolecular system, the performance of a covalent motor-porphyrin hybrid **2** was examined by UV/vis absorption and CD spectroscopy. When irradiated at 532 nm (6 ns, 10 Hz) for 10 s, the PSS of an argon purged solution of **2** was reached, and this resulted in an increase in absorbance between 450 nm and 500 nm with a concomitant minor red-shift of the shoulder around 375 nm (Figure 10). The isomerization was performed repeatedly, with irradiation at 532 nm for 10 s followed by standing in the dark for 20 min for four cycles, with the change in absorbance monitored at 460 nm (Figure 10, inset). The excellent reversibility of the UV/vis absorption spectral changes of **2** indicates that the photoisomerization of the motor part is reversible and degradation does not occur.

The changes in the UV/vis absorption spectrum upon irradiation are somewhat obscured by overlap of the strong Soret band of the porphyrin. However, with CD spectroscopy characteristic spectral changes are also expected in the 250-350 nm region, where the porphyrin has negligible absorption. Indeed, when a solution of (*R*)-**2a** is irradiated at 532 nm, a distinct decrease in the intensity of the CD signal is observed (Figure 11). As was the case for **1**, complete inversion was not observed, presumably due to a relatively poor PSS (*vide infra*). The observed spectral changes are fully reversible when thermal helix inversion is allowed to take place by heating to 40 °C for 20 min.
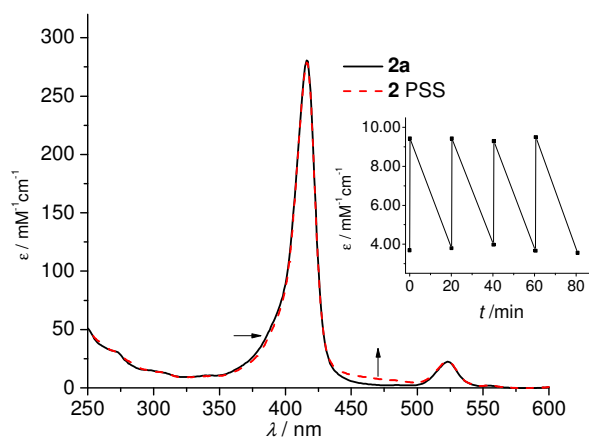

Figure 10. UV/vis absorption spectrum of **2a** (full line) and the mixture of **2a** and **2b** obtained after irradiation at 532 nm (dashed line). Inset: Molar absorptivity at 460 nm of a solution of **2** irradiated at 532 nm for 10 s and left in the dark at rt for 20 min over 4 cycles.
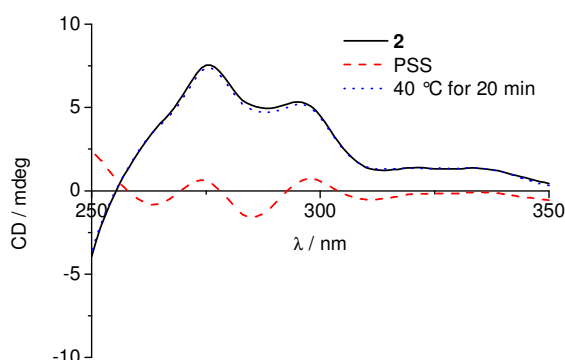

Figure 11. CD spectra of **2a** (full line) and the mixture of **2a** and **2b** obtained after 10 s irradiation at 532 nm (dashed line) and the mixture after the thermal step (dotted line). Note that the opposite stereoisomer is used compared with **1** (Figure 9).

It is worth pointing out that if molecular motor **1** is attached covalently to a non-palladated porphyrin (**3**) instead, no changes are observed in either the UV/vis absorption or the CD spectra. Prolonged irradiation led to irreversible changes in the CD spectrum, which are attributed to degradation. Subsequent standing in the dark for more than 20 min, did not lead to a reversal to the original spectrum (Figure 12). The results of the irradiation experiments using non-metallated motor-porphyrin hybrid **3** implied that the rotation upon visible light irradiation proceeds via triplet energy transfer and not via energy transfer involving a singlet excited state.

3
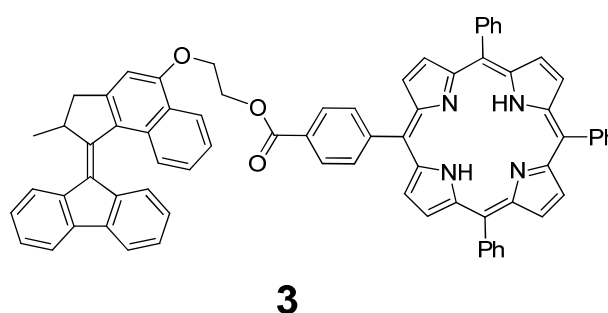
Scheme 7. Molecular structure of molecular motor **1** attached covalently to non-palladated porphyrin **3**.
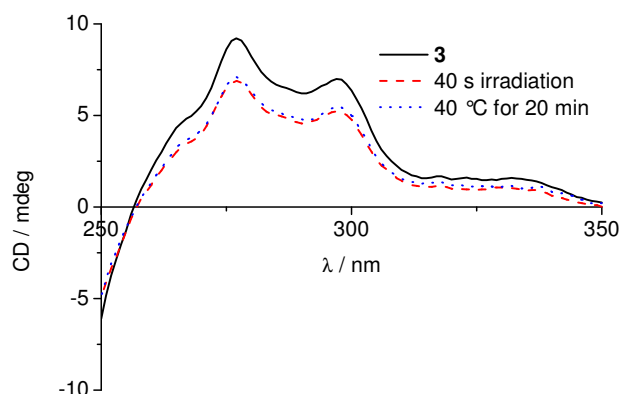

Figure 12. CD spectra of **3** before (solid line) and after 40 s irradiation at 532 nm (dashed line) and after heating at 40 °C for 20 min (dotted line).

4.3.2.3 Luminescence lifetime and quenching

Conclusive demonstration that energy transfer from the triplet state occurs was provided by luminescence spectroscopy and lifetimes of the porphyrins. Steady-state emission spectra of PdTPP, a mixture of PdTPP and **1** with a ratio of 1:2.5 and motor-PdTPP hybrid **2** were recorded (Figure 13) in 1,2-dichloroethane under argon atmosphere. PdTPP, irradiated with visible light (e.g. 532 nm), gives fluorescence at 610 nm and phosphorescence at 710 nm.[26] The phosphorescence quantum yield for PdTPP is significantly reduced by the molecular motor, both in inter- and intramolecular fashion, which is attributed to energy transfer from PdTPP to the motor (Table 1). The quenching of phosphorescence in **2** was greater than in the mixture of **1** and PdTPP under the same conditions (Figure 13 a). In contrast, the fluorescence quantum yield for PdTPP was not influenced by the presence of the molecular motor. This confirms that energy transfer is not via singlet energy transfer but via triplet energy transfer. As a control, the steady-state fluorescence of H_2TPP was compared to that of **3**; quenching of singlet excited state and energy transfer was not observed and there was no change in the fluorescence quantum yield (Figure 13(b)).
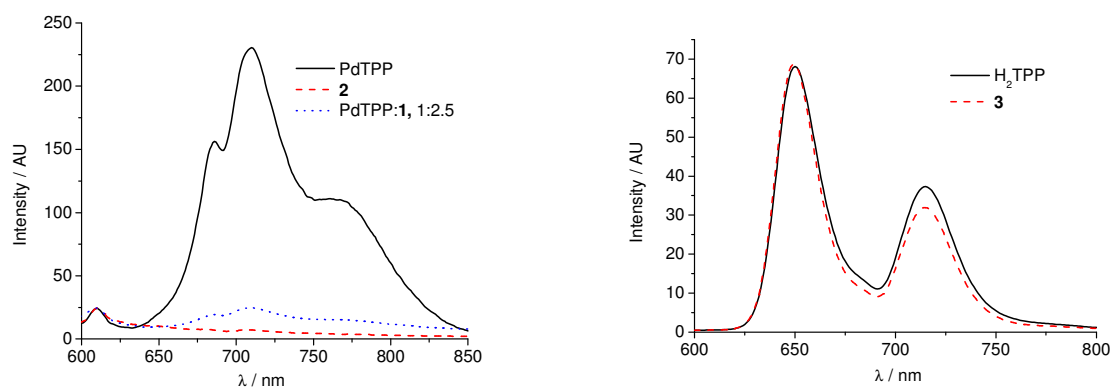
Figure 13. (a) Emission spectra of PdTPP (2×10^{-5} M, solid line), a 1:2.5 mixture of PdTPP and **1** (PdTPP 2×10^{-5} M, **1** 5×10^{-5} M, dashed line), and **2** (2×10^{-5} M, dotted line) under Ar atmosphere, λ_{exc} = 532 nm. (b) Emission spectra of H_2TPP (solid line) and **3** (dashed line) excited at 418 nm (in chloroform, 1×10^{-5} M).

Intra- and intermolecular energy transfer were further studied by measuring phosphorescence lifetime by laser flash photolysis spectroscopy. The phosphorescence decay curves of PdTPP, a 1:2.5 mixture of PdTPP and **1**, and **2** were recorded at 710 nm (Figure 14 and Table 1). The lifetimes were fitted with first order exponential decays. The phosphorescence lifetime was reduced from

34 µs for PdTPP to 9 µs for the mixture of PdTPP and **1**, and to 0.41 µs for **2**, which confirms that quenching of PdTPP triplet excited state occurs. As expected, the covalent system **2** shows more efficient energy transfer than the mixture of PdTPP and **1**, as the latter relies on diffusion controlled quenching.
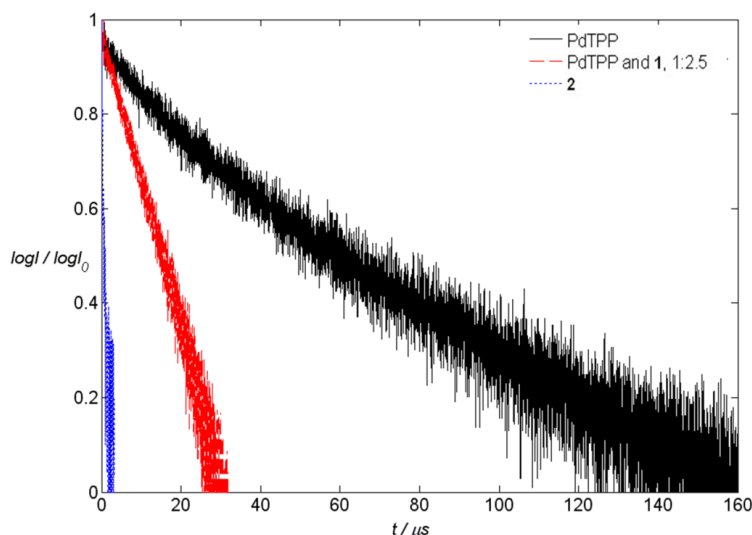

Figure 14. Room temperature phosphorescence lifetime measurements of PdTPP (black line), a 1:2.5 mixture of PdTPP and **1** (red line), and **2** (blue line) in 1,2-dichloroethane in Argon-saturated solution. Measured at 710 nm with excitation at 532 nm (6 ns, 10 Hz).

Table 1. Photophysical properties of PdTPP, PdTPP with **1**, **3**. [a]

	Fluor. λ_{max}(nm)	Phosphor. λ_{max} (nm)	Φ_f (%)[b]	Φ_p (%)[b]	τ_T (µs)
PdTPP	610	710	~0.01	0.5±0.1	36±4
PdTPP:**1**	610	710	~0.01	~0.05	9±1
2	610	-	~0.01	<0.04	~0.41

[a] All the measurement were performed in Ar-saturated 1,2-dichloroethane. Fluorescence quantum yield Φ_f, phosphorescence quantum yield Φ_p and triplet lifetime τ_T. [b] The quantum yields were determined using [Ru(bpy)$_3$](PF$_6$)$_2$ in water as reference ($\Phi = 0.028$).

The phosphorescence lifetime of PdTPP in the presence of the motor at concentrations between 0.0 and 0.5 mM in (argon-saturated) 1,2-dichloroethane were determined and the data is shown in the form of a Stern-Volmer plot (τ_0/τ vs **1** concentration, Figure 15). A linear fit yielded a bimolecular quenching rate constant k_q of 1.8×10^9 M^{-1} s^{-1} for the quenching of ^{3}PdTPP* by **1**. The diffusion-

controlled rate constant in 1,2-dichloroethane is approximately 8.9×10^9 M^{-1} s^{-1} at 25 °C.[27] This indicates that energy transfer is diffusion controlled in the present intermolecular system.
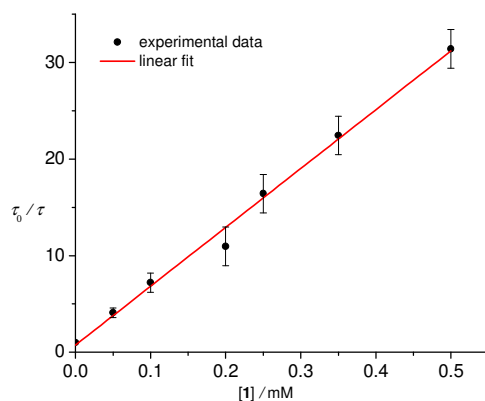

Figure 15. Stern-Volmer plot for quenching of PdTPP by **1** (points) and linear fit (solid line).

4.4 Summary

In the graphene-TPP and graphene-PdTPP hybrid materials studies, the presence of porphyrins was confirmed by UV/vis absorption spectroscopy. Energy and/or electron transfer quenching between graphene and the covalently bound porphyrin molecules was demonstrated by fluorescence and phosphorescence quenching, in which the intensity of emission is significantly decreased. Furthermore by TCSPC and laser flash photolysis spectroscopy, a concomitant decrease in excited state lifetimes is observed. Considering the remarkable properties of both graphene and porphyrin, these two hybrid materials may have potential applications in a number of areas, such as solar cells, sensors and catalysis.

In the second part of this chapter, driving unidirectional molecular rotary motors with visible light by intra- and intermolecular energy transfer from palladium porphyrins was investigated. The photoisomerization was characterized by UV/vis and CD spectroscopy and it was found that the sensitized photoisomerization proceeds similar to photoisomerization by direct irradiation by UV light. Energy transfer from the triplet excited state was confirmed by steady state emission and laser flash photolysis spectroscopy with a dramatic decrease in phosphorescence intensity and lifetime, and this is further confirmed by comparison with a non-metallated motor-porphyrin hybrid. As expected,

energy transfer from the porphyrin to the motor takes place in an intermolecular fashion to drive the photoisomerization. However, covalent linking of the motor to the porphyrin increases the efficiency of energy transfer from the porphyrin to the motor substantially compared with intermolecular energy transfer in driven the photoisomerization. Driving molecular motors with visible light expands their use to biological systems and might have potential applications in molecular information processing.

4.5 Experimental Section

Details ofg syntheses and preparation of graphene hybrid materials and porphyrin motor hybrid are described in reference [28] and [29].

General remarks

All spectra were recorded in 1×1 cm quartz cuvettes. UV/Vis absorption spectra were measured on JASCO V-630 spectrometer. Emission spectra were measured using a JASCO FP-6200 spectrofluorimeter. CD spectra were measured on JASCO J-815 CD spectrometer. Room temperature phosphorescence spectra were obtained in 1,2-dichloroethane under an Argon atmosphere with degassing by at least three freeze-pump-thaw cycles. Phosphorescence lifetimes were obtained using a home built system. Excitation was performed using the second harmonic (532 nm, 10 Hz, 2 mJ, 6 ns) of a Q-switched Nd:YAG laser (Innolas 400) with a Si-diode trigger sensor. The emission from the sample was focused into a Zolix Omni-λ 300 monochromator coupled with a Zolix PMTH-S1-CR131 side-on PMT. Emission decay traces were recorded with 50 Ohm termination on a Tetronix DPO 4032 digital phosphor Oscilloscope and transferred to a PC for data analysis using homebuilt software written in National Instruments LabVIEW 8.2. Quantum yield measurements were determined using $[Ru(bpy)_3](PF_6)_2$ in water as a reference (0.028). Fluorescence lifetime measurements were performed using a time-correlated single photon counting system, and detected using a microchannel plate PMT coupled with 630 nm long pass filter. The light source was a Ti:Sapphire laser (400 nm, 1.9 MHz).

Motor porphyrin solutions were bubbled with Argon for at least two minutes before irradiation. Irradiation was carried out with a fluorescent lamp and a 546±5 nm bandpass filter, and the solutions were cooled to -40 °C using a

cryostat. Depending on the concentration, irradiation times were up to 1 h at ~10^{-5} M and overnight for samples used for NMR spectroscopy (~10^{-3} M). Irradiation with a pulsed laser at 532 nm was carried out at 20 °C with measurement performed within 30 s. In general, a PSS was reached within 10 s of irradiation. To confirm that the photostationary states were reached, several spectra at set intervals were recorded. Thermal isomerization was performed by leaving the solutions in the dark at 20-40 °C for at least 20 min. The solution was then cooled again to the temperature at which irradiation was performed previously before further measurement.

4.5 References

[1] K. M. Kadish, K. M. Smith, R. Guilard, *The Porphyrin Handbook*, Academic Press, the Netherlands, **2003**.

[2] E. D. Sternberg, D. Dolphin, C. Bruckner, *Tetrahedron*, **1998**, *54*, 4151-4202.

[3] W. M. Campbell, K. W. Jolley, P. Wagner, K. Wagner, P. J. Walsh , K. C. Gordon, L. Schmidt-Mende, M. K. Nazeeruddin, Q. Wang, M. Grätzel, D. L. Officer, *J. Phys. Chem. C*, **2007**, *111*, 11760–11762.

[4] D. M. Guldi, G. M. A. Rahman, V. Sgobba, C. Ehli, *Chem. Soc. Rev.* **2006**, *35*, 471-487.

[5] (a) A. K. Geim, K. S. Novoselov, *Nat. Mater.*, **2007**, *6*, 183-191; (b) A. K. Geim, *Science,* **2009**, *324*, 1530-1534; (c) M. J. Allen, V. C. Tung, R. B. Kaner, *Chem. Rev.,* **2010**, *110*, 132-145; (d) C. N. R. Rao, A. K. Sood, K. S. Subrahmanyam, A. Govindaraj, *Angew. Chem.,* **2009**, *121*, 7890-7816; *Angew. Chem. Int. Ed.,* **2009**, *48*, 7752-7777; (e) K. P. Loh, Q. Bao, P. K. Ang, J. Yang, *J. Mater. Chem.,* **2010**, *20*, 2277-2289; (f) Y. Zhu, S. Murali, W. Cai, X. Li, J. W. Suk, J. R. Potts, R. R. Ruoff, *Adv. Mater.,* **2010**, *22*, 3906-3924.

[6] (a) M. D. Stoller, S. Park, Y. Zhu, J. An, R. S. Ruoff, *Nano Lett.,* **2008**, *8*, 3498-3502; (b) H. Wang, H. S. Casalongue, Y. Liang, H. Dai, *J. Am. Chem. Soc.,* **2010**, *132*, 7472-7477; (c) Z. S. Wu, W. Ren, D. W. Wang, F. Li, B. Liu, H. M. Cheng, *ACS Nano,* **2010**, *4*, 5835-5842; (d) C. Liu, Z. Yu, D. Neff, A. Zhuma, B. Z. Jand, *Nano Lett.,* **2010**, *10*, 4863-4868.

[7] (a) C. Jozsa, M. Popinciuc, N. Tombros, H. T. Jonkman, B. J. van Wees, *Phys. Rev. Lett.,* **2008**, *100*, 236603; (b) K. S. Kim, Y. Zhao, H. Jang, S. Y. Lee, J. M. Kim, K. S. Kim, J. H. Ahn, P. Kim, J. Y. Choi, B. H. Hong, *Nature,* **2009**, *457*, 706-710; (c) X. Wang, L. Zhi, K. Müllen, *Nano Lett.,* **2008**, *8*, 323-327; (d) X. Wang, Y. Ouyang, X. Li, H. Wang, J. Guo, H. Dai, *Phys. Rev. Lett.,* **2008**, *100*, 206803; (e) C. Di, D. Wei, G. Yu, Y. Liu, Y. Guo, D. Zhu, *Adv. Mater.,* **2008**, *20*, 3289-3293.

[8] (a) F. Schedin, A. K. Geim, S. V. Morozov, E. W. Hill, P. Blake, M. I. Katsnelson, K. S. Novoselov, *Nat. Mater.,* **2007**, *6*, 652-655; (b) J. D. Fowler, M. J. Allen, V. C. Tung, Y. Yang, R. B. Kaner, B. H. Weiller, *ACS Nano,* **2009**, *3*, 301-306; (c) Y. Wen, F. Xing, S. He, S. Song, L. Wang, Y. Long, D. Li, C. Fan, *Chem. Commun.,* **2010**, *46*, 2596-2598; (d) C. Lu, J. Li, J. Liu, H. Yang, X. Chen, G. Chen, *Chem. Eur. J.,* **2010**, *16*, 4889-4894; (e) Q. Zhang, Y. Qiao, F. Hao, L. Zhang, S. Wu, Y. Li, J. Li, X. Song, *Chem. Eur. J.,* **2010**, *16*, 8133-8139.

[9] (a) S. Stankovich, D. A. Dikin, G. H. B. Dommett, K. M. Kohlhaas, E. J. Zimney, E. A. Stach, R. D. Piner, S. T. Nguyen, R. S. Ruoff, *Nature,* **2006**, *442*, 282-286; (b) J. Shen, Y. Hu, C. Li, C. Qin, M. Ye, *Small,* **2009**, *5*, 82-85; (c) D. Cai, M. Song, *J. Mater. Chem.,* **2010**, *20*, 7906-7915; (d) T. Ramanathan, A. A. Abdala, S. Stankovich, D. A. Dikin, M. Herrera-Alonso, R. D. Piner, D. H. Adamson, H. C. Schniepp, X. Chen, R. S. Ruoff, S. T. Nguyen, I. A. Aksay, R. K. Prud'Homme, L.C. Brinson, *Nat. Nanotechnol.,* **2008**, *3*, 327-331.

[10] X. Zhang, L. Hou, A. Cnossen, A. C. Coleman, O. Ivashenko, P. Rudolf, B. J. van Wees, W. R. Browne, B. L. Feringa, *Chem. Eur. J.,* **2011**, *17*, 8957-8964.

[11] (a) B. L. Feringa, *J. Org. Chem.,* **2007**, *72*, 6635-6652; (b) M. M. Pollard, M. Klok, D. Pijper, B. L. Feringa, *Adv. Funct. Mater.,* **2007**, *17*, 718-729.

[12] J. Wang, B. L. Feringa. *Science,* **2011**, *331*, 1429-1432.

[13] (a) R. A. Van Delden, M. K. J. Ter Wiel, M. M. Pollard, J. Vicario, N. Koumura, B. L. Feringa, *Nature,* **2005**, *437*, 1337-1340; (b) M. M. Pollard, M. Lubomska, P. Rudolf, B. L. Feringa, *Angew. Chem. Int. Ed.*, **2007**, *46*, 1278-1280; (C) G. London, G. T. Carroll, T. F. Landaluce, M. M. Pollard, P. Rudolf, B. L. Feringa, *Chem. Commun.,* **2009**, 1712-1714.

[14] T. Kudernac, N. Ruangsupapichat, M. Parschau, B. Macia, N. Katsonic, S. R. Harutyunyan, K. H. Ernst, B. L. Feringa, *Nature*, **2011**, *479*, 208-211.

[15] (a) R. H. Douglas, J. C. Partridge, K. S. Dulai, D. M. Hunt, C. W. Mullineaux, P. H. Hynninen, *Vision Res.,* **1999**, *39*, 2817-2832; (b) T. Okada, O. P. Ernst, K. Palczewski, K. P. Hofmann, *Trends Biochem. Sci.,* **2001**, *26*, 318-324.

[16] (a) G. S. Hammond, J. Saltiel, A. A. Lamola, N. J. Turro, J. S. Bradshaw, D. O. Cowan, R. C. Counsell, V. Vogt, C. Dalton, *J. Am. Chem. Soc.* **1964**, *86*, 3197-3217. (b) R. Benson, D. F. Williams, *J. Phys. Chem.* **1977**, *81*, 215-220.

[17] (a) A. S. Lukas, M. R. Wasielewski, *Molecular Switches* (Ed.: B. L. Feringa,), Wiley-VCH, Weinheim, **2001**, pp. 1-35; (b) D. Gust, T. A. Moore, A. L. Moore, *Chem. Commun.,* **2006**, 1169-1178.

[18] (a) M. Quintana, K. Spyrou, M. Grzelczak, W. R. Browne, P. Rudolf, M. Prato, *ACS Nano,* **2010**, *4*, 3527-3533; (b) V. Georgakilas, A. B. Bourlinos, R. Zboril, T. A. Steriotis, P. Dallas, A. K. Stubos, C. Trapalis, *Chem. Commun.,* **2010**, *46*, 1766-1768; (c) X. Zhong, J. Jin, S. Li, Z.

Niu, W. Hu, R. Li, J. Ma, *Chem. Commun.,* **2010**, *46*, 7340-7342; (d) T. A. Strom, E. P. Dillon, C. E. Hamilton, A. R. Barron, *Chem. Commun.,* **2010**, *46*, 4097-4099; (e) L. H. Liu, M. M. Lerner, M. Yan, *Nano Lett.* **2010**, *10*, 3754-3756.

[19] D. Eastwood, M. Gouterman, *J. Mol. Spectrosc.*, **1970,** *35,* 359-375.

[20] (a) S. Campidelli, C. Sooambar, E. Lozano Diz, C. Ehli, D. M. Guldi, M. Prato, *J. Am. Chem. Soc.,* **2006**, *128*, 12544-12552; (b) F. D'Souza, R. Chitta, A. S. D. Sandanayaka, N. K. Subbaiyan, L. D'Souza, Y. Araki, O. Ito, *Chem. Eur. J.,* **2007**, *13*, 8277-8284.

[21] (a) N. Koumura, R. W. J. Zijlstra, R.A. van Delden, N. Harada, B. L. Feringa, *Nature*, **1999,** *401*, 152-155; (b) B. L.Feringa, *Acc. Chem. Res.,* **2001,** *34,* 504-513.

[22] A. D. Becke, *J. Chem. Phys*., **1993**, *98*, 1372-1377.

[23] T. C. Lee, W. T. Yang, R. G. Parr, *Phys. Rev. B,* **1988**, *37*, 785-789.

[24] R. Krishnan, J. S. Binkley, R. Seeger, J. A. Pople, *J. Chem. Phys.* **1980**, *72*, 650-654.

[25] These calculations are known to have a significant margin in the determination of the energy of electronically excited states, see S. Grimme, F. Neese, *J. Chem. Phys.* **2007**, *127*, 154116.

[26] J. E. Rogers, K. A. Nguyen, D. C. Hufnagle, D. G. McLean, W. Su, K. M. Gossett, A. R. Burke, S. A. Vinogradov, R. Pachter, P. A. Fleitz, *J. Phys. Chem. A,* **2003**, *107*, 11331-11339.

[27] M. Montalti, A. Credi, L. Prodi, M. T. Gandolfi, *Handbook of Photochemistry*, CRC Press, Boca Raton, **2006**, pp. 424.

[28] X. Zhang, L. Hou, A. Cnossen, A. C. Coleman, O. Ivashenko, P. Rudolf, B. J. van Wees, W. R. Browne, B. L. Feringa, *Chem. Eur. J.* **2011**, *17*, 8957-8964.

[29] A. Cnossen, L. Hou, M. M. Pollard, P. V. Wesenhagen, W. R. Browne, B. L. Feringa, *J. Am. Chem. Soc*. **2012**, *134*, 17613-17619.

CHAPTER 5

Photochemical Control of Singlet Oxygen Generation Using Diarylethene Switches [1]

In this chapter, the ability of diarylethene switches to control the photosensitized generation of singlet oxygen is demonstrated. The generation of singlet oxygen by a porphyrin photosensitizer is observed when the diarylethene is in the ring open form. After switching to the closed form by UV irradiation, singlet oxygen generation is not observed. Irradiation of the closed form with green light leads to a recovery in singlet oxygen generation. The non-invasive control of singlet oxygen generation by light has potential for further application in photodynamic therapy.

---

[1] L. Hou, X. Zhang, T. Pijper, W. R. Browne, B. L. Feringa, to be submitted

5.1 Introduction

Singlet oxygen ($^1O_2$), the first excited state of molecular oxygen, is highly reactive and can damage organic materials and biological tissues.[1] $^1O_2$ has been studied intensely over several decades to understand a variety of processes, including photodegradation, photobleaching, photochemical synthesis, etc.[2] One of the most important applications of singlet oxygen generation is in photodynamic therapy (PDT),[3] which is used clinically to treat diseases by exposing targets to light.[4] The use of a non-toxic photosensitizer and its ability to generate $^1O_2$ are crucial to the success of PDT. Upon irradiation with light, localized photosensitizers transfer energy to triplet oxygen ($^3O_2$) and generate $^1O_2$, which can react with tumors or diseased cells and destroy them chemically.

Considerable effort has been devoted to improving the performance of photosensitizers to generate $^1O_2$ efficiently.[5,6,7] Besides this, developing controllable and regulated singlet oxygen sensitizers has received increasing attention recently, since it could provide efficient and selective control in PDT, and limit nonspecific photodamage in the body.[8,9] Several approaches for controlling generation and deactivation of $^1O_2$ have been reported, e.g., through environmental changes (including solvent[10] or pH[11,12]), programming with enzymes or DNA,[13,14] or interacting with nanomaterials,[15] e.g., carbon nanotubes,[16] and quantum dots.[17] These controllable systems provide two states of the sensitizers, on and off, towards generation of $^1O_2$, which can minimize side effects under prolonged exposure to light. However, changing environments generally need invasive treatments during PDT and the reversible control is complicated. Moreover, some effective changes needed to control the activation of $^1O_2$ are not tolerant and/or toxic in the body, which limits further applications in PDT. Photosensitizers, that are cleaved from a polymer or short peptide sequence upon enzymatic digestion or dissociated from the nanomaterials and bound to the targets, cannot be controlled to reverse to the off state of $^1O_2$ generation. Therefore, it is a challenging task to design a system that can non-invasively switch on and off of $^1O_2$ generation efficiently and reversibly.

Here, a non-covalent strategy to regulate $^1O_2$ generation by photosensitizers using the two states of diarylethene switches is described, in which on and off switching of $^1O_2$ generation is fully reversible and can be achieved upon irradiation with light at distinct wavelengths. Diarylethene molecular switches

can be reversed between a ring open and ring closed forms with UV and visible light, respectively. [18,19] The structural differences between the states result in large difference in properties, e.g., energy levels, color, polarizability, conformation and flexibility. Due to the thermal stability, fatigue resistance and high efficiency in photoisomerization, diarylethene switches have been applied in areas such as information storage in nanotechnology,[20,21,22] photonic devices, [23] biochemical reactivity, [24] etc. Zinc-tetraphenylporphyrin (ZnTPP), a widely used photosensitizer and whose derivatives has been applied in clinical PDT,[3,25] was chosen as the photosensitizer unit because of its high quantum yield (Φ=0.84) towards $^1O_2$ formation and well-understand photochemistry. [26] Moreover, the partial overlap of the emission spectrum of ZnTPP with the absorption spectrum of the closed form of diarylethene switches, but not with the open form, might allow for switching on and off of energy transfer to $^3O_2$. Instead of a covalent link between switches and photosensitizer, a non-covalent approach is taken, which can reduce the cost of synthesis, especially when considering the challenge of synthesis on a large scale to meet the demand for in vivo imaging and PDT. In addition, a non-covalent system can avoid loss of photochemical performance of both switches and photosensitizer. The current system also shows the possibility to modulate fluorescence of the photosensitizer, which can be applied in super resolution fluorescence microscopy to image and locate drugs during therapy.

5.2 System design

In the current system (Scheme 1 (a)), ZnTPP is mixed with diarylethene switches in air equilibrated solution. Two diarylethene switches were used (Scheme 1(b)) to modulate the generation of singlet oxygen. The pyridine unit of **1** can coordinate to ZnTPP and the presence of a dimethylamine substituent will increase binding affinity in the closed state. The other diarylethene switch, 1,2-bis(2'-methyl-5'-phenylthien-3'-yl)cyclopentene (**2**),[27] is used to compare the capability of regulation of generation of $^1O_2$ and fluorescence without coordination.

Switching between on and off state of $^1O_2$ generation is controlled upon irradiation. ZnTPP is excited at the Soret band ca. 420 nm, and energy transfer from the excited photosensitizer to $^3O_2$ occurs, generating $^1O_2$ (on state), while energy transfer between ZnTPP and the open form of the diarylethene is thermo-dynamically unfavorable, because the energy of the lowest triplet states of the

open switches lies much higher than those of ZnTPP (vide infra). The off state for $^1O_2$ generation can be achieved by irradiating the solution with UV light, resulting in switching the diarylethene to the closed state. The lower triplet energy of the closed form allows for energy transfer from ZnTPP to the ring closed switches, which is highly competitive with energy transfer to oxygen. The on and off states of $^1O_2$ generation can be accessed by alternate irradiation with UV ($\lambda=312$ nm) and visible light (e.g., >470 nm). It should be noted that irradiation at the Soret band of ZnTPP corresponds to a minimum in absorption of both the open and closed switches, minimizing photoinduced changes to the structure of the switches (Figure 1).
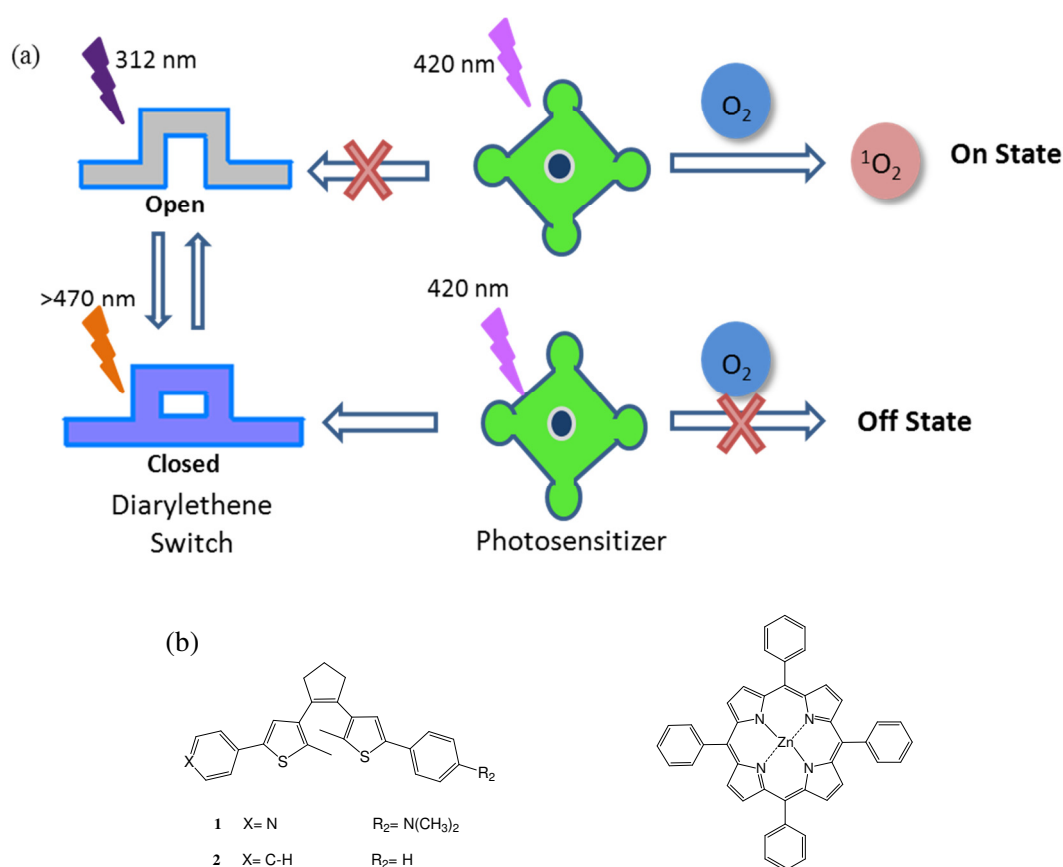
Scheme 1. (a) Photochemical control of the generation of $^1O_2$ by a photosensitizer using diarylethene switches. (b) Structures of the two diarylethene switches and photosensitizer (ZnTPP).

5.3 Results and Discussion

The open form of **1** absorbs in the UV region with the maximum at 324 nm (Figure 1, solid line). UV irradiation (e.g., 312 nm) of the open form of **1** leads to a decrease in absorption between 280 nm to 350 nm, with a concomitant

increase in two new bands at 375 nm and 576 nm of the closed form (Figure 1, dash line). The photostationary state (PSS) was determined by ^{1}H NMR spectroscopy. Irradiation at 312 nm results in 88% conversion to the closed form. The closed form of **1** can be ring opened by irradiation with visible light (>470 nm), with the initial spectrum fully recovered. The presence of the electron withdrawing pyridine group and the electron donating dimethylamine group at each side causes a red shift in the absorption spectra in both forms compared with the phenyl substituted compound **2**.[22] The UV/vis absorption spectrum of ZnTPP is also shown in Figure 1. The Soret band at 423 nm is located at the point of the least absorbance of both open and closed forms of **1** (Figure 1). This minimal overlap can minimize photoinduced changes to **1** upon excitation into the Soret band.
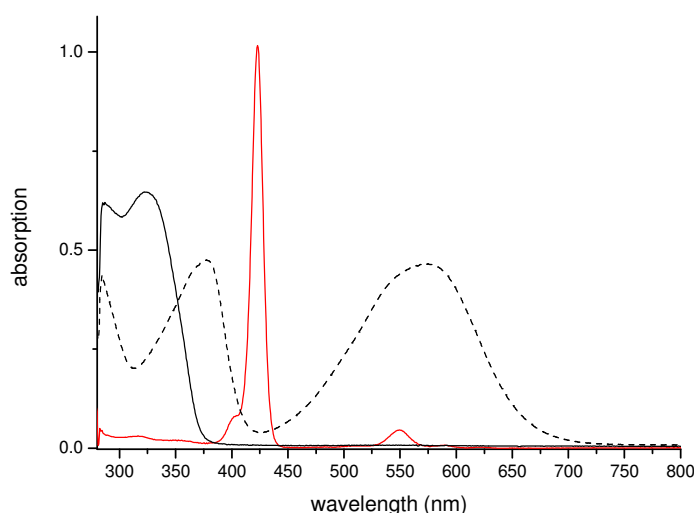

Figure 1. UV/vis absorption spectra of the open form of **1** (20 μM) (solid line) and PSS$_{312\ nm}$ **1** (dash line), and of ZnTPP (2 μM) (red solid line) at room temperature in toluene.

The coordination of **1** to ZnTPP was studied by UV/vis absorption spectroscopy. Titration of ZnTPP with the open or closed form (PSS$_{312\ nm}$ solution) of **1** induced a clear red shift of the Soret band (Figure 2 and Figure 3), and the change in absorbance indicates the formation of 1:1 axially coordinated complexes.[28] The association constants of the open and closed forms are 12000±3000 M^{-1} and 15000±3000 M^{-1}, respectively.
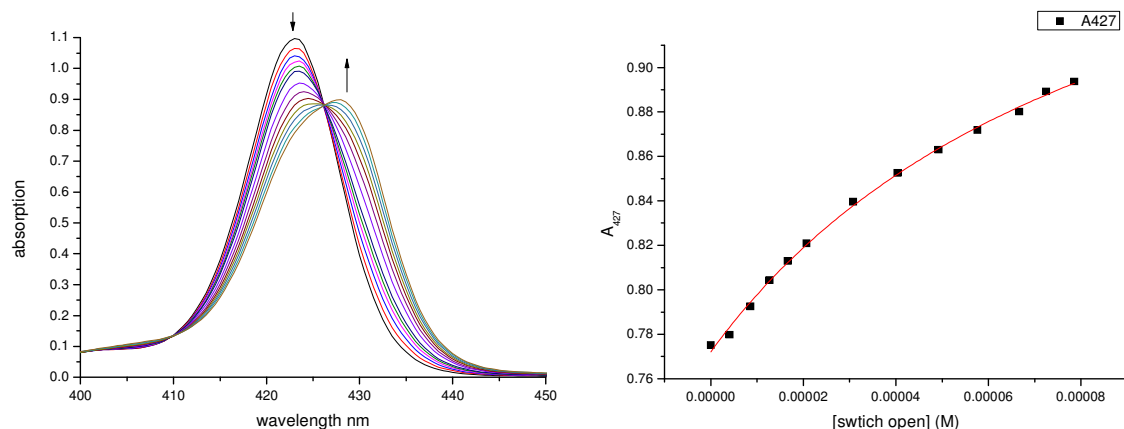
Figure 2. Titration of ZnTPP with the open form of **1** in toluene monitored by UV/vis absorption spectroscopy (left) and absorbance change at 427 nm (right).
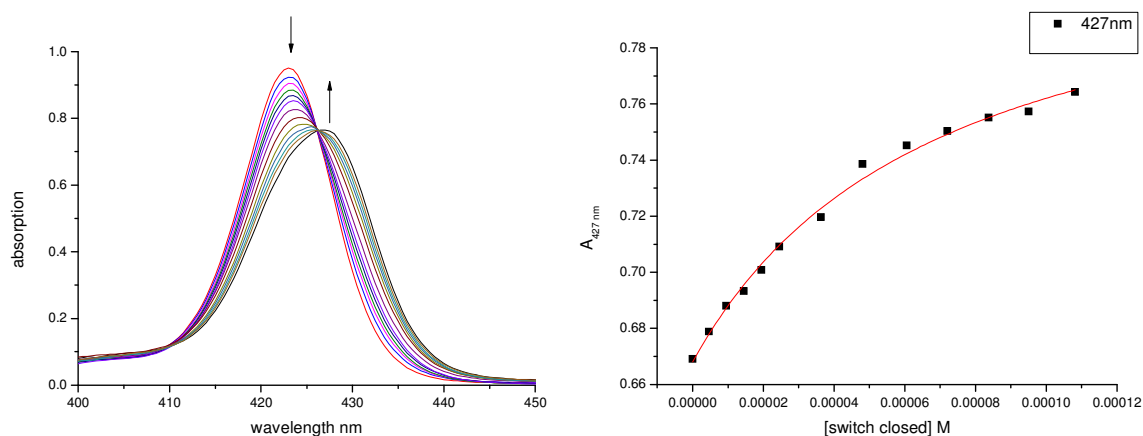

Figure 3. Titration of ZnTPP with the closed form of **1** ($PSS_{312\ nm}$) in toluene monitored by UV/vis absorption spectroscopy (left, the overlap of absorption with ZnTPP was subtracted using a reference titration with equal closed form **1** concentrations without ZnTPP) and absorbance change at 427 nm (right).

The UV/vis absorption spectra of **1** (40 μM) with ZnTPP (2 μM) is shown in Figure 4. The Soret band of ZnTPP is seen at 424 nm and the absorbance is lower compared to that in Figure 1 because of coordination of **1** to ZnTPP. The presence of ZnTPP does not affect the photoswitching behavior of **1** significantly.
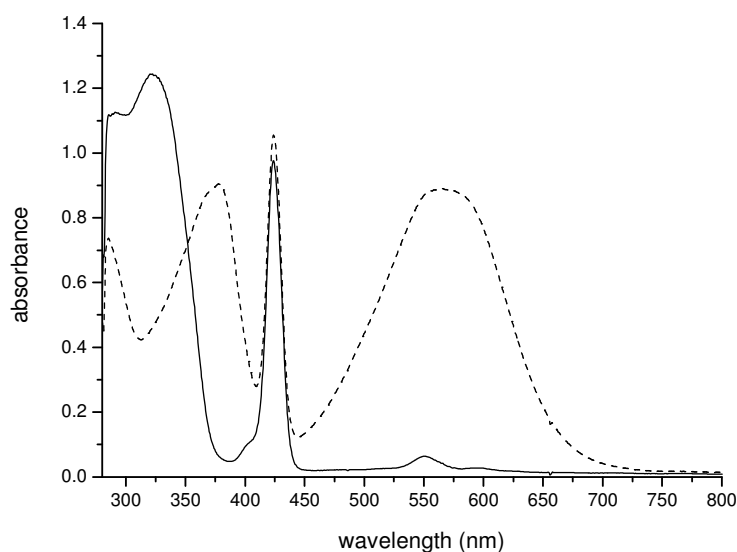
Figure 4. UV/vis absorption spectra of **1** (40 μM) and ZnTPP (2 μM) in aerated toluene at room temperature. The open form of **1** with ZnTPP (solid line), and at the PSS (312 nm) state (dash line).

Photosensitized $^1O_2$ generation was monitored by near-infrared emission spectroscopy, through the phosphorescence of $^1O_2$ at ca. 1270 nm.[2] The emission spectrum of $^1O_2$ in ZnTPP solution is identical in the absence and presence of the open form of **1** (Figure 5, black curve). Irradiating the solution of ZnTPP and **1** at 312 nm converts **1** to its closed form. Remarkably, a more than 93% decrease in $^1O_2$ emission at 1270 nm was observed (Figure 5, red curve). Increasing the concentration of the closed form of **1** in ZnTPP solution can result in a further decrease $^1O_2$ emission. Following irradiation of the solution with visible light (>470 nm), to convert **1** back to the open form, a recovery of $^1O_2$ emission at 1270 nm was observed (Figure 5, blue curve). The change of emission at 1270 nm was monitored over four cycles of switching between open and closed states of **1** (Figure 5, right). These changes indicate that the switching on and off of $^1O_2$ generation is reversible and the switching system is stable. Compound **2**, which cannot bind to ZnTPP, shows similar on and off switching behavior of $^1O_2$ generation (Figure 6). The change in phosphorescence from $^1O_2$ sensitized by ZnTPP in the presence of the closed form of **1** and of **2**, gives quenching constants of $1.03 \pm 0.03 \times 10^{10}$ $M^{-1}s^{-1}$ and $0.82 \pm 0.03 \times 10^{10}$ $M^{-1}s^{-1}$, respectively (Figure 8), which indicates that the energy transfer from ZnTPP to the closed switches is a diffusion controlled process, and that coordination enhances the quenching rate slightly. Switching on and off of $^1O_2$ generation by ZnTPP in the

presence of diarylethene switches is also observed in other solvents, including cyclohexane, THF, ethanol, and ethanol with D_2O (4:1) (Figure 7).
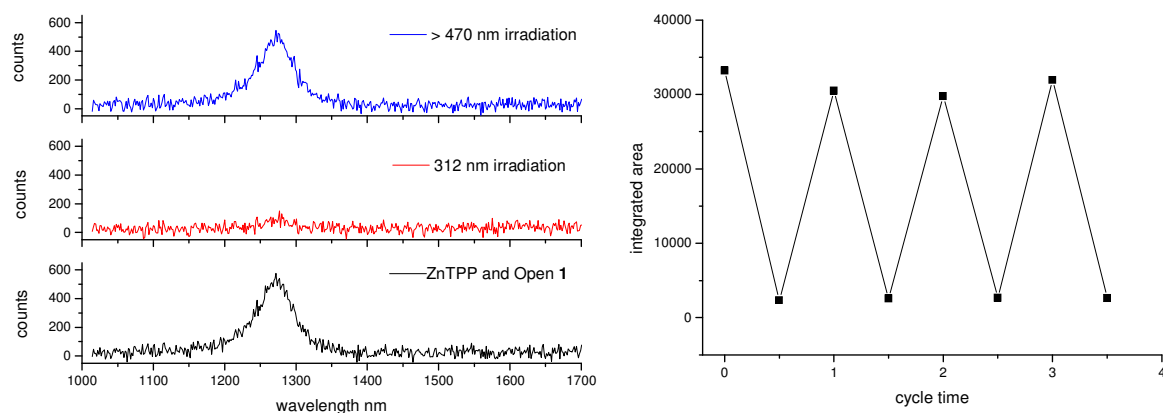

Figure 5. NIR emission of $^1O_2$ generated by ZnTPP (6 µM) in the presence of **1** (30 µM) in air equilibrated toluene; excitation at 405 nm (4 mW). $^1O_2$ generation occurs with the open form of **1** present (left, black) can be switched off (left, red) by irradiation at 312 nm. $^1O_2$ generation was recovered by irradiation at >470 nm (left, blue). The reversibility of $^1O_2$ generation was monitored through the integrated area of the emission band at 1270 nm over four cycles (right).
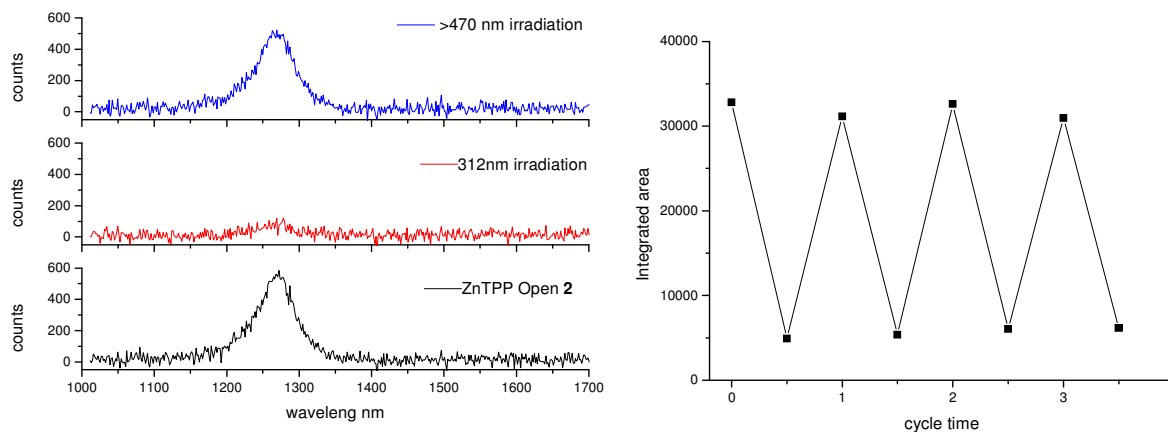

Figure 6. NIR emission of $^1O_2$ generated by ZnTPP (6 µM) in the presence of **2** (30 µM) and in air equilibrated toluene; excitation at 405 nm (4 mW). $^1O_2$ generation was observed (left, black) with the open form of **2** present, and not (left, red) when irradiation at 312 nm generated the closed form. $^1O_2$ generation was recovered by irradiation at >470 nm (left, blue). The reversibility was monitored by the integrated area of the emission band at 1270 nm over four cycles (right).
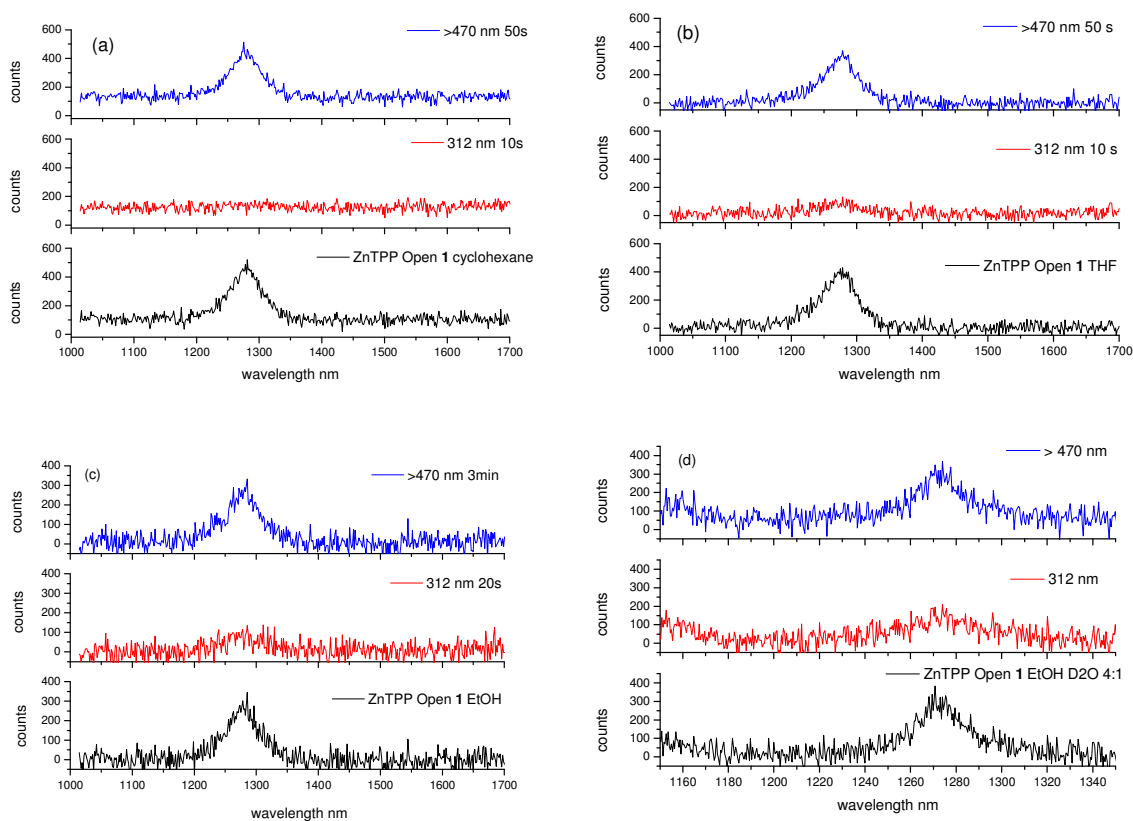
Figure 7. Switching on and off of $^1O_2$ generation by ZnTPP (6 µM) using **1** (30 µM) in (a) cyclohexane, (b) THF, (c) ethanol, and (d) ethanol mixed with D_2O (4:1).
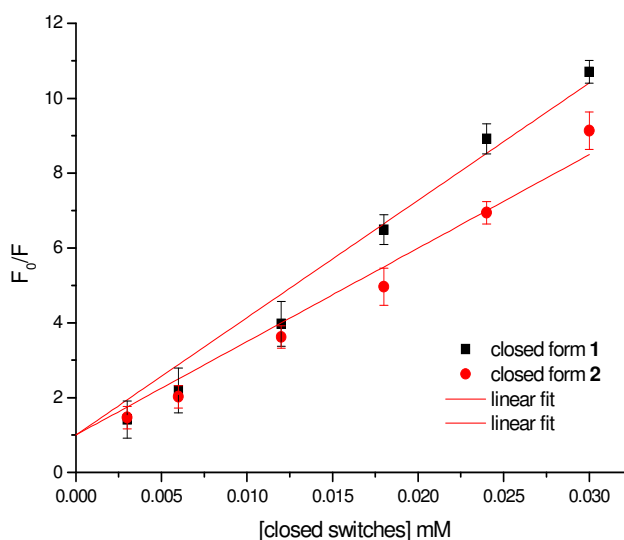

Figure 8. Stern-Volmer plot of $^1O_2$ emission in the presence of closed form **1** (black) and closed form **2** (red) in ZnTPP solution in toluene.

The effect of the switches in the open and closed states on the fluorescence of ZnTPP was examined also. The emission spectrum of ZnTPP (2 µM) with **1** (40 µM) in toluene was measured with excitation at 405 nm (Figure 9, black line).

ZnTPP shows two emission bands with maxima at 596 nm and 645 nm in toluene. Neither open nor closed form of **1** shows emission in this region. In the presence of the open form of **1**, the emission of ZnTPP shifts to 598 nm and 646 nm, respectively, because of coordination of **1** to the Zn (II) ion. A decrease in fluorescence intensity of ZnTPP was observed when irradiated the solution with UV light (Figure 9, red line). The ratio of fluorescence intensity in the open and closed states is ca. 1/0.8, which is comparable to related systems used to control the fluorescence of zinc-porphyrins. [29, 30] The change in intensity at 645 nm was monitored by alternate irradiation at 312 nm and >470 nm over four cycles (Figure 9 (b)). Good reversibility was observed. Compound **2** in the open and closed form does not affect the fluorescence of ZnTPP as expected, due to the intermolecular nature of the quenching and the short fluorescence lifetime of ZnTPP (2.0 ns).[31]
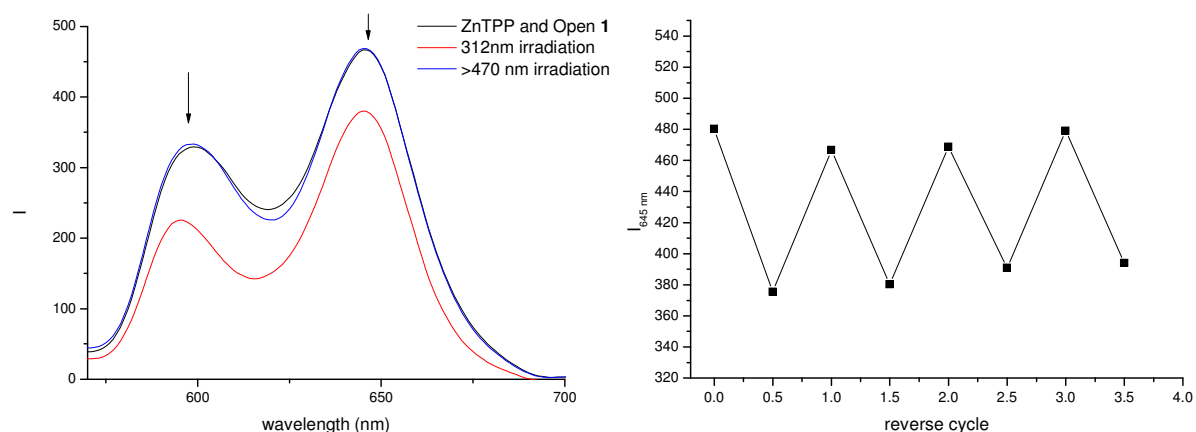

Figure 9. Emission spectra (left) of ZnTPP in the presence of the open form of **1** (black line), under UV irradiation to the PSS (red line), and recovery upon visible irradiation (>470 nm) (blue line). Reversibility of fluorescence quenching was monitored by the change in intensity at 645 nm over four cycles (right).

DFT calculations (at the B3LYP/6-31G(d) level) of the energies of the lowest singlet and triplet state were performed on compounds **1** and **2** (table 1). The energy differences between of the open and closed forms of the switches at the lowest singlet and triplet excited states are relatively large, ca. 1.3 eV for the singlet and ca. 1.6 eV for the triplet, respectively. Therefore, it provides the possibility to switch on and off energy transfer to and from a photosensitizer that has a singlet and/or triplet energy located in between. The lowest triplet excited state of the closed switches (1.23 eV of the closed **1** and 1.30 eV of the closed **2**,

respectively) is higher than the lowest excited state of $^3O_2$ (0.97 eV), which allows a significant competition with $^1O_2$ generation in the photosensitizer.

Table 1. Calculated energies of the first singlet and triplet excited states and the energies of two low-lying excited states of molecular oxygen.

	ZnTPP	*Open 1*	*Closed 1*	*Open 2*	*Closed 2*	$^1O_2$
S_1(eV)	2.30	3.64	2.30	3.74	2.41	1.6 ($^1O_{2\Sigma}$)
T_1(eV)	1.61	2.89	1.23	2.98	1.30	0.97 ($^1O_{2\Delta}$)

The mechanism of switching on and off of $^1O_2$ generation in ZnTPP by diarylethene switches is demonstrated in Scheme 2. Considering the first triplet energy of ZnTPP (1.61 eV),[32] energy transfer can only occur from ZnTPP to the closed form of the switches (1.23 eV), but not to the open form (2.30 eV), and it is highly competitive with energy transfer to $^3O_2$, which thus switches off the generation of $^1O_2$ (scheme 2, right). The first singlet excited state of ZnTPP (2.30 eV) is also close to the closed form of **1** (2.30 eV), but not to the open form (3.64 eV), and hence fluorescence quenching is possible if ZnTPP and switches are close enough to each other and the emission spectrum of ZnTPP overlaps the absorption spectrum of the closed switches.
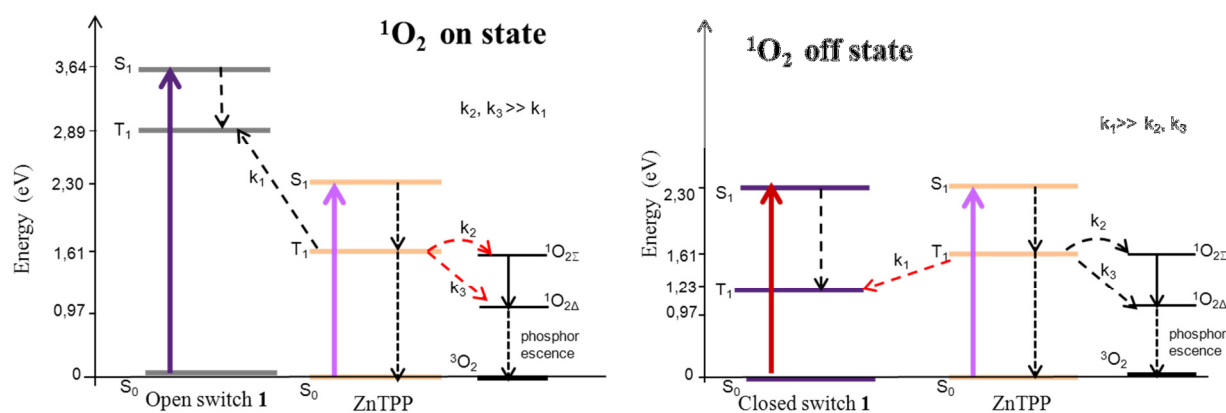
Scheme 2. Photophysical processes for switching on and off of $^1O_2$ generation in ZnTPP using the open and closed form of **1**
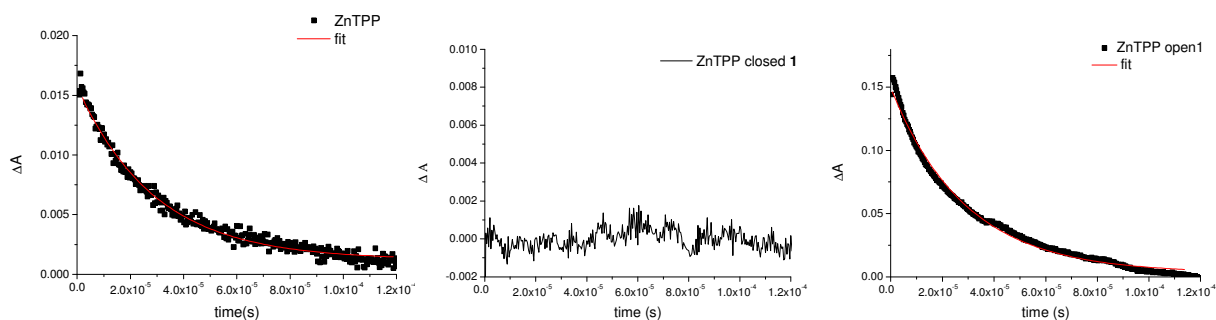
Figure 10. Transient absorption at 460 nm of ZnTPP (40 μM) (left), ZnTPP (40μM) mixed with the closed form of **1**(80 μM) (middle) upon excitation at 355 nm, and ZnTPP (100 μM) mixed with the open form of **1**(100 μM) in toluene upon with excitation at 532 nm (right). All samples were prepared by at least three freeze-pump-thaw cycles.

Energy transfer between the triplet state of ZnTPP and the closed form of **1**, while not the open form, was further confirmed by transient absorption spectroscopy (Figure 10). ZnTPP solution and ZnTPP in the presence of the closed form of **1** were excited at 355 nm, which cannot switch the closed form to the open form during the measurement. ZnTPP in the presence of the open form of **1** was excited at 532 nm at relatively high concentration because of the lower molar absorption at 532 nm compared with that at 355 nm. The triplet lifetime was monitored at 460 nm. ZnTPP has a triplet life of ca.30 μs (Figure 10, left),[33] even in the presence of the open form of **1** (Figure 10, right). When mixed with the closed form of **1**, excited ZnTPP triplet lifetime was highly quenched result in less than 0.5 μs (Figure 10, middle), which indicates the efficient triplet energy transfer between ZnTPP and the closed form of **1**.

5.4 Conclusion

In conclusion, the generation of $^1O_2$ by ZnTPP can be reversibly switched on and off by diarylethene switches through a non-covalent approach by alternate irradiation with UV and visible light. The $^1O_2$ generation is effectively switched off when diarylethenes are in the closed form. Both coordinated and non-coordinated systems can switch of $^1O_2$ generation. The coordination system also shows switching of the fluorescence of ZnTPP. The photoisomerization of the diarylethenes switches is not affected by the presence of ZnTPP, which was confirmed by UV/vis absorption spectroscopy. NIR emission spectroscopy was used to monitor switching on and off $^1O_2$ generation, and the two states of $^1O_2$

generation can be reversed for several cycles in various solvents. Triplet lifetime measurements and DFT calculations further demonstrated that the energy transfer from the photosensitizer proceeds to the closed form, but not the open form, of the diarylethene switches, which is highly competitive with the generation of $^1O_2$.

The large energy difference between the open and closed forms of the diarylethenes enables control of $^1O_2$ generation in other photosensitizers in general, by altering the substituents to reach the required wavelength range. The simple preparation and full optical control of the current systems for switching of $^1O_2$ generation hold potential for application in PDT. Patients, who take or are injected with photosensitizers together with water-soluble diarylethene switches, can be treated by light in a non-invasive manner to control whether or not to activate the generation of $^1O_2$ during PDT.

5.5 Experimental Section

General remarks

Fresh distilled toluene was used for spectroscopy. The UV/vis absorption spectra were recorded on a Specord S 600 (Analytic Jena) spectrometer. The UV/vis emission spectra were measured on a Jasco FP-6200 spectrofluorimeter. To reduce interfilter effects, a 3 x 3 mm cuvette was used for the measurements, or otherwise with 1 x 1 cm cuvette. Near-infrared emission spectra were recorded on Andor iDus InGaAs detector coupled with a Sharmrock 163 spectrograph, and the excitation was performed using a 405 nm laser diode with the power of 4 mW (Thorlabs LDM 405). The irradiation at 312 nm was carried out using a spectroline lamp at 312 nm, and visible irradiation using by a high intensity fiber optic white light source combined with a 470 nm long pass filter. In general, the PSS can be reached within 10 s of irradiation in the UV and the recovery of the open form occurs within 1 min by visible irradiation.

Transient absorption spectroscopy

The triplet absorption lifetimes were obtained using a home built system as described in chapter 2. Excitation was performed using the second harmonic (532 nm, 1-3 mJ, 6 ns) or the third harmonic (355 nm, 1-3 mJ, 6 ns) of a Q-switched Nd:YAG laser (Innolas 400) with a Si-diode trigger sensor. The probe light is from pulsed xenon light source (Applied Photophysics).The change in

absorbance of the sample was measured using a Zolix Omni-λ 300 monochromator coupled with a 5-stage photomultiplier tube (Gilden Photonics). The decay traces were recorded with 1kΩ termination on a Tektronix DPO 4032 digital phosphor Oscilloscope.

Determination of binding constant

The binding constants of the open and closed forms of **1** to ZnTPP were determined by Uv/vis titration monitored by UV/vis absorption spectroscopy. 4 µl of a stock solution containing a mixture of 2 mM of open or closed form **1** and 2 µM ZnTPP in toluene (to keep ZnTPP concentration constant during the titration), was added into a 2 µM ZnTPP solution (2 ml) repeatedly. A red shift of the Soret band of ZnTPP was observed with the isosbestic point at 426 nm both for the open and closed form of **1.** For the closed form, the overlap in absorption with ZnTPP was subtracted using a reference titration with equal closed form **1** concentrations without ZnTPP. The binding constants were obtained by fitting with 1:1 complex equation: [34]

$$A = A_0 - \frac{1}{2}\varepsilon_r[[H_{tot}] + [G_{tot}] + \frac{1}{k_a} - \sqrt{([H_{tot}] + [G_{tot}] + \frac{1}{k_a})^2 - 4[H_{tot}][G_{tot}]}$$

Where A is the absorbance of the Soret band, A_0 is the absorbance without **1** present. ε_r is the relative molar absorption, $[H_{tot}]$ is the total concentration of ZnTPP, and $[G_{tot}]$ is the total concentration of **1.**

Determination of singlet oxygen quenching constant

The quenching constant was calculated by Stern-Volmer equation.

$$\frac{F_0}{F} = 1 + k_q\tau_0[Q]$$

Where F_0 is the intensity of the emission at 1270 nm without switches present, F is the intensity of the emission at 1270 nm with different concentration of closed form **1** and **2**, k_q is the quench constant, τ_0 is the lifetime of singlet oxygen in toluene, and $[Q]$ is the concentration of closed form **1** and **2**. The lifetime of singlet oxygen generated in a ZnTPP toluene solution is taken as 30.3 µs. [35]

Computational details

Geometries of open **1**, closed **1**, open **2**, and closed **2** were optimized with DFT, using the B3LYP hybrid functional[36] and a 6-31G(d) basis set.[37] The energy of the T_1 state was then calculated by a single-point energy calculation at the B3LYP/6-31G(d) level using an unrestricted wavefunction, after which subtraction of the S_0 energy from the T_1 energy provided the S_0–T_1 energy difference. The S_0–S_1 energy difference was calculated using time–dependent DFT, using the CAM–B3LYP functional[38] and a 6–31+G(d,p) basis set. All calculations assumed an isolated molecule in the gas-phase and were performed with Gaussian 09 revision C.01.[39]

Synthesis of switch **1**
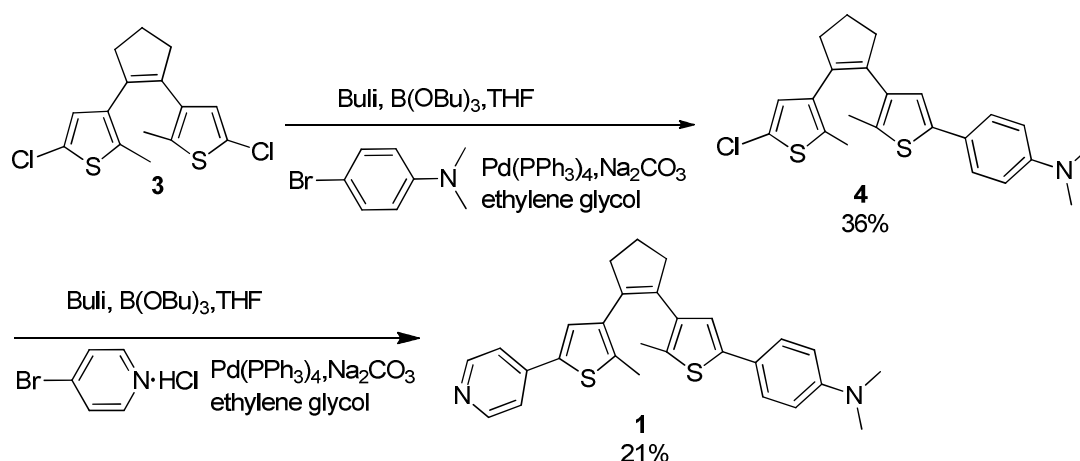
1,2-Bis(5'-chloro-2'-methylthien-3'-yl)cyclopentene[1] **3** (1.003 g, 3.046 mmol) was dissolved in anhydrous THF (40 ml) under nitrogen atmosphere, and *n*-BuLi (1.6 M in hexane, 3.198 mmol) was added dropwise. The solution was stirred at room temperature for 1 h and then B(*n*-OBu)$_3$ (3.503 mmol) was added. The reddish solution was stirred for 1 h at room temperature and was then used directly for the Suzuki cross-coupling reaction.

Meanwhile, in a separate flask, 4-bromo-*N,N*-dimethylaniline (691.1 mg, 3.35 mmol), Pd(PPh$_3$)$_4$ (703.9 mg, 0.609 mmol), aqueous Na$_2$CO$_3$ (2 M, 16 ml) and ethyleneglycol (0.4 ml) in THF (24 ml) were heated to 70 °C. The above crude boronic ester was added and the mixture was heated at reflux overnight. Subsequently, the mixture was diluted with diethyl ether and H$_2$O. The organic layer was dried on Na$_2$SO$_4$, concentrated *in vacuo* and subjected to column chromatography (SiO$_2$, 30% DCM in pentane) to give solid **4** (454 mg, 36%). [1]H

NMR (400 MHz, CD$_2$Cl$_2$) δ 1.89 (s, 3H), 1.95 (s, 3H), 1.99-2.06 (m, 2H), 2.72 (t, J = 8.0 Hz, 2H), 2.78 (t, J = 8.0 Hz, 2H), 2.93 (s, 6H), 6.62 (s, 1H), 6.66 (d, J = 8.0 Hz, 2H), 6.81 (s, 1H), 7.32 (d, J = 8.0 Hz, 2H). ^{13}C NMR (75 MHz, CD$_2$Cl$_2$) δ 14.0, 14.1, 23.0, 38.4, 38.5, 40.3, 112.5, 121.4, 122.8, 124.6, 126.1, 127.1, 132.2, 133.4, 135.5, 135.8, 136.2, 140.7, 149.9. HRMS (ESI) cal. for C$_{28}$H$_{25}$ClNS$_2$ [M+H] 414.11, found 414.11.

Switch **4** (400 mg, 0.966 mmol) was dissolved in anhydrous THF (40 ml) under a nitrogen atomosphere, and *n*-BuLi (1.6 M in hexane, 1.105 mmol) was added dropwise. The solution was stirred at room temperature for 1 h and then B(*n*-OBu)$_3$ (1.111 mmol) was added. The reddish solution was stirred for 1 h at room temperature and was then used directly for the Suzuki cross-coupling reaction.

Meanwhile, in a separate flask, a mixture of 4-bromopyridine hydrochloride (206.7, 1.063 mmol) Pd(PPh$_3$)$_4$ (223.3 mg, 0.193 mmol), aqueous Na$_2$CO$_3$ (2 M, 10 ml) and ethyleneglycol (0.3 ml) in THF (20 ml) was heated to 70 $^{\circ}$C. The above crude boronic ester was added and the mixture was heated at reflux overnight. Subsequently, the mixture was diluted with diethyl ether and H$_2$O. The organic layer was dried on Na$_2$SO$_4$, concentrated *in vacuo* and subjected to column chromatography (SiO$_2$, 5% ethyl acetate in DCM) to give solid **1** (92.6 mg, 21%). ^{1}H NMR (400 MHz, CD$_2$Cl$_2$) δ 1.95 (s, 3H), 2.03 (s, 3H), 2.05-2.12 (m, 2H), 2.82 (t, J = 8.0 Hz, 4H), 2.93 (s, 6H), 6.65 (d, 2H), 6.84 (s, 1H), 7.26 (s, 1H), 7.32 (dd, J = 8.0 Hz, 4H), 8.47 (bs, 2H). ^{13}C NMR (75 MHz, CD$_2$Cl$_2$) δ 14.0, 14.5, 23.0, 38.3, 38.4, 40.2, 112.4, 121.5, 122.7, 126.0, 127.5, 132.2, 133.5, 136.0, 136.2, 137.9, 138.5, 140.6, 149.8. HRMS (ESI) cal. for C$_{28}$H$_{28}$N$_2$S$_2$ [M+H] 457.18, found 457.18. Elemental analysis: cal.: C 73.6%, H 6.2%, N: 6.1% S: 14.0%; found: C 73.3%, H 6.2%, N: 6.1%, S: 13.9%.

2
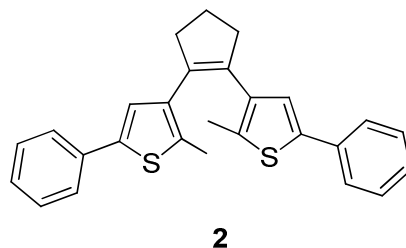
1,2-Bis(2'-methyl-5'-phenylthien-3'-yl)cyclopentene **2** was synthesized according to previous procedures.[22]

Acknowledgments

5.6 References

[1] P. R. Ogilby, *Chem. Soc. Rev.,* **2010**, *39*, 3181-3209.

[2] C. Schweitzer, R. Schmidt, *Chem. Rev.,* **2003**, *103*, 1685-1757.

[3] E. D. Sternberg, D. Dolphin, C. Brückner, *Tetrahedron*, **1998**, *54,* 4151-4202.

[4] D. E. Dolmans, D. Fukumura, R. K. Jain, *Nat. Rev. Cancer*, **2003**, *3*, 380-387.

[5] R. Bonnett, *Chem. Soc. Rev.,* **1995**, *24*, 19-33.

[6] M. R. Detty, S. L. Gibson, S. J. Wagner, *J. Med. Chem.,* **2004**, *47*, 3897-3915.

[7] A. E. O'Connor, W. M. Gallagher, A. T. Byrne, *Photochem. Photobiol.*, **2009**, *85*, 1053-1074.

[8] E. Clo, J. W. Snyder, P. R. Ogilby, K. V. Gothelf, *Chem. Bio. Chem.,* **2007**, *8*, 475-481.

[9] J. F. Lovell, T. W. B. Liu, J. Chen, G. Zheng, *Chem. Rev.*, **2010**, *110*, 2839-2857.

[10] Y. Vakrat-Haglili, L. Weiner, V. Brumfeld, A. Brandis, Y. Salomon, B. Mcllroy, B. C. Wilson, A. Pawlak, M. Rozanowska, T. Sarna, A. Scherz, *J. Am. Chem. Soc.,* **2005**, *127*, 6487-6497.

[11] S. O. McDonnell, M. J. Hall, L. T. Allen, A. Byrne, W. M. Gallagher, D. F. O'Shea, *J. Am. Chem. Soc.,* **2005**, *127*, 16360-16361.

[12] T. Tørring, R. Toftegaard, J. Arnbjerg, P. R. Ogilby, K. V. Gothelf, *Angew. Chem.* **2010**, *122*, 8095-8097.

[13] J. Chen, K. Stefflova, M. J. Niedre, B. C. Wilson, B. Chance, J. D. Glickson, G. Zheng, *J. Am. Chem. Soc.*, **2004**, *126*, 11450-11451.

[14] E. Cló, J. W. Snyder, N. V. Voigt, P. R. Ogilby, K. V. Gothelf*, J. Am. Chem. Soc.,* **2006**, *128*, 4200-4201.

[15] E. S. Shibu, M. Hamada, N. Murase, V. Biju, *J. Photochem. Photobiol., C,* **2013**, *15*, 53-72.

[16] Z. Zhu, Z. Tang, J. A. Phillips, R. Yang, H. Wang, W. Tan, *J. Am. Chem. Soc.,* **2008**, *130*, 10856-10857.

[17] L. Shi, B. Hernandez, M. Selke, *J. Am. Chem. Soc.,* **2006**, *128*, 6278-6279.

[18] K. Matsuda, M. Irie, *J. Photochem and Photobio C*, **2004**, *5*, 169-182.

[19] B. L. Feringa, W. R. Browne, *Molecular Switches,* Vol 1-2, Wiley-VCH, Weinheim, Germany, **2011**.

[20] M. Irie, *Chem. Rev.,* **2000**, *100*, 1685–1716.

[21] N. Katsonis, T. Kudernac, M. Walko, S. J. van der Molen, B. J. van Wees, B. L. Feringa, *Adv. Mater.* **2006**, *18*, 1397-1400.

[22] C. Denekamp, B. L. Feringa, *Adv. Mater.,* **1998**, *10*, 1080-1082.

[23] A. J. Kronemeijer, H. B. Akkerman, T. Kudernac, B. J. van Wees, B. L. Feringa, P. W. M. Blom, B. de Boer, *Adv. Mater.,* **2008**, *20*, 1467-1473.

[24] M. Goeldner, R. S. Givens, *Dynamic Studies in Biology: Phototriggers, Photoswitches and Caged Biomolecules*, Wiley-VCH, Weinheim, Germany, **2005**.

[25] R. R. Allison, G. H. Downie, R. Cuenca, X. H. Hu, C. J. H. Childs, C. H. Sibata, *Photodiagn. Photodyn. Ther.,* **2004**, *1*, 27-42.

[26] K. M. Kadish, K. M. Smith, R. Guilard, *The Porphyrin Handbook*, Academic Press, San Diego, California, USA, **2003**.

[27] J. J. D. de Jong, L. N. Lucas, R. Hania, A. Pugzlys, R. M. Kellogg, B. L. Feringa, K. Duppen, J. H. van Esch, *Eur. J. Org. Chem.*, **2003**, *10*, 1887-1893.

[28] J. Visser, N. Katsonis, J. Vicario, B. L. Feringa, *Langmuir*, **2009**, *25*, 5980-5985.

[29] J. Otsuki, A. Suka, K.Yamazaki, H. Abe, Y. Araki, O. Ito, *Chem. Commun.*, **2004**, 1290-1291.

[30] J. Otsuki, K. Narutaki, J. M. Bakke, *Chem. Lett.*, **2004**, *33*, 356-357.

[31] M. R. Wasielewski, M. P. Niemczyk, *J. Am. Chem. Soc.,* **1984**, *106*, 5043-5045.

[32] J. E. Rogers, K. A. Nguyen, D. C. Hufnagle, D. G. McLean, W. Su, K. M. Gossett, A. R. Burke, S. A. Vinogradov, R. Pachter, P. A. Fleitz, *J. Phys. Chem. A*, **2003**, *107*, 11331–11339.

[33] M. Pineiro, A. L. Carvalho, M. M. Pereira, A. M. d'A. R. Gonsalves, L. G. Arnaut, S. J. Formosinho, *Chem. Eur. J.* **1998**, *4*, 2299-2307.

[34] J. L. Atwood, J. E. D. Davies, D. D. MacNicol, F. Vogtle, J. A. Ripmeester, J. -M. Lehn, *Comprehensive Supramolecular Chemistry*, Elsevier Science, Pergamon, New York, **1996**; Vol.*8*, pp 425-482.

[35] R. L. Jensen, J. Arnbjerg, P. R. Ogilby, *J. Am. Chem. Soc.*, **2010**, *132* , 8098–8105.

[36] a) A. D. Becke, *J. Chem. Phys.,* **1993**, *98*, 5648-5652. b) C. Lee, W. Yang, R. G. Parr, *Phys. Rev. B,* **1998**, *37*, 785-789. c) S. H. Vosko, L. Wilk, M. Nusair, *Can. J. Phys.,* **1980**, *58*, 1200-1211.

[37] a) W. J. Hehre, R. Ditchfield, J. A. Pople, *J. Chem. Phys.,* **1972**, *56*, 2257-2261. b) P. C. Hariharan, J. A. Pople, *Theoret. Chimica Acta,* **1973**, *28*, 213-222. c) M. M. Francl, W. J. Petro, W. J. Hehre, J. S. Binkley, M. S. Gordon, D. J. DeFrees, J. A. Pople, *J. Chem. Phys.,* **1982**, *77*, 3654-3665.

[38] T. Yanai, D. Tew, N. Handy, *Chem. Phys. Lett.,* **2004**, *393*, 51-57.

[39] Gaussian 09, Revision C.01, M. J. Frisch, G. W. Trucks, H. B. Schlegel, G. E. Scuseria, M. A. Robb, J. R. Cheeseman, G. Scalmani, V. Barone, B. Mennucci, G. A. Petersson, H. Nakatsuji, M. Caricato, X. Li, H. P. Hratchian, A. F. Izmaylov, J. Bloino, G. Zheng, J. L. Sonnenberg, M. Hada, M. Ehara, K. Toyota, R. Fukuda, J. Hasegawa, M. Ishida, T. Nakajima, Y. Honda, O. Kitao, H. Nakai, T. Vreven, Jr., J. A. Montgomery, J. E. Peralta, F. Ogliaro, M. Bearpark, J. J. Heyd, E. Brothers, K. N. Kudin, V. N. Staroverov, T. Keith, R. Kobayashi, J. Normand, K. Raghavachari, A. Rendell, J. C. Burant, S. S. Iyengar, J. Tomasi, M. Cossi, N. Rega, J. M. Millam, M. Klene, J. E. Knox, J. B. Cross, V. Bakken, C. Adamo, J. Jaramillo, R. Gomperts, R. E. Stratmann, O. Yazyev, A. J. Austin, R. Cammi, C. Pomelli, J. W. Ochterski, R. L. Martin, K. Morokuma, V. G. Zakrzewski, G. A. Voth, P. Salvador, J. J. Dannenberg, S. Dapprich, A. D. Daniels, O. Farkas, J. B. Foresman, J. V. Ortiz, J. Cioslowski, D. J. Fox, Gaussian, Inc., Wallingford CT, 2010.

CHAPTER 6

Laser Flash Photolysis Study of Molecular Motors

The rotatory speed of overcrowded alkene based molecular motors is a crucial parameter in achieving their unidirectional motor function. Faster rotation can efficiently compete with Brownian motion and accelerate the processes in which molecular motors are involved. However, characterization of these fast motors (i.e., the kHz or MHz regime), specifically the rate and energy barriers to the helix inversion, are challenging. In this chapter, the home-built laser flash photolysis system, described in chapter 2, together with steady state UV/vis absorption spectroscopy is used to monitor the change in absorption with time after excitation, by which the rotary speed and energy barrier to helix inversion of variously substituted molecular motors are determined.

6.1 Introduction

Overcrowded alkene-based molecular motors were first synthesized in Feringa's group nearly two decades ago, and these systems can be driven by a combination of light and heat.[1] The process involves unidirectional rotation of the upper half relative to the lower half of the molecules, by light induced isomerization of the central double bond, followed by thermal helix inversion. Several theoretical and experimental studies also have been performed to understand the mechanisms[2,3,4,5,6] and dynamics of the photochemistry of molecular motors.[7,8] A number of molecular motors have been applied in switchable asymmetric catalysis,[9] modified surfaces,[10] rotation of microscopic objects by doping of liquid crystals,[11] and nanoscale machines,[12] etc.

A key challenge presented by overcrowded alkene-based molecular motors is to achieve comparable or superior speeds to the biological rotary motors, which are fast enough to overcome Brownian motion. ATP (adenosine 5'-triphosphate), one of the motors in nature, transforms the energy of the hydrolysis of approximately 390 molecules of ATP per second into rotational motion at a rate of 130 revolutions per second.[13] The rotary speed of overcrowded alkene-based molecular motors is limited by thermally activated isomerization reactions, since the photoisomerisation occurs over a few picoseconds.[2] The structure units at the lower and/or upper parts of the motors allow to lower the energy barriers of thermal helix inversion and can modify the rotary speed from nanoseconds to hours.[14] The size of the rotor bridging atoms and the size of the rings are also found to be directly related to the rate constant of thermal helix inversion due to its effect on steric crowding with the stator. The fastest rotary rates have been reported can reach the MHz regime.[15]

With the increase of rotary speed, another challenge arises: how can we characterize these high speed molecular motors? The conventional methods for monitoring the rotary motion of the motors are usually UV/vis absorption, CD and NMR spectroscopies. The photoisomerization of the central carbon-carbon double of the motors typically induces a red shift in the lowest energy UV/vis absorption band because of the lower HOMO/LUMO gap of the unstable isomer and the subsequent thermal step results in a restoration of the original spectrum. The inversion of the intrinsic helicity of the molecule can be also observed by CD spectroscopy. The signals corresponding to the unstable isomers appear in the

NMR spectra upon irradiation of the stable isomer also. It takes from seconds to minutes to acquire one spectrum for all of these steady state spectroscopic techniques. If the rate of rotation is faster than the time-resolution of these spectroscopies, cooling the samples to slow down the thermal process can be used for characterizations. However this can only be extended to motors for which the lifetime is longer than the millisecond regime at room temperature, while for the faster motors other techniques are needed.

In this chapter, the laser flash photolysis system as described in chapter 2 is used to measure the transient absorption of a series of molecular motors, for which the lifetime for thermal inversion ranges from nanoseconds to seconds. A pulsed laser is used to generate the unstable form of the motors within several nanoseconds. Since the photoisomerization occurs within several picoseconds, the relaxation to the ground state of unstable form to the stable form can be followed on the nano- to milli-second time scale on a fast response photo detector. By monitoring the change in absorbance upon pulsed laser excitation at a certain wavelength, the rate of the thermal inversion can be obtained. The energy barriers for the thermal helix inversion were calculated also by measuring the lifetime of the unstable isomer over a certain temperature range.

6.2 Molecular motors

Molecular motor **1** is expected to be the fastest motor, and have the lowest barrier to thermal helix inversion to date.[16] However, only a rough indication of the activation parameters have been obtained, and the lifetime of unstable **1** was uncertain (between 8 ns to 100 ns at room temperature), because of experimental limitations.[16]

The rotary speed of molecular motor **2**, **5**, **6** have been determined by steady state spectroscopy,[15, 17, 18] with the half-lives of thermal helix inversion at room temperature being 2.3×10^{-6} s, 40 s, 190 s, respectively. This indicates that a motor with the upper part comprising a five-membered ring (**2**) has a faster rotary speed than the one with the upper part being a six-membered ring (**5**), whereas a five-membered ring lower part (**6**) slows down the rotary speed compared with a six-membered ring lower part (**2**, **5**). Introducing a substantial electronic effect on the thermal isomerization around the central double bond could result in a remarkable increase in the rate of thermal inversion also, e.g. the electronic push-

pull effect in **5**. [19,20] Moreover, the structure substituents at upper and lower part of the motors can affect the rotary speed also. For example, substituting a fluorene-based molecular motor with a p-xylene group to decrease the size of rotor unit accelerates the rate by up to 12 fold, and additional steric bulk, e.g. replacing the methyl for a *tert*-butyl substituent, at the stereocenter at the upper part results in a 3×10^4 fold acceleration. [21, 22] Molecular motor **3,** containing a new structural motif combines a p-xylene unit and a *tert*-butyl substituted stereocenter in the upper part, was designed with the expectation of even faster unidirectional rotation.
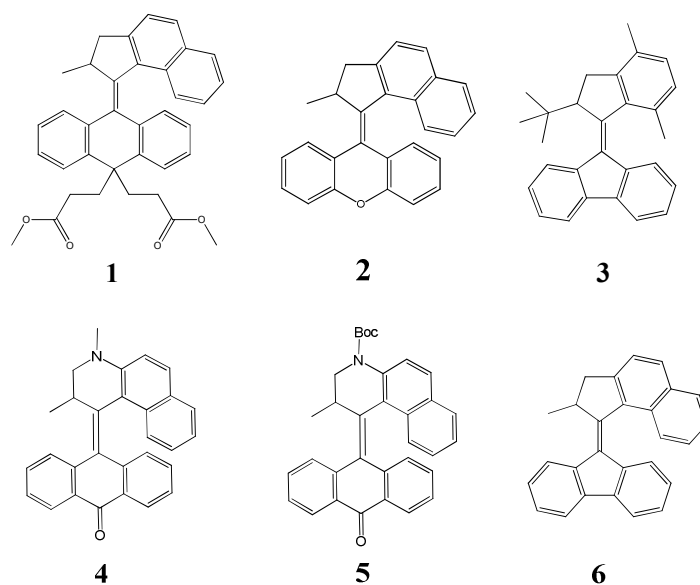
Scheme 1. Structures of molecular motors described in this chapter.

Molecular motor **4**, containing a strongly electron-donating amine group without a Boc protection group in the upper half (compared with **5**) and an electron-withdrawing ketone group in the lower half, was synthesized with the expectation of a stronger electronic push-pull effect. [19] The electronic push-pull effect would reduce steric hindrance because of the contribution of resonance structures where the central olefinic bond has single bond character, which might cause a lowering of the energy barrier to thermal helix inversion (Scheme 2). However, *cis-trans* isomerization of **4** was not observed by ^{1}H NMR spectroscopy even when irradiated in toluene-d$_8$ for 5 h at -80 °C. [23]
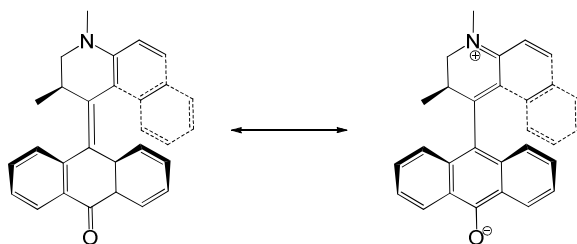
Scheme 2. Resonance structures of **4**, displaying the possible single-bond character of the central double bond in the zwitterionic form.

The lifetimes and energy barrier to thermal helix inversion of **1**-**4** were obtained by measuring the time-resolved absorption spectra using laser flash photolysis. Steady state UV/vis absorption spectroscopy was used to characterize **5** and **6** because of the relative slow thermal step. The electronic effects in **4** and **5** were further examined in various solvent with differing polarity.

6.3 Results and Discussion

6.3.1 UV/vis absorption spectroscopy

UV/vis absorption spectroscopy was used to study the ground state absorption properties of molecular motor **1**-**6** in solvents of low polarity at room temperature (Figure 1). The presence of an oxygen atom in the central bridging group in the lower part of molecular motor **2** (Figure 1, red) induces a red shift in absorption, relative to the methylene bridged analogue motor **1** (Figure 1, black). Replacement of a methyl for a *tert*-butyl substituent at the stereocenter in the upper part in the case of **3** results in a small blue shift with an absorption maximum at 351 nm (Figure 1, blue). Replacing p-xylene with naphthalene in the upper part, motor **6**, (Figure **1**, orange) shows a red shift to 390 nm. The two "electronic push-pull" molecules **4** and **5** (Figure 1, pink and green) show relatively long wavelength absorptions, 457 nm and 371 nm, respectively, with the stronger electronic push-pull effect in **4** inducing the largest red shift.
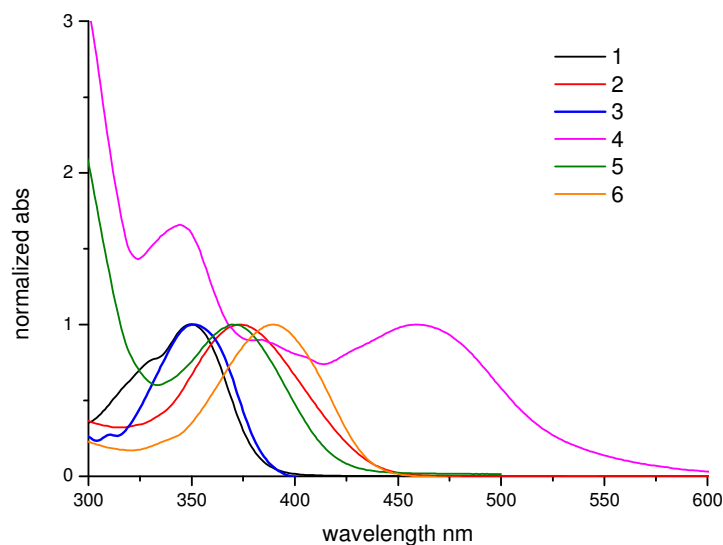
Figure 1. Normalized UV/vis absorption spectra (normalized to the lowest energy UV/vis absorption band) of molecular motor **1** in isopentane (black), **2** in *n*-hexane (black red), **3** in *n*-heptane (blue), **4** in toluene, (pink), **5** in toluene,(green), and **6** in chloroform (orange).

6.3.2 Nanoseconds molecular motor **1**

The change in absorption of **1** upon UV irradiation was not observed at room temperature, even with using laser flash photolysis. This means that either no photoisomerization occurs or the rate of the thermal isomerization is faster than the time resolution of the setup, i.e. sub microsecond. A change in steady state UV/vis absorption spectra was obtained previously at extremely low temperature (in methylcyclohexane: methylcyclopentane =1:1 at 98 K and in propane 85 K) previously.[16] The measurements were carried out at 173 K in isopentane using laser flash photolysis upon 355 nm excitation (6 ns pulses), with the expectation of slowing down the thermal helix inversion step in the measureable range of the system.

Upon 355 nm pulsed excitation, the absorption immediately increased at 430 nm and decreased at 350 nm and the decay trace showed complete recovery within 160 µs in isopentane at 173 K (Figure 2, left). Fitting to a single exponential, a lifetime of 47 µs at 173 K was determined. The change in absorbance was also studied at other wavelengths. The UV/vis absorption difference spectrum of **1** at 100 ns after excitation is shown on the right of Figure 2, which indicates that the absorption band between 300 nm and 375 nm decreases and a new band between

375 nm and 500 nm appears upon photoisomerization, The change in absorption spectra upon irradiation was similar to that observed for molecular motor **6** (*vide infra*).
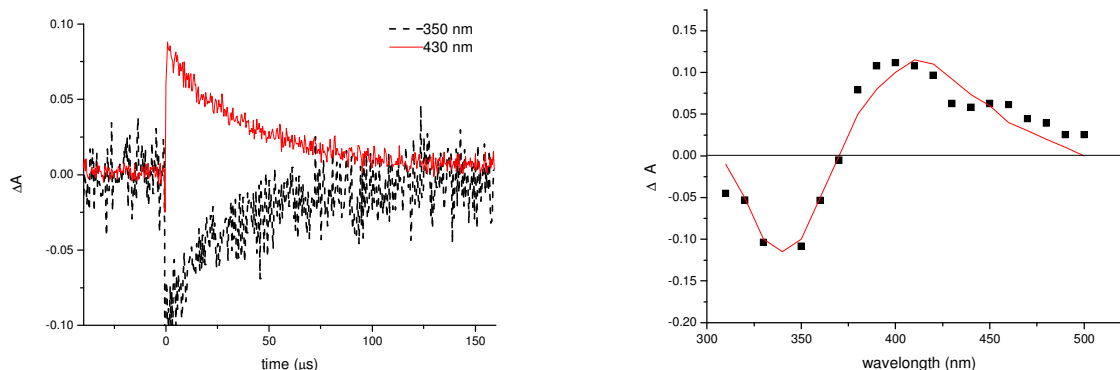

Figure 2. Transient decay and recovery following pulsed excitation of **1** in isopentane at 173 K at 350 nm and 430 nm (left), and the UV/vis difference spectrum at the 100 ns after excitation (right).

The energy barrier to thermal helix inversion was determined by transient absorption spectroscopy. Following the change of absorbance of the sample at the PSS after irradiation at a series of constant temperatures, the rate of conversion to the lowest energy isomer allows for Eyring and /or Arrhenius plots to be drawn (equation 6.1 and 6.2), from the former of which the standard change in Gibbs energy of activation ($\Delta^{\ddagger}G^{o}$) can be determined.

$$ln\frac{k}{T} = \frac{-\Delta H^{\ddagger}}{R} \cdot \frac{1}{T} + ln\frac{k_B}{h} + \frac{\Delta S^{\ddagger}}{R} \qquad (6.1)$$

$$\Delta^{\ddagger}G^{0} = -RTln(\frac{k}{k_B T}) \qquad (6.2)$$

Where k reaction rate constant, T is absolute temperature, $\Delta H^{\ddagger}$ is enthalpy of activation, R is gas constant, k_B is Boltzamnn constant, $\Delta S^{\ddagger}$ is entropy of activation.

The energy barrier to the thermal helix inversion was determined by measuring the lifetimes of **1** in the temperature range of 168 K to 193 K (Figure 3, a, b and c). The Eyring plot (Figure 3, d) provides activation parameters for the thermal process: the enthalpy of activation $\Delta^{\ddagger}H^{o}$ is 24.6 ± 0.5 kJ/mol, the entropy of

activation $\Delta^{\ddagger}S^{o}$ is -18.3 ± 0.5 J/mol.K, and the energy of activation $\Delta^{\ddagger}G^{o}$ at 20 °C is 29.6 ± 0.5 J/mol. The half-life of thermal step in isopentane at 20 °C can be calculated from the Eyring plot, which gives 36 ns. The result is as expected between 8 ns to 100 ns at room temperature. With the rate of thermal helix inversion at 20 °C being 2.0×10^{7} s^{-1}, molecular motor **1**, under suitable irradiation conditions, is capable of achieving unidirectional rotation at 10 MHz at room temperature.
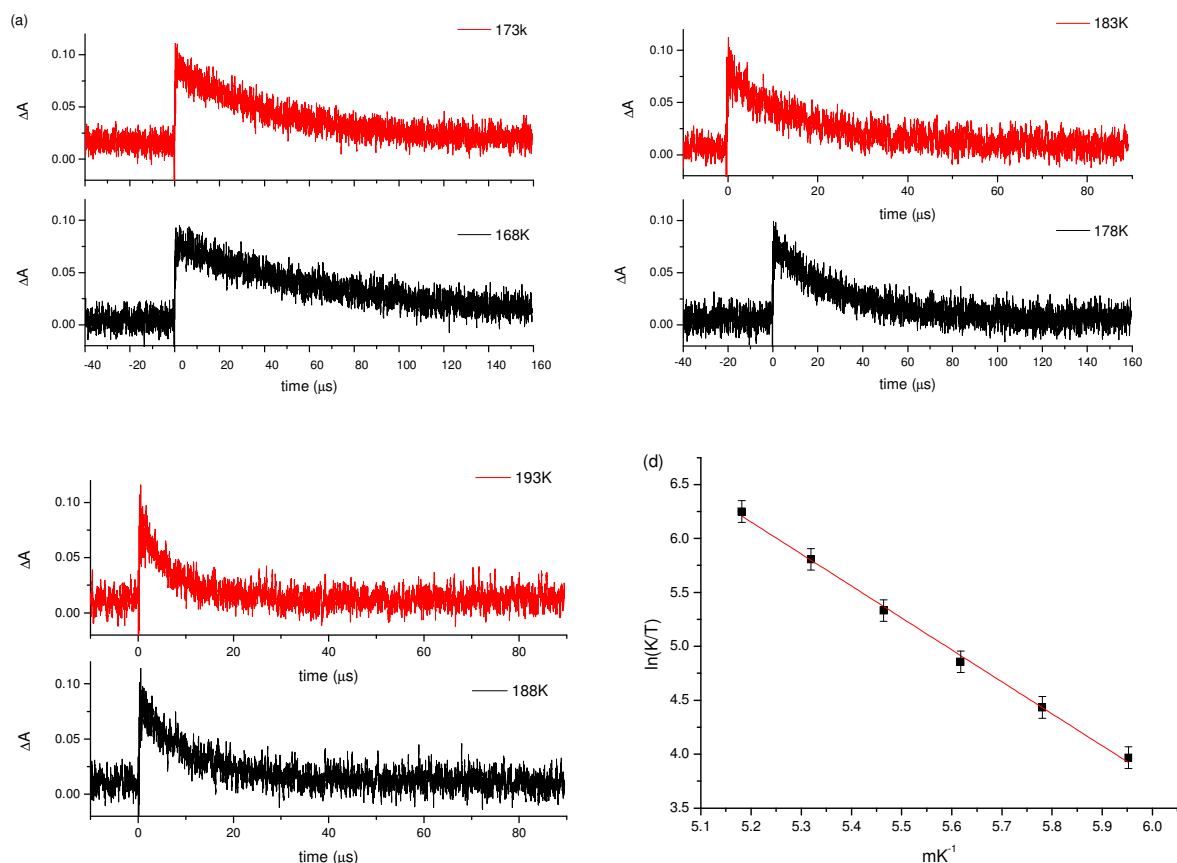
Figure 3. Transient recoveries for **1** (at 430 nm, in isopentane) upon pulsed irradiation at 355 nm at various temperatures (from 168 K to 193 K, a, b, c), and Eyring plot for the thermal helix inversion (d).

6.3.3 Microsecond molecular motor **2**

Transient absorption data for molecular motor **2** gave the same result for the isomerization process as those published.[13] Figure 4 shows the change in absorption of **2** at 475 nm upon laser pulsed excitation, fitted with a single exponential decay, the lifetime was determined to be 3.0 µs at 290 K. Barriers of activation to thermal helix inversion of **3** were described in ref. 13, with $\Delta^{\ddagger}G^{o}$=41.0 KJ/mol at 26°C.
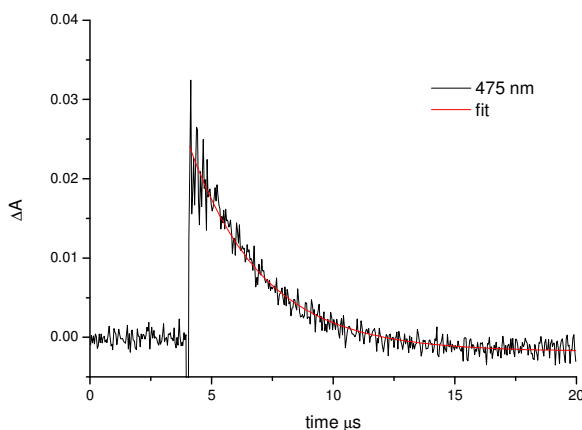
Figure 4. Transient recovery of **2** at 475 nm in hexane upon laser pulsed excitation at 355 nm at 290 K.

6.3.4 Millisecond molecular motor **3**

No changes to the UV/vis absorption spectrum of **3** were observed upon UV irradiation using a steady state UV/vis spectrometer at room temperature, which means that the rotary speed of **3** is faster than the time resolution of the spectrometer. When transient absorption spectroscopy was applied, a decrease in absorbance at 350 nm was observed upon 355 nm pulsed laser excitation, with a concomitant increase when monitored at 450 nm (Figure 5, left). Detection of the change in absorbance in the range 300 nm to 500 nm upon pulsed laser excitation shows a very similar change as for **1** (Figure 5, right). The half-life for thermal helix inversion of **3** was determined to be 2.0 ms at 293 K.
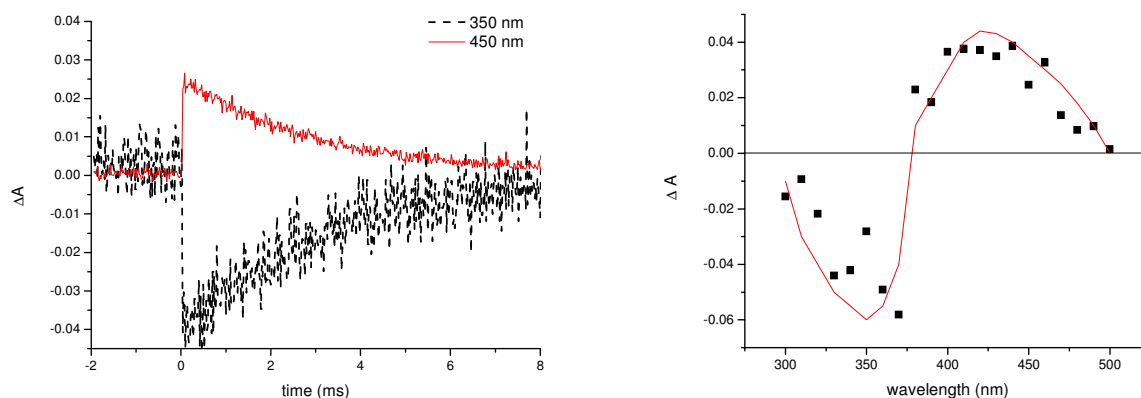
Figure 5. Change in absorption at 350 nm and 450 nm shows interconversion of unstable **3** to stable **3** in heptane at 288 K (left), and the UV/vis difference spectra immediately after the 8 ns pulsed laser (right).

The energy barrier to thermal helix inversion in **3** was determined by the change in absorbance at 430 nm at several constant temperatures (from 288 K to 318 K, Figure 6, left). The rate of thermal helix inversion for unstable **3** to stable **3** was used to determinate of the Gibbs energy of activation using an Eyring plot (Figure 6, right), with the enthalpy of activation $\Delta^{\ddagger}H^{o}=54.8\pm0.5$ kJ/mol, the entropy of activation $\Delta^{\ddagger}S^{o}=-12.4\pm0.5$ J/mol.K and the energy of activation $\Delta^{\ddagger}G^{o}=58.4\pm0.5$ kJ/mol at 293K.
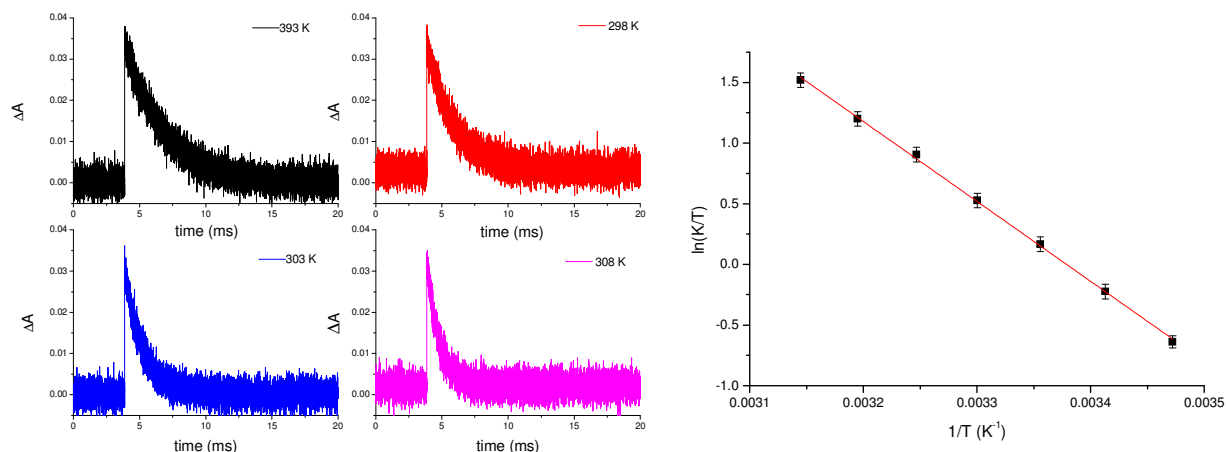
Figure 6. Change in absorption for **3** at 430 nm in heptane upon pulsed laser excitation at 355 nm at various temperatures (from 293 K to 308 K) (left), and Eyring plot (from 288 k to 318K) for the thermal helix inversion.

6.3.4 Electronic push-pull molecular motors **4**, **5**

Due to the relatively slow thermal step, the photochemical and thermal helix inversion of **4** and **5** was firstly studied with UV/vis absorption spectroscopy at low temperature and room temperature, respectively. UV irradiation of *n*-hexane solutions of **4** at 238 K led to the appearance of an absorption band at 500 nm (Figure 7, left). Leaving the sample at room temperature for several minutes resulted in a restoration of the original spectra. This observation is similar to that found in the previous study.[23] The change in absorbance of **4** upon UV irradiation was not observed in other polar solvents, e.g. THF, even at low temperature. Irradiation **5** in toluene at room temperature led to the appearance of an absorption band at 460 nm (Figure 7, right), and leaving in dark for 20 min, these spectral changes had reversed again.
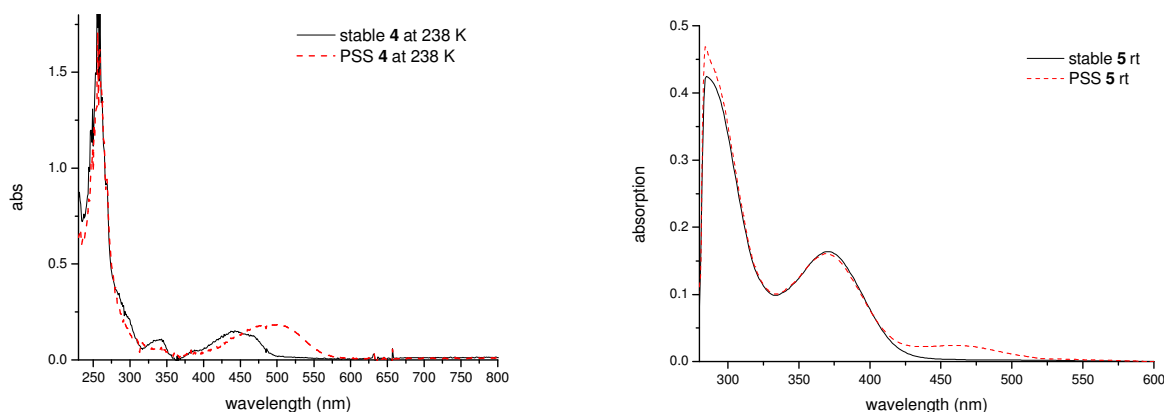
Figure 7. UV/vis absorption spectra of stable **4**, the photostationary state (PSS at 312 nm) mixture of stable and unstable **4** in *n*-hexane at 238 K upon UV irradiation (left). UV/vis absorption spectra of stable **5**, the photostationary state (PSS at 312 nm) mixture of stable and unstable **5** in toluene at 238 K upon UV irradiation (right).

Compound **4** and **5** were further dissolved in other solvents of differing polarities to study the electronic push-pull effect on the central double bond. The steady state absorption spectra of **4** show a ca. 30 nm solvatochromic shift from a non-polar to a polar solvent (Figure 8, left), while the solvatochromic shift of **5** is only ca. 10 nm (Figure 8, right). This shift means that the excited state of **4** is more polar than that of **5**, which may be because of a stronger electronic push-pull effect.
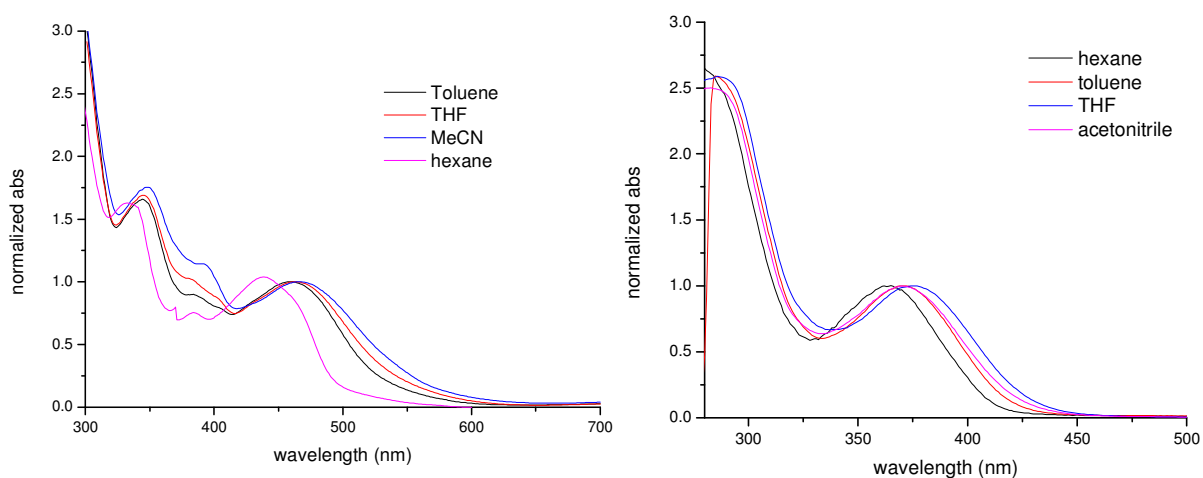
Figure 8. The UV/vis absorption spectra of **4** (left) and **5** (right) in solvent of *n*-hexane, toluene, THF and acetonitrile.

The energy barriers to unstable forms of **4** and **5** relaxing back to their stables form were also determined in solvents of different polarities. Steady state UV/vis absorption spectroscopy was used to examine the relatively slow thermal processes. Transient absorption spectroscopy was used to study the relaxation of **4** in polar solvents, e.g. THF and acetonitrile. Figure 9 (a) shows the change in absorbance at 470 nm of motor **5** with time at five different temperatures, and the activation energy of the thermal step at room temperature was determined using an Eyring plot (Figure 9, b), giving $\Delta^{\ddagger}G^{o}$=81.3 kJ/mol in toluene, and a half-life of the thermal helix inversion was 40 s at room temperature (20 ^{o}C). The energy barrier to thermal helix inversion in **5** in other solvents (tetrahydrofuran, acetonitrile), and the Eyring plots are shown in Figure 9 (c) and (d). Together with the previous study of **5** in *n*-hexane,[17] the energy barriers ($\Delta^{\ddagger}G^{o}$) and half-lives of **5** in these four solvents are listed in Table 1. Compound **5** shows almost identical activation energies in both low and high polarity solvents, and it can exclude significant electronic push-pull effect in motor **5.**
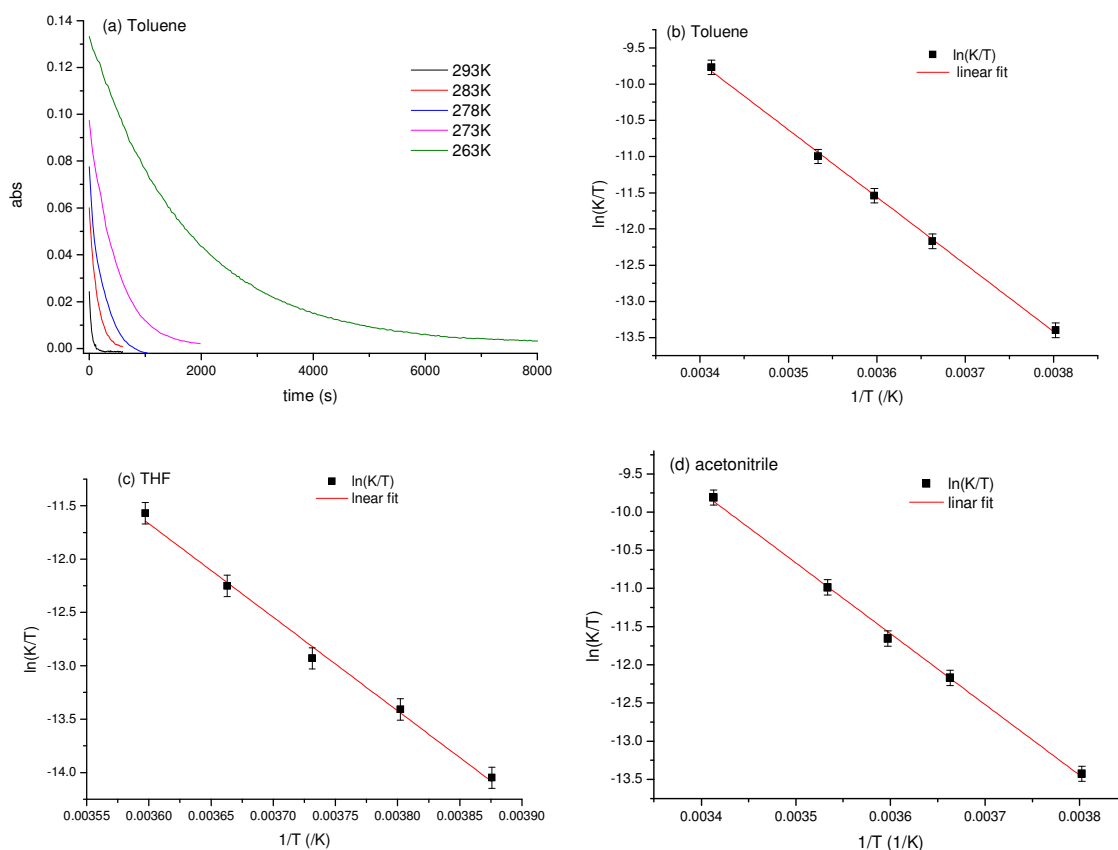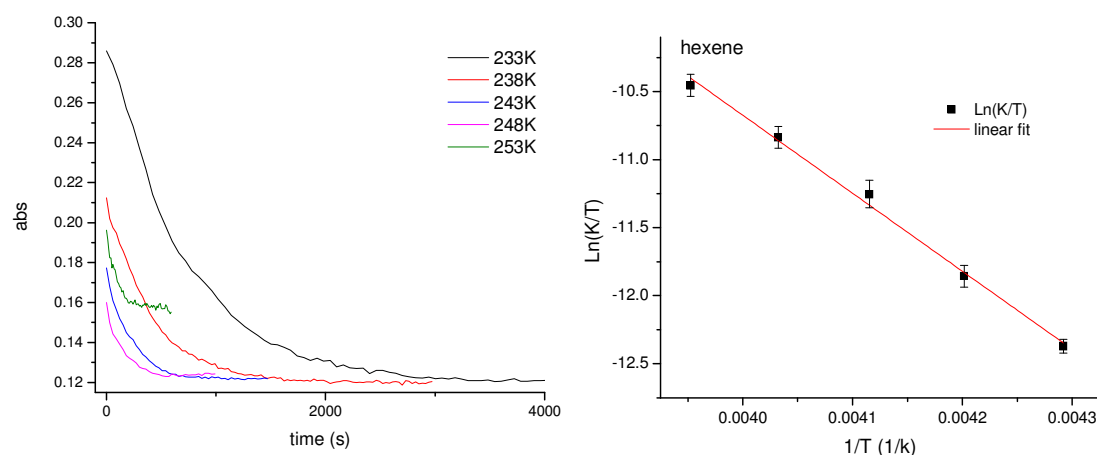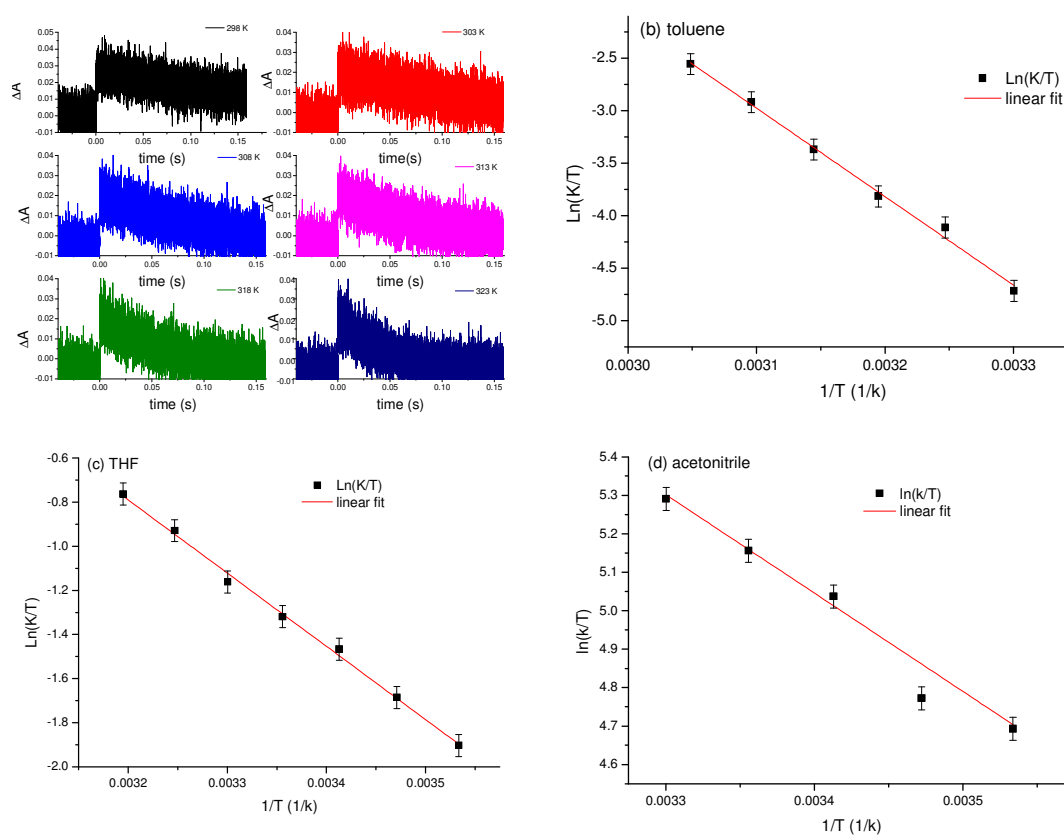

Figure 9. UV/vis absorption monitored at 470 nm over time for conversion from PSS to stable **5** at several temperatures (from 263 K to 293 K) in toluene (a), and an Eyring plot for the thermal helix inversion in toluene (b), THF (c) and acetonitrile (d).

Table 1. Solvent dependence of energy barriers and half-lives to thermal helix inversion of **5**.

Solvent	*hexane*	*toluene*	*THF*	*acetonitrile*
Polarity	0.06	2.4	4.2	6.2
$\Delta^{\ddagger}G^{o}$ (kJ/mol) (+/- 2%)	81.7	81.3	81.6	81.5
$\Delta^{\ddagger}H^{o}$ (kJ/mol) (+/- 2%)	76.7	77.0	72.9	77.1
$\Delta^{\ddagger}S^{o}$ (J/mol.K) (+/- 5%)	17.1	-15.7	-32.0	-16.5
$\tau_{1/2}$(s) RT (+/- 10%)	40	40	40	40

Figure 10 (left) shows the thermal recovery of **4** at 510 nm upon UV irradiation between 233 K and 253 K, which was monitored by steady state UV/vis absorption spectroscopy. The first-order exponential decay fits were used to extract the lifetime data. Figure 10 (right) shows Erying plot, from which the following activation parameters are determined: the enthalpy of activation $\Delta^{\ddagger}H^{o}$=47.6±0.5 kJ/mol, the entropy of activation $\Delta^{\ddagger}S^{o}$=-96.8 J/mol.K, and the energy of activation $\Delta^{\ddagger}G^{o}$=75.9±0.5 kJ/mol at 293 K.

Figure 10. Change in UV/vis absorption (at 510 nm, in n-hexane) monitored over time for conversion from PSS to stable **5** at several temperature (from 233 K to 253 K) (left), and Eyring plot for the thermal helix inversion

In more polar solvents, no obvious change in absorption upon UV irradiation was observed by steady state UV/vis spectroscopy even at low temperature. Transient absorption spectroscopy was used to monitor the change in absorbance upon ns pulsed laser excitation, and the changes in absorbance at 540 nm were followed over a range of temperatures to determine the activation energy. Figure 11 (a) shows the change in absorbance of **4** in toluene over millisecond scale, and the Eyring plots in toluene, THF and acetonitrile are shown in Figure 11 (b), (c) and (d). Together with the result in *n*-hexane, the activation energy and half-lives of **4** in these solvents are summarized in Table 2.

Figure 11. UV/vis absorption monitored at 540 nm over time for conversion from PSS to stable **4** at several temperatures (from 298 K to 323 K) in toluene (a), and an Eyring plot for unstable **4** thermally relaxing to stable **4** in toluene (b), THF (c) and acetonitrile (d).

Table 2. Solvent dependence of energy barriers and half-lives to thermal relaxation of unstable **4**.

Solvent	*Hexane*	*Toluene*	*THF*	*Acetonitrile*
Polarity	0.06	2.4	4.2	6.2
$\Delta^{\ddagger}G^{o}$ (kJ/mol) (+/- 2%)	75.9	75.0	61.5	45.7
$\Delta^{\ddagger}H^{o}$ (kJ/mol) (+/- 2%)	50.3	48.7	27.6	21.8
$\Delta^{\ddagger}S^{o}$ (J/mol.K) (+/- 5%)	-84.7	-88.3	-115.7	-83.2
$\tau_{1/2}$ (s) RT (Error 10%)	3.86	2.38	0.01	2×10^{-5}

The activation energy and the half-lives to the thermal relaxation of unstable **4**, which is formed upon UV irradiation, is highly dependent on the polarity of the solvent, by increasing polarity, the energy barrier is lowered and a much shorter lifetime from seconds to microseconds observed. The solvent effect on the thermal step might be ascribed to the strong electronic push-pull effect of **4**: a zwitterionic structure might be formed (Scheme 2). The zwitterionic structure can be stabilized more in polar solvents than nonpolar solvents. In addition, the central olefinic structure has substantial single-bond character, and the more flexible zwitterion suffers less steric hindrance and therefore lower barriers to thermal helix inversion are observed.

However, the full rotation, unstable isomer and PSS upon irradiation of **4** could not be confirmed. Several attempts by ^{1}H NMR spectroscopy to determine the PSS of **4** upon irradiation failed.[23] Transient absorption spectroscopy of **4** gives a lifetime in toluene at -80 ^{o}C (calculated from the Erying plot) of ca. 2 hour, which is long enough for a single ^{1}H NMR measurement at -80 ^{o}C, however, no changes in ^{1}H NMR spectra were detected after irradiation for 4 h in toluene-d_{8}.

A study of the photoisomerization of **4** over a range of concentrations was carried out also. The change in absorbance at several concentrations upon UV irradiation was monitored by UV/vis absorption spectroscopy at 203 K in toluene (Figure 12). The absorption of the new band with the maximum at ca. 520 nm reaches a maximum as the concentration of **4** increases in toluene. This saturation means that the unstable species formed from **4** upon UV irradiation is limited to a certain concentration, less than 50 μM even at low temperature. This might be the reason that the thermally unstable isomer of **4** cannot be detected by ^{1}H NMR spectroscopy. At higher concentration, limitations to photoisomerization were also observed with some thioindigoid and stilbene derivatives.[24,25] Possible reasons for the concentration limit of PSS discussed in the literature are that a catalytic process or electron transfer reaction between *trans* and *cis* isomers is involved, or an exciplex or dimer is formed at high concentration.
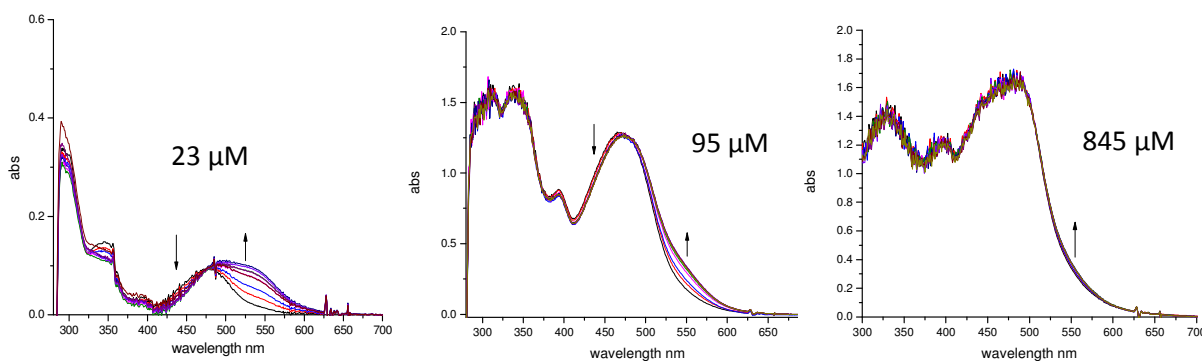

Figure 12. UV/vis spectra at several concentration of **4** (left 23 μM, middle 95 μM and right 845 μM) in toluene at 203 K upon UV irradiation over 1 h to reach the PSS state.

6.3.6 Minute molecular motor **6**

The photochemical and thermal helix inversion of molecular motor **6** was monitored by UV/vis absorption spectroscopy at room temperature. UV irradiation of **6** in toluene led to a red shift of the lowest absorption band from 390 nm to 410 nm (Figure 13), and leaving the solution in dark for 20 min at room temperature resulted in a restoration of the original spectrum.
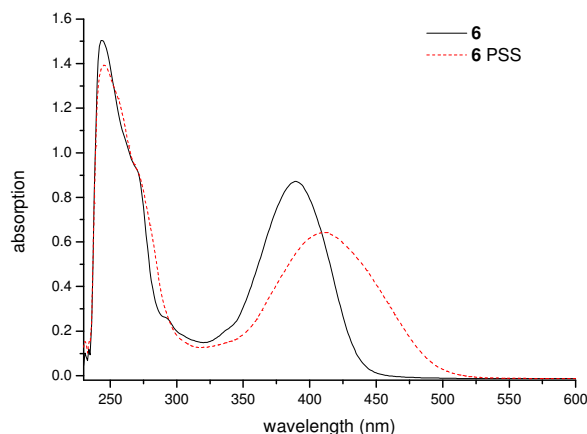
Figure 13. UV/vis absorption spectra of stable-**6**, the PSS (at 312 nm) mixture of stable and unstable-**6** in chloroform upon UV irradiation .

The energy barriers and half-life of **6** were studied in detail previously.[23] Together with other molecules investigated in this chapter, the main properties of these motor functional molecules are summarized in Table 3, in which the half-lives range from ns to min as expected from motors with different substituents in upper and lower parts.

Table 3. Properties of molecular motor **1-6**.

	λ_{max} *(nm)*	$\Delta^{\ddagger}G^{o}$ *(kJ/mol)*	$\tau_{1/2}$ *at RT*
1	349	29.98	36 ns
2	371	41.0	2.8 μs
3	351	58.4	1.4 ms
4	459	71.6	2.38 s
5	370	81.5	40 s
6	390	85	3 min

6.4 Conclusion

In conclusion, a series of molecular motors were characterized by UV/vis steady state absorption and transient absorption spectroscopies. Transient absorption spectroscopy is shown to be an efficient method to detect the transient behavior of molecular motors, especially those with relatively high rates of rotation. By

measuring the lifetime of the thermal relaxation at several temperatures, the energy barrier between thermally unstable and stable forms in the ground state can be determined.

Motor **1** was shown to have a half-life of 36 ns at room temperature, which is the fastest motor reported to date. The transient absorption measurements show the same results as the published data for motor **2**.[13] Motor **3** has a millisecond half-life. Molecular motor **5**, with an N-Boc protected group in the upper part, did not show an obvious electronic push-pull effect, which was confirmed by measuring the thermal lifetime in the solvents of differing polarity. In case of **4**, a strong push-pull effect was observed, however, the fully rotary motor function cannot be detected by ^{1}H NMR spectroscopy because of the low PSS at the relative high concentration needed (>100 μM). The accurate determination of the rotary speed and energy barrier of these molecular motors can provide useful insights and will support diverse applications of molecular motors.

6.5 Experimental Section

Details of syntheses and characterizations of the molecular motors in this chapter are described in references [16], [22], [23] and [26].

General remarks

All spectra were recorded in 1 × 1 cm quartz cuvettes. For transient absorption measurements, the absorbance at the excitation wavelength was between 0.5 and 1.0, and UV/vis absorption spectra of the samples were measured to ensure that photodegradation did not occur. UV/Vis absorption spectra were measured on a Hewlett-Packard HP 8543 FT spectrophotometer, and Cyro-UV/vis and transient absorption were performed using an Oxford Instruments OptistatDN variable temperature liquid nitrogen cryostat.

Transient absorption spectroscopy

The laser flash photolysis setup includes one nanosecond Nd:YAG laser worked as a pump light source and one pulsed Xenon lamp worked as a probe light source. The laser (Innolas 400) with a 6 ns pulsed width was set at the third harmonic 355 nm, 2-8 mJ pulse, 10 Hz. The Xenon lamp (Applied Photophysis) with its pulse unit (Applied Photophysis ARC Lamp Pulser) have synchronized to

the flash lamp of pulsed laser. When the transient signal is strong enough, the xenon lamp can work without the pulse function. The pump and probe light source were perpendicular to each other. The signal was detected by photo multiplier tube (Zolix PMTH-S1-CR131) which coupled with a monochromator (Zolix Omni-λ 300) to select the wavelength. The transient was record on digital phosphor oscilloscope (Tektronix DPO 4032) and it was triggered by a Si-diode sensor which detects the scattering light of the laser. The transients were transferred to a PC for data analysis using homebuilt software written in National Instruments LabVIEW 8.2, see chapter 2 and appendix.

6.5 References

[1] N. Koumura, E. W. J. Zijlstra, R. A. van Delden, N. Harada, B. L. Feringa, *Nature*, **1999**, *401*,152-155.

[2] A. Kazaryan, M. Filatov, *J. Phys. Chem. A*, **2009**, *113*, 11630–11634.

[3] A. Kazaryan, J. C. M. Kistemaker, L. V. Schäfer, W. R. Browne, B. L. Feringa , M. Filatov, *J. Phys. Chem. A*, **2010**, *114*, 5058–5067.

[4] M. Klok, M. Walko, E. M. Geertsema, N. Ruangsupapichat, J. C. M. Kistemaker, A. Meetsma, B. L. Feringa, *Chem. Eur. J.,* **2008**, *14*, 11183-11193.

[5] G. Pérez-Hernández, L. González, *Phys. Chem. Chem. Phys.*, 2010, **12**, 12279-12289.

[6] F. Liu, K. Morokuma, *J. Am. Chem. Soc.*, **2012**, *134*, 4864–4876.

[7] R. Augulis, M. Klok, B. L. Feringa, P. H. M. van Loosdrecht, *Phys Stat. Sol. (c)* **2009**, *6*,181-184.

[8] J. Conyard, K. Addison, I. A. Heisler, A. Cnossen, W. R. Browne, B. L. Feringa S. R. Meech, *Nat. Chem.*, **2012**, *4*, 547–551.

[9] J. Wang, B. L. Feringa, *Science,* **2011**, *331*, 1429-1432.

[10] R. A. van Delden, M. K. J. ter Wiel, M. M. Pollard, J. Vicario, N. Koumura, B. L. Feringa, *Nature,* **2005**, *437*, 1337-1340.

[11] R. Eelkema, M. M. Pollard, J. Vicario, N. Katsonis, B. S. Ramon, C. W. M. Bastiaansen, D. J. Broer, B. L. Feringa, *Nature,* **2006**, *440*, 163.

[12] T. Kudernac, N. Ruangsupapichat, M. Parschau, B. Maciá, N. Katsonis, S. R. Harutyunyan, K. Ernst, R. Eelkema, M. M. Pollard, J. Vicario, N. Katsonis, B. S. Ramon, C. W. M.

Bastiaansen, D. J. Broer, B. L. Feringa, *Nature,* **2006**, *440*, 163. B. L. Feringa, *Nature*, **2011**, *479*, 208–211.

[13] K. Kinosita, Jr., K. Adachi, H. Itoh, *Annu. Rev. Biophys. Biomol. Struct.,* **2004**, *33*, 245-268.

[14] N. Koumura, E. M. Geertsema, M. B. van Gelder, A. Meetsma, B. L. Feringa, *J. Am. Chem. Soc.*, **2002**, *124*, 5037–5051.

[15] M. Klok, N. Boyle, M. T. Pryce, A. Meetsma, W. R. Browne, B. L. Feringa, *J. Am. Chem. Soc.,* **2008**, *130*, 10484–10485.

[16] M. Klok, *Ph. D. Thesis*, University of Groningen, **2009**.

[17] D. Pijper, R. A. van Delden, A. Meetsma, B. L. Feringa, *J. Am. Chem. Soc.*, **2005**, *127*, 17612-17613.

[18] J. Vicario, A. Meetsma, B. L. Feringa, *Chem. Comm.,* **2005**, 5910-5912.

[19] R. A. van Delden, N. Koumura, A. M. Schoevaars, A. Meetsma, B. L. Feringa, *Org. Biomol. Chem.* **2003**, *1*, 33-35.

[20] W. F. Jager, J. C. de Jong, B. de Lange, N. P. M. Huck, A. Meetsma, B. L. Feringa, *Angew. Chem. Int. Ed.,* **1995**, *34*, 348-350.

[21] M. M. Pollard, A. Meetsmaa, B. L. Feringa, *Org. Biomol. Chem.,* **2008**, *6*, 507-512.

[22] A. Cnossen, *Ph. D Thesis,* University of Groningen, **2013**.

[23] D. Pijper, *Ph. D Thesis*, University of Groningen, **2008**.

[24] C. P. Klages, K. Kobs, R. Memming, *Ber. Bunsen Ges. Phys. Chem.,* **1982**, *86*, 716-720.

[25] D. S. Frohlinde, H. Blume, H. Gusten, *J. Phys. Chem.*, **1962**, *66,* 2486–2491.

[26] J. Bauer, *Ph. D Thesis,* University of Groningen, **2013**.

Molecular photochemistry is the study of transformations upon interaction with light. Molecules that absorb the energy of photons are promoted to electronically excited states, from where they relax rapidly to the lowest vibrational level of the ground state or yield new chemical species by emission of photons or vibrational heat, or encounter other molecules to transfer electrons, protons, H atoms or energy. Understanding photochemical processes is crucial to investigate photosynthesis in nature and artificial photoresponsive systems. In the Characterization of photochemical processes generally two types of measurements are employed: steady state and time resolved spectroscopy. Steady state spectroscopy is relative simple to implement with the use of a continuous light source for illumination and recording continuous light intensity. Much of the dynamic information of molecules is lost through the time averaging of processes in steady state measurements. Time-resolved spectroscopy requires more complex systems, using a short pulsed light source, where the pulse width is much shorter than the decay time of the excited state, to generate time-dependent information of molecules of interest and reveals more molecular information, e.g. quenching, energy transfer and electron transfer rates.

The research described in this thesis applies both steady state and time-resolved spectroscopy to investigate several photoswitchable molecular systems, in which the functions and properties can be controlled by light, or modified through photoinduced energy transfer or electron transfer. These photoswitchable molecular systems are designed for the application in nanotechnology and developing new materials, e.g. photoswitching of magnetic interactions, graphene-porphyrin hybrid materials; or for future application in biology, e.g. driving molecular motors with visible light, control of singlet oxygen generation in photodynamic therapy, etc.

Chapter 1 introduced the main concepts and processes in molecular organic photochemistry. Fundamental photophysical processes (absorption, emission) and some typical photochemical reactions (photocycloaddition, photoreduction and photoisomerization) are discussed. Bimolecular photochemistry, including collisional quenching, electron transfer and energy transfer, is also described, and

several examples are given to illustrate some applications based on photochemistry.

Chapter 2 described three home-built spectroscopic systems. The first system was developed to measure time resolved luminescence, as well as measuring steady state emission spectra. The second is a laser flash photolysis system that can be used to measure time resolved absorption as well as steady state absorption spectra. The last system is designed to measure steady state NIR emission. The software for system control, data acquisition and analysis is described in the appendix. These systems together with other spectroscopies were used to study photoswitchable molecular systems described in this thesis.

In chapter 3 an intramolecular photoswitchable system is described, in which through-space magnetic interactions can be switched on and off. The interaction between two TEMPO spin centers connected to a photoswitchable overcrowded alkene changes from noncoupled in the *trans* state, to strongly coupled in the *cis* state. Switching magnetic interaction can be achieved at room temperature without compromising the efficiency of the photoswitching processes. Steady state UV/vis absorption, EPR and ^{1}H NMR spectroscopies were used to study the functioning of this system.
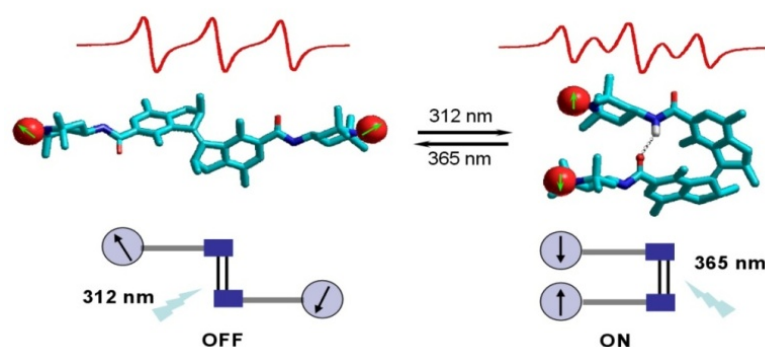
In Chapter 4 two porphyrin modified systems are described. Porphyrins were used to modify graphene through a covalent approach in the first system. The presence of porphyrin on graphene was studied by steady state UV/vis absorption spectroscopy, and energy/electron transfer was demonstrated by steady state and time resolved luminescence spectroscopy. The second system uses a porphyrin to drive the unidirectional rotation of a molecular motor. The unidirectional rotation of the hybrid system was characterized by steady state UV/Vis absorption and

CD spectroscopies, and energy transfer via triplet excited states was demonstrated by steady state and time resolved luminescence measurements.
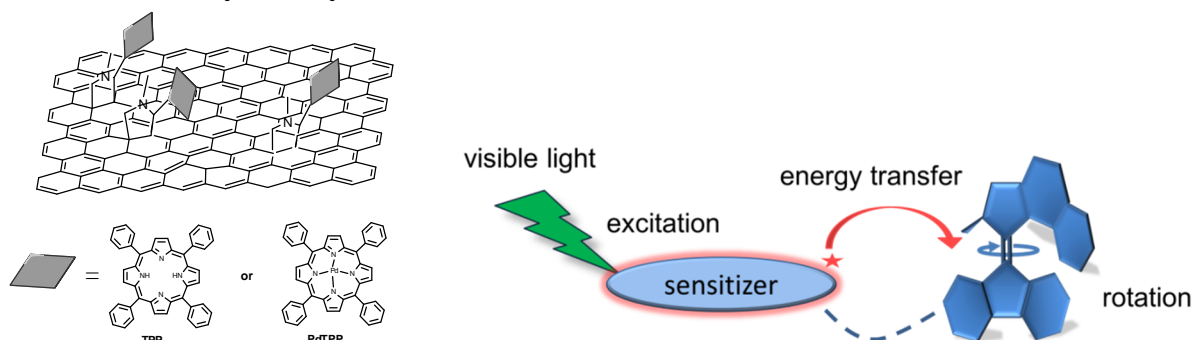
In Chapter 5 diarylethene switches were used to control singlet oxygen generation in zinc porphyrin through intermolecular energy transfer. Singlet oxygen can be generated by excitation of zinc porphyrin in the presence of the open form of diarylethene. Switching the diarylethene to its closed form by UV irradiation, results in singlet oxygen generation not being observed. Singlet oxygen generation was monitored by steady state NIR emission spectroscopy, and energy transfer through triplet excited state study was studied by time resolved absorption spectroscopy.
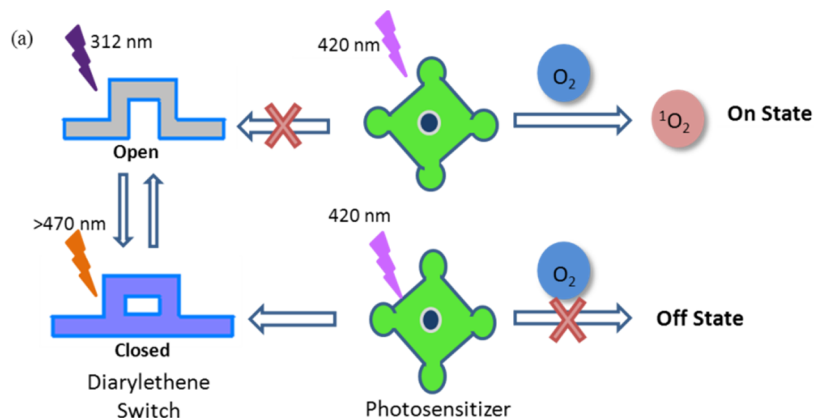
Chapter 6 is focused on the characterization of six light driven molecular rotary motors with various rotatory speeds. Time resolved absorption spectroscopy was used to study the relatively fast thermal relaxation, from ns to ms, and steady state UV/vis absorption spectroscopy was used to study slow molecular motors in the sec to min time domain. By measuring lifetimes of the thermal relaxation at several temperatures, the energy barriers between thermally unstable and stable forms of six compounds in the ground states were determined.

Summary

Moleculaire fotochemie is de studie van transformaties onder invloed van licht. Moleculen die fotonen absorberen kunnen in een elektronisch aangeslagen toestand worden gebracht, vanwaar zij kunnen relaxeren naar de laagste vibrationele toestand door middel van de uitzending van fotonen of warmte. Andere processen die kunnen plaatsvinden vanuit de elektronisch aangeslagen toestand zijn de overdracht van electronen, protonen, waterstofatomen of energie naar andere moleculen. Het begrijpen van fotochemische processen is cruciaal voor het onderzoek naar fotosynthese in de natuur en kunstmatige fotoresponsieve systemen. Bij het bestuderen van fotochemische processen worden in het algemeen twee soorten spectroscopie gebruikt: steady state en time resolved spectroscopie. Steady state spectroscopie is relatief gemakkelijk toe te passen door het gebruik van een continue lichtbron voor bestraling en het continu meten van de lichtintensiteit. Met steady state spectroscopie gaat veel informatie over het dynamische gedrag van moleculen verloren door het uitmiddelen van verscheidene processen over tijd. Time resolved spectroscopie vergt complexere systemen met een korte puls lichtbron, waarvan de pulsbreedte korter is dan de vervaltijd van de aangeslagen toestand van de te bestuderen moleculen. Met deze meettechniek kan informatie vergaard worden over moleculaire processen zoals quenching, energie-overdracht en de snelheid van elektronenoverdracht.

In het onderzoek beschreven in dit proefschrift is zowel gebruik gemaakt van steady state als time resolved spectroscopie om verschillende met licht schakelbare moleculaire systemen te bestuderen. De functies en eigenschappen van deze systemen kunnen bediend of veranderd worden door middel van licht. Deze moleculaire, met licht schakelbare systemen zijn ontworpen voor toepassing in de nanotechnologie en voor de ontwikkeling van nieuwe materialen zoals grafeen porfyrine hybride materialen. Toekomstige toepassingen in de biologie behoren ook tot de mogelijkheden, zoals de controle over singlet zuurstof productie voor fotodynamische therapie.

In hoofdstuk 1 worden de algemene concepten en processen in de moleculaire organische fotochemie geïntroduceerd. Fundamentele processen (absorptie, emissie) en verscheidene fotochemische reacties (fotocycloadditie, fotoreductie en fotoisomerizatie) worden besproken. Bimoleculaire fotochemie, zoals collisional quenching, elektronoverdracht en energie-overdracht, wordt

beschreven en verscheidene voorbeelden zijn gegeven ter illustratie van verschillende toepassingen gebaseerd op fotochemie.

Hoofdstuk 2 beschrijft drie zelf opgezette spectroscopische systemen. Het eerste systeem was ontwikkeld om time resolved luminescentie als ook steady state emissie te meten. Het tweede systeem is een laser flash fotolyse systeem dat gebruikt kan worden voor metingen aan time resolved en steady state absorptie. Het laatste systeem is ontworpen voor het meten van steady state NIR emissie. De software voor het beheren van het systeem, data acquisitie en analyse is beschreven in de appendix. Deze drie systemen tezamen met andere spectroscopische methodes zijn gebruikt om met licht schakelbare moleculaire systemen te bestuderen.

In hoofdstuk 3 is een met licht schakelbaar systeem beschreven, waarvan de intramoleculaire magnetische interactie aan- en uitgezet kan worden. De interactie tussen twee TEMPO spin centra, met elkaar verbonden door een met licht schakelbaar overbezet alkeen, kan geschakeld worden van niet-gekoppeld in de trans vorm naar sterk gekoppeld in de cis vorm. Het schakelen van magnetische interactie kan worden bewerkstelligd zonder de efficiëntie van het schakelproces te hinderen. Steady state UV/vis absorptie, EPR en 1H NMR spectroscopie zijn gebruikt voor het bestuderen van het functioneren van dit systeem.
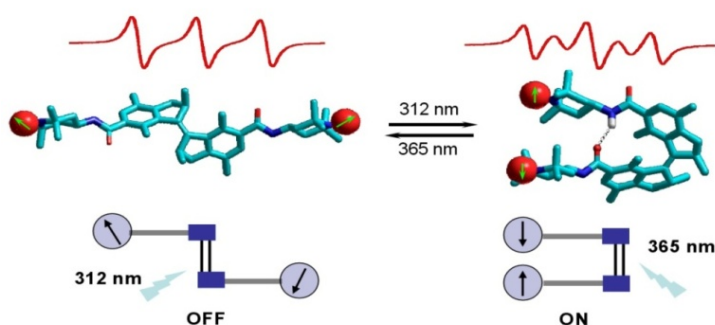
In hoofdstuk 4 zijn twee gemodificeerde porfyrine systemen beschreven. In het eerste systeem zijn porfyrines gebruikt om grafeen te modificeren door middel van een covalente aanpak. De porfyrines op grafeen zijn bestudeerd met steady state UV/vis absorptie spectroscopie en energie/elektron overdracht was aangetoond door middel van steady state en time resolved luminescentie spectroscopie. Het tweede systeem gebruikt een porfyrine om de unidirectionele rotatie van een moleculaire motor aan te drijven. De unidirectionele rotatie van

dit hybride systeem is gekarakteriseerd met steady state UV/vis absorptie en CD spectroscopie. Energie-overdracht via triplet aangeslagen toestanden is aangetoond met steady state en time resolved luminescentie metingen.
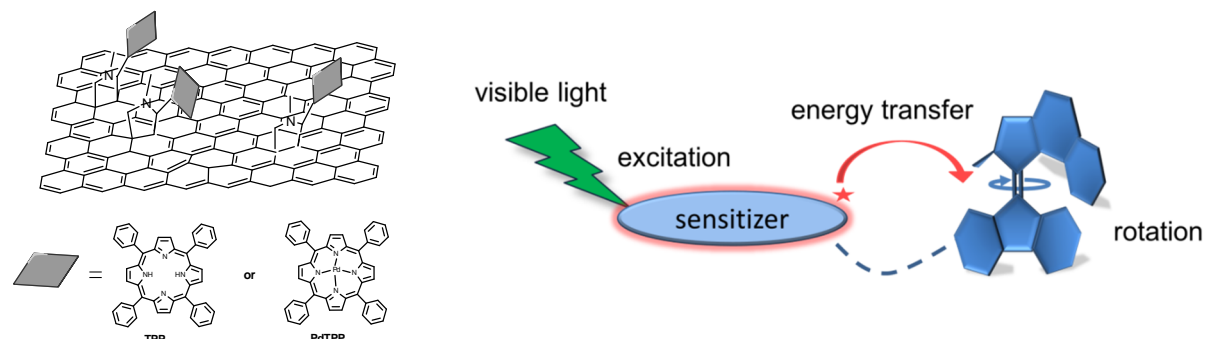
In hoofdstuk 5 zijn diaryletheen schakelaars gebruikt om de genereratie van singlet zuurstof te reguleren. Singlet zuurstof kan worden gemaakt door de excitatie van zink porfyrine in de aanwezigheid van de open vorm van een diaryletheen. Het schakelen van de diaryletheen naar zijn gesloten vorm door middel van UV bestraling, resulteert in het stopzetten van het genereren van singlet zuurstof. De productie van singlet zuurstof werd gevolgd met steady state NIR emissie spectroscopie. Energie-overdracht is bestudeerd door middel van time resolved absorptie spectroscopie.
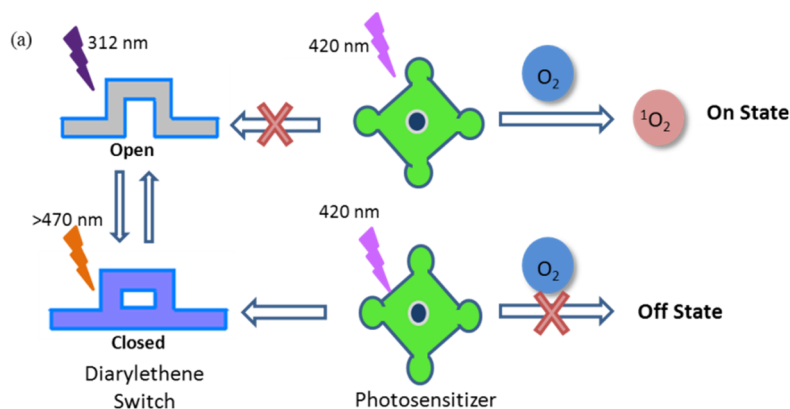
Hoofdstuk 6 richt zich op de karakterisering van zes door licht aangedreven moleculaire rotatie motoren. Time resolved spectroscopie is gebruikt voor het bestuderen van de relatief snelle thermische relaxatie, van ns tot ms, en steady state spectroscopie is gebruikt voor het bestuderen van langzame moleculaire motoren. Door het meten van de halveringstijd van de thermische relaxatie bij verschillende temperaturen, zijn de energiebarrières tussen de thermische instabiele en stabiele vorm van zes moleculen bepaald.

Samenvatting

有机分子光化学是一门研究有机分子与光相互作用的学科。分子通过吸收光子能量，跃迁到激发态电子能级。而后，以发射光子或热量的形式，从激发态电子能级跃迁回基态的最低震动能级，或者生成新的化学物质。在从激发态能级向基态能级跃迁过程中，被激发的分子有可能与其它分子相遇，从而导致分子间的电子转移、质子转移、氢原子转移或能级转移。掌握光化学过程对研究自然中的光合成过程以及人工合成光敏系统有着极其重要的作用。研究光化学过程通常使用两种方法：稳态光谱法和瞬态光谱法。稳态光谱法实现起来相对容易：通过连续光源激发样品，同时记录和时间无关的光强信息。由于对所测光强在时间上做了平均处理，基态光谱法无法捕捉分子的动态信息。瞬态光谱法实现起来相对复杂：需要使用脉冲光源，且要保证光脉冲宽度远远小于所研究的动态过程寿命。瞬态光谱法可以用来获取与时间相关的光信号，从而揭示所研究分子的更多特性，比如光淬灭、能量转移、电子转移等过程。

在本论文中，通过稳态光谱法和瞬态光谱法，深入研究了几种不同特性的光控分子系统。在这些系统中，光照能够转变分子系统的功能和特性，或者导致能量或电子转移。这些光控分子系统在纳米技术及新材料设计方面有着潜在的应用价值，比如，光控磁性开合可以应用于分子范围内的数据处理及储存，石墨烯卟啉复合材料可以应用于太阳能存储。此外本论文中所研究的其他光控分子系统，比如，可见光驱动分子马达，控制光动力疗法中单线态氧的产生，能够为未来生物领域的应用提供借鉴意义。

第一章主要介绍了有机分子光化学的概念及主要的光化学过程，其中，列举了基本的光化学过程，如光吸收过程，光发射过程，及典型的光化学反应，如光加成反应，光还原反应和光致异构反应。此外，本章还讨论了几种典型的双分子光化学过程，如碰撞致光淬灭、电子转移、能量转移，并用相应的例证阐明了光化学过程在实际中的应用。

第二章详细介绍了三个自主搭建的光谱系统。第一个光谱系统能够用来测量时间分辨的发光光谱和稳态发光光谱。第二个光谱系统，基于激光闪光

光解技术，能够用来测量时间分辨的吸收光谱和基态吸收光谱。第三个光谱系统可以用来测量稳态近红外发光光谱。通过在 LabVIEW 中编译的一系列软件实现对这些系统的控制，数据采集和分析，软件部分设计参见附录。对本论文中讲述的几种光控分子系统的研究正是基于本章所搭建的光谱系统，及一些常见的其它光谱技术完成。

第三章介绍了一个能够控制分子内部空间磁性开合的光控分子系统。该分子系统的设计基于在挤迫型多烯的两端各连接了一个四甲基哌啶氧化物自由基（TEMPO）。当挤迫型多烯处于反式构型时，两个四甲基哌啶氧化物自由基之间不存在相互耦合作用。光照拥挤烯烃使之处于顺式构型时，两个四甲基哌啶氧化物自由基之间存在强烈的磁性耦合。该分子系统通过不同波长的光照能够实现室温下的磁性开合控制，并且分子本身的光化学性能未受到影响。在本章中通过基态紫外-可见光吸收光谱、电子自旋共振（EPR）及氢谱核磁共振（^{1}H NMR）手段对该分子系统的性能进行了深入探讨。
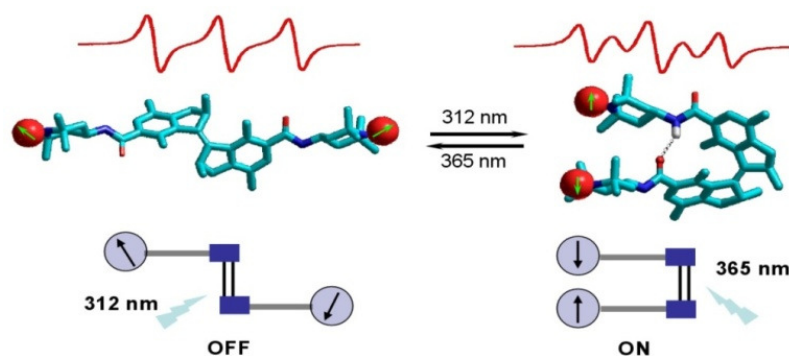
第四章介绍了两个卟啉修饰的系统。在第一个系统中，通过环加成反应，共价连接卟啉与石墨烯。通过基态紫外-可见光吸收光谱分析证明了卟啉存在于复合材料中。稳态和瞬态发光光谱表明了在复合材料中存在的电子或能量转移。第二个系统使用卟啉驱动分子马达，通过能量转移，实现了利用可见光驱动分子马达。基态紫外-可见光吸收光谱、圆二色谱（CD）表明了分子马达在可见光驱动下的单向转动。稳态和瞬态发光光谱证明了分子系统中的三线态能量转移。
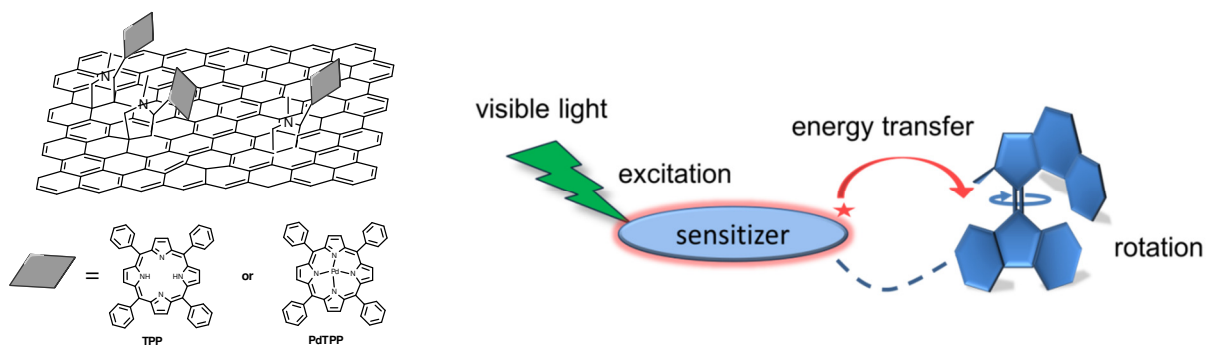
在第五章中，利用了二芳基乙烯分子开关，控制锌卟啉产生单线态氧的能力。当二芳基乙烯处于开环构型时，光照（420 nm）锌卟啉能够产生单线态氧。然而，当紫外光照射，使二芳基乙烯处于闭环构型时，光照（420 nm）锌卟啉不能产生单线态氧。在本章中，单线态氧的检测通过近红外发光光谱，三线态能量转移的检测通过瞬态吸收光谱。
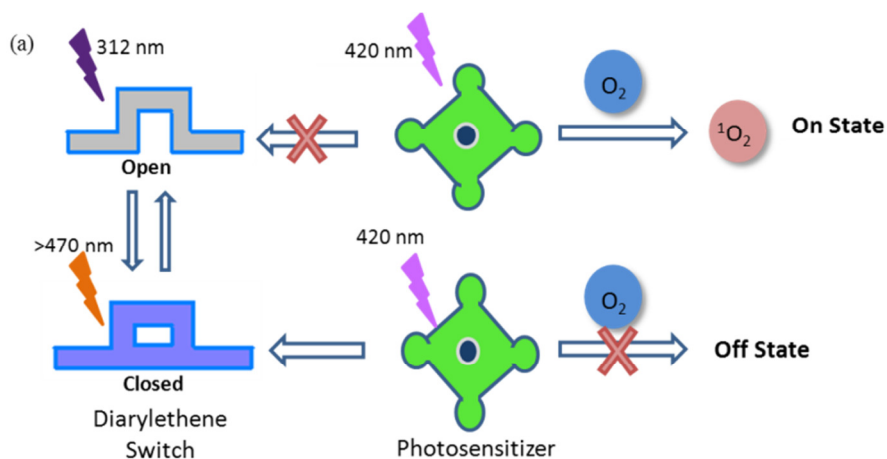
第六章主要研究了六个不同转动速度的分子马达的特性。对拥有相对较快热弛豫的分子马达（纳米到毫秒级别），使用了瞬态吸收光谱技术进行分析。对有相对较慢热弛豫的分子马达，使用了基态紫外-可见光光谱技术进行分析。通过测定在不同温度下热弛豫的寿命，确定了分子马达在热稳态和非热稳态间的基态能量位垒。

总结

总结

APPENDIX

Software for Home-built Spectroscopic Systems Based on LabVIEW

A series of programs to control the home-built spectroscopic systems described in chapter 2 were developed in the LabVIEW programming enviroment. The software enables recording and preliminary analysis of spectra and transients. Some common features of the home-built spectroscopic systems allow the software to be used for steady state and time resolved experiments.

I.1 Introduction

All the systems described in chapter 2 need to be controlled via a computer, which should control the devices to accomplish their mission in proper order without conflict and record data for further analysis. These operations are completed by custom built software packages. Since there are three distinct systems, which are used to measure both steady and time resolved absorption and emission, a series of software packages were designed to meet the various requirements. Thanks to the common features and devices (e.g., monochromator, oscilliscope) of the systems, the software can be applied universally with minimal customization. All the software was developed in a visual programming language (graphical language 'G') based on LabVIEW, which is commonly used for data acquisition, instrument control, and industrial automation.[1]

LabVIEW programs/subroutines are called virtual instruments (VIs). Each VI has two components: a front panel and a block diagram. The front panel, built using controls and indicators, is the window through which the user can interact with the programs, e.g., inputting data, executing the program, monitor the output. The block diagram contains the graphical source code of programming. Once built, a VI can be used in other VIs by building a connector pane and creating an icon. A VI called from the block diagram of another VI is called a sub-VI. Sub-VIs are widely used in these software packages.

There are in total 9 programs that are divided into three parts: a laser as an excitation source, a lamp as an excitation source, and some applications of basic control and preliminary spectral analysis. When a laser is used as an excitation light source, only one emission monochromator is needed to obtain a spectrum which is relatively simple in terms of device control. When the excitation light source is a white light lamp (e.g., xenon lamp), an additional monochromator as excitation monochromator is required. Two monochromators working in parallel complicates communication with the computer. Additional programming is needed for two monochromators to be controlled, since the basic drivers available only support the control of a single monochromator. The basic applications are used to set the monochromators, directly record the waveform shown on the oscilloscope, and read and fit of the recorded data.

Two wavelength scanning modes are available for each excitation light source; continuous and step scanning of the monochromator, respectively. Continuous scanning mode is a recording method where the monochromator is set to scan through the whole wavelength range of interest with a relatively high speed with simultaneously recording of the spectrum by the oscilloscope and transfer to the control software. Continuous scanning mode allows for a quick assessment of the spectrum of interest albeit compromising resolution. Step scanning mode records the signal at each wavelength with preliminary data processing, e.g., averaging before moving to the next wavelength. The spectrum recorded in step scanning mode has much higher resolution but with a longer aquisition time. The signal can be recorded in either two dimensional, wavelength *vs.* signal intensity, which is generally used to obtain steady state spectra, or three dimensional, wavelength *vs.* time *vs.* signal intensity, which is used to obtain transient spectra.

The reason for separating the software based on each of different excitation light sources is that an extra monochromator is used to select the wavelength when white light excitation is used. Therefore, the two monochromators need to control and work together. The software should allow setting and controlling the two monochromators at the same time without conflict. The continuous scanning mode is used to do the fast measurement by setting the monochromator to scan while recording the spectrum. The step scanning mode sets the wavelength stably and then records the signal, before moving to the next wavelength. The wavelength of the monochromator is no reliable when fast scanning as it needs some time to respond and sit at the correct wavelength. The step scanning mode provides more accurate measurement with a cost in the time required.

I. 2 Software list

The programs with the functions described above are compiled within a main window by using a tree control (Figure 1, the front panel). This window is called the 'software list', in which the target program included can be selected by double clicking.

All programs included in 'software list' are defined as sub-VIs and called as an individual case in a case structure. This case structure is wired to the tag of the tree control, which responds to doubling clicking. An outer layer event structure enables the program to keep running unless the 'Exit' button on the front panel, a

Boolean control, is clicked. Clicking the button results in activating the stop event of the event structure, therefore, a true constant transfers to the outer layer while loop thereby stopping the whole program (Figure 1, the block diagram).
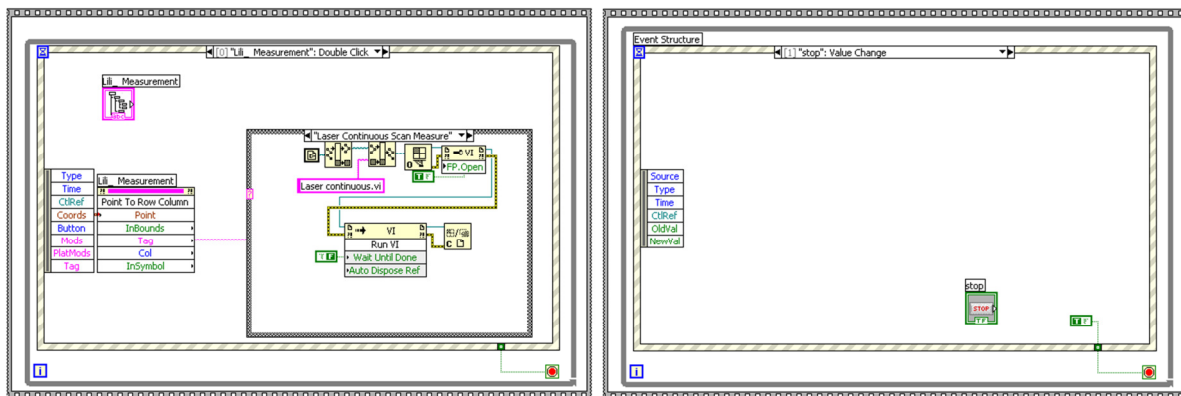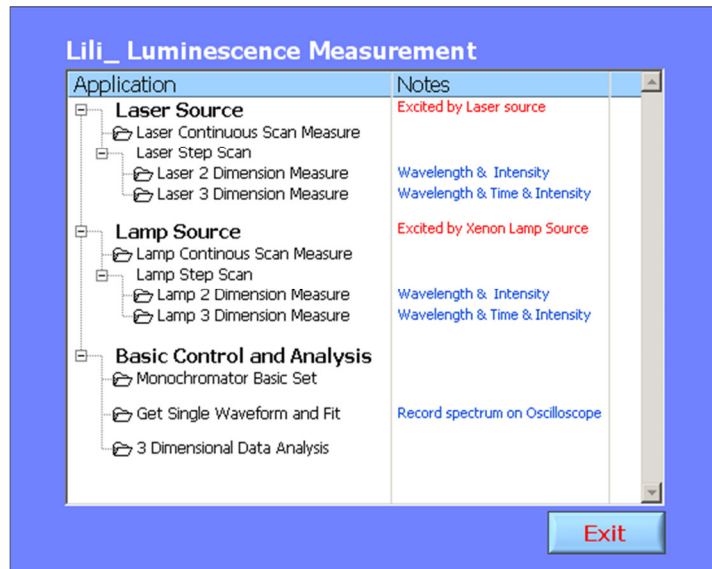

Figure 1. The front panel and block diagram for the software list.

I. 3 Continuous scanning mode (with laser excitation)

Figure 2 shows the main interface for continuous scanning measurements, when a laser is used as excitation source. The left area of the panel is used to set the device connection, parameters and end the whole process. The left bottom section shows the status of the monochromator during the measurement. The right area shows the real-time oscilloscope display and the final spectrum when the measurement is finished. The right bottom displays the parameters, which can be used to monitor whether the devices respond correctly by comparison with the left bottom part. The indicators of "index of element" and "handle" in the right

corner are the parameters for the rear diagram running monitor. Index of element is used to indicate the starting point of synchronization between the monochromator scanning and oscilloscope recording. Handle is a parameter generated by the monochromator when communication with the computer is established. It is a basic parameter to enable control of the monochromator.
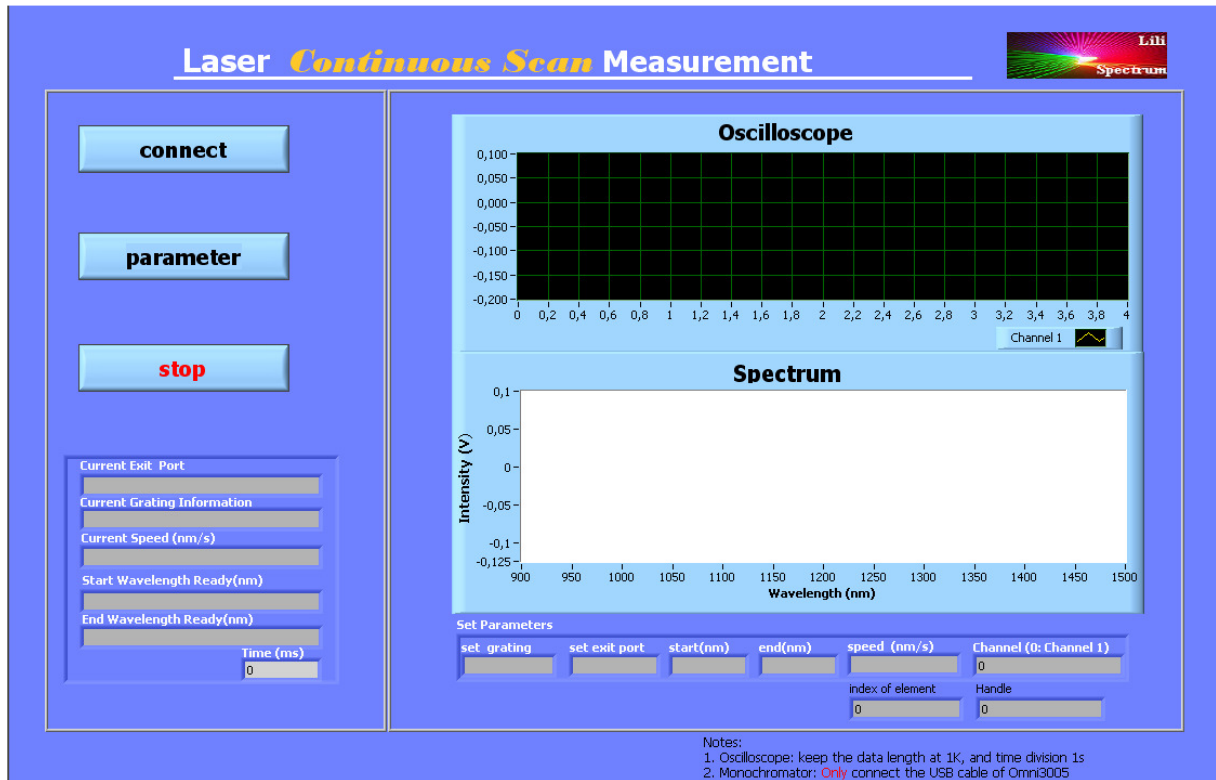
Figure 2. Front panel for continuous scanning measurements with laser excitation.

Figure 3 shows the block diagram for the graphical source code. It is separated into two frames in a flat sequence structure. The first frame codes the connection of the devices by calling a Sub-VI named "connect" in an event structure. Clicking the connect button on the front panel calls the sub-window of the connection, in which the devices can be selected and status of the connection can be monitored. The graphical source code of Sub-VI 'connect' is subsequently introduced. Setting the parameters, running the measurement and ending the program are compiled in the second frames. An event structure is used to respond to clicking to set parameters and end the program in the front panel, through use of two event cases named 'parameter' and 'stop'. A while loop is used in the outer layer of the event case, which allows repeated measurement without initializing the connection of devices. Disconnection only occurs when

the stop button is clicked on the front panel. A true constant transfers from the 'stop' event case to the outer layer while loop, thus ending the whole program.
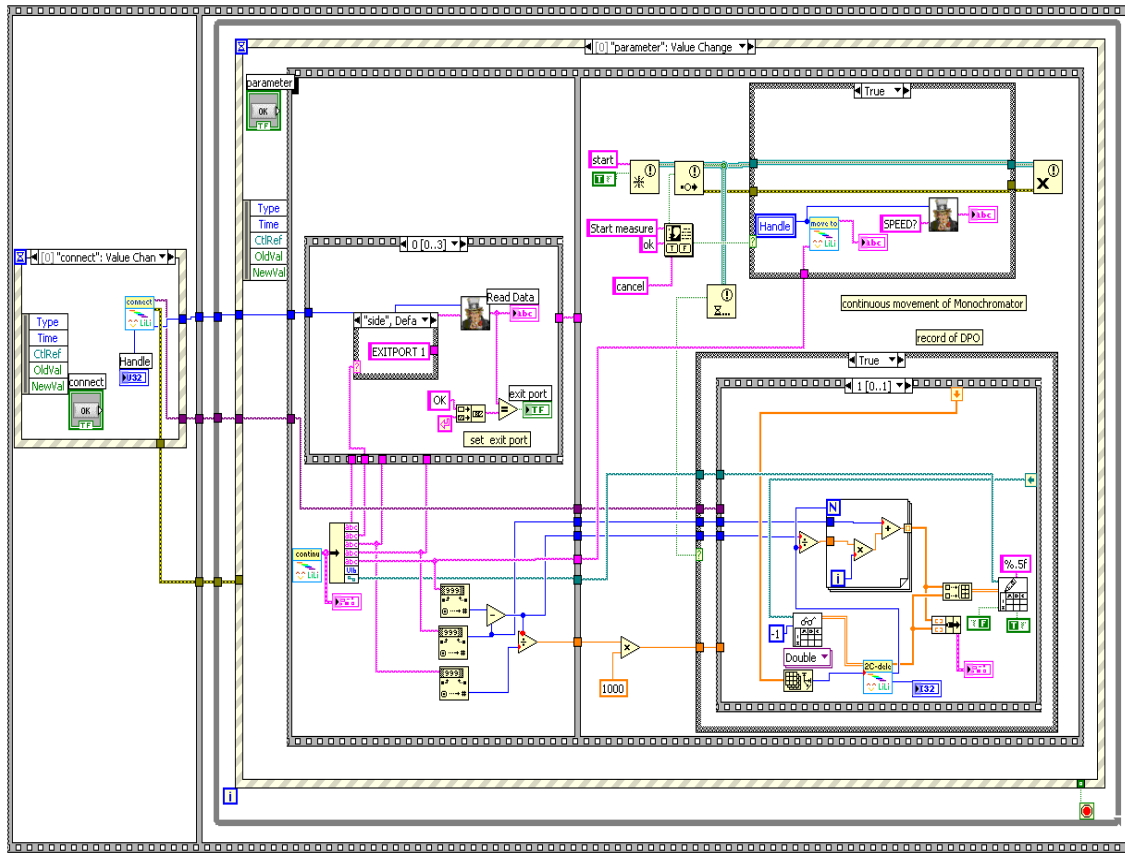
Figure 3. The block diagram for continuous scanning measurements with laser excitation.

Setting the parameters and processing the measurements are the major functions of this program. These two functions are further separated in chronological order by using a flat sequence structure in the event case 'parameter'. A Sub-VI named 'continu' is called for inputting the parameters in a sub-window. The graphical source code of Sub-VI 'continu' is subsequently introduced. Setting the monochromator according to the parameters is accomplished in a stacked sequence structure. This stacked sequence structure is unfolded into a flat sequence structure and shown in Figure 4, in which the exit port, grating and wavelength of the monochromator are set in sequence. The functions of all Sub-VIs in this sequence can be found in the manual of the monochromator. There is a Sub-VI named 'move to', as shown in Figure 5, which is used to convert the input string constant to the command that the monochromator can respond to and read the current wavelength position.
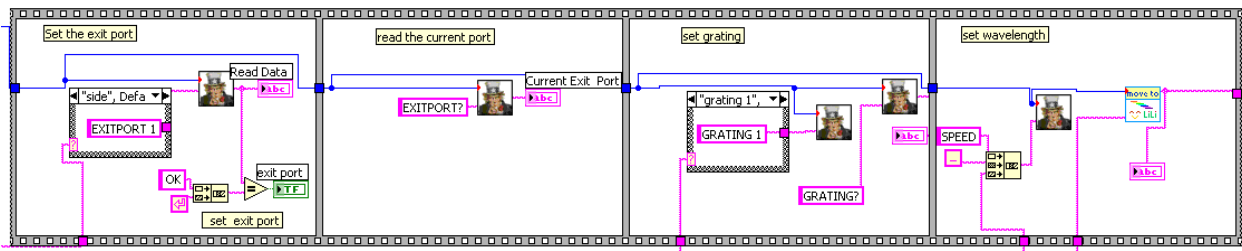
Figure 4. Unfolded the sequence structure for setting the monochromator in Figure 3.
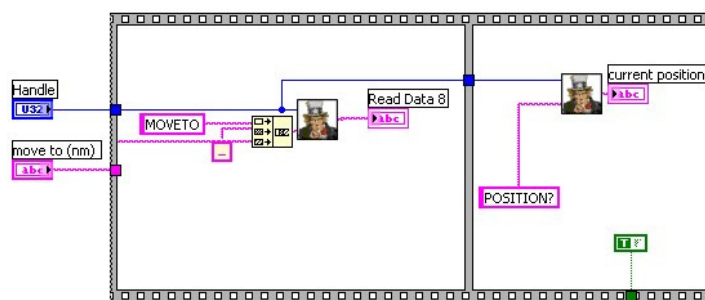
Figure 5. The block diagram for the 'move to' Sub-VI.

After the monochromator is set according to the input parameters, a dialog for starting the measurement appears. Clicking it sends a notification to the monochromator and starts recording by the oscilloscope. Acquiring a spectrum with the correct wavelength in continuous scanning mode needs synchronization between the oscilloscope and monochromator, however, a hardware connection between the devices is not available. Therefore, a software synchronization method is programed through notifier operations.

The case structure in the upper right corner in Figure 3 is used to start a continuous scan by the monochromator when the notification is received. The case structure in the bottom right corner is used to display and save the waveform displayed on the screen of the oscilloscope. The functions of displaying and saving are coded in chronological order by using a sequence structure, which is unfolded in Figure 6.
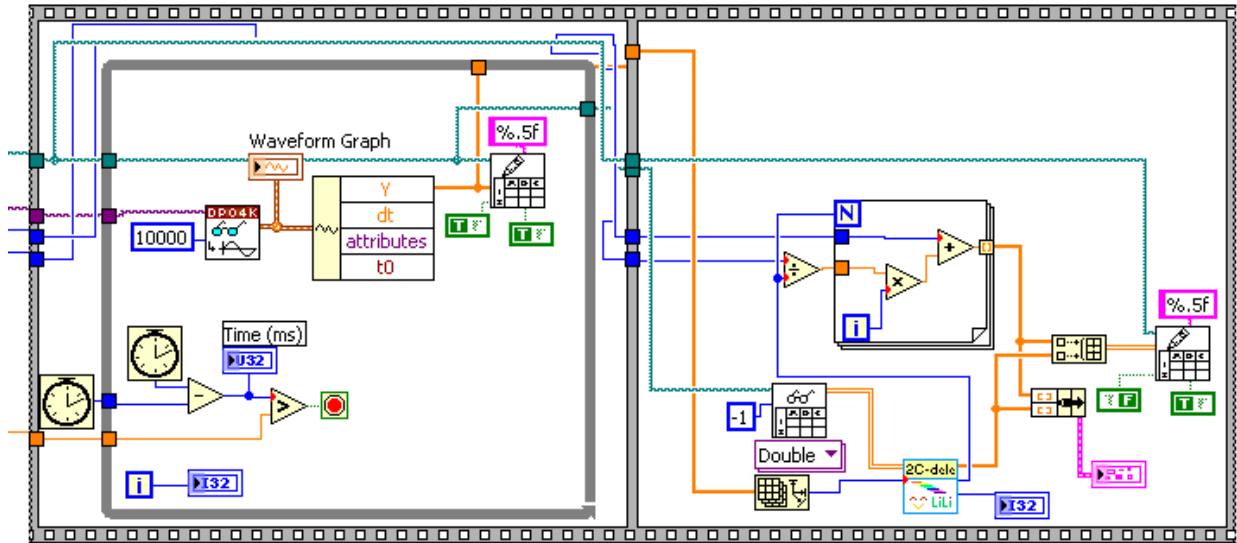
Figure 6. Unfolded sequence structure in the right corner of Figure 3.

Sub-VIs in this program are described as follow:

(1)   Sub-VI 'connect'

The front panel of this Sub-VI is shown in Figure 7. The sources of oscilloscope connection are listed in a combo box. Selecting the right source and clicking the button of 'Connect It' enables the connection between the oscilloscope and the computer. The status of connection is displayed on the right of the panel. The connection with the monochromator is achieved by clicking 'Connect It' in the monochromator box. The name and status of the monochromator are shown in the right corner of the panel. Clicking the button 'Exit' ends the process of connection.

Figure 7. The front panel of 'connect' Sub-VI.

An event structure is used to respond to the clicking operations on the front panel, in which three event cases are possible (Figure 8). The first event case is connection (Figure 8(a)). The initialization of the oscilloscope is accomplished by citing a Sub-VI named 'Initialize', whose detailed description refers to the driver of the oscilloscope.[2] A pop-up window is programed by using a case structure, to which the status of the oscilloscope is wired. The pop-up shows the status and instructions for the connection. The second event case is the monochromator connection. A stacked sequence structure is used to obtain the device description, open the device, write a string, obtain a queue status and read the string, which are unfolded in Figure 9. A time delay between the two frames is used to wait for the response. Detailed information on the Sub-VIs used here can be found in the manual of the monochromator. The parameter named 'Handle' is a crucial parameter to access all of the remote controls of the monochromator, and this parameter is generated uniquely once the connection is established. The last event case is exiting the program, which is achieved through the output of a true constant to the outside while loop (Figure 8 (C)).
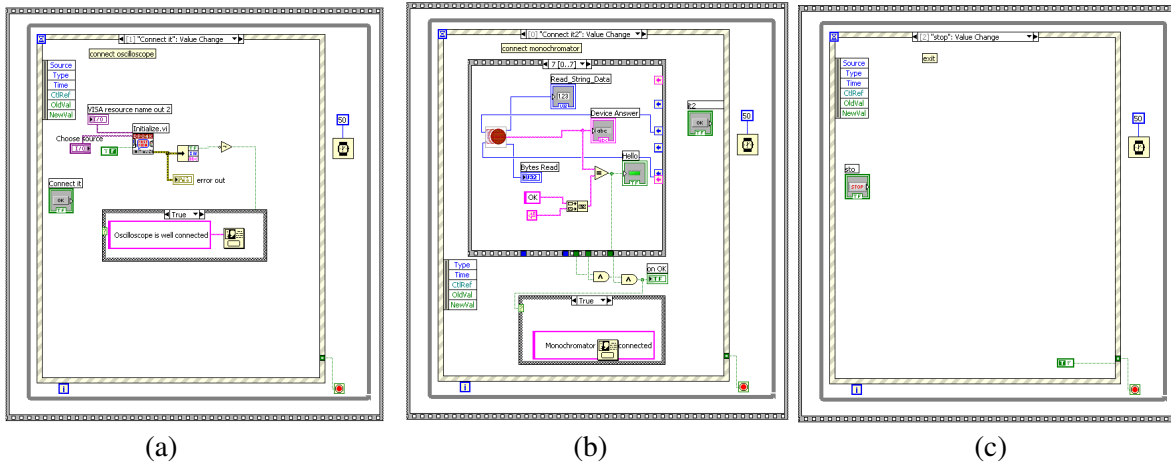
Figure 8. The block diagram of the 'connect' Sub-VI.
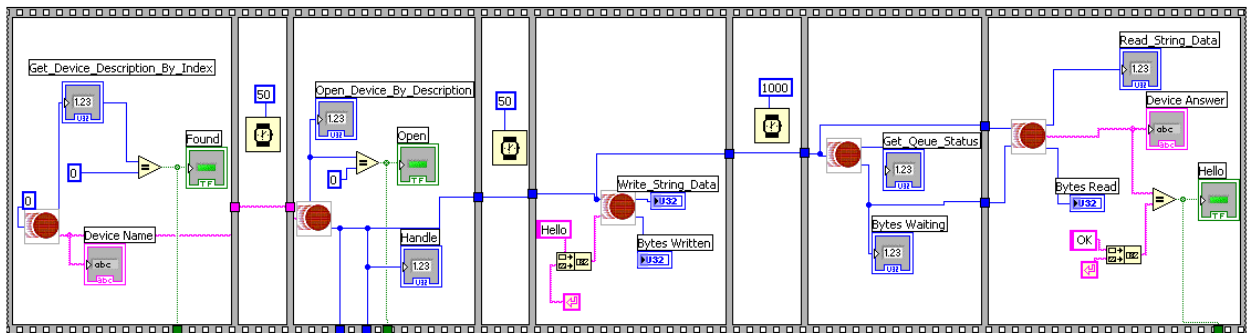

Figure 9. Unfolded sequence structure of the monochromator connection shown in Figure 8.

(2)   Sub-VI 'Laser_conti_para'

The front panel for the Sub-VI with the name of Laser_conti_para is used to input the parameters for the continuous scan measurements (Figure 10), which can be accessed by clicking the parameter button on the front panel that is shown in Figure 2. These parameters can be input either by selecting the items in a combo box or entering the number in a string control box. All of the input parameters are bundled and delivered to the main program. Clicking the 'Set OK' button on the front panel can exit this Sub-VI through stopping the while loop in the block diagram.
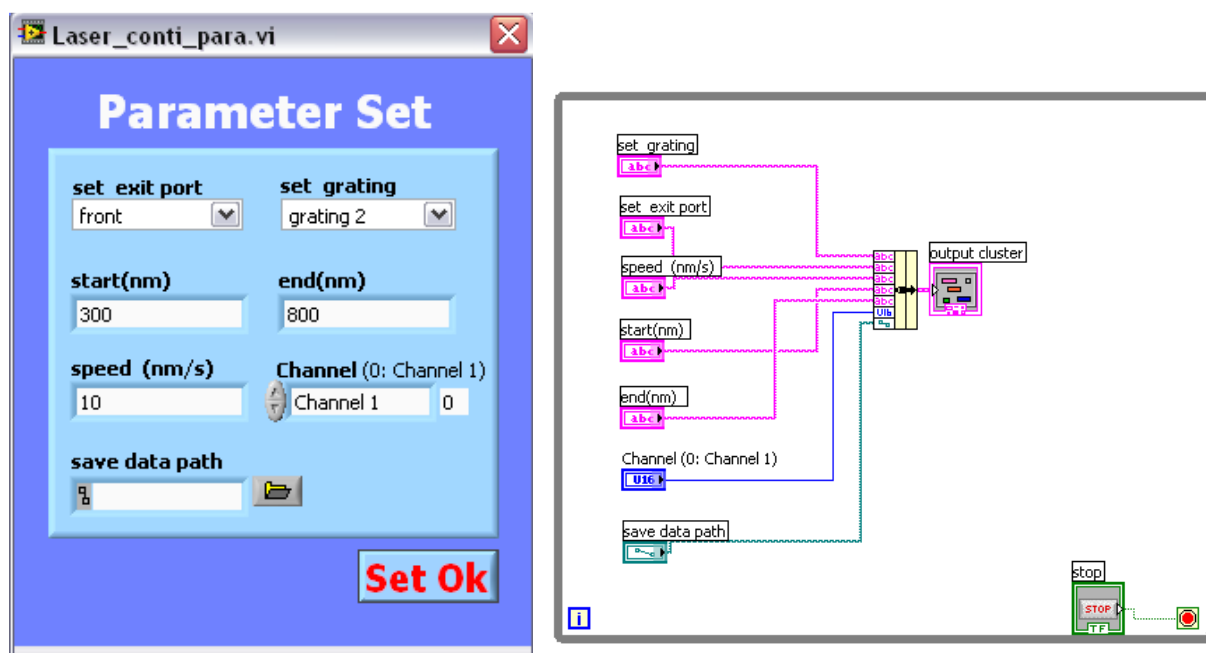
Figure 10 The front panel and block diagram of Sub-VI 'Laser_conti_para'.

I. 4 Step scanning measurements (2D mode, with a laser excitation)

The step scanning measurement in 2D mode is used to obtain a high quality steady state spectrum. The spectrum is plotted in the form of intensity (or absorbance) *vs.* wavelength. Figure 11 shows the front panel of this program. The left part is the control area, in which connecting the devices, inputting of parameters, starting the measurement and ending the program can be carried out. The left bottom panel shows the status of the monochromator and the status of wavelength movement in real-time. The right part is a synchronous display of the oscilloscope. The spectrum is shown in a chart, which is below the oscilloscope display window. The right bottom area shows the set parameters.
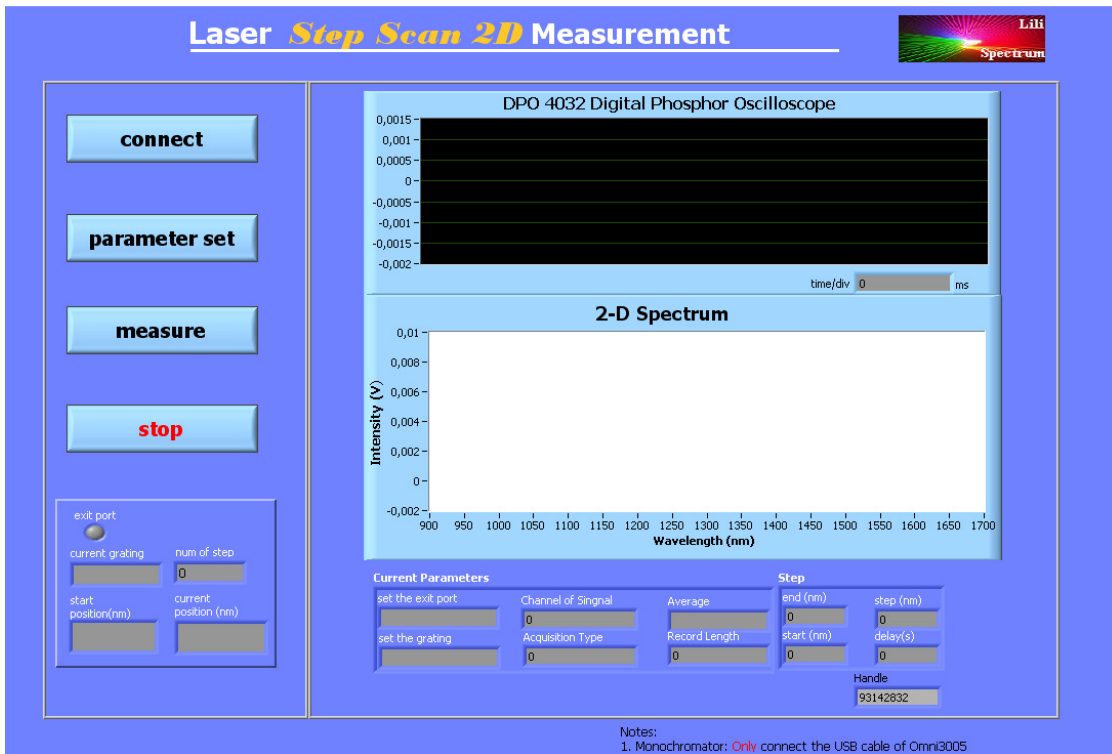
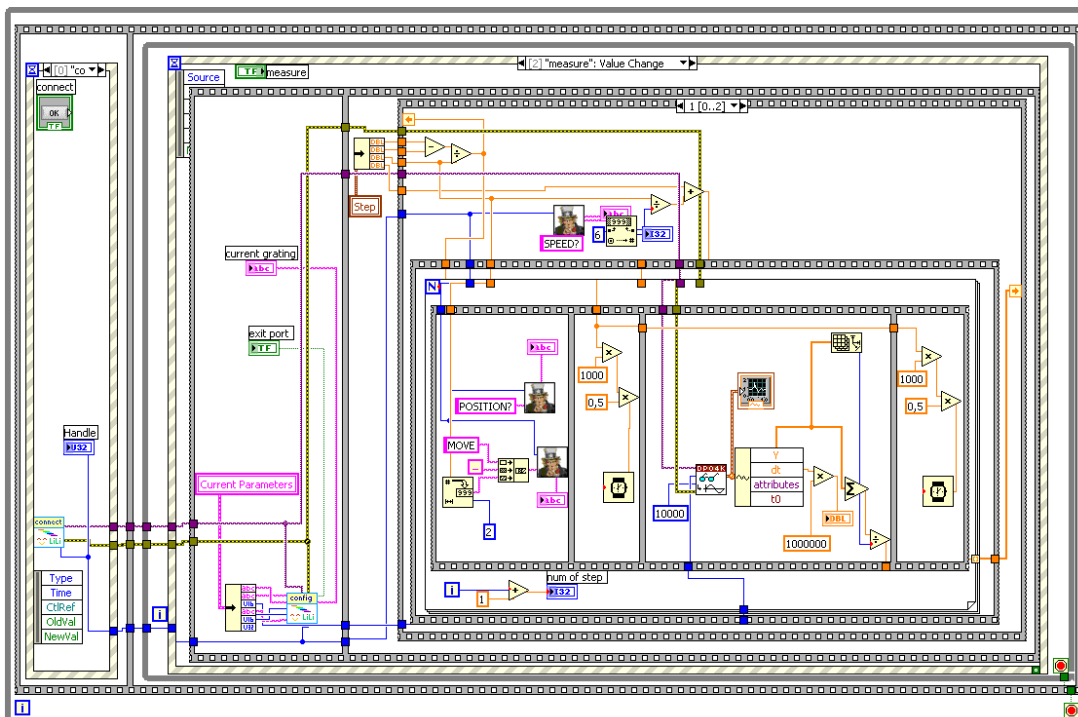**Figure 11.** The front panel for step scanning measurements (2D mode, with laser excitation).

Figure 12. The block diagram for step scanning measurements (2D mode, with laser excitation).

Figure 12 shows the block diagram for this program, a while loop is used in the outer layer to enable the program to keep running until a stop command is received. A flat sequence structure in the inside layer is used to execute the commands in sequence: first device connection and then other operations. Device connections in this program are accomplished by citing the same Sub-VI as the program described in section I.3, since the same devices are used and connected.

Setting parameters, starting a measurement and ending the program are defined as individual event cases in an event structure. The event case responds to the clicking action made in the front panel of the program. Using an event case instead of a sequence structure enables repeating each operation without processing in sequence. The event case of ending the program uses the same protocol as that section I.3, i.e., ending a while loop.

The event case for setting parameters is achieved by citing a Sub-VI named 'Lase_2D-para'. The differences between continuous and step scanning are the manner by which the parameters are set, e.g. step size and delay for the step scanning. The front panel and block diagram of this Sub-VI is shown in Figure 13. Monochromator and oscilloscope settings are separated into two boxes on the front panel, and the input parameters are bundled into clusters as outputs in the block diagram.
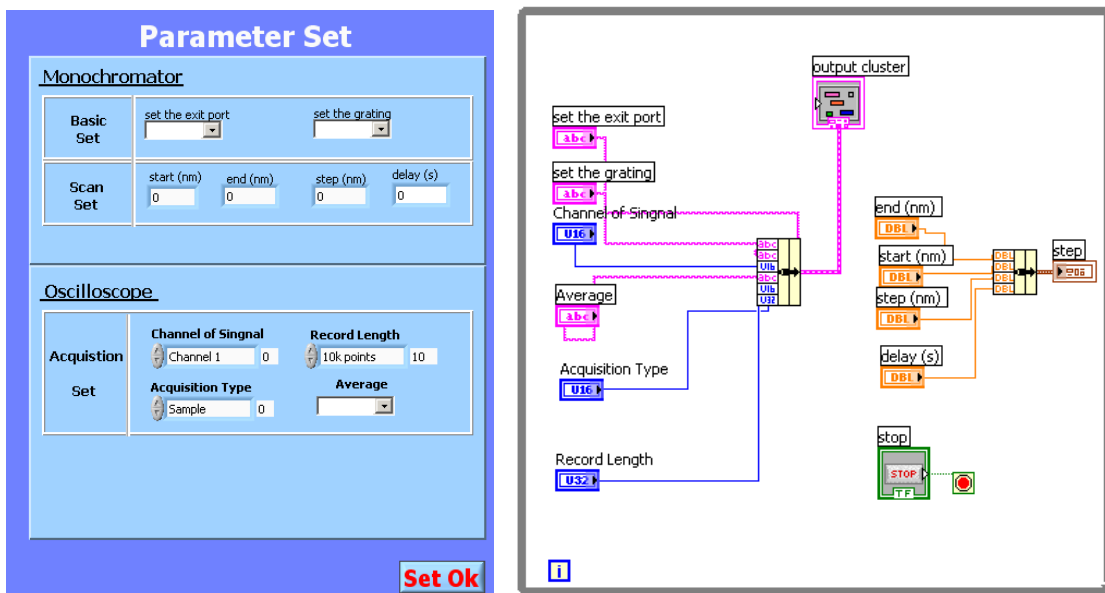

Figure 13. The front panel and block diagram for the Sub-VI 'Lase_2D-para'.

The event case for the measurement is the central function of this program, which is shown in Figure 12. A flat sequence structure with two frames is used. The first frame configures the devices according to the parameters set, in which the parameters in the Sub-VI 'Lase_2D-para' are defined as a local variable and sent to the devices through a Sub-VI named 'config'. The block diagram of the Sub-VI 'config' is shown in Figure 14. The design of this Sub-VI is similar to the unfolded sequence structure in Figure 4 and Figure 5. The second frame is the process for the step scanning measurements. It is accomplished by another main stacked sequence structure, which is unfolded in Figure 15. In the first frame, the monochromater moves to the start wavelength by calling the Sub-VI of 'move to'. In the middle frame, the step scanning movement is processed, and simultaneously transfers the waveform of the oscilloscope to the front panel of the program. The upper part in this frame is the working section for some mathematical calculations of the stepping parameters. A for loop structure below is used to execute moving the wavelength in steps and displaying the waveform. The cycle count of the loop is wired to the number of the step. Inside of this for loop structure, a further flat sequence structure is used to execute the measurement in chronological order, moving first and then acquiring the waveform. A waiting time is used in between to allow for stabilization of the measurement and avoids conflict. In the third frame in Figure 15, the spectrum is recorded to a file by a file I/O item of writing to a spreadsheet file. The intensity of the spectrum at each wavelength is calculated by averaging the waveform at that wavelength.
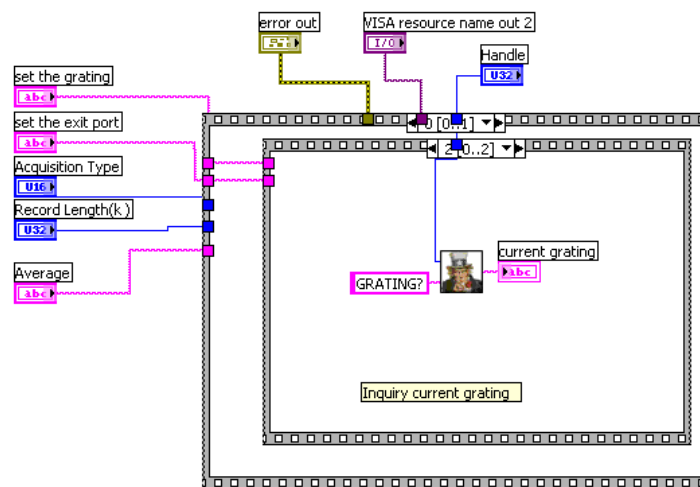

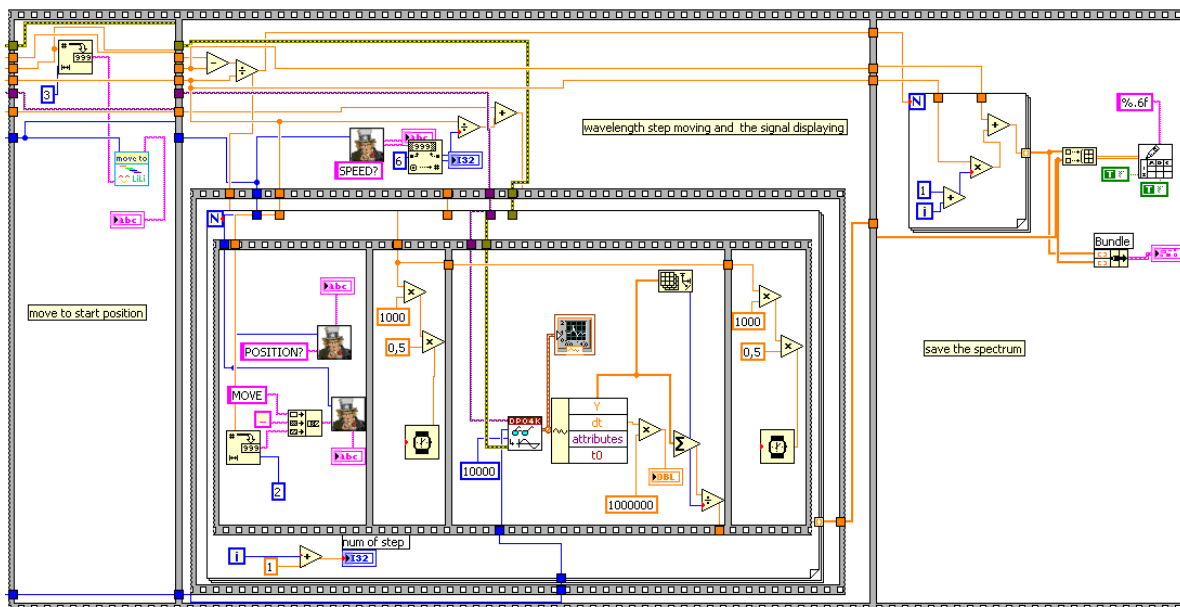**Figure 14.** The block diagram for the 'config' Sub-VI.

Figure 15. Unfolded sequence structure in the event case of measurement in Figure 12.

I. 5 Step scanning measurements (3D mode, with pulsed laser excitation)

The function of step scanning measurement in 3D mode is similar to 2D mode, when a pulsed laser is used as an excitation source. The main difference is that the 3D mode is used to record the transient signal and 2D mode is used for steady state measurement, which holds no temporal information, and this difference is accessed by using different devices, e.g. a pulsed laser is used in 3D mode and a continuous wave laser is used in 2D mode. The recorded signal in 3D mode includes information both of time and wavelength *vs.* light intensity (or absorbance). The front panel for the step scanning measurement in 3D mode is shown in Figure 16. For convenience of operation, the front panel is designed as for the 2D mode and can be distinguished by the title on top.

A 3D spectrum is plotted by using a 3D surface graph based on the data recorded by the oscilloscope in the form of an array. Information on intensity *vs.* time *vs.* wavelength is saved to a text file and a 3D image is saved as a bmp file in the sequence structure shown in Figure 17.
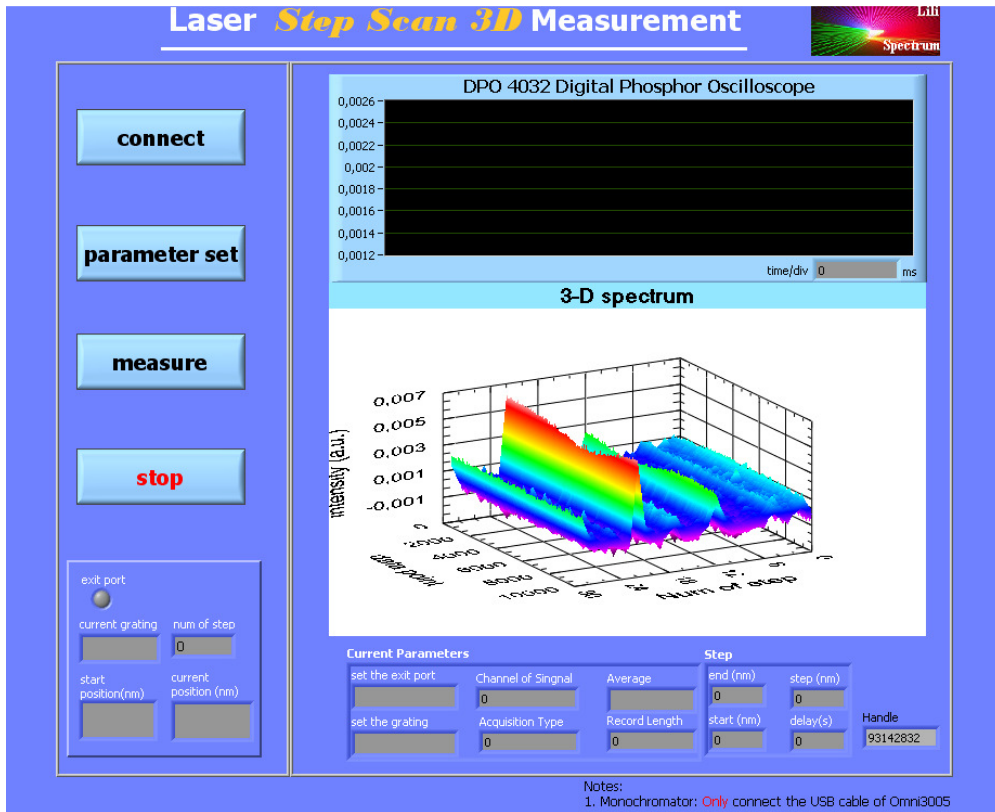
Figure 16. The front panel for the step scanning measurement in 3D mode with pulsed laser excitation.
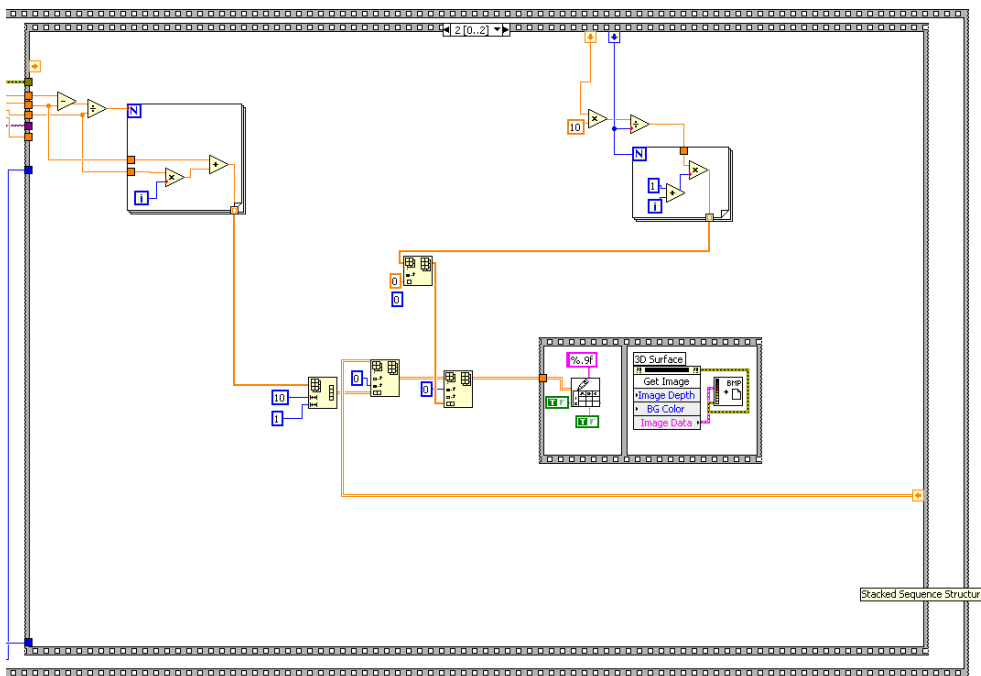

Figure 17. The sequence structure for saving and plotting data in 3D mode.

I. 6 Continuous scanning mode (with white light source excitation)

The front panel for this program is shown in Figure 18. The color of the background and the color of operation and function are reversed relative to that when a laser is used as an excitation source. When white light source is used as an excitation source, it is required that an additional monochromator is used to select the excitation wavelength. This requirement needs to be programmed to allow the connection to the additional monochromator and setting the excitation wavelength.   Other functions of this program are designed as with those described in section I.2. The connection to an additional monochromator is accessed by calling a Sub-VI with the name 'lamp_connect_2 mono', and the front panel and block diagram is shown in Figure 19. In the event case for monochromator connection, the communications of the excitation and emission monochromators are established sequentially, and the names are shown in the front panel. This Sub-VI is called for all the measurements when using white light source excitation.
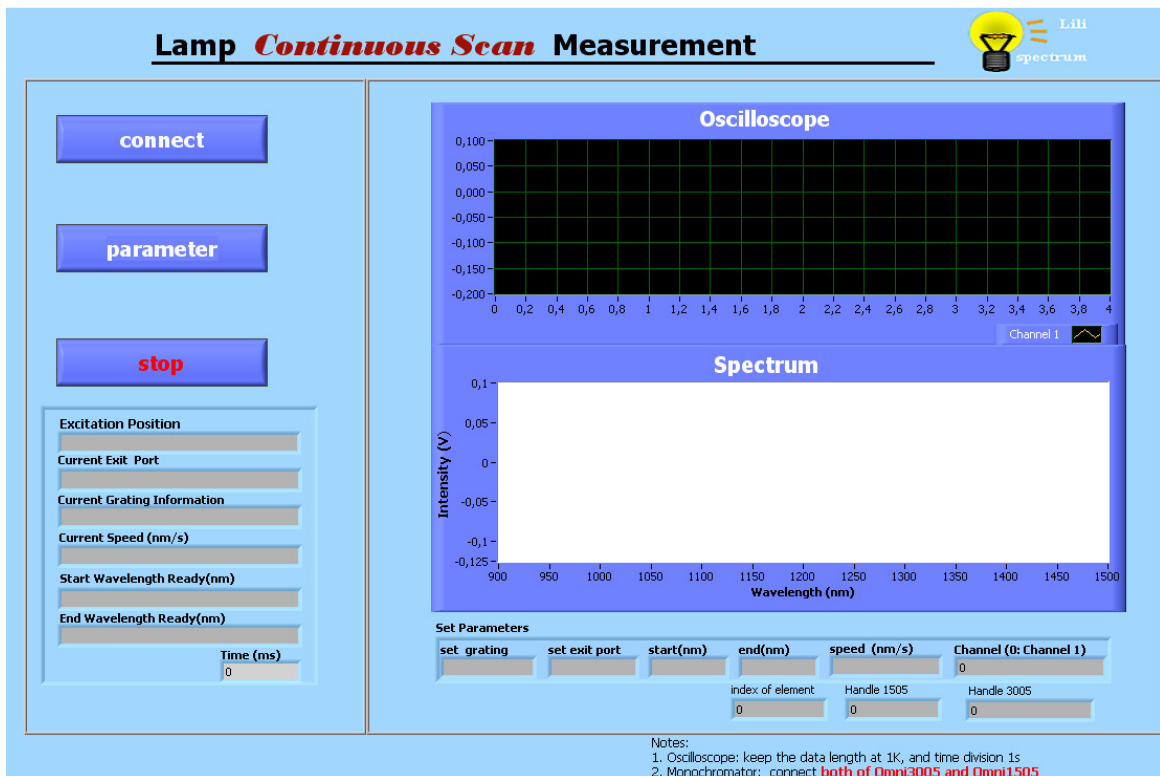

Figure 18. The front panel for the continuous scanning measurements with white light excitation.
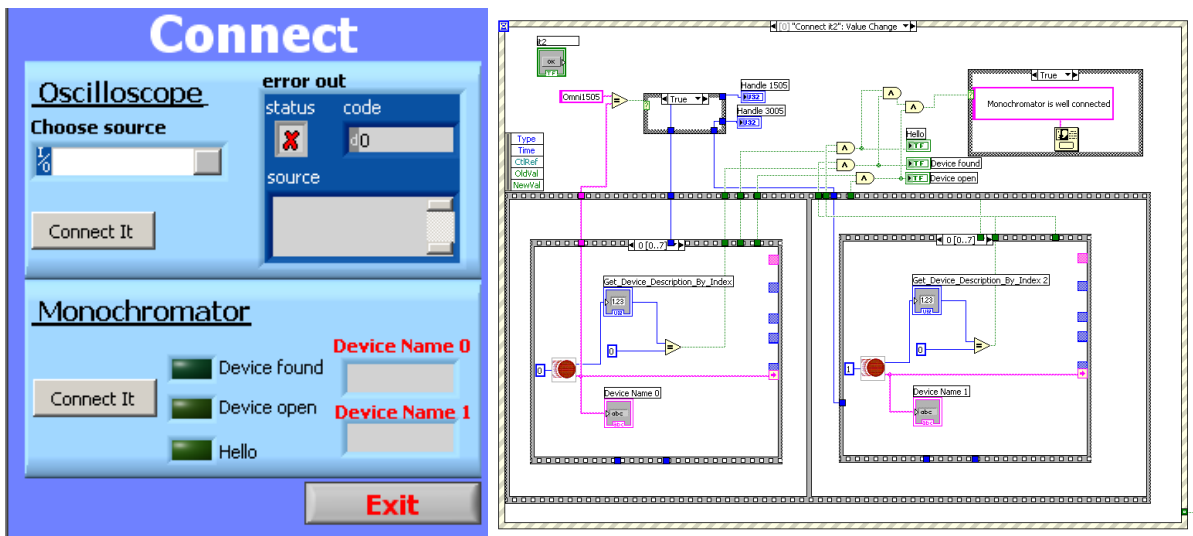
Figure 19. The front panel and block diagram for the Sub-VI 'lamp_connect_2 mono'.

The Sub-VI for setting parameters in this program, shown in Figure 20, is programmed similarly to that shown in Figure 10. A parameter named 'excited wavelength' is added in this Sub-VI, which is used to select the wavelength of the lamp. This parameter is not bounded with other parameters as the output is due to the separated operation of the excitation monochromator.
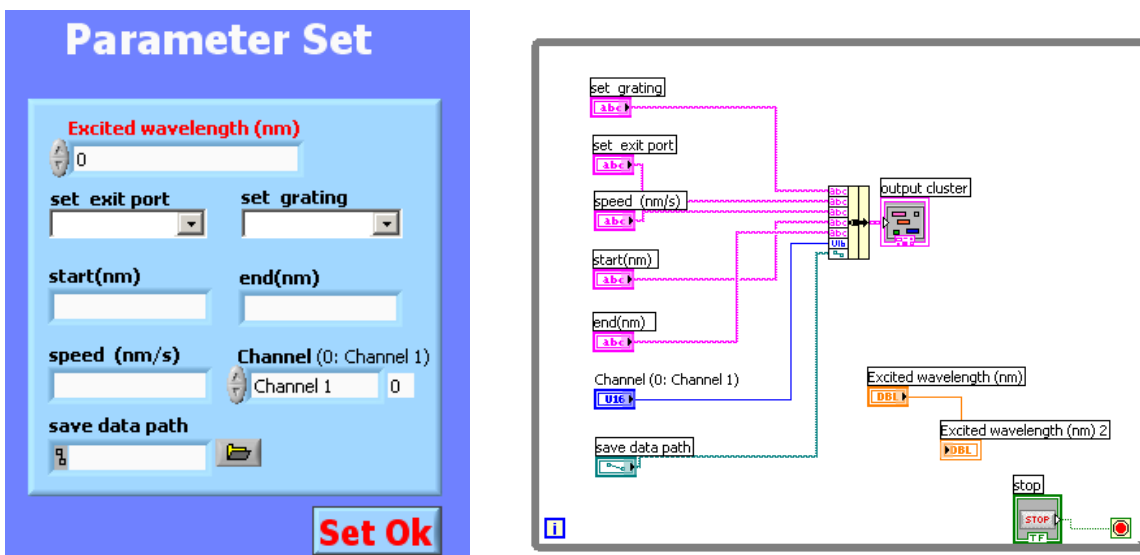

Figure 20. The front panel and block diagram for the Sub-VI 'lamp_conti_para'.

I. 7 Step scanning measurements (2D mode, with white light excitation)

This program is designed similarly to that described in section I.4. The front panel is shown in Figure 21. The reminders for setting excitation wavelength and connecting two monochromators are marked in red at the bottom of the panel. The difference is that the connection of the monochromators and setting parameters, which are accomplished by calling the Sub-VI 'lamp_connect_2 mono' described in section I.6 and the Sub-VI 'Lamp-2D-para' (Figure 22). The Sub-VI for setting parameters in this program is programmed similarly to the one shown in Figure 13. A parameter named 'excited wavelength' is added in this Sub-VI, which is used to select the wavelength of the lamp. This parameter is not bundled with other parameters as the output is because of the separate operation of the excitation monochromator. The detailed design of this program is described in section I.4.
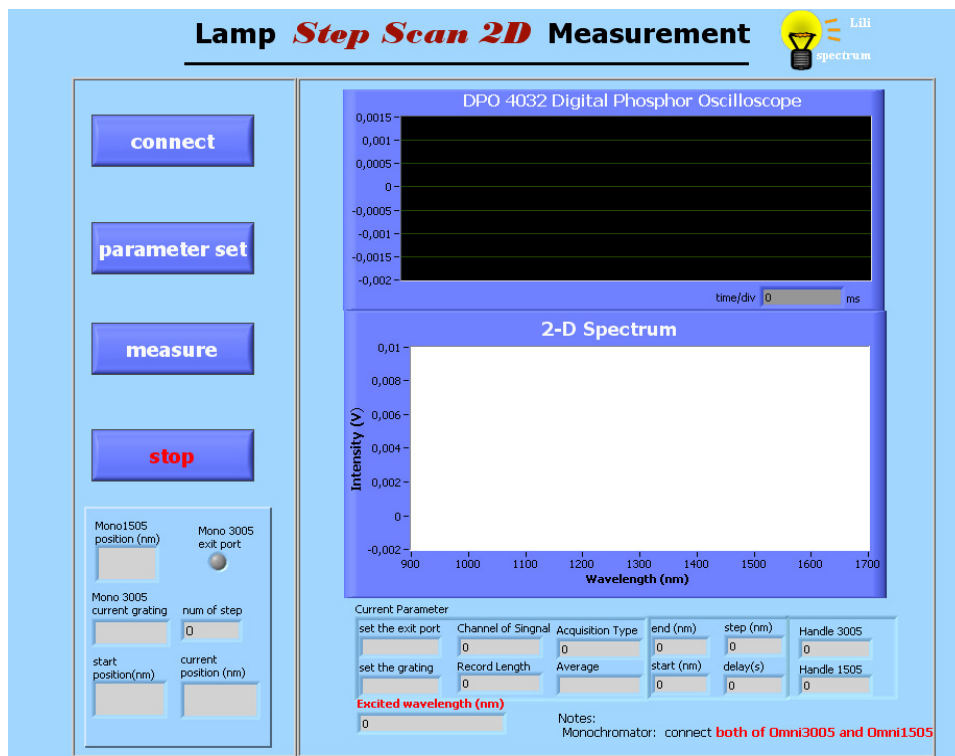

Figure 21. The front panel for the step scanning measurements (2D mode, with white light source).
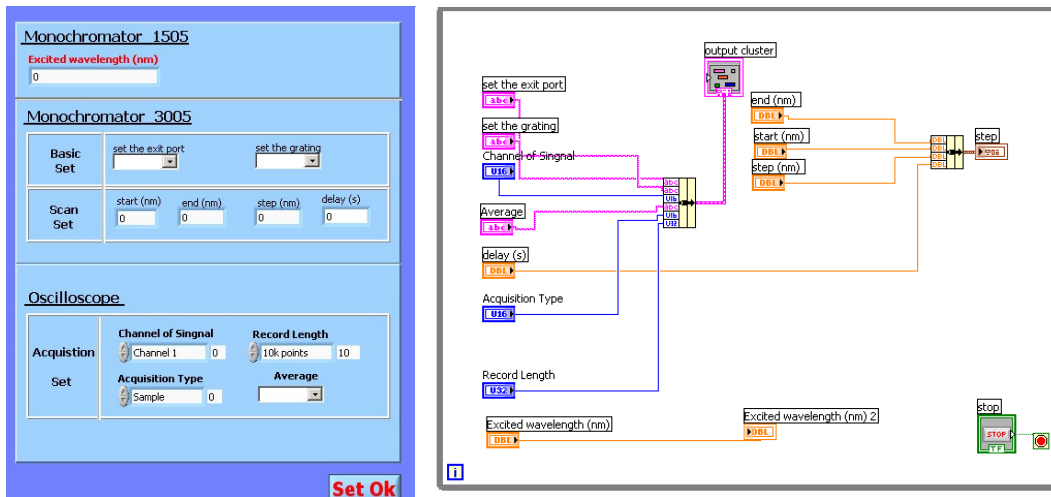
Figure 22. The front panel and block diagram for the Sub-VI 'Lamp-2D-para'.

I. 8 Step scanning measurements (3D mode, with white light excitation)

The front panel of this program is shown in Figure 23. The design is similar to that described in section I.4. The connection and parameters settings call on the same Sub-VIs as used in section I.7.
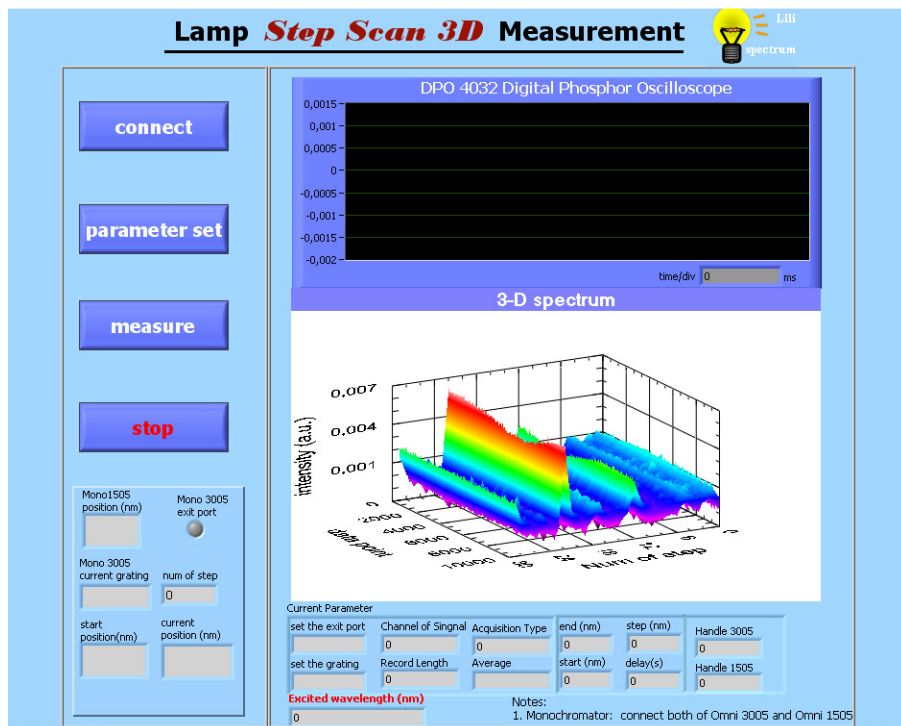

Figure 23. The front panel for the step scanning measurements (3D mode, with white light excitation).

I. 9 Basic control of the monochromator

The monochromator is also used independently of the previous measurements, so that it is set without further measurement being programmed. The front panel of this program is shown in Figure 24, in which the monochromator can be connected to the computer and the parameters set. Selecting gratings, setting exit ports and moving to the set wavelength are programmed in three event cases in a tab control. The basic codes in these event cases are the same as that for controlling the monochromator described above. The current status is read and refreshed on the current information box in the light bottom part. This software can used to set either the excitation or emission monochromator.
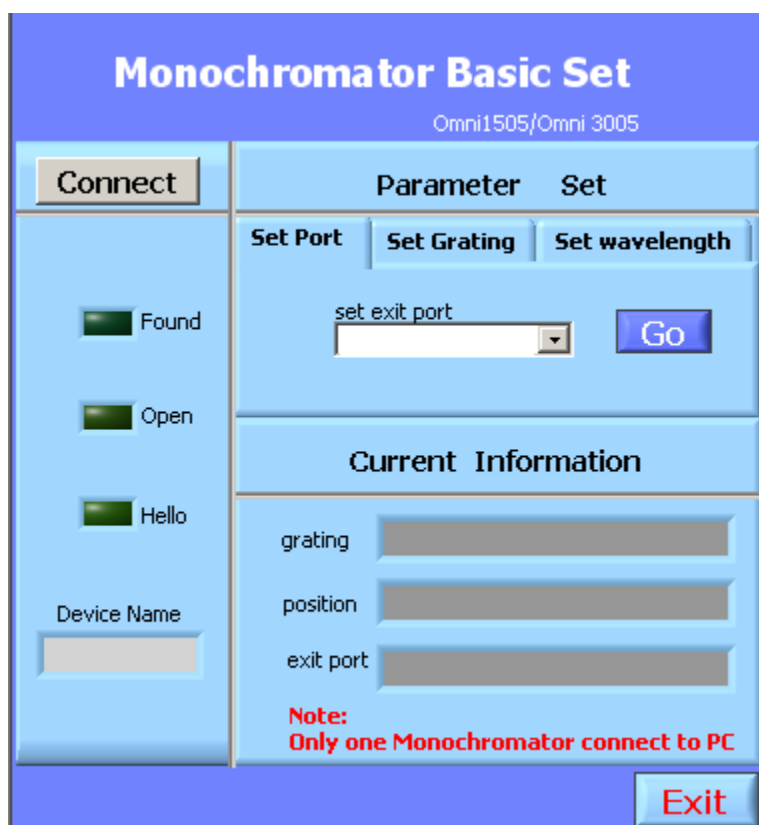

Figure 24. The front panel for the basic control of the monochromator.

I. 10 Record and read a single waveform

It is not always worth recording the transient signal at each wavelength, especially, when only the lifetime of the transient species is of interest and not the entire transient spectrum. This program is used to record a transient signal at a wavelength, where generally the largest change of emission or absorbance occurs

when pulse excitation is used. The front panel of this program is shown in Figure 25. There are two main functions, recording and reading the waveform, which are programmed as two individual event cases in a tab controlled event structure. Clicking the tab on the top shows the individual interface (Figure 25 (a) and (b)). Recording a single waveform is programmed the same way as all the cases for displaying the oscilloscope in real-time in the front panel described above.
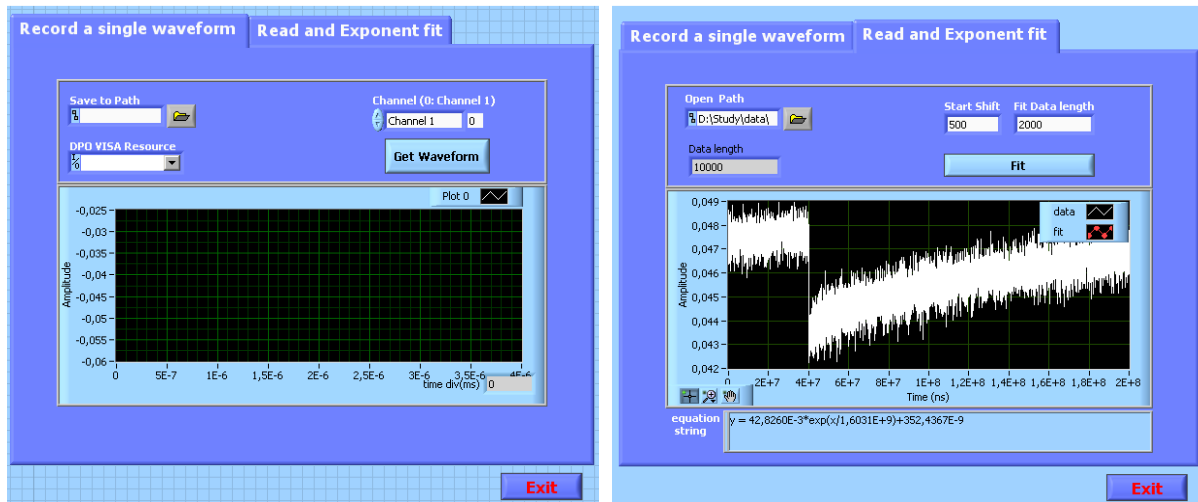
(a) the interface for recording   (b) the interface for reading and fitting

Figure 25. The front panel for recording and reading a single waveform.

Reading a recorded waveform and fitting with an exponential equation are programmed in an event case, which is shown in Figure 26. A file I/O function control of 'read from spreadsheet' is used to open the recorded data. With the help of some operations of the recorded array, this signal is transferred and displayed in a graph indicator. The fitting is accomplished by using a mathematical control of 'exponential fit'. The point of pump pulse arrival is calculated by finding the maximum or minimum of the recorded data. A shift length from the arrival point input in the front panel sets the starting point of the exponential fitting. The fitting equation concatenated as a string displays on the bottom of the front panel, from which the lifetime of the transient signal can be read.
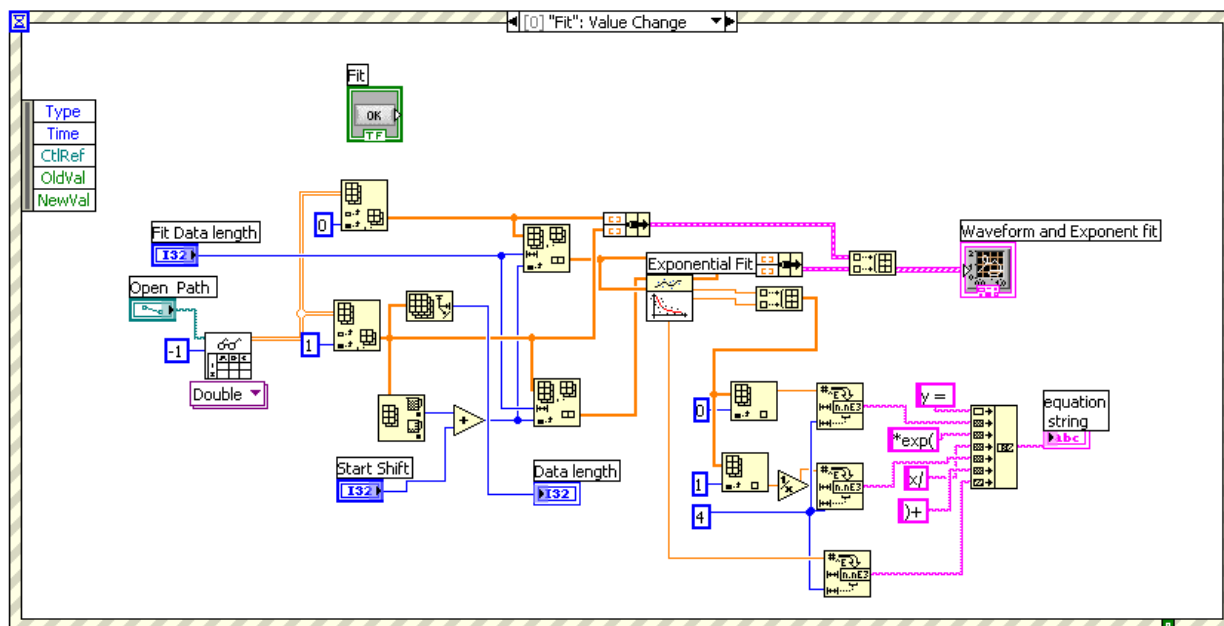
Figure 26. The block diagram for reading and fitting.

I. 11 Read 3D data

The function for plotting data in 3D in LabVIEW is relatively poor, because it is not allowed to rotate the 3D view to an arbitrary angle for consideration of the information as a whole. To this end, a program for reading data saved in 3D form and preliminary analysis was designed. The front panel is shown in Figure 27 (a). There are three main functions to this program, replotting 3D spectra, extracting 2D spectra in the form of intensity *vs.* time and intensity *vs.* wavelength. These three functions are defined as three individual event cases in an event structure.

The 3D spectrum is replotted in a figure window of Matlab by calling a section code in Matlab through a Matlab script node. The replotted spectrum is shown in Figure 27(b). The 3D replotting occurs in response to the action of clicking the button '3D plot' in the front panel, which is accomplished by calling the event case '3D plot' (Figure 28). The figure window of Matlab can allow for zooming in or out, rotating and saving the image of the 3D spectrum.
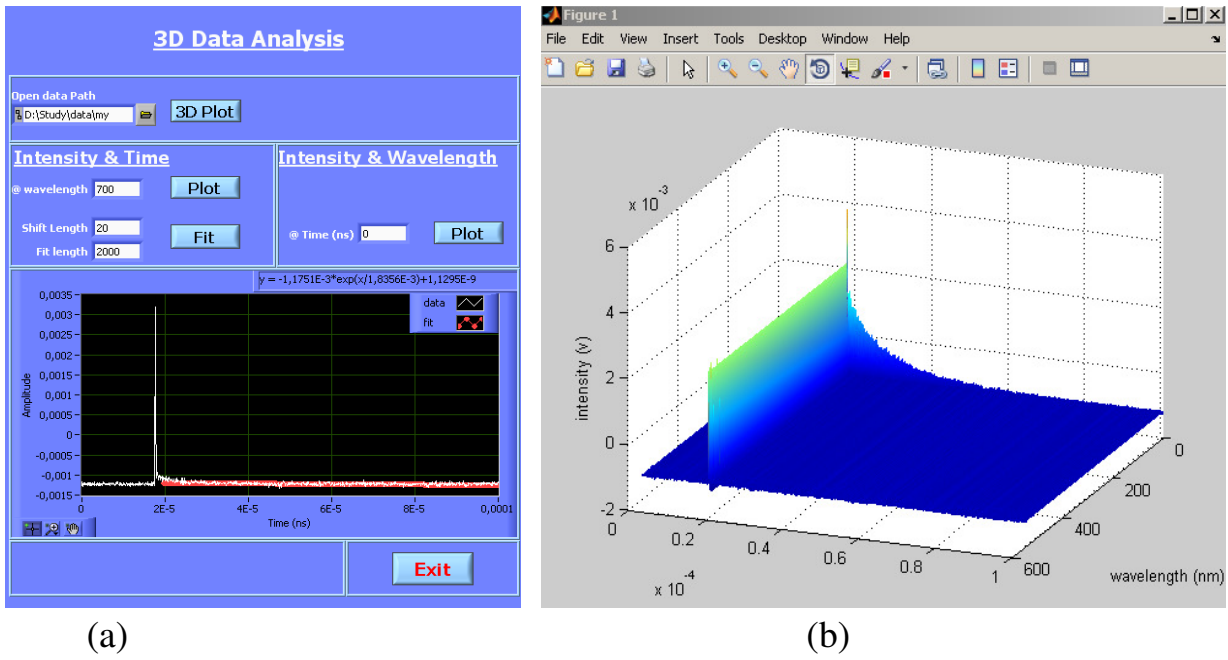
(a)   (b)

Figure 27. The front panel for reading 3D data (a), and replotting the image in 3D in Matlab (b).

By inputting the time or the wavelength of interest, a 2D spectrum can be extracted from the 3D image by clicking the plot button in the box of 'Intensity & Times' or 'Intensity & Wavelength', and the 2D spectrum is shown in the graph window in lower area of the front panel.

The graphs of two individual 2D spectra share the same graph window to keep the user interface simple. This is accomplished by using a property node 'visible' of the waveform graph. The unselected 2D graph is set to be invisible according to the false constant of the property node, and spectrum of interest is set to be visible and shown in the main panel. The event cases for extracting 2D spectra in the form of intensity *vs.* wavelength and intensity *vs.* time are shown in Figure 29 and Figure 30, respectively. Figure 30 shows that the 2D signal with the transient information can be fitted with an exponential equation, and the design of this case is similar to the function for exponential fitting in section I.10. The fitting equation is shown on the right top of the graph in the main panel by calling a property node 'visible ' of the equation string.
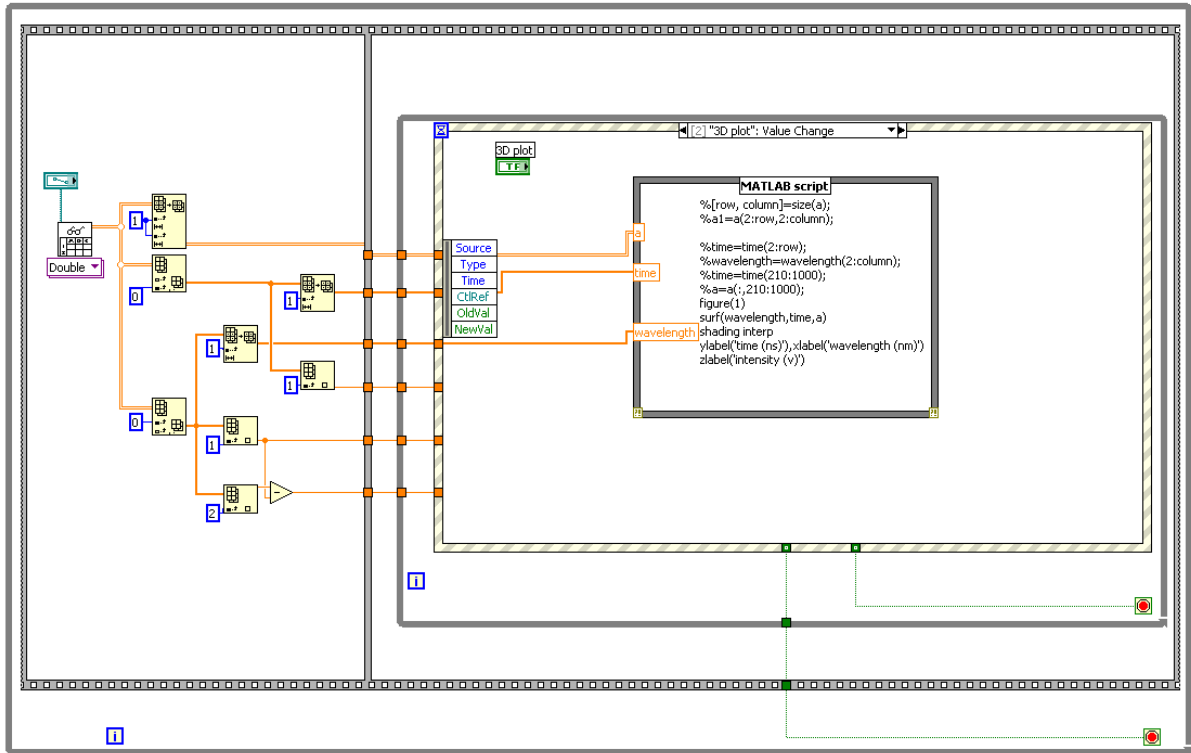
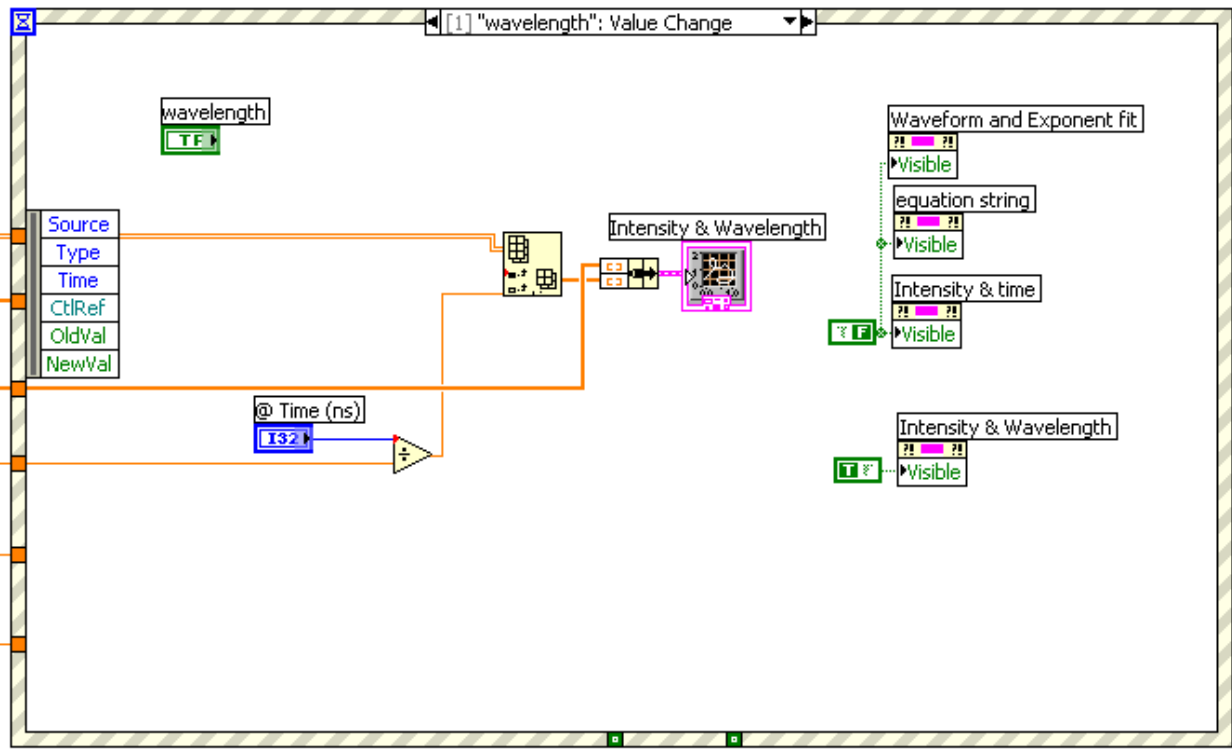**Figure 28.** The block diagram for3D data analysis.

Figure 29. The event case for 2D plot in intensity *vs.* wavelength.
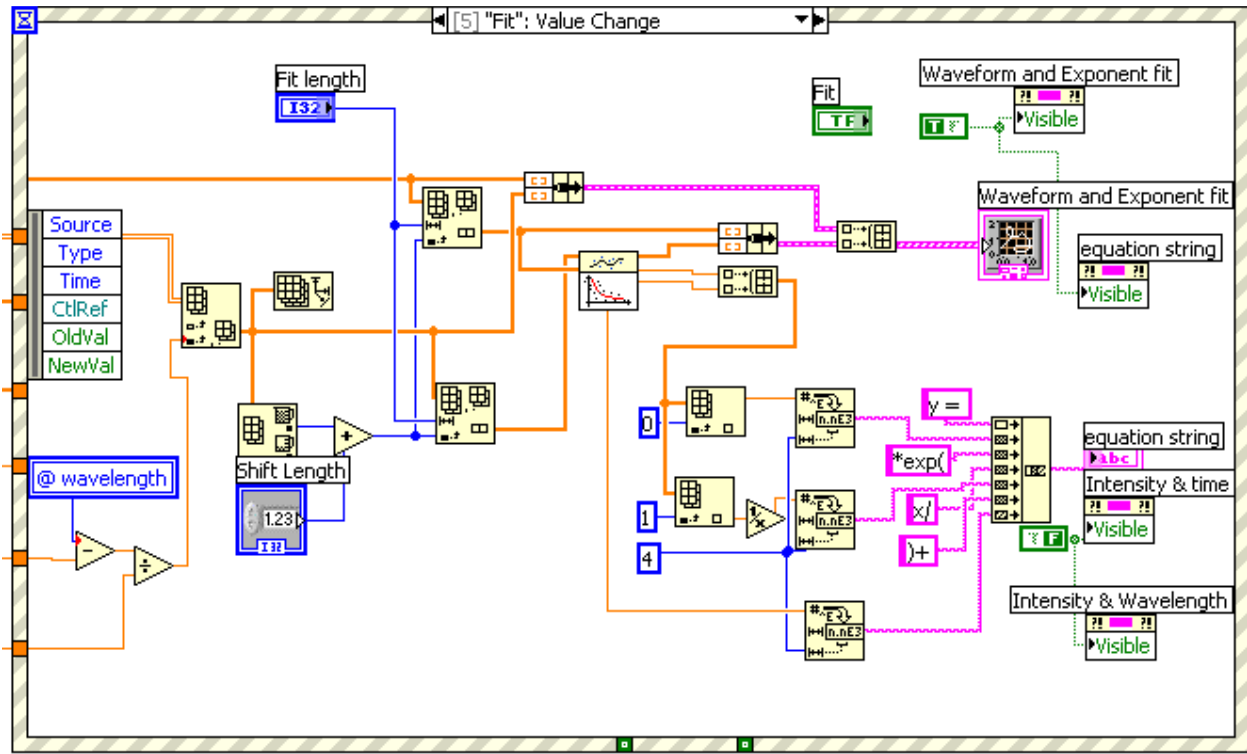
Figure 30. The event case for 2D plot in intensity *vs.* time and fitting.

I.12 References

[1] J. Travis, J. Kring, *LabVIEW For Everyone: Graphical Programming Made Easy and Fun*.3rd ed, Boston, US, Prentice Hall, **2007**.

[2] Data accesses to the driver for Tektronix DPO MSO 2000 4000 Series Oscilloscope are vailable online.
http://sine.ni.com/apps/utf8/niid_web_display.download_page?p_id_guid=6E23DB10D9FC2B 05E04400144FB7D21D.

Acknowledgements

Six years ago, I studied in an optical fiber lab and played with lasers and optical elements every day. I remember that one day someone mixed up acetone with ethanol for cleaning the interface of an optical fiber causing a huge panic in the lab, and the group took this issue very seriously. Time sometimes can drive life into the opposite direction. Working in a chemical group for four years, I had a chance to play with all kinds of solvents and have to protect super seriously when working with lasers. This great adventure I have experienced would not have been as colorful without all the chemists and friends here, to whom I want to give my sincere acknowledgements.

First of all, my deep gratitude goes to Prof. Ben L. Feringa, my first promotor, for offering me the opportunity to study in such an outstanding group. Dear Ben, you are the one who always has brilliant ideas and can give illuminating suggestions, and I deeply appreciate your kind and valuable instructions for my writing and presentation. You give an example of how an excellent scientist should be, infinite passion and enthusiasm for research, precise and strict discussions of experimental results. What I learnt from you is a precious treasure for all my life.

Second, I want to express my heartfelt gratitude to Prof. Wesley R. Browne for the guidance and supervision during these four years. Dear Wes, you are always there to help me with instruments, data analysis, writing and presentation. I am really impressed on your broad knowledge and can consult almost everything from you. I am very grateful for your arrangement for my PhD study with consideration of my background. Moreover, I also appreciate your pushing on my thesis writing, although at some stage you drove me really crazy because of forbidding any lab work when I was curious about experimental results, while without your pushing this thesis would have needed much more time to be finished.

I also want to express my sincere acknowledgement to Prof. John M. Kelly, Prof. Syuzanna Harutyunyan and Prof. Wybren Jan Buma, for their time and patience as my reading committee. I really appreciate your willingness of reading and evaluating my manuscript. Your comments and suggestions helped to polish this thesis a lot.

Next, to my dear paranimfs Jiajia and Francesca, I am so glad and grateful to meet both of you in Groningen and have you be my side during my defense ceremony. I do believe that your company will ease my nervers a lot during the defence. Both of you will finish your PhD study next year, and I wish you all the best for your own defense.

Jiaobing, I am very grateful for your instruction and help in the first two years of my PhD. I still remember your patient explanation of the projects on the first day of my PhD. It is you who showed me how to do accurate measurements, work efficiently and design beautiful photochemical systems.

Arjen, I very much enjoyed our collaboration on the motor-porphyrin project and it was a nice experience to work with such a smart chemist. Also thanks for your help with NMR measurements and analysis, calculations and enlightening discussions for other projects.

Paula, you are the one who taught me how to do real chemical reaction. With your help, after mixing, stirring, TLC, columns, evaporation, NMR analysis, I could survive together with my compounds. I really appreciated your help and also the days we spent together in the measurement room.

Thanks for all the staff in the Stratingh institute helping me deal with daily issues and analysis: Tineke, Hilda, Cristina, Alphons, Theodora, Hans, and Monique, thank you very much.

I was stuck in the same office during my entire PhD period, which rare happens in our group. The time with former and current officemates in 5116.0231 was very pleasant, thanks to Jiaobing, Giuseppe, Francesca, Derk-Jan, Paula, Bin, Martin, Robby, Manuel, Tom, Thomas, Petra, Sonia, Romina and Sander. Martin, thank you for always making a happy environment in the office and always kindly helping me to read Ben's writing. Thanks for the childish games, Jiaobing and Derk-Jan's plugging in and out of mouse and keyboard, Bin and Manuel's endless lifting up and down the desks, Romina's scare, and all the interesting talks in English, Dutch, Spanish, Italian, Deutsch and Chinese, although I was usually quiet, I enjoyed a lot all of the fun stories in our office. A special thanks goes to Tom, for the help to translate the summary into Dutch, and also thanks for Sander helping me with the Dutch correction.

I also thank other labmates in the C-wing, Jiawen, Kuang-Yen, Wen-Hao, Matea, Ana, Nathalie, Jort, Jurica, Jochem, Peter, Diederik, Stefeno, for the friendly working environment. Special thanks for Jos and Anouk, our lab assistants, for their work of keeping our lab tidy and organized. I also thank Thom and Jos for calculations of my compounds and discussions. Moreover, I thank other colleagues in the group, Wiktor, Claudia, Valentin, Almudena, Suresh, Wim, Depeng, Anne, Krzysztof, Massimo, Celine, Carlos, Lorina, Tao, and some others I may forgot to mention here. Thank all of you for the happy time in the institute.

During my PhD study, I was also involved a lot in the Brownie's group. It is pleasant to see the group growing. Thanks Appu, Hella, Heloise, Pattama, Shaghayegh, Nikki, Davide, Hans, Emma, Francesco, Sandeep, Peter, Luuk, Duenpen, for the nice environment and always giving me clues to where Wes was.

Thanks to our Chinese group in Groningen, Jiajia Dong, Depeng Zhao, Kun Yue, Jiawen Chen, Beibei Zhang, Zhongtao Wu, Lei Zhang, Yun Liu, Zhiyuan Zhao, Zheng Zhang, Shuo Yang, Jingyi Huang, Jianwei Li, Jiawei Rong, Yange Huang, Stella Zhang, because of all of you, the life here is more interesting and enjoyable.

我想在这里特别感谢是我亲爱的爸爸妈妈，感谢你们对我从小到大一路上的培养和付出，以及你们无限的支持和鼓励。谢谢我的其他家人们，在我远离家里的这段日子，是你们对家里的照顾，使我能够安心于国外的生活和学习。还要感谢我可爱的好朋友们，哼哼，圆圆，青青，小娜，小牛，离开学校这些年，我们的生活都发生了很大的变化，虽然远隔万里，依然能够分享生活的喜怒哀乐。最后，我要感谢我的老公，张小岩同学，我的阿胖，我原来从没想过嫁给你不仅意味着走入你的日常生活，还意味着走进了同一个实验室，不过现在看来也不错。我们莫名其妙的被安排在了同一天答辩，看来也是缘分使然吧。随着这几年你体重的增长，你在我生命中所占的分量也越来越重，感谢你在这些年里的陪伴和鼓励，我想这将是我们人生中很美好的一段时光。

Lili 丽丽

Groningen, 2013